

Research Grants Program

2004 Winner Researches

Research Grants

Book 2004

Language Revision

Bibliotheca Alexandrina Translation and Language Control Unit

© 2011, Bibliotheca Alexandrina

NON-COMMERCIAL REPRODUCTION

Information in this publication has been produced with the intent that it be readily available for personal and public non-commercial use and may be reproduced, in part or in whole and by any means, without charge or further permission from the Bibliotheca Alexandrina. We ask only that: Users exercise due diligence in ensuring the accuracy of the materials reproduced; Bibliotheca Alexandrina be identified as the source; and The reproduction is not represented as an official version of the materials reproduced, nor as having been made in affiliation with or with the endorsement of the Bibliotheca Alexandrina.

Foreword

At the dawn of the 21st century, the Bibliotheca Alexandrina (BA) takes its place in the world as one of the centers of knowledge and intellect. As we move on in the revival of the roles of the Ancient Library of Alexandria, we take into account its having been the focal point of where many of the fundamental rules of science were born.

The BA aims to empower the country's science capabilities and to invest in young scientists of high potential; those who would like to dedicate themselves to research, where their love for knowledge and discovery is what drives them on. We would also like Egyptian scientists to explore the potential of international linkage and its advantage to the scientific community. Societies need to hear the dissenting voices, the contrarian views, the new ideas and the new findings in research.

This booklet summarizes and highlights progress of our outstanding BA/CSSP Research Grants 2004 winners. We aim to combining, focusing, and enhancing research efforts by promoting the research papers, and to explore the potential for international collaboration and its advantage to the scientific and business communities.



Ismail Serageldin
Librarian of Alexandria
Director of the Bibliotheca Alexandrina

Preface

This age is the knowledge-driven era. Challenges faced by nations today are numerous, and keys to overcoming the hurdles include the correct application of scientific knowledge and technology. Enhancing science and technology in developing countries has therefore become a true necessity and not a luxury. Hand-in-hand with it is research advancement. But improvement of research involves various actors, and each has a vital role to play. The Center for Special Studies and Programs (CSSP) at Bibliotheca Alexandrina (BA) hopes to contribute to this goal through its BA/CSSP Research Grants Program, and other projects that support researchers.

In Egypt there are over 52,000 researchers in R&D (617 per million people). Professionals and scholars such as PhD holders, who obtained their degrees abroad, can remain in the foreign country and continue the pursuit of their professional or academic careers, provided they can secure funding for their research. This ultimately leads to brain drain. They could also return to their original Egyptian institutions where research funds are scarce and they risk losing the knowledge they acquired, or they could pursue a career in the business sector, where their acquired knowledge can be applied.

CSSP would like to tackle the alienation problem faced by Egyptian researchers upon their return to Egypt and their original institutions. It also recognizes the existence of a pool of untapped potential available in young researchers all over Egypt that are eager to collaborate with international institutions, however lack the process needed for such collaborations.

CSSP is especially concerned with the young Egyptian post-doctoral scientists from Egyptian universities. It also recognizes that cooperation between scientific and technological communities is critical to enhance technology transfer, maintain high research quality, as well as provide opportunities for scientific contacts.

The Library of Alexandria has therefore launched a research grant program, through CSSP, to fund outstanding young postdoctoral scientists in Egypt, who undertake collaborative projects in the Natural Sciences, Mathematics and Information Technology. A new field has been added; Pre-University Education.

The BA/CSSP Research Grants program aims to support Egyptian S&T research and development, as well as decrease the widening scientific achievement gap between local scientists and their peers in developed countries. It tackles the unavailability of sufficient financing while evading bureaucracy faced by researchers in acquirement of funds. It also limits impediments faced by some, since selection is based on research excellence and not seniority, leading to equal opportunities for all researchers. CSSP hopes to act as a focal point, creating and sustaining networks of international collaboration through these research grants.

For further information, please visit the BA/CSSP Research Grants program webpage: www.bibalex.org/cssp/rg



Mohamed El-Faham
Director
Center for Special Studies and Programs
Bibliotheca Alexandrina

Introduction

The ancient Library of Alexandria has survived in the memory of all scholars to this day, not only by being the largest in antiquity, but also by being a vibrant center of scientific and intellectual debate. Aiming to revive its past historical scientific mission, the Bibliotheca Alexandrina (BA) launched the Center for Special Studies and Programs (CSSP) in July 2003 with the aim of being recognized again by scientists all over the world as one of the best global linkage venues to eminent researchers and scientific institutions.

The CSSP is an independent scientific non-profit institution affiliated to the BA and chaired by the BA Director. It was established by the Egyptian Presidential Decree no. 361 of 2002. The CSSP has its own Director and selected Board of Directors. It aims to support the country's science, math and engineering capabilities and promote their utilization to serve society. This is via promotion and support of research through the conduction of conferences and workshops, at international and local levels, aiming to increase public awareness of the significance of science and technology which will in turn promote the rise of professional scientists.

Since the beginning of 2004, the BA; through CSSP, has been offering annual research grants for young Egyptian postdoctoral researchers below the age of 35, who have completed their PhD within the past 5 years, or are expecting to complete it within the year of submitting their application. The objective of the Research Grants program is to support outstanding young postdoctoral Egyptian researchers who perform cutting edge research and undertake collaborative investigation approaches across the science and technology spectrum, by offering them postdoctoral research grants as well as helping them establish connections with Egyptian and international scientists and researchers.

The whole application procedure for the Research Grants takes place online, where candidates upload their personal information and proposals. A blind review process follows to evaluate each proposal. Therefore no reference is made to the person, institution, or specific location that would otherwise identify the researcher in the documents submitted for reviewing, thus preventing biased selection.

Acknowledgment

This dissertation is dedicated to those who contributed in making the BA/CSSP Research Grants program feasible and recognized by Egyptian researchers and international scholars. It would not have succeeded without the full support of the Director of the BA and the Director of the CSSP.

Special thanks to all reviewers and foreign counterparts who participated in all of the researches accomplished in the research grants program.

Finally, we thank all our researchers who took the initiative to research for the sake of their home country Egypt, willing to step up with its highly motivated calibers.

Table of Contents

AGRICULTURAL SCIENCES

- 1. Marker Assisted Selection for Orobanche Crenata Resistance in Faba Bean** 3
Mahmoud Mohamed Zeid, Faculty of Agriculture, Alexandria University
- 2. Optimization of Mass Production Entomopathogenic Nematodes (EPN's) in Egypt** 13
Mona Ahmed Hussein, Center of Excellence for Advanced Sciences (CEAS), National Research Center

BIOLOGY AND BIOTECHNOLOGY

- 3. Desert Actinomycetes as a Novel Source of New Antimicrobial Agents** 31
Wael Nabil Hozzein, Faculty of Science, Cairo University, Beni-Suef Branch

CHEMISTRY SCIENCES

- 4. Some Studies for Preparing Superamolecules Species via Thiocalixarenes and Their Applications Acknowledgment** 43
Omran Abd-Ellah Omran, Faculty of Science, South Valley University

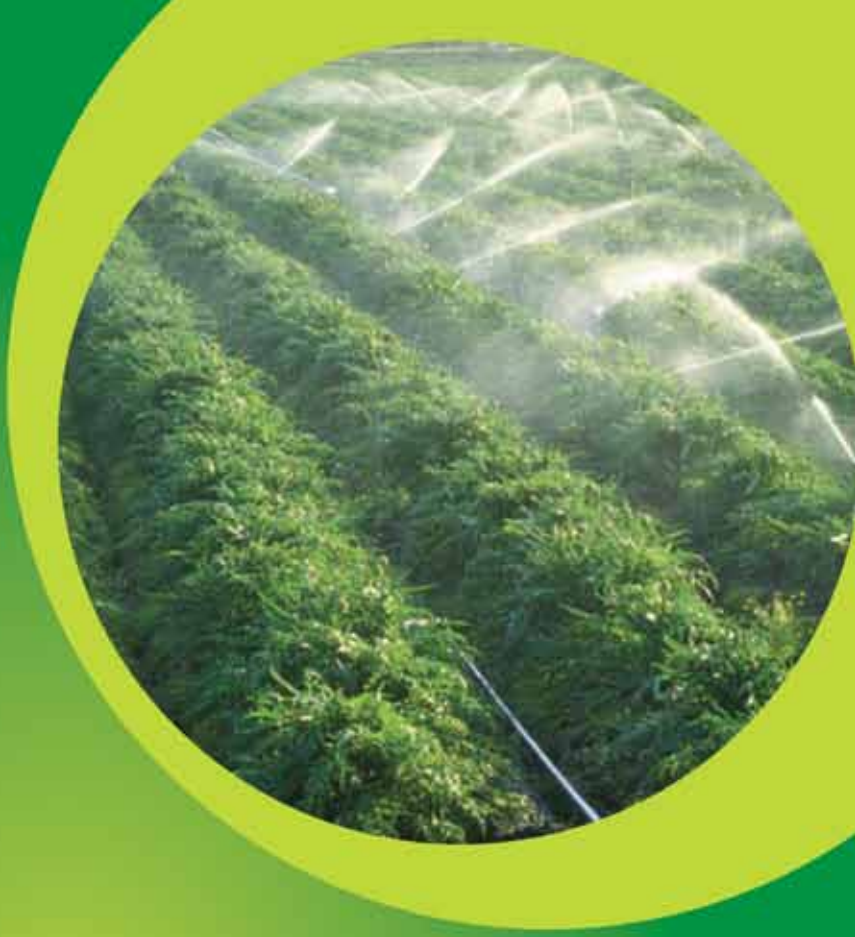
ENGINEERING SCIENCES AND TECHNOLOGIES

- 5. Flexural Behavior of Externally Prestressed Continuous Concrete Beams** 59
Ahmed Hassan Ghallab, Faculty of Engineering, Ain Shams University
- 6. Deployable Structures** 143
Ehab Mahmoud El-Kassas, College of Engineering and Technology, Arab Academy for Science and Technology and Maritime Transport

INFORMATION TECHNOLOGY

- 7. Towards Engineering Web-Services and Agent-Oriented Applications** 161
Amir Farouk Zeid, Computer Sciences, American University in Cairo
- 8. Using Change Propagation Probabilities to Assess Quality Attributes of Software Architectures** 169
Amir Farouk Zeid, Computer Sciences, American University in Cairo
- 9. Providing Secure Communications for Wireless and Wireline Applications** 179
Shymaa M. Arafaat, Faculty of Computer and Information Sciences, Ain Shams University





Agricultural Science



Mahmoud Mohamed Kamel Zeid

Assistant professor, Department of Crop Sciences, Alexandria University, Alexandria, Egypt. Mahmoud Zeid was born on 26 December 1970, in Alexandria, Egypt. He graduated from Victoria College High School and attended the University of Alexandria in 1989. In 1992, he received his Bachelor of Science in Agriculture from Alexandria University. He has been working at the Department of Crop Sciences, Alexandria University, Alexandria, Egypt since 1992 and received his Master's degree from the same department in 1997. In 1998, he traveled to Germany, on a DAAD scholarship to pursue his PhD studies. In 2003, he completed his PhD program at Georg-August-Universität Göttingen, Germany.

Mahmoud received training in the field of applying molecular tools in plant breeding in Greece, Spain, and Netherlands and most recently in USA, where he was awarded the African Scientist Fellowship at Cornell University, New York, USA. He was awarded the Bibliotheca Alexandrina (BA) Research Grants, Alexandria, Egypt in 2004. Through the BA/CSSP Research Grants, he collaborated with researchers in Germany and the USA and was able to develop the first of type microsatellite markers in faba bean.

Marker Assisted Selection for *Orobanche Crenata* Resistance in Faba Bean

Mahmoud Mohamed Kamel Zeid

Faculty of Agriculture, Alexandria University, Alexandria, Egypt

EXECUTIVE SUMMARY

Faba bean (*Vicia faba* L.) is by far the most important legume crop grown in Egypt, with 110,000 hectares grown annually (FAO, 2005). Although progress has been achieved in yield improvement, the problem of the parasitic weed *Orobanche crenata* Forsk is considered a constraint to faba bean production in the Mediterranean basin. Accurate and rapid methods of screening faba bean lines for resistance to *O. crenata* are critical in assisting breeders in precise selection, thus reducing the number of lines in resistance breeding programs as early as possible. The use of molecular markers can facilitate the identification and selection of resistant material once genes for resistance are tagged. A key point in this work is based on the fact that up to date, the Egyptian line F 402 (now known as the cultivar Giza 402) is considered the only true source of resistance genes to the parasite on faba bean, not only in Egypt, but in the whole Mediterranean region. The objective of this project was to tag genes for *O. crenata* resistance in a faba bean in F3 population segregating for this trait. The markers employed were Randomly Amplified Polymorphic DNA (RAPD), Microsatellites (SSR), Inter Simple Repeats (ISSR) markers and Resistance Gene Analogs (RGAs). The resistance source was the Egyptian cultivar Giza 402 known to be the donor of resistance genes in all resistant varieties in Egypt and Spain.

Two hundred and twenty F3 families derived from a cross between a resistant (Giza 402) and a susceptible (Giza 3) inbred line were tested for *O. crenata* resistance in a pot experiment with soil infested with *O. crenata* seeds. Transgressive segregation was observed where some F3 families surpassed either parental line in their level of resistance expressed as the number of parasite attacks or the dry weight of the host plant, providing an excellent material for the molecular studies. A total of 330 RAPD, 12 ISSR, six RGAs and 10 SSR markers, either based on previous work on faba bean or screened for the first time, were tested to search for polymorphism between the two parental lines.

When polymorphism was detected, a Bulk Segregant Analysis method (BSA) was employed to search for possible genes of major effect for resistance. Bulks were formed from two contrasting groups each of 16 individuals from the screened F3 families (resistant and susceptible bulks). None of the tested markers was useful in tagging any major gene for resistance.

Since the majority of the markers were dominant RAPD markers (*i.e.* were unable to differentiate between homozygous and heterozygous resistant lines), and were not reproducible between laboratories (in Spain, Germany and Egypt), the need for a co-dominant marker that is transferable between laboratories and between populations was recognized. We tested the latest technique for SSR development, known as FIASCO (Fast Isolation by AFLP of Sequences Containing repeats), proposed by Zane *et al.* (2002) for non plant species. We succeeded in developing 40 *de novo* SSR markers from the line Giza 402. The significance of these SSR markers not only relies on their being the first SSR markers to be developed from the whole faba bean genome (not restricted to a specific chromosome), but also in their amplification across *O. crenata* resistant materials from Egypt and Spain where almost all of the research on *O. crenata* is conducted. Furthermore, the markers amplified across a broad range of germplasm, signalling their importance for faba bean breeding programs. To reliably identify QTL for *O. crenata* resistance in faba bean, more SSR markers are being produced.

1. Project Background

1.1 The Problem

The parasitic weed *Orobanche crenata* Forsk. is almost restricted to the Mediterranean basin, extending only few hundred kilometers south into Africa (Algeria, Egypt, Morocco and Tunisia), north into Europe (including Spain, Italy, Greece, Malta, and Cyprus) and east into Iran. The parasite affects faba bean, pea, lentil, chickpea, carrot, safflower, lettuce and sunflower.

The most important of these, by far, is faba bean, (*Vicia faba* L.). Estimates of actual area infested or at risk in the Mediterranean region and western Asia amounts to 1 million hectares of faba bean, which is almost the total area of the crop grown in the region (Parker, 1994). In Portugal more than 13,500 ha, in Spain the area amounts to 50,000 ha and in Egypt, more than 28,000 ha are infested with the parasite, causing losses that exceed 10 million dollars annually. Because of the large number of seeds deposited by the parasite and their exceptional viability and longevity, being able to survive in the soil for more than 15 years (Linke and Saxena, 1991), farmers are being forced to abandon the cultivation of faba bean. This in turn leads to a decrease in the production of vegetable proteins and an increase in costs of nitrogen fertilization, which mainly affects small scale farmers who cannot afford the costs of the additional nitrogen fertilizers needed

to compensate for the drop in soil nitrogen when faba bean is excluded from the rotation.

1.2 Opportunities for a Solution

Control measures for the noxious parasitic weed *Orobanche crenata* including late sowing, handpulling, glyphosate spraying and trap crops have all been shown to reduce levels of infestation, however, no totally effective methods have yet been introduced. The use of resistant cultivars is known to be the easiest and most economic way to fight against parasitic weeds. Prior to the detection of the line F402 in Egypt (Nassib *et al.*, 1978), very few sources of resistance had been found. In fact, they showed differences in susceptibility rather than agronomic useful resistance (Cubero, 1984). Breeding for resistant varieties has successfully resulted in the development of the cultivar Giza 402 (Nassib *et al.*, 1978), expressing moderate resistance to the parasite accompanied by appreciable seed yield under parasite infestation. Continuous improvement through classical breeding methods in this cultivar resulted in improving the level of resistance to the weed (Khalil *et al.*, 1994). Up to date, Giza 402 is considered the only source of resistance to the parasite in Egypt, where all resistant material produced, (Giza 429, Giza 674 and X-843), have their genes of resistance from Giza 402 (Saber *et al.*, 1999). In Spain, the F402 line provided the basic material for obtaining a valid resistant cultivar. The result was the line VF1071, which became the

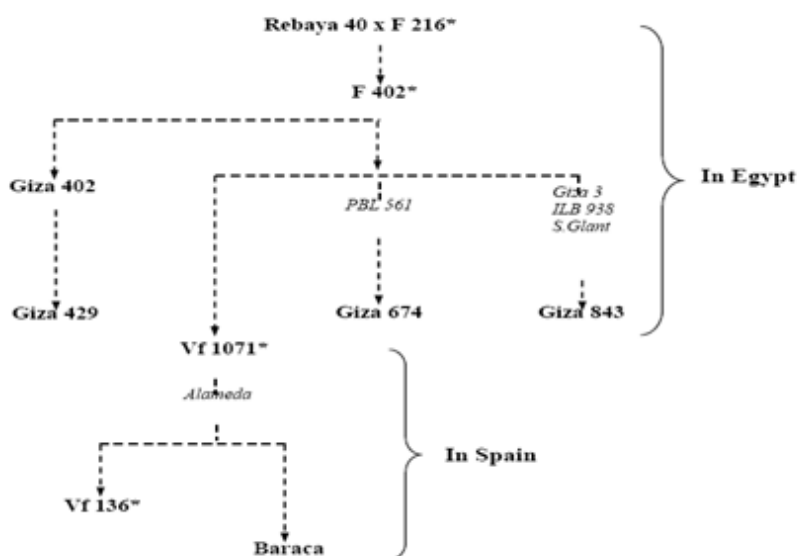


Figure 1 Pedigree showing the origin of *O. crenata* resistance and pedigrees of resistant cultivars/lines (*) in Egypt and Spain. (Alameda: Spanish cultivar, PBL 561: breeding line from ICARDA, Giza 3: Egyptian cultivar, ILB938: Colombian accession, S.Glant: Spani)

resistant parental line for breeding programs in Spain yielding the resistant cultivar Baraka, released in 2002 (Nadel *et al.*, 2004). Fig. 1 summarizes the origin of *O. crenata* resistance in faba bean in Egypt and Spain.

Accurate and rapid methods for screening faba bean lines for resistance to *Orobanche crenata* are critical in assisting breeders in precise selection, thus reducing the number of lines in resistance breeding programs as early as possible.

The best screening method for resistance involves growing the tested material under parasite infestation in pot experiments, where scoring for resistance is performed after carefully washing the roots of the host and counting the successful parasite attachments. Assessing resistance in this form however, is a demanding and time consuming job, with only a limited number of pots that could be examined at a time.

Proposed Solution

An alternative method, Marker Assisted Selection (MAS), circumvents many of these problems. MAS is faster and more accurate because it is not affected by the environment and requires less labor and space, making it possible to screen large numbers of faba bean lines within the laboratory setting. Few published work on using molecular markers in faba bean breeding programs in general could be cited. The work of Vaz Patto *et al.* (1999) is one of the significant studies devoted to the development of a composite map in faba bean. A breakthrough for employing molecular markers to study faba bean resistance to the parasite was the mapping of quantitative trait loci (QTLs) for *O. crenata* resistance in faba bean (Roman *et al.*, 2002). The identified QTLs were based on RAPD markers and screening for resistance was performed in the field, counting the number of spikes of the parasite/plant of the host under infestation of Spanish parasite races.

2. Project Objectives

- To develop a population segregating for *O. crenata* resistance from a cross between a susceptible inbred line and a resistant inbred line having the genes of resistance from Giza 402.
- To test the segregating population for their resistance levels under controlled conditions.
- To screen as many molecular markers as possible for variation between the two parental lines, especially those previously published.
- To use the Bulk Segregant Analysis (BSA) method to identify major genes controlling resistance.
- To employ all possible marker types to identify markers that are linked to *O. crenata* resistance in faba bean.

3. Achievements

3.1 Plant Material and Screening for Resistance

We were able to achieve a total of 220F3 families with plenty of seeds to perform the pot experiments with seeds left over for future work. It is noteworthy that plants had to be grown under insect proof tents (Figure A.1) to avoid the contamination of pollen by bees; flowers had to be tripped to insure a reasonable seed set.

We succeeded in screening all 220F3 families in five replicates, the parental lines and many other different lines as a control for our experiment under the infestation of fixed inoculums of the parasite. Screening for resistance was performed by thoroughly washing roots of the host, counting the number of attacks (Figure A.2 to A.6) and measuring the dry weight of both the host and the parasite.

As shown in Figs. 2 and 3 we obtained quite a good range of segregation among the F3 families for both the number of infections and the faba bean dry weight. This type of information was needed to perform the steps employing the molecular markers.

Today those F3 families are being advanced into recombinant inbred lines for future work.

3.2 Molecular Marker Analysis

DNA extraction from leaf tissues is another time consuming step besides screening for resistance in pot experiments. DNA extraction was extracted from individual plants of the F3 families, the parental lines and control lines.

A total of 330 RAPD, 12 ISSR, six RGAs and 10 SSR markers, either based on previous work on faba bean or screened for the first time, were tested to search for polymorphism between the two parental lines. When polymorphism was detected, the BSA was employed to search for possible genes of major effect for resistance. Bulks were formed from two contrasting groups each composed of 16 individuals from the screened F3 families (resistant and susceptible bulks). None of the tested markers was useful in tagging any major gene for resistance.

A problem we faced during the course of this work was the inconsistency of RAPD results between laboratories (Germany and Egypt) and the difficulty in repeating published results from Spain where almost all the work on *O. crenata* resistance on the molecular level has been conducted (Figure A.7). Another obstacle was that the segregating population we were using is different from the Spanish population that was used in previous work. Consequently, the need for the type of markers that would not vary in results between laboratories and would target the same genomic region even in differ-

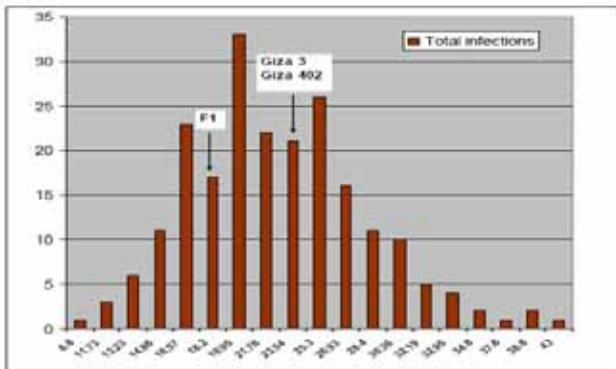


Figure 2 Histogram showing the distribution of the total number of parasite infections of the F3 segregating population (220 lines), the parental lines and the F1 hybrid

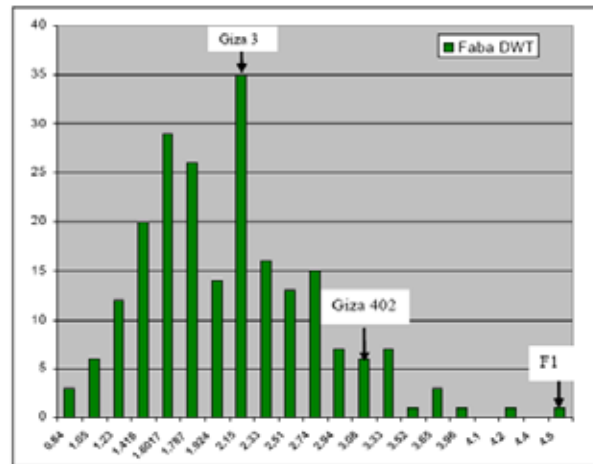


Figure 3 Histogram showing the distribution of faba bean dry weight of the F3 segregating population

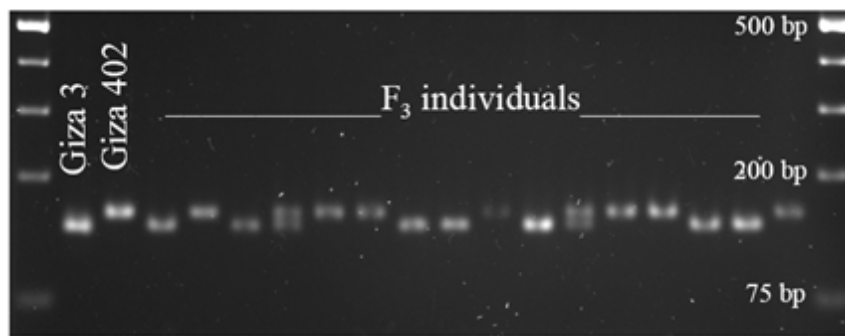


Figure 4 Segregation pattern of marker VfG 9 for 16 F3 individuals and their parental lines Giza 3 and Giza 402

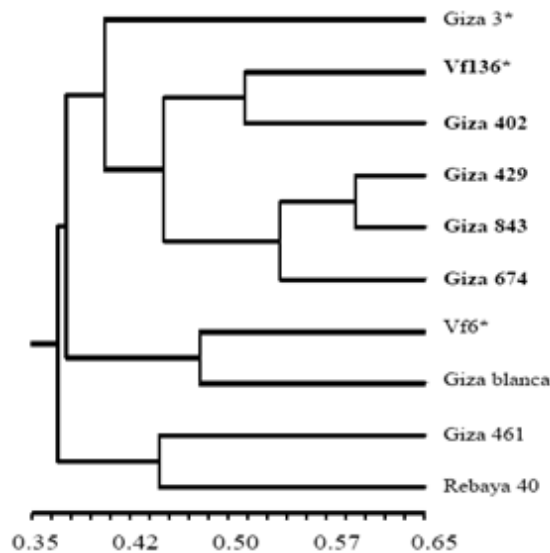


Figure 5 UPGMA dendrogram showing relationships among faba bean cultivars and inbred lines. Orobanche-resistant genotypes are in bold type and asterisks(*) denote inbred lines. Dendrogram based on data from 40 SSR loci

Table 1 Faba bean cultivars and lines tested for SSR amplification and used to construct the dendrogram

| Cultivar | Year of release | Area bred for | Pedigree |
|-------------------------------|-----------------|---|-------------------------------------|
| <i>O. crenata</i> resistant | | | |
| Giza 402 | 1979 | Middle & Upper Egypt | Figure 1 |
| Giza 429 | 1995 | Middle Egypt | Figure 1 |
| Giza 674 | 1995 | Middle & Upper Egypt | Figure 1 |
| Giza 843 | 1998 | North Delta, Egypt | Figure 1 |
| Vf 136 | – | Breeding Line, Spain | Figure 1 |
| <i>O. crenata</i> susceptible | | | |
| Giza 3 | 1979 | Replacement for Giza 1 | Giza 1 X NA 29 (Netherlands) |
| Giza blanca | 1994 | Newly reclaimed areas, Egypt | Selection from Spanish Reina blanca |
| Giza 461 | 1995 | North Delta, Egypt | Giza3xILB938 (ICARDA) 1980s |
| Rebaya 40 | late 1960s | Replacement for Rebaya 8 in Upper Egypt | Landrace |
| Vf6 | – | Breeding line, Spain | Asynaptic breeding line |

ent populations was recognized. The most appropriate type of marker with such features was the Microsatellite marker also known as SSRs. The few available SSR markers for faba bean were tested here in this work and were proven to be useless; after all they were not linked to resistance genes in previous studies and were only developed to chromosome 1 in faba bean.

The use of SSRs has been limited in genetic studies of organisms that lack extensive genomic DNA sequence data like faba bean because isolation and development costs (in terms of labor, time and reagents) are very high compared to other markers such as RAPDs and AFLP. We tested the latest technique for SSR development, known as FIASCO (Fast Isolation by AFLP of Sequences

Containing repeats), proposed by Zane *et al.* (2002) for non plant species. We succeeded in developing 40 *de novo* SSR markers from the resistant line Giza 402. We confirmed the co-dominant nature of 25 SSRs that were polymorphic between parental lines Giza 3 and Giza 402 by observing the banding pattern of their F1 hybrid. The Mendelian inheritance of four of SSRs was also verified by comparing genotypes of 16 individuals from a Giza 3 and Giza 402 segregating population (Fig. 4).

The significance of these SSR markers not only relies on their being the first SSR markers to be developed from the whole faba bean genome (not restricted to a specific chromosome), but also in their amplification across *O. crenata* resistant materials from Egypt and Spain where almost all of the research on *O. crenata* is conducted. Furthermore, the markers amplified across a broad range of germplasm (Table 1), signalling their importance for faba bean breeding programs. Relationships among the ten faba bean genotypes, including both *Orobanche*-susceptible and *Orobanche*-resistant genotypes were tested

by constructing a UPGMA dendrogram (Fig. 5). Results from the dendrogram showed one main cluster that comprised all *Orobanche*-resistant genotypes; *Orobanche*-susceptible genotypes on the other hand were observed in a loose cluster. These results were consistent with the pedigree information since all resistant genotypes, including the Spanish inbred line Vf136 (Cubero, 1991), have a common progenitor, F 402, which was the source of the resistance (Figs. 1 and 5).

4. Forms of Collaboration

The scientific collaboration between the Crop Science Department, Faculty of Agriculture, Alexandria University, resembled in the holder of this project and both the Institute of Plant Breeding, Georg-August-University, Goettingen, Germany and the Institute of Genomic Diversity at Cornell University, USA, did not end at the financial inputs from both foreign institutes, but was rather extended to the collaborative publication of two posters (see Appendix B) and a manuscript in preparation for submitting in the *Theoretical and Applied Genetics* Journal (TAG). Furthermore, abiding by the terms and guide lines of the TAG Journal and the idea of sharing of knowledge, all sequences obtained from this work will be made available to the public domain by placing them in Genbank databases.

Collaboration also continues in the future, where the plant material is being preserved and advanced to reach the stage of Recombinant Inbred Lines (RILS) for future work. Crosses between elite Egyptian and foreign plant material are also taking place on yearly basis to open doors for future research.

5. Conclusions

After two years of starting this project and an extremely broad and diverse level of cooperation between scientists and institutes in three different continents we were able to conclude the following:

1. The issue of resistance of *O. crenata* to faba bean is a very hard problem to tackle, especially since the host and parasite are both of plant nature. The resistance is quantitative (controlled by many genes) as shown in the transgressive segregation at the F3 level. The issue of how to define resistance per se is challenging. We have decided to take the number of parasites on the roots of the host and their growth stage as an indicator for resistance, provided that the host plant stays healthy.
2. We have succeeded in preparing an excellent plant material for marker assisted selection in faba bean especially for resistance to *O. crenata*.
3. The use of molecular markers is a very efficient tool provided that the correct type of marker is applied. Here the use of RGAs was expected to be of great success as it was in many other crops, however, our results have shown that with the available knowledge on this matter, for leguminous crops in general and for faba bean as a special case, it is much lagging as compared to cereals. Faba bean poses a challenge for scientists because of its huge genome (1C mean = 20.36 pg) making it larger than in most diploid plants. RPAD markers, although widely used in

developing countries, because of their low cost/sample and the minimal equipment needed (a PCR machine), are not the best choice especially when more than one laboratory is involved in a project.

4. The method employed to develop the SSR markers is very efficient and although it was not designed for plants, our results have shown that the method fits very well to plants too.
5. The development of the set of SSR markers from the DNA of the *O. crenata* resistant line presented in this work is by far a great step, not only towards improving studies on faba bean that are related to *O. crenata* resistance, but also towards improving many aspects related to molecular studies on that crop because of their reproducibility and how they are applicable to a diverse group of genotypes.

6. Recommendations

To reliably identify markers linked to *O. crenata* resistance in faba bean, more SSR markers should be produced before the quantitative trait loci work is launched. These SSRs are currently in the pipeline. Further collaboration with other institutes is a must to achieve this goal.

Appendix B. Poster Presentations

Abstract of a poster presented at the BioVision 2006, The New Life Sciences Ethics, Patents and the Poor, 26–29 April, Alexandria, Egypt.

Appendix A. Plant Material and Screening for Resistance



Figure 1 Screening of 220 F3 families for *O. crenata* resistance



Figure 2 Growth of the parasite on the roots of the faba bean plant



Figure 3 Viewing the infection under the soil surface



Figure 4 Separation and counting of the infection from the roots of the host plant



Figure 5 Infections on a susceptible host



Figure 6 Infections on a resistant host

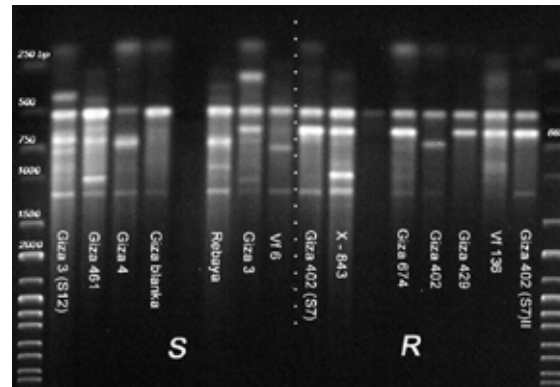


Figure 7 The banding pattern of RAPD analysis for eight resistant and eight susceptible genotypes tested using the primer U9. The arrow shows the band linked to a QTL for resistance on the resistant parent Vf136 as indicated by Roman (personal communication)

Quest for *Orobanche Crenata* Resistance Genes in Faba Bean

| | |
|-------------------|--|
| Mahmoud Zeid | Crop Science Department, Faculty of Agriculture, Alexandria, Egypt. |
| Abdel-Halim Ghazy | Plant Pathology Institute, Department of Seed Pathology, Agricultural Research Institute, Alexandria, Egypt. |
| Wolfgang Link | Institute of Agronomy and Plant Breeding, Georg-August- University, Goettingen, Germany. |

The parasitic weed *O. crenata* is a serious problem for agricultural production in the whole Mediterranean basin. Large areas planted with faba bean are infested by the parasite causing great losses annually. Farmers are forced to abandon the cultivation of faba bean, which reflects negatively on the production of vegetable proteins and increases costs of nitrogen fertilization. Breeding for *O. crenata* resistance in Egypt has successfully identified the only available source of resistance in faba bean; the line F402. Since then, breeding programs have yielded many resistant cultivars (Giza 402, Giza 429 and X-843) in Egypt and (Baraka) in Spain. Assessing resistance however, is very demanding and involves many laborious scoring procedures. Molecular markers can, once genes for resistance are tagged, facilitate the identification and selection of resistant material early in the breeding program and are environment independent. Because all resistant cultivars have their genes of resistance inherited from the same parental cultivar Giza 402, we tested the hypothesis that resistant genotypes inherited certain markers linked to resistance from their common resistant parent. Molecular markers from 330 RAPD (Randomly Amplified Polymorphic DNA), 12 ISSR (Inter-Simple-Sequence Repeat) primers, and six RGAs (Resistance Gene Analogues) primer pairs were employed to search for contrasting markers among four resistant and four susceptible genotypes. A single band of the primer (OP-U9), previously mapped close to a QTL for resistance to *O. crenata* (Roman *et al.*, 2002) appeared to be marking almost all resistant genotypes. Ongoing work involves screening the genotypes employed in pot experiments for resistance to confirm their resistance susceptibility and validate the usefulness of the marker for future work. Results shall be illustrated by a chart for the pedigree of the tested genotypes, a picture showing RAPD products and a cluster analysis.

Abstract of a poster presented at the Post doctoral research day at Cornell University, NY, USA on the 5th of April 2007.

Development of SSR Markers in Faba Bean

Zeid, M1., M. Carter¹, S. Mitchell¹, W. Link², T. Fulton¹, S. Kresovich¹

1. Institute for Genomic Diversity, Cornell University, US.

2. Georg-August- University, Goettingen, Germany.

Vicia faba L. (faba bean) is a legume crop planted for human consumption, as a source of plant protein, in North Africa, Ethiopia, and China and mostly as stockfeed in Europe and recently in Australia. The plant is a diploid ($2n = 2x = 12$) and its few and large chromosomes make it one of the cytogenetically best characterized plant species. The amount of DNA per nucleus ($1C_{mean} = 20.36$ pg) is more than most diploid crop plants, thus posing a challenge for nuclear DNA studies. All mapping studies published to date rely mainly on RAPDs, in addition to a few isozymes, RFLPs and only four SSR markers that are specific to chromosome 1. In a recent study, EST-SSR markers from *Medicago truncatula*, widely accepted as a model legume, showed no size polymorphism among the tested faba bean genotypes, although 40% of the 242 SSRs assayed cross amplified products in faba bean. The need for co-dominant markers that are PCR based, reliable and transferable across populations is crucial if improvement in this crop is to be realized. We used the FIASCO (Fast Isolation by AFLP of Sequences containing repeats) technique to develop 89 primer pairs flanking repetitive motifs, forty-one of which were polymorphic and were inherited in a Mendelian fashion. Markers were used to construct a dendrogram showing the genetic relationships between a number of Egyptian faba bean cultivars bred for resistance to the parasitic weed *O. crenata* and genotypes used in resistance susceptibility studies in Egypt and Spain.

References

1. Cubero, J. I. (1984). Parasitic Diseases in *Vicia faba* with Special Reference to Broomrape (*Orobanche crenata* Forsk.) p. 493-521. In P.D. Hebblethwaite (ed.) *The Faba Bean (Vicia Faba L.)*, Butterworths, London.
2. Cubero, J.I. (1991). Breeding for Resistance to *Orobanche* Species: A Review. In K.Wegmann and L.J. Musselman (eds), *Progress in Orobanche Research*, Eberhard-Karls-Universitaet, Tubingen, FRG, p. 257–277.
3. Cubero, J.I., A.H. Pieterse, S.A. Khalil and J. Sauerborn (1994). Screening Techniques and Sources of Resistance to Parasitic Angiosperms. *Euphytica* 73: 51–58. FAO, 2005. Food and Agriculture Organization. Production year book, Rome, Italy.
4. Khalil, S.A., H.A. Saber, M.H. El-Sherbeeney, M.M. El-Hady, and S.R. Saleeb (1994). Present State of *Orobanche* Resistance Breeding in Faba Bean in Egypt. In: A.H. Pieterse, J.A.C. Verkleij and S.J.ter Borg (eds) *Biology and Management of Orobanche*. Proc. 3rd Inter. Workshop on *Orobanche* and related *Striga* research. Amsterdam, Royal Tropical Institute, the Netherlands, 455–464.
5. Linke, K.H., and M.C. Saxena (1991). Study on Viability and Longevity of *Orobanche* Seed under Laboratory Conditions. In: K. Wegmann and L.J. Musselman (eds) Proc. of the Int. Workshop on *Orobanche* research Obermarchtal, FRG, 110–114.
6. Nadel, S. M.T. Moreno, and J.I. Cubero. 2004. Registration of Baraca Faba Bean. *Crop Sci.* 44:1864–1865.
7. Nassib, A.M., A.A. Ibrahim, and H.A. Saber. (1979). Broomrape (*Orobanche crenata*) Resistance in Broad Beans: Breeding Work in Egypt. In: G. Hawtin and G.C. Chancellor (eds) *Food Legume Improvement and Development*. Proc. of a workshop held at the University of Aleppo, Syria, 133–135.
8. Parker, C. (1994). The Present State of the *Orobanche* Problem. In: A.H. Pieterse, J.A.C. Verkleij and S.J. Ter Borg (eds) *Biology and Management of Orobanche*. Proc. 3rd Inter. Workshop on *Orobanche* and related *Striga* research. Amsterdam, Royal Tropical Institute, the Netherlands, 17–26
9. Roman, B., A.M. Torres, D. Rubiales, J.I. Cubero, and Z. Satovic (2002).
10. Mapping of Quantitative Trait Loci Controlling Broomrape (*Orobanche crenata*)
11. Forsk.) Resistance in Faba Bean (*Vicia faba* L.) *Genome* 45(6): 1057–1063.
12. Saber, H.A., M.A. Omar, M.M. El-Hady, S.A. Mahmoud, N.M. Abou-Zeid and M.M. Radi. Performance of a Newly Bred Faba Bean Line (X-843)
13. Resistant to *Orobanche* in Egypt. (1999). In: J. Kroschel, M. Abderabihi, H. Betz (eds.), *Advances in Parasitic Weed Control at On-farm Level*.
14. Vol.II. Joint Action to Control *Orobanche* in the WANA Region. Magraf Verlag, Weikersheim, Germany, 227–237.
15. Vaz Patto, M.C., A.M. Torres, A. Koblizkova, J. Macas, J.I. Cubero (1999). Development of a Genetic Composite Map of *Vicia faba* Using F2 Populations Derived from Trisomic Plants. *Theor. Appl.Genet.* 98: 736–743.
16. Zane L., L. Bargelloni and T. Patarnello (2002). Strategies for Microsatellite Isolation: A Review. *Molecular Ecology* 11:1–16.



Mona Ahmed Hussein

Associate Professor of Entomology and Nematology, Center of Excellence for Advanced Sciences (CEAS), National Research Center, Cairo. She obtained her Master's scholarship from New Mexico State University, New Mexico, USA (1993–1995).

Her Master's thesis was entitled General Survey for Phytophagous Insects Attacking Snakeweed with Emphasis on the Bud, Flower and Seedfeeding Weevil *Anthonomus Tenius* Fall (Coleoptera: Curculionidae). In (2004), she obtained her PhD in Entomology with an emphasis on Utilization of Entomopathogenic Nematodes for the Biological Control of Some Lepidopterous Pest. The same year she was nominated and won the BA/CSSP Research Grant to continue her research on *Optimization of Mass Production of Entomopathogenic Nematodes*.

Member of several scientific and social organizations such as the Organization of Nematologist of Tropical America (ONTA), USA; Entomological Society of America (ESA), USA; Sam Steel Society, New Mexico, USA; Association of Egyptian American Scholars (AEAS), USA; Arab Society for Plant Protection (ASPP); Egyptian Society of Nematologists, (ESN); Egyptian Society of Biological Pest Control and an effective member of Society for Women in Science in Developing Countries (SWSDC).

She was rewarded the *Innovation Award* from the European Union EU-Research and Development Innovations RDI-Program in association with Heliopolis Academy (2009). Nematology and Biological Control Consultant for SEKEM Group for Development (2009–present).

Optimization of Mass Production Entomopathogenic Nematodes (EPN's) in Egypt

Mona Ahmed Hussein

Center of Excellence for Advanced Science (CEAS), National Research Center, Cairo, Egypt

1. Project Background

Entomopathogenic Nematodes (EPN) have many qualities that make them highly effective biological agents and excellent alternatives to chemical pesticides. EPN carry symbiotic bacteria in their lumen, which are responsible for killing the target host. The bacteria provide antibiotic protection against contaminants as well as nutrients and enable the nematodes to reproduce within the insect cadaver. These bacteria are found in two phases, primary and secondary. Only the primary phase supports the nematode development. Nematodes feed upon the bacterial cells and the host tissue, mature, mate and produce progeny, which emerge from the cadaver as infective juveniles carrying the bacteria, in search for new hosts. Infective stages of the EPN search for an insect host in the soil, penetrate the insect, move into the haemocoel, and release the bacteria, which they carry in their intestinal lumen. The bacteria start multiplying and kill the host, supported by excretion products of the nematode. Phase variation factors, which are characterized as phase 1 and phase 2 or, primary and secondary forms, play an important role for nematode reproduction and virulence.

The project will focus on production, storage and applied technology. It will study mass production and factors affecting in vivo or in vitro production. In addition, the project will focus on developing the technology and expertise required for the commercial use of entomopathogenic nematodes as bioinsecticides.

2. Project Objectives

1. Increasing the EPN strains by isolation and identification of the new strains from soil samples containing EPNs through making field visits to many places in Egypt.
2. Improving in vivo production of EPN through:
 - a. Improving rearing method of the natural host *G. mellonella* through changing the ingredients of semi artificial diet using cheap, locally available components as side products of sugar industry as fodder yeast and molasses.
 - b. Improving rearing procedures of the nematodes on *G. mellonella* larvae by using locally available materials, and easier procedures for inoculation, extraction and purification of the yielded nematodes.
3. Improving in vitro production of EPN through:
 - a. Depending on bedding technique of solid media production, the project will improve the aeration method of bedding flasks and the components of ingredients used in culturing the nematodes and the symbiotic bacteria. Such ingredients include: (Soya flour, wheat flour, yeast extract, egg yolk, fat and distilled water).
 - b. Optimizing quantity of medium per flask (inoculum size).
 - c. Optimizing conditions that affect growth of both nematodes and bacteria.
 - d. Suitability of local nematode species and strains for the modified culturing conditions.
5. Improving the shelf-life of produced biopesticide through:
 - a. Optimization of formulations used in storage and transportation.
 - b. Using locally available materials for formulation of the biopesticides and facilitation of agriculture.

3. Project Findings and Conclusions

1. Many new isolates and new species of EPN were isolated from Egypt through this find.
2. Some of these new isolates were found to be superior to the current strain of nematodes in their capacity to infect different pests.
3. Reducing costs of in vivo production of EPN.
4. Improving rearing procedures of the nematodes on *G. mellonella* larvae.
5. Improving in vitro production of EPN on solid culture.
6. Optimization of inoculum size per flask.
7. Optimization of growth condition for nematodes and bacteria.
8. Selection of suitable strains for mass propagation.
9. Selection of suitable formulation for the new Egyptian strains.
10. Improving shelf-life of EPN.
11. The project explained methods for the large scale production, harvesting and formulation of entomopathogenic nematodes.

4. Discussion

Result 1. Isolation of EPN

101 soil samples were collected from 6 governorates: Sinai, Fayoum, Behira, Sharkia, Bahria Oasis; Giza and Beni Swaif. The nematodes were isolated according to Woodring and Kaya (1988) and Kaya and Styock (1997) techniques.

Six samples were positive. Three new strains of nematodes recovered from soil samples and went through identification process. Two strains (BA1 and BAA2) belonging to heterorhabtid nematodes and (BA2) to steinernematids were selected to be identified. Another new species was isolated from Belpas, Sharkia gover-

norate and went through molecular and morphological identification. This species coded MH and it is going through publication process.

Result 2. Identification of EPN

Based upon the morphometric characters and cross-breeding tests, BA1 and AA2 were identified as two different strains of *Heterorhabditis bacteriophora*, whereas BA2 was identified as *Steinernema carpocapsae*. The new species coded MH were identified as *Heterorhabditis baujardi*. The tables 1, 2, 3, 4, 5 and 6 present the data obtained. The productivity of these strains was assessed and it ranged between 62.000 and 100.000 infective juveniles/larva.

Table 1 Comparative measurements of infective juveniles of the Egyptian isolates of *Heterorhabditis bacteriophora* and *Steinernema carpocapsae* and those of the original description

| Character | Heterorhabditis bacteriophora | | | Steinernema carpocapsae | |
|-----------------------|-------------------------------|-----------|------------------|-------------------------|------------------|
| | Egyptian | | Original | Egyptian | Original |
| | BAA1 | BA1 | HB | BA2 | All |
| Body length | d560±40.6 | 624±36.7 | 588 (512-671) | 594±28.6 | 558 (438-650) |
| Maximum body diameter | 20±2.7 | 20±2.1 | 23 (18-31) | 25±3.2 | 25 (20-30) |
| ^a EP | 88±4.8 | 100±6.3 | 103 (87-110) | 36±4.5 | 38 (30-56) |
| ^b NR | 76±3.3 | 82±2.8 | 85 (72-93) | 78±6.2 | 85 (76-99) |
| ^c ES | 100±12.6 | 112±7.4 | 125 (100-139) | 106±12.7 | 120 (103-190) |
| Tail length | 86±5.3 | 90±2.8 | 98(83-112) | 54±4.3 | 53 (47-59) |
| Ratio A | 26.1±0.7 | 26.4±0.9 | 25 (17-30) | 23.7±2.1 | 21 (19-24) |
| Ratio B | 4.5±0.8 | 4.3±0.6 | 4.5 (4-5.1) | 5.2±0.4 | 4.4 (4-4.8) |
| Ratio C | 5.7±0.5 | 6.2±0.3 | 6.2 (5.5-7) | 11.1±0.4 | 10 (9.1-11.2) |
| Ratio D | 0.78±0.07 | 0.91±0.04 | 0.84 (0.76-0.92) | 0.26±0.02 | 0.26 (0.23-0.28) |
| Ratio E | 1.02±0.04 | 1.2±0.1 | 1.12 (1.03-1.3) | 0.65±0.06 | 0.60 (0.54-0.66) |
| Ratio F | 0.23±0.03 | 0.23±0.02 | 0.25 (0.22-0.36) | 0.44±0.04 | 0.47 (0.43-0.51) |

^aEP, distance from anterior end to excretory pore; ^bNR, distance from anterior end to nerve ring; ^cES, distance from anterior end to the base of esophagus; ^dMeans ± SD and range in µm, n = 20

$$\text{Ratio A} = \frac{\text{Body length}}{\text{Body diameter}}$$

$$\text{Ratio B} = \frac{\text{Body length}}{\text{ES}}$$

$$\text{Ratio C} = \frac{\text{Body length}}{\text{Tail length}}$$

$$\text{Ratio D} = \frac{\text{EP}}{\text{ES}}$$

$$\text{Ratio E} = \frac{\text{EP}}{\text{Tail length}}$$

$$\text{Ratio F} = \frac{\text{Body diameter}}{\text{Tail length}}$$

Table 2 Comparative measurements of the hermaphroditic and amphimictic females of the Egyptian and original populations of *Heterorhabditis bacteriophora*

| Character | First generation (Hermaphroditic female) | | | Second generation (Amphimictic female) | | |
|---------------------|---|----------|---------------------|---|----------|---------------------|
| | BAA1 | BA1 | Original HB | BAA1 | BA1 | Original HB |
| Total body length | 3840±520 | 4160±470 | 4030 (3630–4390) | 2880±420 | 3190±330 | 3500 (3180–3850) |
| Greatest body width | 180±22 | 210±15 | 165 (160–180) | 160±22 | 172±15 | 190 (160–220) |
| Length of stoma | 6.6±2.9 | 7.8±1.7 | 8 (6–9) | 6.1±0.8 | 7.3±1.2 | 7 (6–9) |
| Width of stoma | 10.2±0.8 | 8.1±1.0 | 8 (6–9) | 8.3±1.2 | 8.4±1.4 | 7 (6–9) |
| *aEP | 196±7.3 | 210±5.6 | 209 (189–217) | 184±6.1 | 191±4.7 | 192 (174–214) |
| *bNR | 126±2.1 | 132±3.1 | 126 (121–130) | 98±5.8 | 102±6.3 | 103 (93–118) |
| *cES | 186±5.4 | 200±4.2 | 197 (189–205) | 156±7.3 | 160±4.8 | 168 (155–183) |
| % Vulva | 44.8±2.7 | 47.0±3.3 | 44 (41–47) | 42.6±2.2 | 47.2±3.1 | 47 (42–53) |
| Tail length | 83±5.5 | 86±3.4 | 90 (81–93) | 76±6.2 | 83±5.5 | 82 (71–93) |
| Width at anus level | 48.4±3.8 | 50.6±2.8 | 46 (40–53) | 22.6±2.8 | 27.3±3.4 | 28 (22–31) |
| Anal Swelling | 3.7±0.4 | 4.1±0.3 |** | 1.7±0.3 | 2.4±0.4 |** |

*See footnote in Table 1. **These measurements were not recorded in the original description

Table 3 Comparative measurements between normal and giant females of the first generation and the second generation of the Egyptian and original population of *Steinernema carpocapsae*

| Character | First generation | | | Second generation | | |
|---------------------|------------------|------------|------------------------|---------------------|-----------|---------------------|
| | N. females | G. females | Original N. females | Original G. females | BA2 | Original |
| Total body length | 3620±220 | 8320±670 | 510670 (9560–17400) |** | 2840±360 | 12550 (750–4600) |
| Greatest body width | 180±17.6 | 260±45 | 351 (225–410) | | 156±12.6 | 3146 (58–216) |
| Length of stoma | 5.6±0.3 | 9.2±2.2 | 10 (5–10) | | 6.4±0.7 | 6 (3–9) |
| Width of stoma | 8.7±0.8 | 12.6±1.4 | 12 (10–14) | | 8.1±1.3 | 7 (6–10) |
| *aEP | 63.4±6.2 | 86±7.3 | 122 (88–157) | | 58.6±10.8 | 70 (55–96) |
| *bNR | 158±16.4 | 220±13.8 | 245 (213–275) | | 136±14.4 | 159 (125–183) |
| *cES | 181±37 | 260±64.5 | 306 (226–385) | | 162±22.3 | 200 (157–262) |
| % Vulva | 49.6±4.2 | 55.4±2.7 | 56 (50–57) | | 51.3±2.6 | 55 (52–58) |
| Tail length | 59.4±4.8 | 71.7±5.6 | 68 (53–81) | | 48.7±6.1 | 39 (28–47) |
| Width at anus level | 70.4±8.2 | 140±12.8 | 115 (97–115) | | 47.4±4.2 | 58 (4–77) |
| Anal Swelling | 6.5±0.4 | 9.2±0.8 | | | 6.2±0.6 | |

*See footnote in Table 1. N. females = Normal females, G. females = Giant females

Table 4 Comparative measurements of adult males of the Egyptian isolate and the original population of *Steinernema carpocapsae*

| Character | Males of <i>Steinernema carpocapsae</i> | | | |
|-----------------------------|---|------------------|----------------|-----------------|
| | 1st Generation | | 2nd Generation | |
| | BA2 | Original | BA2 | Original |
| Body length | 1640±111 | 1730 (1500–2750) | 1280±76 | 1130 (720–1580) |
| Greatest width | 128±34 | 136 (80–235) | 62.6±11.4 | 58 (43–61) |
| Length of stoma | 5.8±0.9 | 6 (4–7) | 4.7±0.6 | 5 (3–8) |
| Width of stoma | 6.1±0.42 | 4 (3–7) | 6.4±1.2 | 6 (3–8) |
| *aEP | 68.5±10.4 | 82 (61–108) | 56.7±4.8 | 39 (32–43) |
| *bNR | 148.6±17.3 | 178 (134–190) | 107±12.6 | 105 (85–116) |
| *cES | 178.5±15.4 | 190 (170–200) | 157.4±14.2 | 142 (131–156) |
| Tail length | 38.8±4.4 | 47 (36–50) | 27.5±2.6 | 35 (27–42) |
| Length reflection of testis | 660.7±62.3 | 721 (414–967) | 570.6±42.8 | 589 (350–946) |
| Width of cloaca | 52.6±3.6 | 51 (46–55) | 41.7±4.8 | 44 (34–47) |
| Length of spicule | 69.7±6.5 | 85 (69–93) | 61.3±5.2 | 66 (55–73) |
| Width of spicules | 11.4±1.1 | | 9.7±0.8 | |
| Length of gubernaculum | 52.4±4.3 | 52 (46–57) | 43.2±2.7 | 45 (39–50) |
| Width of gubernaculum | 4.9±0.8 | | 4.2±0.3 | |

*See footnote in Table 1. 1st Generation = First generation, 2nd Generation = Second generation

Table 5 Comparative measurements of adult males of the Egyptian isolates and the original population of *Heterorhabditis bacteriophora*

| Character | Males of <i>Heterorhabditis bacteriophora</i> | | |
|-----------------------------|---|----------|---------------|
| | BAA1 | BA1 | Original |
| Body length | 690±48 | 726±39 | 820 (780–960) |
| Greatest width | 40.8±2.7 | 41.4±3.4 | 43 (38–46) |
| Length of stoma | 4.3±1.1 | 4.8±1.2 | 3 (2–4) |
| Width of stoma | 5.6±1.2 | 6.2±1.0 | 2 (1–3) |
| *aEP | 126±5.4 | 130±3.1 | 121 (114–130) |
| *bNR | 75.4±3.7 | 79.1±4.4 | 72 (65–81) |
| *cES | 102±3.8 | 108±2.6 | 103 (99–105) |
| Tail length | 31.7±4.2 | 33.5±3.7 | 28 (22–36) |
| Length reflection of testis | 73.4±8.2 | 82.8±5.5 | 79 (59–87) |
| Width of cloaca | 23.4±3.2 | 24±2.6 | 23 (22–25) |
| Length of spicule | 39.6±3.1 | 41.5±3.3 | 40 (36–44) |
| Width of spicules | 4.7±0.8 | 5.2±0.6 | |
| Length of gubernaculum | 21.8±2.1 | 23±1.3 | 20 (18–25) |
| Width of gubernaculum | 1.2±0.2 | 1.4±0.2 | |

*See Footnote in Table 1.

Table 6 Results of cross-breeding experiments between *H. bacteriophora* (H.bac) and (H.ind.) or *H. maralata* (H.m) with the isolates from Egypt (BA1 and BAA1), and between *Steinernema carpocapsae* (All) and the Egyptian isolate (BA2)

| Female | Male | | | | | | |
|---------|------|------|---------|---------|---------|-----|------|
| | BA1 | BAA1 | H. bac. | H. ind. | H. mar. | BA2 | S.c. |
| BA1 | F2 | F1 | F2 | - | - | _* | _* |
| BAA1 | F1 | F2 | F2 | - | - | _* | _* |
| H. bac. | F2 | F2 | F2 | - | - | _* | _* |
| H. ind. | - | - | - | F2 | - | _* | _* |
| H. mar. | - | - | - | - | F2 | _* | _* |
| BA2 | _* | _* | _* | _* | _* | F2 | F2 |
| S.c. | _* | _* | _* | _* | _* | F2 | F2 |

BA1, BAA1 and BA2: the tested isolates *H. bac.* = *Heterorhabditis bacteriophora*,
H. ind. = *H. indica*, *H. mar.* = *H. maralata* and *S.c.* = *Steinernema carpocapsae*

Table 7 List of the insect pests used to measure the virulence of the Egyptian isolates of *Entomopathogenic nematodes*, *Heterorhabditis bacteriophora* BA1 and *Steinernema bacteriophora* BA2

| Pest | Latin name | Taxonomy | | Tested larval instar | Host Crops |
|--------------------------|------------------------------|-------------|--------------|------------------------------------|-----------------------------|
| | | Order | Family | | |
| Greater Wax moth | <i>Galleria mellonella</i> | Lepidoptera | Pyralidae | 5 th | Stored Wax Comb |
| Cotton Leaf worm | <i>Spodoptera littoralis</i> | | Noctuidae | 5 th | Cotton and Vegetables |
| Cut worm | <i>Agrotis ipsilon</i> | | Noctuidae | 4 th | Cotton, Corn and Vegetables |
| European corn borer | <i>Osterinia nubilalis</i> | | Pyralidae | 4 th or 5 th | Corn |
| Greater sugar cane borer | <i>Sesamia cretica</i> | | Noctuidae | 4 th or 5 th | Corn and sugar cane |
| Apple tree borer | <i>Zeuzera pyrina</i> | | Pyralidae | 5 th | Apple, peach and Grapes |
| Sugar beet fly | <i>Pegomyia mixta</i> | Diptera | Muscidae | 3 rd | Sugar beet |
| Tortoise beetle | <i>Cassida vittata</i> | Coleoptera | Curculionide | 3 rd | Sugar beet |

Result 3. The virulence of BA1 and BA2 against some insect pests

The EPN BA1 and BA2 were chosen to study the efficiency of two of the new isolated strains against some economically important insect pests. These pests are listed in Table 7 as follows: The greater wax moth larvae, *Galleria mellonella*; the Cotton Leaf worm, *Spodoptera littoralis*; the Cut worm, *Agrotis ipsilon*; the European corn borer, *Osterinia nubilalis*; the Greater sugar cane borer, *Sesamia cretica*; the Apple tree borer, *Zeuzera pyrina*; the Sugar beet fly, *Pegomyia mixta* and the Tortoise beetle, *Cassida vittata*. The virulence of EPN against the melon fruit fly, *Dacus cilatus*; the peach fruit fly, *Bactocera zonata* and the fruit fly, *Ceratitidis capitata* were tested in details. Table 8 shows the virulence of BA1 and BA2 against eight different insect pests. The data are represented as a percentage of mortality.

The European corn borer, *O. nubilalis*, showed high sensitivity to both nematode strains. The mortality percentages recorded for *H. bacteriophora* were 85%, 65% and 45% for the concentrations 1000, 500 and 250 IJ/ml H₂O, respectively. While the percentages were 95%, 75% and 60% for *S. carpocapsae*.

The results also revealed the susceptibility of the greater sugar cane borer larvae, *S. cretica* to infection with EPN. The mortality reached 100% for the concentration 1000 IJ/ml H₂O and recorded 84% and 64% for the concentration 500 and 250 Ij/ml H₂O, respectively for *H. bacteriophora*. BA2 caused 84%, 64% and 52% for the concentration 1000, 500, 250 IJ/ml H₂o, respectively. On the other hand, the apple tree borer larvae, *Z. pyrina*, showed more susceptibility to *S. carpocapsae* than to *H. bacteriophora*. The mortality percentages ranged from 100% to 90% for 1000, 500 and 250 IJ/ml H₂O, and 90%, 75% and 60% for the same concentration, respectively.

Table 8 Mortality of different economically important insect pests treated with two *heterorhabditid* BA1 and *steinernematid* BA2 nematodes at 27°C using filter bioassay

| Insect Host | Nematode Strain | Replicates | Nematode Concentration IJ/ml | % Mortality after | | | | Accumulated Mortality |
|------------------------------|-----------------|------------|------------------------------|-------------------|--------|--------|--------|-----------------------|
| | | | | 24 hrs | 48 hrs | 72 hrs | 96 hrs | |
| <i>Galleria mellonella</i> | <i>H.b.</i> | 30 | 1000 | 50 | 33.33 | 16.66 | 0.00 | 100 |
| | | 30 | 500 | 56.66 | 30 | 10 | 3.33 | 100 |
| | | 30 | 250 | 33.33 | 16.66 | 30 | 10.00 | 90 |
| | <i>S.c.</i> | 30 | 1000 | 16.66 | 53.33 | 0.00 | 0.00 | 100 |
| | | 30 | 500 | 30 | 43.33 | 10 | 6.66 | 90 |
| | | 30 | 250 | 13.33 | 26.66 | 10 | 3.33 | 76.66 |
| <i>Spodoptera littoralis</i> | <i>H.b.</i> | 30 | 1000 | 96.67 | 3.33 | 0.00 | 0.00 | 100 |
| | | 30 | 500 | 90 | 10 | 0.00 | 0.00 | 100 |
| | | 30 | 250 | 70 | 20 | 3.33 | 0.00 | 93.33 |
| | <i>S.c.</i> | 30 | 1000 | 60 | 33.33 | 3.33 | 3.33 | 100 |
| | | 30 | 500 | 40 | 23.33 | 23.33 | 0.00 | 86.66 |
| | | 30 | 250 | 23.33 | 26.66 | 30 | 3.33 | 83.33 |
| <i>Agrotis ipsilon</i> | <i>H.b.</i> | 30 | 1000 | 33.33 | 53.33 | 6.66 | 3.33 | 96.66 |
| | | 30 | 500 | 26.67 | 50 | 6.66 | 3.33 | 86.66 |
| | | 30 | 250 | 20 | 13.33 | 10 | 3.33 | 46.66 |
| | <i>S.c.</i> | 30 | 1000 | 26.66 | 36.33 | 10 | 6.66 | 80 |
| | | 30 | 500 | 30 | 20 | 10 | 3.33 | 63.33 |
| | | 30 | 250 | 13.33 | 23.33 | 6.66 | 3.33 | 46.66 |
| <i>Osterinia nubilalis</i> | <i>H.b.</i> | 20 | 1000 | 25 | 30 | 20 | 10 | 85 |
| | | 20 | 500 | 15 | 35 | 10 | 5 | 65 |
| | | 20 | 250 | 5 | 15 | 20 | 5 | 45 |
| | <i>S.c.</i> | 20 | 1000 | 45 | 35 | 10 | 5 | 95 |
| | | 20 | 500 | 20 | 25 | 20 | 10 | 75 |
| | | 20 | 250 | 15 | 25 | 15 | 5 | 60 |

Data in Table 8 shows that both sugar beet pests are susceptible to the infection with nematodes to a variable extent. The 3rd instar larvae of the sugar beet fly (Leaf miner), *P. mixta*, were more susceptible to steinernematid nematodes than heterorhabditids. The results showed the high sensitivity of sugar beet pests for both nematode strains. This sensitivity varied with different concentrations. For example, the sugar beet fly, *P. mixta*, which is considered as a leaf miner insect was more susceptible to *S. carpocapsae* BA2 than the strain *H. bacteriophora* BA1. Meanwhile, the opposite was true with the tortoise sugar beet beetle, *C. vitatta*, which recorded the highest

mortality when treated with *H. bacteriophora* BA1. The percentage mortality ranged between 100%, 96.66% and 73.33% for BA1; 93.33% and 66.66% for the strain BA2 at concentrations of 1000, 500 and 250 IJ/ml H₂O, respectively. For the melon fruit fly, *Dacus ciliatus*, the nematode *H. bacteriophora* BA1 was compared with four different nematode species against the larvae, pupae and adults of the flies (Table 9).

The tables from 10–13 show the data obtained from this laboratory bioassay.

Screening five species of entomopathogenic *Heterorhabditis* and *Steinernema* nematodes against *D. cili-*

| Insect Host | Nematode Strain | Replicates | Nematode Concentration | | % Mortality after | | | | Accumulated Mortality |
|------------------------|-----------------|------------|------------------------|--------|-------------------|--------|--------|-------|-----------------------|
| | | | IJ/ml | 24 hrs | 48 hrs | 72 hrs | 96 hrs | | |
| <i>Sesamia critica</i> | <i>H.b.</i> | 25 | 1000 | 24 | 60 | 12 | 4 | 100 | |
| | | 25 | 500 | 12 | 32 | 28 | 12 | 84 | |
| | | 25 | 250 | 16 | 20 | 24 | 4 | 64 | |
| | <i>S.c.</i> | 25 | 1000 | 24 | 28 | 12 | 20 | 84 | |
| | | 25 | 500 | 32 | 20 | 8 | 4 | 64 | |
| | | 25 | 250 | 8 | 16 | 12 | 16 | 52 | |
| <i>Zeuzera pyrina</i> | <i>H.b.</i> | 20 | 1000 | 25 | 35 | 25 | 5 | 90 | |
| | | 20 | 500 | 15 | 30 | 20 | 10 | 75 | |
| | | 20 | 250 | 20 | 20 | 15 | 5 | 60 | |
| | <i>S.c.</i> | 20 | 1000 | 45 | 50 | 5 | 0 | 100 | |
| | | 30 | 500 | 40 | 35 | 10 | 5 | 90 | |
| | | 20 | 250 | 15 | 45 | 20 | 5 | 90 | |
| <i>Pegomyia mixta</i> | <i>H.b.</i> | 30 | 1000 | 6.66 | 26.66 | 33.33 | 16.66 | 83.33 | |
| | | 30 | 500 | 0.00 | 16.66 | 50 | 6.66 | 73.33 | |
| | | 30 | 250 | 0.00 | 10 | 26.66 | 23.33 | 60 | |
| | <i>S.c.</i> | 30 | 1000 | 16.66 | 33.33 | 40 | 10 | 100 | |
| | | 30 | 500 | 10 | 33.33 | 46.66 | 3.33 | 93.33 | |
| | | 30 | 250 | 0.00 | 16.66 | 43.33 | 6.66 | 66.66 | |
| <i>Cassida vittata</i> | <i>H.b.</i> | 30 | 1000 | 26.66 | 50 | 23.33 | 0.00 | 100 | |
| | | 30 | 500 | 16.66 | 30 | 23.33 | 26.66 | 96.66 | |
| | | 30 | 250 | 3.33 | 23.33 | 26.66 | 20 | 73.33 | |
| | <i>S.c.</i> | 30 | 1000 | 16.66 | 40 | 26.66 | 10 | 93.33 | |
| | | 30 | 500 | 6.66 | 23.33 | 33.33 | 3.33 | 66.66 | |
| | | 30 | 250 | 0.00 | 26.66 | 30 | 10 | 66.66 | |

atus revealed that *S. feltiae* and *H. bacteriophora* (BA1) produced significant levels of melon fruit fly mortalities in the filter paper assay compared to the others. *S. feltiae* and *H. bacteriophora* were the most promising EPN; however, *S. feltiae* varied greatly in its virulence. No differences were observed between pupae survival and adults emergence. Data showed that *S. feltiae* was the most virulent species towards larvae and pupae followed by *H. bacteriophora* (BA1 and HB), and *S. ab-basi* and *H. indica* in the filter paper assay. The results appear to be comparable with those of Shapiro *et al.*, (1996), who found that nematode virulence is reduced

when added to soil. *H. bacteriophora* was more virulent than *S. feltiae*, as it did not perform as well as in the filter paper assays. Bednarek and Gaugler (1997) found that *S. feltiae* populations actually increased with the addition of soil; which does not support our results.

S. feltiae and *H. bacteriophora* (BA1) could be good biocontrol agents because of their demonstrated activity in our study against other dipterans (Gaugler and Kaya, 1990). With the augmentation of these nematodes in the soil, pupae of *D. ciliatus* will be attacked more; moreover larvae could become infected as they drop onto the ground.

Although Profenofos and Pirimiphos-methyl insecticides caused a higher mortality of the flies compared to EPNs, the latter is considered to be environmentally safe. Data confirmed the potentiality of entomopathogenic nematodes, especially *S. feltiae* followed by *H. bacteriophora* for the biological control of dipterous larvae and pupae. These results are essential for developing an effective pest management program for controlling *D. ciliatus*. Additional research is needed in this field to evaluate the activity of these nematode species against larvae and pupae of melon fruit flies.

Result 4. Virulence of stored infective juveniles against *Galleria mellonella*

The aim of this experiment is to check the effect of long term storage in distilled water on the viability and infectivity of the infective juveniles of the Entomo-

pathogenic nematodes, *Heterorhabditis bacteriophora* BA1 and *Steinernema carpocapsae* BA2.

Materials and Methods

Five ml of nematode suspension, containing approximately 400 IJs/ml were taken in 2 sets, one with distilled water and the other with 0.1% formalin. The suspension was kept in 100 ml conical flasks. Two temperatures levels were chosen to assist the storage ability of *Heterorhabditis bacteriophora* BA1 and *Steinernema carpocapsae* BA2 for 7 weeks.

Survival percentages of infective juveniles were measured at the end of the experiment by counting the live and the dead juveniles. One thousand stored juveniles were used for testing the virulence against larvae of the greater wax moth *Galleria mellonella*. Five replicates were maintained for each temperature regime.

Table 9 List of Entomopathogenic nematodes used, their associated bacteria and their origin

| Nematode | Bacteria | Strain | Geographical origin | Reference |
|-------------------------|---------------------------------|--------|---------------------|-----------------|
| <i>S. abbasi</i> | <i>Xenorhabdus</i> | ABB | Oman | M.S.T. Abass |
| <i>S. feltiae</i> | <i>X. bovenii</i> | NC | Montpellier, France | Noel Boemare |
| <i>H. bacteriophora</i> | <i>Photorhabdus luminescens</i> | BA1 | Egypt | Mona Hussein |
| <i>H. indica</i> | | SAA2 | Egypt | Mona Hussein |
| <i>H. bacteriophora</i> | | HB | Germany | Ralf-Udo Ehlers |

Table 10 Efficiency of five species of Entomopathogenic nematodes on the mortality percentages of 2nd instar of larvae of *D. ciliatus* on filter paper

| Nematode | Concentration | % Larvae mortality at indicated days | | |
|-------------------------------|---------------|--------------------------------------|-----------------|-----------------|
| | | 1 st | 3 rd | 7 th |
| <i>S. abbasi</i> (ABB) | 500 | 20.0 | 80.0 | 100.0 |
| | 1000 | 40.0 | 100.0 | 100.0 |
| <i>S. feltiae</i> (NC) | 500 | 30.0 | 90.0 | 100.0 |
| | 1000 | 50.0 | 100.0 | 100.0 |
| <i>H. bacteriophora</i> (BA1) | 500 | 30.0 | 80.0 | 100.0 |
| | 1000 | 40.0 | 100.0 | 100.0 |
| <i>H. indica</i> (SAA2) | 500 | 20.0 | 80.0 | 100.0 |
| | 1000 | 40.0 | 100.0 | 100.0 |
| <i>H. bacteriophora</i> (HB) | 500 | 20.0 | 70.0 | 100.0 |
| | 1000 | 40.0 | 100.0 | 100.0 |
| Control | | 0.0 | 0.0 | 0.0 |

Table 11 LC₅₀ and LC₉₀ of five species of Entomopathogenic nematodes on larvae and Pupae of *D. ciliatus* on filter paper/Petri dishes

| Nematode | | Larvae | | Pupae | |
|-------------------------------|------------------|-----------------|-----------------|-----------------|-----------------|
| | | 3 rd | 7 th | 3 rd | 7 th |
| <i>S. abbasi</i> (ABB) | LC ₅₀ | 1051.4 | 322.6 | 1833.8 | 716.1 |
| | LC ₉₀ | 6954.8 | 3854.1 | 20010.4 | 8140.1 |
| <i>S. feltiae</i> (NC) | LC ₅₀ | 764.2 | 254.3 | 5400.0 | 586.6 |
| | LC ₉₀ | 1866.6 | 765.2 | 87330.1 | 1548.6 |
| <i>H. bacteriophora</i> (BA1) | LC ₅₀ | 505.6 | 268.6 | 1787.3 | 845.8 |
| | LC ₉₀ | 3773.5 | 1444.1 | 9268.9 | 2874.5 |
| <i>H. indica</i> (SAA2) | LC ₅₀ | 1172.5 | 322.6 | 1895.4 | 859.9 |
| | LC ₉₀ | 6015.6 | 3854.2 | 69297.9 | 6741.1 |
| <i>H. bacteriophora</i> (HB) | LC ₅₀ | 1133.7 | 553.2 | 2140.1 | 1162.6 |
| | LC ₉₀ | 16081.3 | 4930.7 | 16683.6 | 4903.6 |

Table 12 Larval mortality percentages of *D. ciliatus* treated with different species of Entomopathogenic nematodes by dipping application of cucumber fruits

| Nematode | Concentration | % Larval mortality | | |
|-------------------------------|---------------|---------------------|---------------------|---------------------|
| | | 1 st Day | 3 rd Day | 7 th Day |
| <i>S. abbasi</i> (ABB) | 4000 | 20.0 | 40.0 | 60.0 |
| <i>S. feltiae</i> (NC) | 4000 | 50.0 | 66.7 | 80.0 |
| <i>H. bacteriophora</i> (BA1) | 4000 | 40.0 | 57.3 | 73.4 |
| <i>H. indica</i> (SAA2) | 4000 | 30.0 | 43.3 | 60.0 |
| <i>H. bacteriophora</i> (HB) | 4000 | 40.0 | 53.3 | 73.4 |
| Control | | 0.0 | 0.0 | 0.0 |

Table 13 LC₅₀ and LC₉₀ of five species of EPNs on Pupae of melon fruit fly in sand soil

| Nematode | | 3 rd | 7 th |
|-------------------------------|------|-----------------|-----------------|
| <i>S. abbasi</i> (ABB) | LC50 | 987.1 | 900.3 |
| | LC90 | 3812.5 | 1056.4 |
| <i>S. feltiae</i> (NC) | LC50 | 925.3 | 827.7 |
| | LC90 | 3331.2 | 983.5 |
| <i>H. bacteriophora</i> (BA1) | LC50 | 855.4 | 675.6 |
| | LC90 | 7796.3 | 1679.4 |
| <i>H. indica</i> (SAA2) | LC50 | 1467.1 | 787.2 |
| | LC90 | 7564.4 | 4030.9 |
| <i>H. bacteriophora</i> (HB) | LC50 | 1750.4 | 735.1 |
| | LC90 | 11596.8 | 3423.4 |

Table 14 Infectivity of *Heterorhabditis bacteriophora* BA1 and *Steinernema carpocapsae* BA2 infective juveniles stored in distilled water for 7 weeks at two different temperatures

| Nematode Strain | % Infectivity before storage | % Infectivity after 7 weeks | | % Loss in infectivity | |
|--|------------------------------|-----------------------------|------|-----------------------|------|
| | | 10°C | 30°C | 10°C | 30°C |
| <i>Heterorhabditis bacteriophora</i> BA1 | 100 | 85.8 | 66.4 | 14.2 | 33.6 |
| <i>Steinernema carpocapsae</i> BA2 | 100 | 80.3 | 71.7 | 19.7 | 28.3 |

Results

Data in Table 14 shows that the percent of infectivity after 7 weeks of storage in distilled water recorded 85.8% for *H. bacteriophora* BA1 at 10°C. Meanwhile, the viability reached 66.4% at 30°C causing loss in infectivity as 14.2% and 33.6% for the temperatures 10°C and 30°C, respectively. The survival percent of *S. carpocapsae* BA2 reached 80.3% and 71.7% for the temperatures 10°C and 30°C, respectively. The loss in infectivity was 19.7% at temperature 10°C and 28.3% at temperature 30°C. It was noticed that the viability of the stored nematodes was more in distilled water for both tested temperatures.

For the infectivity against *G. mellonella*, it was found that all tested nematodes caused 100% mortality for the wax moth larvae, which means that the storage period of juveniles did not affect their capability to infect host insects. From the above results, it was noticed that the temperature 10°C was better for the storage of *H. bacteriophora* BA1 than for *S. carpocapsae* BA2, and the storage of juveniles in distilled water is better than that in 0.1% formalin.

Result 5. Pathogenicity of the symbiotic bacteria, *Xenorhabdus nematophila* and *Photorhabdus luminecens*

The aim of this experiment is to study the pathogenic effect of the symbiotic bacteria, *Xenorhabdus nematophila* associated with the Entomopathogenic nematode, *Steinernema carpocapsae* and the symbiotic bacteria, *Photorhabdus luminecens*, associated with *Heterorhabditis bacteriophora*.

Three different application methods were used: direct spray feeding, and direct injection of the bacteria cells into the haemolymph of the 3rd instar larvae of the greater wax moth, *Galleria mellonella*.

Materials and Methods Isolation of *X. nematophila* and *P. luminecens*

X. nematophila and *P. luminecens* were obtained from haemolymph of dead *G. mellonella* larvae infected with IJs of *S. carpocapsae* and *Heterorhabditis bacteriophora*. *G. mellonella* larvae were surface sterilised in 70% alcohol for 10 minutes, flamed and allowed to dry in a laminar airflow cabinet. Larvae were opened with sterilised needles, care was taken not to damage the gut, a drop of oozing haemolymph was streaked into nutrient agar and the plates incubated at 28°C in the dark for 24 hours. Single colonies were selected, streaked into nutrient agar and sub-cultured until colonies of uniform size and morphology were obtained. The pathogenicity of these bacterial isolates was confirmed by re-inoculation into *G. mellonella* larvae followed by streaking the haemolymph of the dead larvae into nutrient agar.

Production of bacterial cell suspensions:

A single colony of each bacterium was selected and inoculated into 500 ml of nutrient broth (15 g nutrient broth (BDH) in 500 ml distilled water) in a flask, which was stoppered by sterile cotton wool and placed in a shaking incubator at 150 rpm for 24 hours at 28°C. The concentration of bacterial cells in the broth suspension was determined in a spectrophotometer where the optical density was determined at 600 nm wavelength.

Based on the previous results obtained by pilot experiment, the concentration of cells used in the experiments was adjusted to 8.35×10^3 , 4.17×10^3 , 2.08×10^3 , 1.04×10^3 and 0.52×10^3 cells/ml⁻¹ for *X. nematophila* and adjusted to 5.35×10^3 , 2.67×10^3 , 1.34×10^3 , 0.67×10^3 and 0.33×10^3 with Ringer solution added to dilute the bacterial suspension. All tests were carried out in cups (9×6 cm) lined with double layer of Whatmann no.1 filter paper. After application of the selected method, cups were sealed with parafilm and incubated at 28°C±2°C. Results were checked over 5 day intervals.

Results

Data in Table 15 shows that all different concentrations of direct spray with *X. nematophila* gave reasonable control except for the lowest concentration. 60% mortality in the 3rd instar larvae of *G. mellonella* was recorded 4 days after application of the concentration 8.35×10^3 cells/ml.

When the same bacteria were mixed with the diet of the wax moth larvae (Table 16), also 60% mortality in the larvae was recorded after 5 days of feeding on treated food with the concentrations 8.35×10^3 , 4.17×10^3 and 2.08×10^3 cells/ml. Meanwhile, only 20% mortal-

ity was obtained with the concentration 0.52×10^3 cells ml^{-1} .

In Table 17, when *X. nematophila* cells were injected directly into the haemolymph of the 3rd instar larvae of *G. mellonella*, all insects were dead after only 48 hours of injection. The same results were obtained when *P. luminescens* cells were directly injected into the haemolymph of the 3rd instar larvae of *G. mellonella* (Table 18).

Data in Table 19 shows that feeding the 3rd instar larvae on media treated with five concentrations of the *P. luminescens* recorded 66.6, 60, 46.6 and 13.3 after nine days of application for the concentrations 5.35×10^3 , 2.67×10^3 , 1.34×10^3 and 0.67×10^3 cell ml^{-1} , respectively. However, the direct spray of the bacterial cells on the *Galleria* larvae caused 73.33% mortality for the concentration 5.35×10^3 cell ml^{-1} after 8 days of treatment (Table 20).

Table 15 Effect of direct spray of *Xenorhabdus nematophila* on 3rd larval instars of *Galleria mellonella*

| Concentration (Cell/ml) | Mortality % | | | |
|----------------------------|-------------|-------------|-------------|--------------|
| | 48 hours | 72 hours | 96 hours | 120 hours |
| Control | 0 | 0 | 0 | 0 |
| 8.35×10^3 | 30 | 40 | 60 | 60 |
| 4.17×10^3 | 20 | 40 | 40 | 50 |
| 2.08×10^3 | 30 | 50 | 50 | 60 |
| 1.04×10^3 | 20 | 30 | 40 | 60 |
| 0.52×10^3 | 0 | 0 | 10 | 20 |

Table 17 Effect of different concentrations of *Xenorhabdus nematophila* on 3rd larval instars of *Galleria mellonella* by direct injection into the haemolymph

| Concentration (Cell/ml) | Mortality % | | |
|----------------------------|-------------|----------|----------|
| | 24 hours | 48 hours | 72 hours |
| Control | 0 | 0 | 0 |
| 8.35×10^3 | 100 | 100 | - |
| 4.17×10^3 | 100 | 100 | - |
| 2.08×10^3 | 100 | 100 | - |
| 1.04×10^3 | 80 | 100 | - |
| 0.52×10^3 | 70 | 100 | - |

Table 19 Effect of different concentrations of *Photorhabdus luminescens* on 3rd larval instars of *Galleria mellonella* by direct feeding

| Concentration (Cell/ml) | Mortality % | | |
|----------------------------|-------------|--------|--------|
| | 3 days | 6 days | 9 days |
| Control | 0 | 0 | 0 |
| 5.35×10^3 | 26.6 | 46.6 | 66.6 |
| 2.67×10^3 | 26.6 | 33.3 | 60 |
| 1.34×10^3 | 13.3 | 40 | 46.6 |
| 0.67×10^3 | 0 | 13.3 | 13.3 |
| 0.33×10^3 | 0 | 0 | 13.3 |

From the previous results we can conclude that the performance of the symbiotic bacteria by itself can be enhanced by adding some additives to protect the bacterial cells from environmental effect such as desiccation, UV effect, temperature, etc.

Result 6. Improving in vitro production of EPN on solid culture depending on Wouts and DFA techniques.

Isolation of the *Xenorhabdus* & *Photorhabdus* Bacteria Species

10 last instar larvae of *Galleria mellonella* were infected with about 100 IJ/larva in moist sand (10% RH) in 10 cm Petri dish. After infection (24–48 hours) the dead insect cadavers were washed with 70% alcohol for 5–10 min in a glass staining block. A drop of the insect haemolymph were streaked on NBTA (or McConkey)

Table 16 Effect of *Xenorhabdus nematophila* on 3rd larval instars of *Galleria mellonella* by feeding

| Concentration (Cell/ml) | Mortality % | | | |
|----------------------------|-------------|-------------|-------------|--------------|
| | 48 hours | 72 hours | 96 hours | 120 hours |
| Control | 0 | 0 | 0 | 0 |
| 8.35×10^3 | 0 | 33.3 | 40 | 60 |
| 4.17×10^3 | 0 | 33.3 | 40 | 53.3 |
| 2.08×10^3 | 0 | 40 | 46.6 | 60 |
| 1.04×10^3 | 0 | 0 | 26.6 | 60 |
| 0.52×10^3 | 0 | 0 | 6.6 | 20 |

Table 18 Effect of different concentrations of *Photorhabdus luminescens* on 3rd larval instars of *Galleria mellonella* by direct injection into the haemolymph

| Concentration (Cell/ml) | Mortality % | | |
|----------------------------|-------------|----------|----------|
| | 24 hours | 48 hours | 72 hours |
| Control | 0 | 0 | 0 |
| 5.35×10^3 | 100 | 100 | - |
| 2.67×10^3 | 100 | 100 | - |
| 1.34×10^3 | 100 | 100 | - |
| 0.67×10^3 | 90 | 100 | - |
| 0.33×10^3 | 70 | 100 | - |

Table 20 Effect of direct spray of different concentrations of *Photorhabdus luminescens* on 3rd larval instars of *Galleria mellonella*

| Concentration (Cell/ml) | Mortality % | | | |
|----------------------------|-------------|--------|--------|--------|
| | 2 days | 4 days | 6 days | 8 days |
| Control | 0 | 0 | 0 | 0 |
| 5.35×10^3 | 26.66 | 33.3 | 60 | 73.33 |
| 2.67×10^3 | 13.33 | 20 | 40 | 46.66 |
| 1.34×10^3 | 0 | 20 | 26.66 | 26.66 |
| 0.67×10^3 | 0 | 6.66 | 13.33 | 13.33 |
| 0.33×10^3 | 0 | 0 | 6.66 | 6.66 |

using a sterile loop. After inoculation of plates at 25°C for 48 hours in the dark, a single primary colony was chosen and streaked again on new plates of NBTA or McConkey-Agar.

Preparation of the bacteria stock culture

After 48 hours, single primary colonies were transferred to YS-broth & incubated for 1–2 days at 25°C on an orbital shaker at 200 rpm in the dark; 15% glycerol was added to the culture. After mixing well, culture was transferred in 2ml aliquots into sterile caps and stored at –80°C immediately after filling them. These caps are the stock culture for the in vitro mass propagation of Entomopathogenic nematode.

In Vitro Mass Production of Entomopathogenic Nematodes

Two artificial media were used to mass produce both the Entomopathogenic nematode species *Steinernema carpocapsae* BA2 & *Heterorhabditis bacteriophora* BA1. The first media is Wouts Agar media which consists of 16 gm Bacto® Nutrient broth, 12 gm Bacto® Nutrient agar and 5 gm Corn oil or plant oil in 1 Litre distilled water. The other medium was DFA (Dog Food Agar) which consists of 6.5 gm ground dog food, 1.5 gm peptone, 0.2 gm agar and 100ml phosphate buffer. The infective juveniles (IJ) were surface sterilized with 0.5% Hyamine by washing 3000–4000 IJ for 15 minutes in the hyamine solution and centrifuged for 2 minutes on 3000 rpm followed by several times washing in distilled water. Three replicates of each medium were inoculated with one ml of the specific bacteria (*Xenorhabdus* and *Photorhabdus*) and kept for 24 hours in a dark room. Each plate was inoculated with 3000 IJ and kept for two weeks. Cultures were checked daily for contamination and nematode development.

Results

According to the data obtained, it was noticed that both Wouts and DFA media were suitable for mass propagation of *S. carpocapsae* BA2 and *H. bacteriophora* B1. The infective juveniles yield was apparently variable according to the media and the nematode species.

Wouts medium was obviously better than DFA medium regarding the amount of juveniles produced for both BA1 and BA2. In Wouts plates, the mean number of infective juveniles produced recorded 1.8×10^6 and 4.7×10^6 IJ/Petri dish for BA1 and BA2, respectively. Meanwhile, the mean number of infective juveniles over DFA produced 1.14×10^6 & 0.57×10^6 IJ/Petri dish for BA1 and BA2, respectively.

Although *S. carpocapsae* BA2 were able to propagate on DFA medium supplemented with peptone, its reproductive rate was far lower than that of *H. bacterio-*

phora B1. Therefore, it was assumed that DFA media lacked specific nutrient (s) for *S. carpocapsae* BA2.

All Entomopathogenic nematodes have specific bacteria which proliferate in the host haemocoel and also in artificial media. The nematodes feed these bacteria and reproduce many off-springs.

Therefore, it is possible that the nutrients may be deficient for these bacteria rather than for the nematodes.

Improving in vitro production of EPN on solid culture depending on Bedding technique of solid media production

The effect of culture components on the production of Dauer juveniles was assessed. The media contained 20 g Bacto® nutrient broth (Difco), 10 g Yeast extract (Merck), 260 g sunflower oil, 385 g Soy-flour and 1200 g distilled water mix. Erlenmeyers flasks of 100 ml were filled with 15 g solid medium mixed into 0.8 g foamed polyether polyurethane.

The flasks were inoculated with 2 ml of the two bacterial cultures (BA1 and BA2) in liquid culture and incubated at 25°C for 48 hours prior to nematode inoculation. The cultures were kept 20 days and then the contents of each flask were spread over a sieve of 50 µm mesh size. The sieves were dipped into tap water. Active DJs were collected from the tap water and counted. The highest mean yield per flask was 7.9×10^6 .

Result 7. The suitability of the two Egyptian entomopathogenic nematodes, *Heterorhabditis bacteriophora* BA1 and *Steinernema carpocapsae* BA2 for formulation

Different formulations were surveyed to check the suitable form for longer nematode survival as follows:

1. Sponge
2. Liqua gel
3. Calcium alginate
4. Kaoline clay

The formulations were compared with the water suspension as control. Some adjuvants such as ascorbic acid, citric acid and sorbic acid were added to check their effect on the nematode survival.

It was noticed that the survival in water and sponge formulations is better in low temperature (5–10°C) but only for keeping the species inocula, not for storage for long periods. As the temperature increased, the survival of the nematodes in water decreased. On the other hand, it was noticed that *Ca alginate* formulation was better for nematode storage for longer time than the other formulations, especially in higher temperatures ranging between 12 and 16°C.

When the suitability of the hydrogel as a carrier for the EPN and as a simple and cheap formula was tested, the nematode *Heterorhabditis bacteriophora* BA1 record-

Table 21 Viability of *Heterorhabditis bacteriophora* formulated with hydrogel

| Storage Period | Repl. | Nematodes | | | % Survival |
|----------------|-------|-----------|-------|--------|------------|
| | | Alive | Dead | Total | |
| 10 Days | R1 | 1567.0 | 97.0 | 1664 | 94.2 |
| | R2 | 1358.0 | 87.0 | 1445 | 94.0 |
| | R3 | 1389.0 | 78.0 | 1467 | 94.7 |
| | Mean | 1438.0 | 87.3 | 1525.3 | 94.3 |
| 20 Days | R1 | 1003.0 | 87.0 | 1090 | 92.0 |
| | R2 | 1143.0 | 76.0 | 1219 | 93.8 |
| | R3 | 1221.0 | 58.0 | 1279 | 95.5 |
| | Mean | 1122.3 | 81.5 | 1384.2 | 94.1 |
| 30 Days | R1 | 875.0 | 190.0 | 1065.0 | 82.2 |
| | R2 | 798.0 | 110.0 | 908.0 | 87.9 |
| | R3 | 654.0 | 289.0 | 943.0 | 69.4 |
| | Mean | 775.6667 | 196.3 | 972.0 | 79.8 |
| 40 Days | R1 | 643 | 340 | 983 | 65.4 |
| | R2 | 843 | 59 | 902 | 93.5 |
| | R3 | 459 | 123 | 582 | 78.9 |
| | Mean | 648.3 | 174.0 | 822.3 | 79.2 |
| 50 Days | R1 | 389 | 567 | 956 | 40.7 |
| | R2 | 546 | 453 | 999 | 54.7 |
| | R3 | 761 | 142 | 903 | 84.3 |
| | Mean | 565.3 | 387.3 | 952.7 | 59.9 |

Table 22 Viability of *Steinernema carpocapsae* formulated with hydrogel

| Storage Period | Repl. | Nematodes | | | % Survival |
|----------------|-------|-----------|-------|--------|------------|
| | | Alive | Dead | Total | |
| 10 Days | R1 | 1234.0 | 90.0 | 1324 | 93.2 |
| | R2 | 1134.0 | 77.0 | 1211 | 93.6 |
| | R3 | 1237.0 | 89.0 | 1326 | 93.3 |
| | Mean | 1201.7 | 85.3 | 1287.0 | 93.4 |
| 20 Days | R1 | 988.0 | 67.0 | 1055 | 93.6 |
| | R2 | 1213.0 | 89.0 | 1302 | 93.2 |
| | R3 | 1114.0 | 78.0 | 1192 | 93.5 |
| | Mean | 1160.2 | 82.2 | 1242.4 | 93.4 |
| 30 Days | R1 | 510.0 | 201.0 | 711.0 | 71.7 |
| | R2 | 546.0 | 124.0 | 670.0 | 81.5 |
| | R3 | 603.0 | 315.0 | 918.0 | 65.7 |
| | Mean | 553.0 | 213.3 | 766.3 | 73.0 |
| 40 Days | R1 | 443 | 289 | 732 | 60.5 |
| | R2 | 612 | 323 | 935 | 65.5 |
| | R3 | 356 | 297 | 653 | 54.5 |

ed 94.3% survival percentage after 10 days of storage and decreased gradually with time to reach 59.9% after 50 days. Meanwhile, the Entomopathogenic nematode, *Steinernema carpocapsae* BA2 recorded 93.4% after 10 days and decreased gradually to reach 37.9%. The temperature seemed to be one of the key factors for the success of any formulation. More studies are needed to select better formulae and to improve the shelf-life of the EPN.

5. Selected Publications

In addition to the production of new Egyptian EPN based bioinsecticide, several research papers were extracted from the project. Moreover, two more are in progress from the project data. Most of these papers were published in international scientific journals. Below is the list of the papers published so far from the project.

- Abd El Rhman, R.A. and Mona A. Hussein (2007). Effect of Different Infection Rates in *Galleria mellonella* Larvae on the Quality of the Produced Heterorhabditis Juveniles. Egypt. J. Biol. Pest Control 17(2): 91–97.
- Farag, N.A., Hussein Mona, A. and Hussein, H.M. (2009). Impact of Liquid Agar on the Efficacy of *Steinernema carpocapsae* to Control *Pieris rapae* Infected Cabbage Plantation. J.Plant Protec. (under press). Poland.
- Hussein A., Mona and Nariman AH. Aly (2009). Insecticidal Activity (virulence) and Genetic Characterization of Some Bacterial Isolates of *Xenorhabdus* and *Photorhabdus* Associated with the Entomopathogenic Nematodes. (under press) USA.
- Hussein A. Mona and A. B Abou El- Soud (2006). Isolation and Characterization of Two Heterorhabditids and One Steinernematid nematodes from Egypt. International J. Nematol. Vol. (16) no.1:7-12. United Kingdom.
- Magda A. Mohamed and Mona A. Hussein (2007). Purification and Characterization of an Alkaline Protease Produced by the Bacterium *Xenorhabdus nematophila* BA2, a Symbiont of the Entomopathogenic nematode *Steinernema carpocapsae*. Res. J. of Agri. and Biologic. Sci., 3(5): 510–521. Pakistan.
- Mona A. Hussein, Nabil El-Wakeil and Talaat El-Sebai (2006). Susceptibility of Melon Fruit Fly, *Dacus ciliatus* (Loew) (Diptera: Tephritidae) to Entomopathogenic Nematodes (Rhabditida: Steinernematidae, Heterorhabditidae) and to Insecticide. International J. Nematol. Vol. (16) no.1:13-18. United Kingdom.
- Nabil El-Wakeil and Mona Hussein (2009). Field Performance of Entomopathogenic Nematodes and an Egg Parasitoid for Suppression of Corn Borers in Egypt. Archives of Phytopathology and Plant Protection (41). United Kingdom.
- Saleh, M.M.E, K.A.A. Draz, M.A. Mansour, Mona A. Hussein and M.F.M. Zawrah (2009). Controlling the Sugar Beet Weevil *Cassida vittata* with Entomopathogenic Nematodes. J. Pest sci. (accepted). Germany.

6. Conclusions and Recommendations

6.1 Conclusions

This work was conducted based on a grant from the Center for Special Studies and Programs (CSSP), Bibliotheca Alexandrina. The main target of this project was to optimize the mass production of the entomopathogenic nematodes (EPNs) as bioinsecticides.

Entomopathogenic nematodes (EPN) of the families *Steinernematidae* Travassos, 1927 and *Heterorhabditidae* Poinar, 1967 have been used as biopesticides for controlling insect pests in niche markets (Bedding, 1998). The need for more effective EPN for controlling insect pests and more new EPN symbiotic bacteria for developing bioactive by-products for various purposes, such as obtaining novel insecticidal toxin genes for developing transgenic insect-resistance crops or antimicrobial substances as agro- or medical-pharmaceuticals, etc. (Webster, 2002), has stimulated efforts on EPN survey worldwide, which resulted in the recovery of many new EPN species.

Indigenous EPN may become more suitable for inundative release against local insect pests because of adaptation to local climate and other population regulators. In addition, many countries are concerned about the introduction of exotic Entomopathogenic nematodes because they may have negative impact on non-target.

A general survey for these pathogens was conducted during 2005 to cover different geographical and climatic areas in Egypt. Seven out of 102 soil samples were positive for EPNs. Three samples were completely identified to the species level and designated as BA1, BAA2 and BA2. Another new species was identified as MH; and now has an accession number in the Gene Bank under the name of Nariman, AH and Mona, AH.

The two EPNs, *Heterorhabditis bacteriophora* BA1 and *Steinernema carpocapsae* BA2 were chosen to scale up in vivo and in vitro cultures of nematode for the first time in Egypt. The associated bacteria of both species were isolated and propagated on selected media. The bacteria were identified using the Polymerase Chain Reaction (PCR) and identified as *Photorhabdus luminescens* and *Xenorhabdus nematophilus* for the nematodes *Heterorhabditis bacteriophora* BA1 and *Steinernema carpocapsae* BA2, respectively. Both the phenotypic

and chemical characterizations of the bacteria were studied. Moreover, the pathological effect of the toxic metabolites produced during the primary phase of the bacteria was investigated.

Virulence of the infective juveniles of *Heterorhabditis bacteriophora* BA1 and *Steinernema carpocapsae* BA2 against major insect pests was discussed. These tested pests were: the greater wax moth larvae; *Galleria mellonella*, the Cotton Leaf worm; *Spodoptera littoralis*, the Cut worm; *Agrotis ipsilon*, the European corn borer; *Osterinia nubilalis*, the Greater sugar cane borer; *Sesamia cretica*, the Apple tree borer; *Zeuzera pyrina*, the Sugar beet fly; *Pegomyia mixta*, and the Tortoise beetle; *Cassida vittata*.

The virulence of EPN against the melon fruit fly, *Dacus ciliatus*; the peach fruit fly, *Bactocera zonata* and the fruit fly, *Ceratitis capitata* were tested in details.

H. bacteriophora BA1 and *S. carpocapsae* BA2 were propagated in vivo using *G. mellonella* mass culture and in vitro using three different techniques: Wouts media, Dog Food Agar (DFA) and Bedding flask.

To extend the shelf-life of the EPNs-based bioinsecticide, different formulations were tested to select the suitable form for longer nematode survival as follows: Sponge, Liqua gel or hydro gel, Calcium alginate and Kaoline. The formulations were compared with the water suspension as control. Some adjuvants such as ascorbic acid, citric acid and sorbic acid were added to check their effect on the nematode survival. The heterorhabditis nematodes were able to survive at room temperature for 50 days on hydrogel with better infectivity than the steinernematids.

By the end of the project a biopesticide based on EPNs was produced. It is known as 'NoBug' and is now available in market.

Recommendations

Based on the data of this project, some points should be taken into consideration:

1. Marketing the new biopesticide should be processed through the Ministry of Agricultural or the Academy of Science and Technology.
2. More studies must be done to improve the production and formulation process especially in the fermentation of these microbial pathogens in biological bioreactors.

References

1. Akhurst, R.J. (1980) Morphological and Functional Dimorphism in *Xenorhabdus* spp. Bacteria Symbiotically Associated with Insect Pathogenic Nematodes Neaplectana and Heterorhabditis. Journal General Microbiology 121, 303–309.
2. Akhurst, R.J., Boemare NE (1988) A numerical Taxonomic Study of the Genus *Xenorhabdus* (Enterobacteriaceae) and Proposed Elevation of the Subspecies of *X. nematophilus* to Species. Journal General Microbiology 134, 1835–1845.
3. Boemare, N.E., Akhurst RJ (1988) Biochemical and Physiological Characterization of Colony form Variants in *Xenorhabdus* spp. (Enterobacteriaceae). Journal General Microbiology 134, 751–761.
4. Boemare, N.E., Akhurst RJ, Mourant RG (1993) DNA Relatedness Between *Xenorhabdus* spp. (Enterobacteriaceae), Symbiotic Bacteria of Entomopathogenic Nematodes, and a Proposal to Transfer *Xenorhabdus Luminescens* to a New Genus, Photorhabdus gen. nov. International Journal Systematic Bacteriology 43, 249–255.
5. Ehlers, R.U (2001) Mass Production of Entomopathogenic Nematodes for Plant Protection. Appl. Microbiol. Biotechnol. 56: 623–633.
6. Georgis, R. (1990) Formulation and Application Technology. In 'Entomopathogenic Nematodes in Biological Control' (R. Gaugler and H. K. Kaya, Eds.), CRC Press, Boca Raton, FL. pp. 173–194.
7. Glazer, I. and Lewis, E.E. (2000): Bioassays for Entomopathogenic Nematodes. In Bioassays for Entomopathogens and Nematodes. Navon A. [ed] Kluwer Academic Publisher, Holland.
8. Grewal, P. (2002) Formulation and Application Technology. In 'Entomopathogenic Nematology' (R. Gaugler, ed.), Chapter 13, CABI Publishing, Wallingford, UK. pp. 265–287.
9. Hussein, M.A. and Ehlers, R.-U. (2001) Significance of the Photorhabdus Luminescens Inclusion Bodies for the Development of Heterorhabditis Bacteriophora. In: Entomopathogenic Nematodes-Virulence Vectors and Secondary Metabolites from Symbiotic Bacteria of Entomopathogenic Nematodes. N. Boemare, R.-U. Ehlers, A. M. Burnell, R. Wegensteiner, E. Koshier, R. Mulder, eds. COST 819. Office for Official Publications of the EC, Luxembourg, pp. 47–53 (2001). Austeria.
10. Kaya HK, Stock SP (1997) Techniques in Insect Nematology. In Lacey L. (ed.) Manual Techniques in Insect Pathology. Academic press, San Diego, pp 281–324.
11. Mona A. Hussein (2004) 'Utilization of Entomopathogenic Nematodes for the Biological Control of Some Lepidopterous Pest' Entomology (BioControl). Entomology Department Faculty of Science, Ain Shams University, Egypt pp.203.
12. Strauch-O, Niemann-I, Neumann-A, Schmidt-AJ, Peters-A, Ehlers-RU (2000) Storage and Formulation of the Entomopathogenic Nematodes Heterorhabditis Indica and *H. bacteriophora*. Bio Control 2000, 45: 4, 483–500.
13. Woodring, J.L., Kaya, H.K. (1988). Steinernematid and Heterorhabditid Nematodes: A Handbook of Techniques. Arkansas Agricultural Experiment Station Southern Cooperative Bulletin 331





Biology and Biotechnology



Wael Nabil Hozzein

Lecturer in the Botany Department, Faculty of Science, Cairo University, Beni-Suef Branch, Egypt. A visiting researcher at the School of Biology, University of New Castle, United Kingdom, and a PhD fellow at the key Laboratory for Microbial Resources of the Ministry of Education, Yunnan Institute of Microbiology, Yunnan University, China.

He was born on 29 May 1972 and graduated from Botany and Microbiology Department, Faculty of Science, Beni-Suef Branch, Cairo University with Honors, and was ranked the first in his department. In 1995, he obtained his Master's Degree in Microbiology from Cairo University, his research was entitled '*The Production of Some Bioactive Compounds by Some Alkalophilic Microorganisms Isolated from Wadi Araba, Egypt*'. His interest in Alkalophilic studies continued with another research entitled '*Biological Studies on some Alkalophilic Actinomycetes Isolated from Wadi Sannur*', and in 2003 he obtained his PhD a year later, he won the BA/CSSP Research Grant and successfully finished his research on '*Desert Actinomycetes as a Novel Source of New Antimicrobial Agents*'.

Desert Actinomycetes as a Novel Source of New Antimicrobial Agents

Wael Nabil Hozzein

Faculty of Science, Beni-Suef Branch, Cairo University, Cairo, Egypt

EXECUTIVE SUMMARY

The main aim of the project was to test the abilities of desert actinomycetes as a new possible source to find a novel lead compound for drug development. For this purpose, a hundred (100) soil samples were collected from six different localities representing different desert and arid regions in Egypt. Different selective isolation techniques and pretreatments were used in isolation to yield, as much as possible, novel and diverse active taxa. About 200 strains have been isolated from the collected soil samples. The results of the selective isolation work were published in a research article in the *World Journal of Microbiology and Biotechnology*, Hozzein, W. N., Ali, M. I. A. and Rabei W. (2008). A new preferential medium for enumeration and isolation of desert actinomycetes. *World Journal of Microbiology and Biotechnology* 24:1547–1552.

The isolated strains have been de-replicated by color grouping and some representatives were selected for the screening process. The selected strains have been screened for the production of antimicrobial agents against different pathogenic test organisms. The results of the preliminary screening were encouraging as about 42.67% of the tested strains were biologically active. The morphological and chemotaxonomical characteristics of some representatives of the selected strains have been studied. These phenotypic characteristics revealed the genus affiliation of the strains and the genus biodiversity of the desert actinomycetes. The results of the antimicrobial activities and genus diversity of the isolated desert actinomycete strains were introduced in the 14th International Conference for Arab Biologists which was held at Suez Canal University from 15 to 19 April. The paper entitled 'Genus Diversity and Antibacterial Activities of Some Desert Actinomycetes' was published in volume 17B in the *Journal of Union of Arab Biologists*.

Based on the bioactivity data, one interesting strain, designated D332, was selected due to its wide broad spectrum and high productivity for further work. The optimization of the production rate of the active metabolites produced by the most potent actinomycete strain was carried out by optimizing the different environmental conditions and nutritional requirements affecting the production rate.

Partial purification of the bioactive compound produced by strain D332 was carried out and the antimicrobial activity during production, extraction and partial purification of the active compound was checked on *Bacillus subtilis* seeded agar plate. The partially purified bioactive compound produced by the most potent isolate was characterized chemically on precoated thin layer chromatography plates after spraying with different spray reagents.

Then the most active actinomycete strain was identified to the species level by studying its morphological (cultural characteristics, spore surface and spore morphology by electron microscopy), chemotaxonomical (diaminopimelic acid (DAP) isomer type, whole-cell sugar and phospholipids pattern) and molecular characteristics (16S rDNA gene sequencing and phylogenetic analysis). All the obtained results confirmed the assignment of strain D332 as a new member of the genus *Streptomyces*.

In conclusion, desert habitats seem to be a new source for the isolation of novel actinomycetes with good biological activities which could provide novel candidates for drug discovery. Finally, a third paper was written from the results and submitted for publication and another article will follow.

The Project Description

The project research design and methodology was as follows:

1. Collection of the Desert Soil Samples

About 100 soil samples representing different desert habitats in the Eastern and Western Desert of Egypt. Soil samples were taken from a depth of 5–20 cm below soil surface with a collecting spatula in clean sterile plastic bags. The soil of the top region (5 cm of the surface) was excluded and most of the collected samples were obtained from the rhizosphere of the dominant plants if present. The soil samples were air-dried at room temperature for 7–10 days and then passed through a 2 mm sieve to remove gravel and debris. A mixture of the samples from each site was made by mixing the samples thoroughly. The sampling and soil preparation took about one month.

2. Characteristics of the Study Area

2.1 Climate

Meteorological parameters of the study areas including temperature, rainfall and relative humidity were obtained from Beni-Suef and Giza weather stations.

2.2 Chemical Analysis of the Soil Samples

Samples were suspended in distilled water at 1:5, shaken vigorously to ensure uniformity, and then allowed to settle down for about 10 min. Hydrogen ion concentration was measured by using a Beckman digital pH meter. Organic matter content was determined by using the wet combustion method of Walkley and Black after Tan (1996). Total carbonates were determined by the rapid titration method according to Grimshaw *et al.* (1989), bicarbonates by titration with standard potassium bisulfate and chlorides by titration with silver nitrate as described by Piper (1944). Total soluble salts were determined by evaporation of the soil extract and expressed as a percent of the soil weight according to Jackson (1967).

3. Microbial Structure and Selective Isolation of Actinomycetes

Soil dilution plate technique (Johnson *et al.* 1959) was used for this purpose. Serial dilutions of the air-dried soil samples were made by aseptically adding 1 g of soil to 9 ml of sterilized distilled water (10⁻¹), mixed by shaking and further tenfold dilutions were made till 10⁻⁶.

Three different agar media were tested for their efficiency for enumeration and isolation of desert actinomycetes; namely, glucose-yeast extract (Gordon and Mihm, 1962), soil extract (Atlas, 1997) and a minimal medium (MM) designed by us, of the following composition (g/l): glucose, 0.5; yeast extract, 0.5; K₂HPO₄, 1; MgSO₄·7H₂O, 0.5 and NaCl, 0.5. All media were supplemented with 18 g agar and MM was supplemented with 1 ml of a microelement stock solution (Labeda and Shearer, 1990). Tenth milliliter aliquots of each soil dilution were spread over the surface of the isolation plates which were then incubated for 21 days at 30°C. Three replicates were used for each dilution and the most suitable dilutions for counting were selected. The average colony count of bacteria, actinomycetes and fungi formed on a plate was calculated. Colonies were recognized by their characteristic cultural and morphological features, and sometimes after microscopic observations. After incubation at 30°C for three weeks, the plates were checked to select the colonies to be purified by streaking on the same isolation medium and subcultured for further work. The isolated strains were preserved in 20% glycerol at –20°C.

4. Study the Genus Biodiversity of the Isolated Desert Actinomycetes in Relation to Environmental Conditions

Identification of the isolated desert actinomycetes to the genus level was conducted by studying the morphological and cultural features according to the guide described in Bergey's Manual of Determinative Bacteriology (Holt *et al.*, 1994). For morphological and cultural examinations, the purified isolates were inoculated on modified Bennett's agar (Jones, 1949) and oatmeal agar (ISP 3; Küster, 1959) plates and were incubated for 14 days at 30°C. Isolates were then assigned to groups based on aerial spore mass color, reverse pigment color and the color of any diffusible pigments. Glass coverslip cultures were prepared as described by Kawato and Shinobu (1959) on yeast extract-malt extract agar (ISP 2 medium; Shirling and Gottlieb, 1966) and the morphology of sporophores and spore chains was observed under the light microscope after incubation for 2 weeks at 30°C. Then, the diaminopimelic acid isomer type was determined as described by Hasegawa *et al.* (1983). The obtained results from the above mentioned experiments were used to assign the isolated desert actinomycetes to the genus level. A relationship between the genus biodiversity in relation to the environmental conditions prevailing in the isolation localities was evaluated.

5. De-replication of the Isolated Desert Actinomycetes

The purified strains were de-replicated to get rid of repeated strains by studying their cultural characteristics (color of aerial and substrate mycelia and soluble pigments) on two different media, notably the isolation medium and oatmeal agar (Shirling and Gottlieb, 1966) to differentiate them into different color groups. The results from color grouping guided us to select different representative organisms for screening. The isolation, purification and de-replication of about 200 actinomycete strains all together took about three months.

6. Screening for Antimicrobial Activities of Selected Strains

Directly after selection, the representative strains were cultured in liquid medium. A preliminary screening was carried out by using the agar blocks method and the classical agar disk diffusion method (Cooper, 1963 & 1972) against some pathogenic test strains. The following pathogenic microorganisms were used as test strains for the antimicrobial activities of the isolated actinomycetes; *Bacillus subtilis*, *Micrococcus luteus*, *Staphylococcus aureus*, Methicillin-resistant *Staphylococcus aureus* (MRSA), *Escherichia coli*, *Mycobacterium pheli*, *Shigella spp.*, *Salmonella typhi*, *Salmonella paratyphi*, *Candida albicans*, *Saccharomyces cerevisiae*, *Aspergillus oryzae* and *Penicillium chrysogenum*. The plates were then incubated at 37°C for 24 hours for bacteria and at 30°C for two or three days for yeast and fungal strains. After incubation, the diameters of the clear zones were measured and used as indication of activity.

7. Optimization of the Production of the Most Interesting Compounds

The effect of some environmental conditions (incubation period, pH and temperature) on the production rate of the active metabolites produced by the most potent actinomycete strain was determined. The effect of using different nutritional requirements (carbon sources, nitrogen sources and mineral salts) in the media on the production rate of the active metabolites was also studied to optimize the production rate in the next phase.

8. Identification of the Most Potent Actinomycete Strain to the Species Level

8.1 Phylogenetic Analysis of the 16S rDNA Gene Sequence

The DNA extraction, PCR-mediated amplification of the 16S rDNA, purification of the PCR products and sequence of the purified products were carried out as previously described (Lane, 1991). The resultant 16S rDNA gene sequence was aligned manually using the software package MEGA version 3.1 (Kumar *et al.*, 2004), against the available corresponding bacterial sequences retrieved from the DDBJ, EMBL and GenBank databases. Phylogenetic trees were inferred using the least-squares (Fitch and Margoliash, 1967), maximum likelihood (Felsenstein, 1981) and neighbor-joining (Saitou and Nei, 1987) tree-making algorithms from the PHYLIP suite of programs (Felsenstein, 1993). The distance model of Jukes and Cantor (1969) was used to generate evolutionary distance matrices. The resultant tree topologies were evaluated by bootstrap analyses (Felsenstein, 1985) of the neighbor-joining method based on 1,000 resamplings using the SEQBOOT and CONSENSE programs from the PHYLIP package (Felsenstein, 1993).

8.2 Chemotaxonomy

Standard analytical procedures were used to extract and analyze the isomeric forms of diaminopimelic acid (Hasegawa *et al.*, 1983), whole-organism sugars (Staneck and Roberts, 1974) and polar lipids (Minnikin *et al.*, 1984).

8.3 Cultural and Morphological Characteristics

The cultural characteristics of the desert actinomycete isolate D332 were recorded as described by Shirling and Gottlieb (1966). The morphological features were observed after examining the coverslip cultures by the light and scanning electron microscopes using a Cambridge Steroscan 240 scanning electron microscope and the procedure described by O'Donnell *et al.* (1993).

8.4 Phenotypic Tests

All the recommended physiological and biochemical tests for characterization of actinomycetes were carried out as described by Williams *et al.* (1983).

9. Production of Antimicrobial Compound(s)

A loopful of seven days old culture of strain D332 grown on MM agar was used to inoculate 500 ml Erlenmeyer flasks each containing 100 ml of ISP2 medium and incubated at 30°C on a shaking incubator at 200 rpm for two days. Then, 10% of the actinomycete inoculum was transferred to starch nitrate production medium (Tadashi, 1975) and incubated at 30°C on a shaking incubator at 200 rpm for five days. The fermentation broth was collected and examined for the antimicrobial activity by using the agar well diffusion method in nutrient agar plate seeded with *Bacillus subtilis*.

10. Extraction and Partial Purification of Antimicrobial Compound(s)

The fermentation broth was filtered and extracted with 1:1 (v/v) ethyl acetate. The organic ethyl acetate phase was collected and evaporated to dryness under reduced pressure by using a rotary evaporator. The antimicrobial activity of the crude extract was tested by using the filter paper disc diffusion method assay on *Bacillus subtilis*. The crude extract was then partially purified by thin layer chromatography (precoated silica gel TLC plates) using a solvent system composed of heptane: ethyl acetate (3:2). The activity at the partial purification stage was checked using the bioautography method in which the developed chromatogram strip was placed on the surface of a *Bacillus subtilis* seeded agar plate. The plate was then incubated at 37°C for 24 hours. The presence of inhibition zones around the active compound(s) was determined and the distance from the starting point, where the crude extract was loaded to the TLC strip, to the center of the clear zones were measured (the R_f value).

This project resulted in establishing a scientific collaboration with a group of scientists from Palermo University, Italy. Additionally, two publications and two other papers are in preparation.

Conclusions

Although previous studies on actinomycetes isolated from the desert habitats are very few, their antimicrobial potential was not reported yet. Therefore, the desert habitats in Egypt can be considered as a new resource for biotechnology and the actinomycetes from these habitats could be new candidates for drug discovery.

While, various media and techniques were developed for selective isolation of actinomycetes in general, none of the studies concentrated on desert actinomy-

cetes. Therefore, we tested the best selective method for isolation of actinomycetes from the desert environments. The results revealed that a new minimal medium designed by us was highly efficient for enumeration and selective isolation of actinomycetes from the desert soils.

The current study is one of the few studies aimed to investigate the genus diversity and antibacterial activities of some desert actinomycetes isolated from the Egyptian arid regions. The results revealed that actinomycetes occurred in high population in these arid regions in Egypt. All of the isolated 75 desert actinomycetes were characterized by their morphological and cultural properties. It was found that they belong to 8 actinomycete genera; *Streptomyces*, *Nocardioopsis*, *Nocardia*, *Amycolatopsis*, *Actinomadura*, *Nonomuraea*, *Microtetraspora* and *Pseudonocardia*.

The isolated desert actinomycete strains were then subjected to a preliminary screening program to investigate their ability to produce antimicrobial compounds. The results of the antimicrobial screening program revealed that 32 out of the isolated 75 strains were active against the tested pathogenic organisms. This means that 42.67% of the isolated desert actinomycetes are biologically active. It was obvious from the results that the activities against Gram-positive bacteria were more frequent than against Gram-negative bacteria and yeast.

With reference to the obtained screening results, the most potent 10 isolates were selected to be identified by 16S rDNA gene sequence analysis to determine their taxonomic status. The phylogenetic analyses of 16S rDNA gene sequence confirmed the classification of the 10 isolates into *Streptomyces*, *Nocardia*, *Nocardioopsis* and *Amycolatopsis*. It is also worth mentioning that no discrepancy was found between the generic identities determined by morphological and cultural features and 16S rDNA gene sequence analysis. The phylogenetic results showed that some of the active strains could be described as new species but further experiments should be done to clarify this. It can also be concluded from the results that the actinomycete diversity in desert habitats is high at both the genus and the subgenus levels.

The desert actinomycete strain D332 was selected for its broad spectrum and high antimicrobial activity for further studies including its classification and partial purification of its antimicrobial compound(s).

The taxonomical position of strain D332 was obtained after a stepwise phylogenetic analysis of the 16S rDNA gene sequence with the closely related similar sequences. It was found that it belongs to genus *Streptomyces* as obvious from the phylogenetic tree. It was evident also from the tree that strain D332 formed a distinct phyletic line in the *Streptomyces* 16S rRNA gene tree and it is most probably representing a new species

of the genus *Streptomyces*. The affiliation of strain D332 to genus *Streptomyces* was supported by its chemotaxonomical characteristics. It contained LL-diaminopimelic acid as the characteristic diamino acid of the peptidoglycan in the whole-cell hydrolysate and glucose and galactose as whole-organism sugars (wall chemotype I (Lechevalier and Lechevalier, 1970)). The polar lipid pattern revealed the presence of phosphatidyl ethanolamine, phosphatidyl inositol mannosides, diphosphatidyl glycerol (phospholipid type II (Lechevalier *et al.*, 1977)). This chemical profile is clearly consistent with the assignment of strain D332 to genus *Streptomyces* (Williams *et al.*, 1989). All the morphological, cultural and phenotypic characteristics were also similar to those reported for members of genus *Streptomyces*. To confirm that D332 is a new species of the genus *Streptomyces*, further comparative studies with the closest phylogenetic neighbours including DNA-DNA hybridization should be carried out (Manfio *et al.*, 1995).

Only one band was detected for the partially purified extract produced by the *Streptomyces* strain D332 on the TLC plate. Moreover, a single sharp inhibition zone in the bioautography assay revealed that strain D332 produce only a single active compound. The results of the bioautography showed also that the Rf value was 0.28. However, further purification and analysis with HPLC should be conducted before characterization of the pure active metabolite produced by the *Streptomyces* strain D332.

In the present study, the results showed that 42.67% of the isolated desert actinomycetes are biologically active. These results are very encouraging to continue screening more actinomycete strains from the desert habitats and strongly support the idea that species of actinomycetes from underexploited environments could be a very fruitful source of novel bioactive secondary

metabolites. Therefore, much interest must be oriented to those poorly studied microorganisms. The results also showed that the *Streptomyces* strain D332, which was isolated from the Egyptian Desert soil, produced one biologically active compound with high broad spectrum activity against Gram-positive and Gram-negative bacteria and yeasts, suggesting this strain as a promising producer of an antimicrobial compound.

Recommendations

1. The results indicated that microorganisms are present and many are in a viable and culturable state within the desert soil samples studied. So, the microbiologically poorly explored areas and extreme environments should be investigated for their microflora because they are likely to harbor new microorganisms.
2. It is very important to study and understand the microbial biodiversity within these habitats to conserve and make better use of the biological resources there.
3. The microbial count was very low from the soil samples collected from the desert. Therefore, more accurate and more effective methods other than the dilution plate technique should be used to estimate the number of microorganisms in extreme environments.
4. It is very important in the future to use or to formulate more selective isolation media to be able to isolate other desert actinomycetes.
5. These results are very encouraging to continue work on extreme actinomycetes and investigate new habitats as a possible way to discover new taxa.
6. Some strains could be identified as new species. This means that, by much more work on actinomycetes from these habitats we can discover many new taxa and consequently many novel useful metabolites.

Appendices

Some Representative Tables of the Results

Table 1 Average of microbial counts (CFU/gram of dry soil x 10⁻³) from the different six sites representing the Eastern (E1-E3) and the Western (W1-W3) deserts of Egypt on the three used media

| Site | GYE | | | Soil Extract | | | MM | | |
|------|-----|------|------|--------------|------|-------|------|-------|------|
| | Aa | B | F | A | B | F | A | B | F |
| E1 | 1.6 | 2 | 0.65 | 0.85 | 12.3 | 0.65 | 4.7 | 4 | 0.65 |
| E2 | 0.1 | 0.5 | 0.65 | 24.6 | 33.9 | 1.97 | 2.3 | 4.3 | 1.3 |
| E3 | 0.5 | 0.2 | 0.6 | 4.7 | 42.3 | 3.1 | 16.5 | 15.19 | 1.3 |
| W1 | 0 | 0.5 | 1.15 | 0.125 | 8.3 | 0.975 | 3.4 | 8 | 0.33 |
| W2 | 1.4 | 4.3 | 1.05 | 6.97 | 26 | 2.7 | 15 | 10.09 | 0 |
| W3 | 3.4 | 11.6 | 1.1 | 22.5 | 19.3 | 0.675 | 34.6 | 22.2 | 0 |

^a A, actinomycetes; B, Bacteria; F, Fungi

Table 2 The antimicrobial activities of the biologically active desert actinomycete isolates expressed as inhibition zones of growth against the used test organisms in mm

| Isolate code | Test organism* | | | | | | | | | | |
|--------------|----------------|-------|------|-------|-------|-------|---------|-------|-------|-------|-------|
| | B. s. | M. p. | MRSA | S. a. | S. l. | E. c. | Sh. sp. | S. p. | S. t. | C. a. | C. k. |
| S11 | 32 | 30 | 26 | 28 | 35 | – | – | – | – | – | – |
| S14 | 22 | 26 | 23 | 23 | 28 | – | – | – | – | – | – |
| S133 | – | – | 16 | 16 | 18 | – | – | 15 | 14 | – | – |
| S134 | 18 | 26 | 17 | 19 | 20 | 17 | – | 16 | 15 | – | – |
| S135 | – | – | 15 | – | – | – | – | 23 | 18 | – | – |
| S139 | 16 | – | – | 14 | 18 | – | – | 18 | 17 | – | – |
| S22 | 25 | 19 | 20 | 26 | 23 | – | – | – | – | – | – |
| S212 | 24 | – | 22 | 23 | 27 | – | – | – | – | – | – |
| S215 | – | – | – | 35 | – | 21 | 24 | 16 | 17 | 23 | 32 |
| S230 | 17 | – | 18 | 20 | 27 | – | – | – | – | – | – |
| S36 | 18 | – | – | – | – | – | – | – | – | – | – |
| S38 | – | 17 | – | – | 25 | – | – | – | – | 16 | – |
| S39 | 20 | – | – | – | 16 | – | – | – | – | – | – |
| S310 | 25 | – | – | 23 | 20 | – | – | – | – | 30 | 19 |
| S319 | – | – | – | – | 20 | – | – | – | – | 28 | 34 |
| S320 | – | – | 19 | – | – | – | 20 | 17 | 22 | 30 | 28 |
| S322 | – | – | – | – | 21 | – | – | – | – | – | – |
| S323 | 25 | – | 16 | 18 | 20 | – | – | – | – | 35 | 30 |
| S325 | 16 | – | – | 23 | 16 | 27 | – | – | – | – | – |
| S328 | – | – | – | 32 | – | 18 | – | – | – | 16 | 16 |
| S329 | – | – | – | – | 16 | – | – | – | – | – | – |
| S331 | – | – | – | – | 16 | 20 | – | – | – | – | – |
| D13 | 18 | 20 | – | – | 26 | – | – | – | – | – | – |
| D17 | 19 | – | – | – | – | – | – | – | – | 19 | – |
| D137 | 14 | 16 | – | – | 16 | – | – | 18 | 16 | – | – |
| D211 | 27 | 30 | – | 21 | 25 | – | – | – | – | – | – |
| D217 | 15 | – | – | 18 | 16 | – | – | – | – | – | – |
| D221 | 17 | – | – | – | 20 | 17 | – | – | – | – | – |
| D224 | – | – | – | 18 | 18 | 16 | 19 | – | – | – | – |
| D226 | 16 | – | – | – | 18 | – | – | – | – | – | – |
| D327 | – | – | – | – | 16 | – | – | – | – | – | – |
| D332 | 35 | – | – | 32 | 31 | 25 | 23 | 39 | 40 | 30 | 35 |

* B. s., *Bacillus subtilis*; M. p., *Mycobacterium pheli*; MRSA, Methicillin-resistant *Staphylococcus aureus*; S. a., *Staphylococcus aureus*; S. l., *Sarcina lutea*; E. c., *Escherichia coli*; Sh. sp., *Shigella spp*; S. p., *Salmonella paratyphi*; S. t., *Salmonella typhi*; C. a., *Candida albicans* and C. k., *Candida kruzei*.

Some Representative Figures from the Results

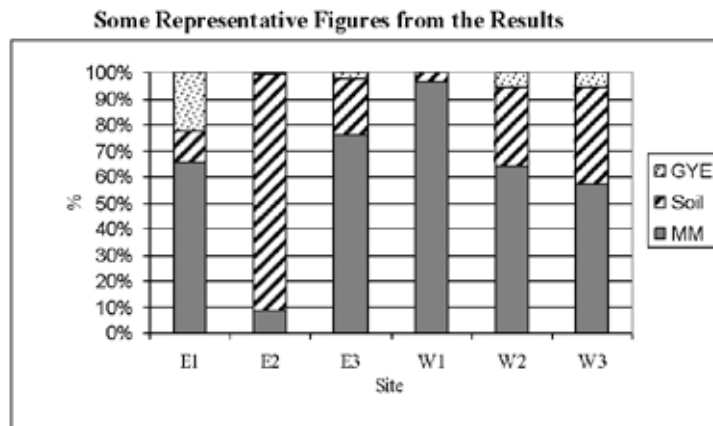


Figure 1 Percentage of actinomycete colonies appeared on MM compared to the other two used media which clearly proved the efficiency of MM in enumeration and isolation of desert actinomycetes

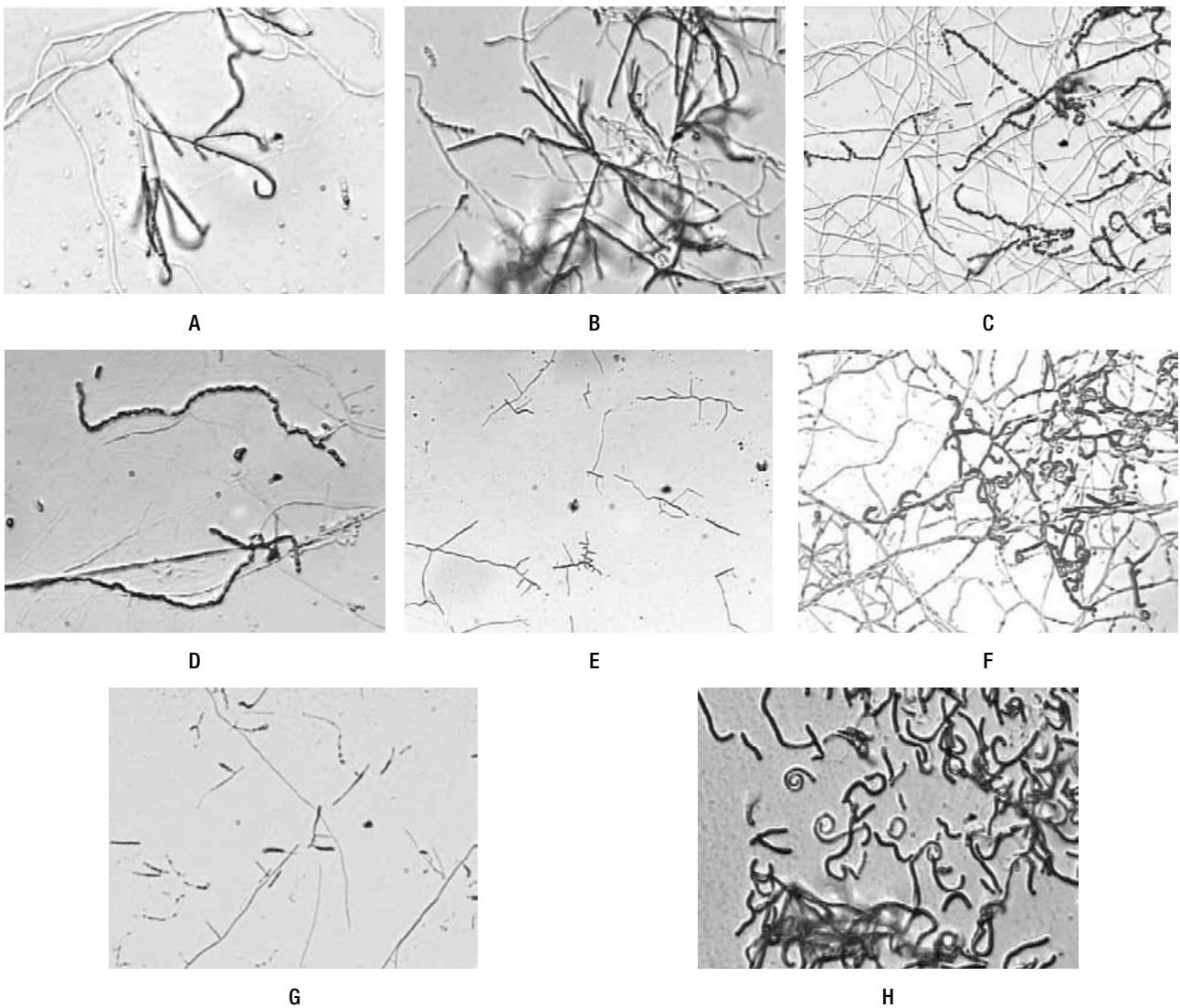


Figure 2 Light micrographs showing the micromorphology of some representative actinomycete genera isolated from the desert habitats in Egypt; A and B are two different *Streptomyces* strains with short coiled spore chains and verticillate spore chains, respectively, C and D are two different *Nocardioopsis* strains with fragmented long spore chains, E is the fragmented substrate mycelium of *Nocardia*, F is aerial hyphae forming short spore chains of genus *Actinomadura*, G is a *Microtetraspora* strain and H is a *Nonomurea* strain

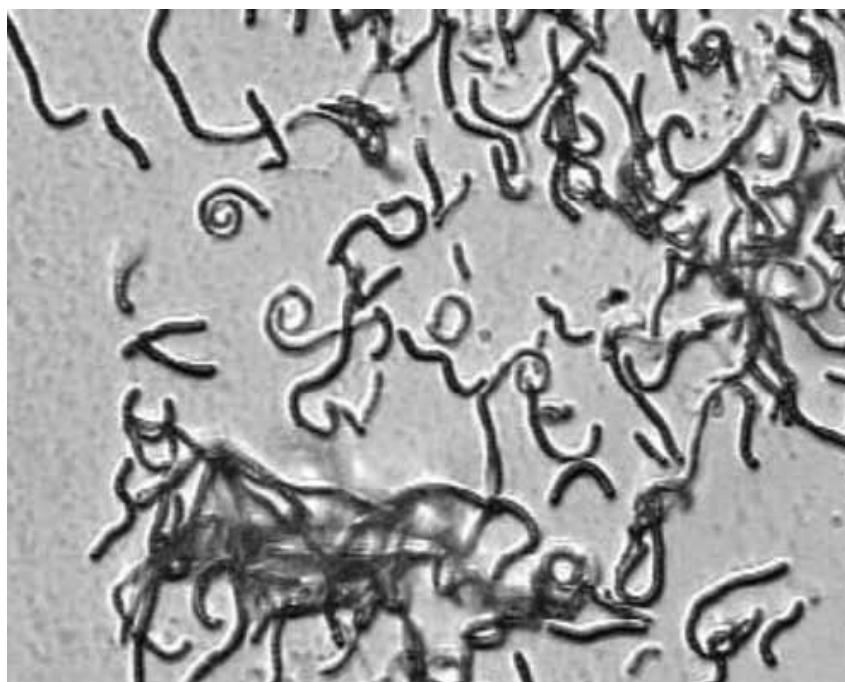


Figure 3 Representative plates showing the antimicrobial activities of some of the isolated desert actinomycetes on different test organisms

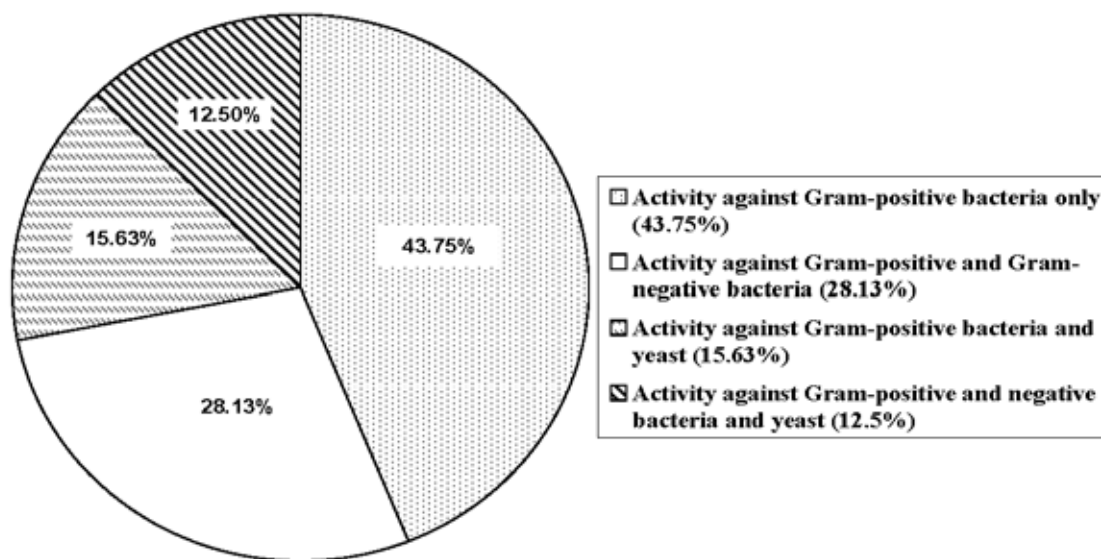


Figure 4 Classification of the active desert actinomycete isolates according to their spectrum of activity

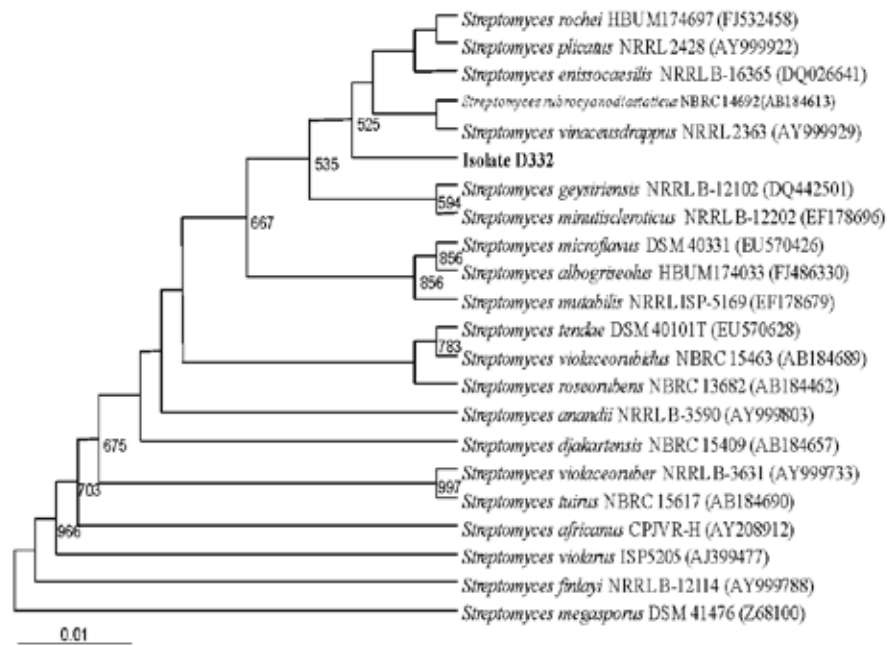


Figure 5 Phylogenetic relationships between strain D332 and closely related members of the genus *Streptomyces* based on nearly complete 16S rRNA gene sequences. Numbers at nodes indicate levels of bootstrap support based on a neighbor joining analysis of 1000 resampled datasets; only values above 50% are given. Bar, 0.01 substitutions per nucleotide position



Figure 6 An electron micrograph of strain D332 showing the spore chains forming coil ends with smooth-surfaced spores.

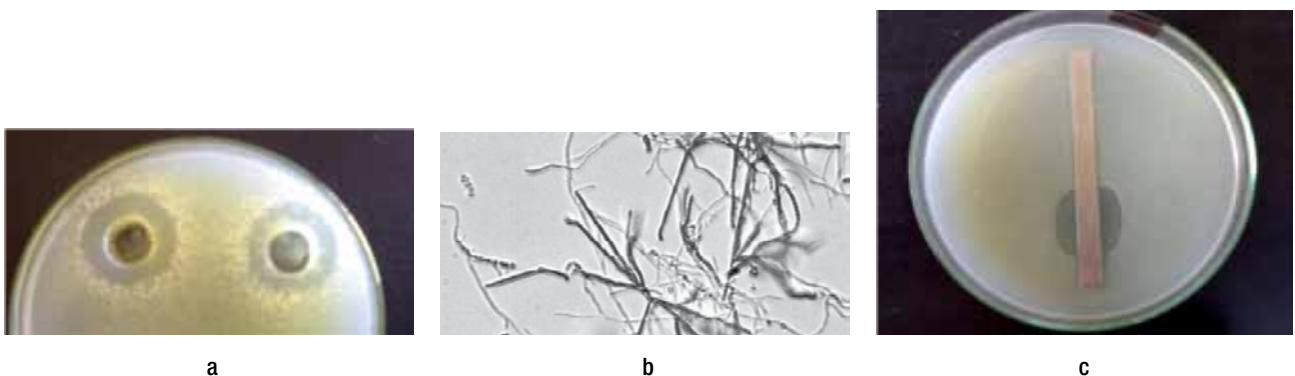


Figure 7 (a) A plate showing the activity of the most potent desert actinomycete; *Streptomyces* strain D332, using the agar well diffusion method, (b) a plate showing the activity of the crude extract using the disc diffusion method and (c) the bioautography bioassay plate showing the single inhibition zone of the active compound; all on *Bacillus subtilis* seeded plate.

References

- Atlas, R. M. (1997). Handbook of microbiological media, 2nd ed. Boca Raton: CRC Press, Florida.
- Cooper, K. E. (1963). In F. Kavanagh (ed.), *Analytical Microbiology*, Vol. 1, pp. 1–86, Academic Press, New York.
- Cooper, K. E. (1972). In F. Kavanagh (ed.), *Analytical Microbiology*, Vol. 2, pp. 13–30, Academic Press, New York.
- Felsenstein, J. (1985). Confidence Limits on Phylogenies: An Approach using the Bootstrap. *Evolution* 39: 783–791.
- Felsenstein, J. (1981). Evolutionary Trees from DNA Sequences: A Maximum Likelihood Approach. *J Mol Evol* 17:368–376.
- Felsenstein, J. (1993). PHYLIP (Phylogenetic Inference Package), version 3. University of Washington, Department of Genetics, Seattle, WA, USA.
- Fitch, W. M. and Margoliash, E. (1967). Construction of Phylogenetic Trees: A Method Based on Mutation Distances as Estimated from Cytochrome C Sequences is of General Applicability. *Science* 155:279–284.
- Gordon, R. E. and Mihm, J. M. (1962). Identification of *Nocardia caviae* (Erikson) nov. comb. *Ann N Y Acad Sci* 98:628–636.
- Grimshaw, H. M., Allen, S. E. and Parkinson, J. A. (1989). Nutrient Elements. In: Allen SE (ed) Chemical Analysis of Ecological Materials, 2nd ed. *Blackwell Sci Publ.*, Oxford, London pp. 81–159.
- Hasegawa, T., Takizawa, M. and Tanida, S. (1983). A Rapid Analysis for Chemical Grouping of Aerobic Actinomycetes. *J Gen Appl Microbiol* 29:319–322.
- Holt, J. G., Krieg, N.R., Sneath, P. H.A., Staley J. T. and Williams S. T. (1994). *Bergey's Manual of Determinative Bacteriology*, 9th ed., Williams & Wilkins, Baltimore, pp. 518–537.
- Jackson, M. L. (1967). *Soil Chemical Analysis*, Prentice Hall Inc., Englewood, Cliffs, N. S.
- Johnson, L. F., Curl, E. A., Bond, J. H., and Fribourg, H. A. (1959). Methods for Studying Soil Microflora-plant Disease Relationships, Burgess, Minneapolis.
- Jones, K. L. (1949). Fresh Isolates of Actinomycetes in which the Presence of Sporogenous Aerial Mycelia is a Fluctuating Characteristic. *J Bacteriol* 57:141–145.
- Jukes, T. H. and Cantor C. R. (1969). Evolution of Protein Molecules. In Munro H. N. (ed.) *Mammalian Protein Metabolism*. Academic Press: New York, pp. 21–131.
- Kawato, N. and Shinobu, R. (1959). On *Streptomyces herbaricolor*, nov. sp. Supplement: A Simple Technique for the Microscopic Observation. *Memoirs of the Osaka University of the Liberal Arts and Education, B Nat Sci* 8:114–119.
- Kumar, S., Tamura, K. and Nei, M. (2004). MEGA3: Integrated Software for Molecular Evolutionary Genetics Analysis and Sequence Alignment. *Briefings in Bioinformatics* 5:150–163.
- Küster, E. (1959). Outline of a Comparative Study of Criteria used in Characterization of the Actinomycetes. *Int Bull Bact Nom Tax* 9:97–104.
- Labeda, D. P. and Shearer, M. C. (1990). Isolation of Actinomycetes for Biotechnological Applications. In: Labeda DP (ed) *Isolation of Biotechnological Organisms from Nature*, McGraw-Hill Publishing Company, New York, pp 1–19.
- Lane, D.J. (1991). 16S/23S rRNA Sequencing. In: Stackebrandt E. and Goodfellow M. (eds), *Nucleic Acid Techniques in Bacterial Systematics*. John Wiley and Sons, Chichester, United Kingdom, pp. 115–175.
- Lechevalier, H. A. and Lechevalier, M. P. (1970). A Critical Evaluation of the Genera of Aerobic Actinomycetes. In: Prauser H (ed) *The Actinomycetales*, VEB Gustav Fischer, Jena, pp. 393–405.
- Lechevalier, M. P., De Bièvre, C. and Lechevalier, H. A. (1977). Chemotaxonomy of Aerobic Actinomycetes: Phospholipid Composition. *Biochem Syst Ecol* 5:249–260.
- Manfio, G. P., Zakrzewska-Czerwinska, J., Atalan, E. and Goodfellow, M. (1995). Towards Minimal Standards for the Description of *Streptomyces* Species. *Biotekhnologija* 8:228–237.
- Minnikin, D. E., O'Donnell, A. G., Goodfellow, M., Alderson, G., Athalye, M., Schaal, K. P. and Parlett, J. H. (1984). An integrated procedure for extraction of bacterial isoprenoid quinones and polar lipids. *J Microbiol Meth* 2:233–241.
- O'Donnell, A. G., Falconer, C., Goodfellow, M., Ward, A. C. and Williams, E. (1993). Biosystematics and Diversity Amongst Novel Carboxydrotrophic Actinomycetes. *Antonie Van Leeuwenhoek* 64:325–340.
- Piper, C. S. (1944). *Soil and Plant Analysis: A Laboratory Manual of Methods for the Examination of Soils and the Determination of Inorganic Constituents of Plants*, A monogr. from the Water Agri Res Inst, University of Adelaide, Adelaide.
- Saitou, N. and Nei M. (1987). The Neighbor-joining Method: A New Method for Reconstructing Phylogenetic Trees. *Mol Biol Evol* 4:406–425.
- Shirling, E. B. and Gottlieb D. (1966). Methods for Characterization of *Streptomyces* Species. *Int J Syst Bacteriol* 16:313–340.
- Staneck, J. L. and Roberts, G. D. (1974). Simplified Approach to Identification of Aerobic Actinomycetes by Thin-layer Chromatography. *Appl Microbiol* 28:226–231.
- Tadashi, A. (1975). *Culture Media for Actinomycetes*. The Society for Actinomycetes. Japan. National Agricultural Library. 1:1–31.
- Tan, K. H. (1996). *Soil Sampling, Preparation and Analysis*, Marcel Dekker Inc., New York.
- Williams, S. T., Goodfellow, M. and Alderson, G. (1989). Genus *Streptomyces* Waksman and Henrici 1943, 339AL. In Williams ST, Sharpe ME, Holt JG (eds) *Bergey's Manual of Systematic Bacteriology*, vol. 4, Williams and Wilkins, Baltimore, pp. 2452–2492.
- Williams, S. T., Goodfellow, M., Alderson, G., Wellington, E. M. H., Sneath, P. H. A. and Sackin, M. J. (1983). Numerical Classification of *Streptomyces* and Related Genera. *J Gen Microbiol* 129: 1743–1813.



Chemistry Sciences



Omran Abd-Allah Omran

A lecturer in the Chemistry Department at the Faculty of Science, South Valley University, Egypt. He has a PhD in “Selective Functionalization” from Kazan State University, Chemistry Department, Russia.

In 1992, he graduated from the Chemistry Department, Assuit University, Egypt with a very good degree. After six years, he finished his MSc with a thesis entitled “Application of secondary Amines in Synthesis of Some New Spiro Heterocyclic Compounds”. Meanwhile, he was an assistant lecturer in the Chemistry Department, South Valley University, Egypt. He was awarded a researcher position in Kazan University, Russia (1998–2002). In 2004, he won the BA/CSSP Research Grants for scientific research; his research covered the preparation of super molecular species through (thia) calixarene compounds.

Some Studies for Preparing Superamolecules Species via Thiacalixarenes and Their Applications

Omran Abd-Ellah Omran

Faculty of Science, South Valley University, Egypt

SUMMARY

I received a grant from the CSSP, Bibliotheca Alexandrina for one year via this grant, I took the opportunity to make a scientific cooperation with the research group at Aalborg University, Denmark for three months. During this short visit, I have participated in a scientific workshop for four days. Where I learned to prepare the starting material (p-tert-butyl thiacalix [4] arenes). I gained great experience working on proton magnetic resonance spectroscopy apparatus. I bought high quality UV lamp for Chromatography detection as well as three important books related to my research fields. I have learned new techniques and new ideas which are very important for my career. After I came back to my home country, I continued working in my project plan. I prepared and introduced two different chiral carbon atoms in the thiacalixarene based compounds, by different spectroscopic methods (IR, Proton NMR and MALDI-TOF spectroscopy). I synthesised some thiacalixarenes based compounds with further sulphur atom which are considered new compounds. One of them is registered at Cambridge Crystallographic Data Center (CCDC), U. K under: (DeDositated Data -CCDC 299162).

As for the scientific publications, I have already submitted one article for publication in an international journal in Japan and the other one is under preparation to be submitted in an international journal. In addition to the above results, there are some data under investigations.

Description of the Research Project and its Results

I signed the project contract in May 10, 2005 with the CSSP. After that, I started preparing the project program. In addition, I made a scientific collaboration with Prof. Kim L. Larsen, Department of Biotechnology, Chemistry and Environmental Engineering, Aalborg University, DK-9000, Aalborg, Denmark, who invited me to visit him and join his group for three months.

Scientific Collaboration

Outcome of my visit to Denmark:

1. I have prepared for the first time the starting material (p-tert-butyl thiacalix [4] arenes) which is very expensive to buy through the chemical companies.
2. Participating in a scientific workshop during the period from 16 to 18 November, 2005: "Novel Technologies to Overcome Drug Delivery and Formulations Barriers; Recent Developments". During the course of this workshop I learned different ideas from a number of Professors working at different Universities in Europe.
3. I have succeeded to buy an apparatus (UV. lamp) for chromatography detection which is very useful to

our Faculty of Science, Sohag. So far 6 undergraduate, 4 graduate students, and 5 faculty staff members are using the UV Lamp in their research work.

4. I gained experience in using the proton magnetic resonance spectroscopy apparatus during my stay in Denmark.
5. I have added three important books to my scientific library. These books are also available for my colleagues here to use anytime in their scientific research.
6. I left a good impression as an Egyptian researcher in Prof. Kim L. Larsen group and we will continue our collaboration.
7. In addition to all the above mentioned items we discussed different scientific research points and transferred some ideas to the group members in Denmark.

Conclusion

I have succeeded to synthesize and introduce two different chiral carbon atoms in the *p-tert-butyl* thiacalix [4] arenes structure; the prepared compounds were characterized by different spectroscopic methods (IR, Proton NMR and MALDI- TOF spectroscopy). The results have been prepared and already submitted for publication. The following is an abstract from the article.

Recommendations

1. Thiaclixarenes compounds as a monograph in supramolecular chemistry is considered a new branch in organic chemistry that should be encouraged especially in Egypt. To the best of my knowledge, I am the only researcher in Egypt working on this subject.
2. I recommend group research plans along with individual research plans for the CSSP Library of Alexandria.
3. X-ray diffraction investigations of Thiaclixarenes crystals compounds should be studied by some theoretical calculation on the intermolecular interactions.
4. The prepared tetrakis ((ethoxythiocarbonyl) methoxy) tetrathiacalix [4] arenes are promising positive sense in complexations.

Acknowledgment

On a lucky day (11 January 2005), I was awarded the BA/CSSP Research Grant from the Bibliotheca Alexandrina. The celebration was great where we listened to

the outstanding talk given by Dr. Ismail Serageldin the Director of the library. I would like to thank him for this fruitful talk. His lecture opened the way for imagination and creation of all the researchers. I would also like to thank the staff members of the Center for Special Studies and Programs (CSSP) especially Dr. Mohamed EI Faham, Director of the CSSP and Professor Salah Soliman; CSSP Board Member for their efforts to create and establish a new unique system for promotion of the scientific research in Egypt which, from my point of view, reinforces the competition and the cooperation between Egyptian researchers as well as their international counterparts.

My warm thanks to the Bibliotheca Alexandrina and the CSSP for giving me the chance to attend the prestigious International Conference (BioVision 2005) Lyon, France from 10 to 15 April 2005.

My great thanks to the staff members at the Department of Biotechnology, Chemistry and Environmental Engineering, Aalborg University, DK-9000, Aalborg, Denmark, for their sincere help during my stay in the

Synthesis and Simple Separation of Thiactalixarene Diastereomers

Omran A. Omran^{a*}, Kim L. Larsen^b, Donghong yu^b and Reinhard Wimmer^b.

^aChemistry Department, Faculty of Science, South Valley University, Sohag, Egypt.

^bDepartment Of Biotechnology, Chemistry and Environmental Engineering, Aalborg University, Aalborg, Denmark.

ABSTRACT

Two different 1, 3-Distal thiactalix [4] arenes were prepared by the reaction of thiactalix [4] arene with phenacyl and/or p-nitro phenacyl bromide in acetone or acetonitrile in the presence of dry CsOH. The prepared 1, 3-distal disubstituted thiactalixarenes afforded two pairs of diastereomers upon bromination in chloroform. The obtained diastereomers were separated by fractional crystallization in a mixture dichloromethane-acetone.

Synthesis of some new thiactalixarenes based compounds which could be applied for complex investigation and used for the purification of some wastes due to having some special properties. The new compounds structures were separated by different separation techniques (Column chromatography and crystallization) and characterized by the different Spectroscopic methods. In addition, one of them has been characterized by X-ray diffraction methods and the crystal structure has been registered at Cambridge Crystallographic Data Center (CCDC), U.K under: ([DeDosltd Data -CCDC 299162](#)).

The following is an abstract from the article.

Studying the Reaction of Lawesson Reagent with Tetrakis (ethoxycarbonyl) methoxy Tetrathiactalix [4] arenas

Omran A. Omran^a, Kim L. Larsen^b, Donghong yu^b and Reinhard Wimmer^b.

^aChemistry Department, Faculty of Science, South Valley University, Egypt.

^bDepartment of Biotechnology, Chemistry and Environmental Engineering, Aalborg University, Aalborg, Denmark.

ABSTRACT

Partially and completely carbonyl thiation of tetrakis ((ethoxycarbonyl) methoxy) tetrathiactalix [4] arenes were prepared by studying its interaction with Lawesson's reagent in dry toluene as solvents under reflux for a week. The prepared compounds were characterized by different spectroscopic methods (IR, ¹HNMR, MALDI- TOF & X-ray). I would like to emphasize that the prepared compounds in the past two points (1, 2) will be synthesized in a large scale for applications.

Under investigation I am studying two different important reactions with thiactalixarenes which are:

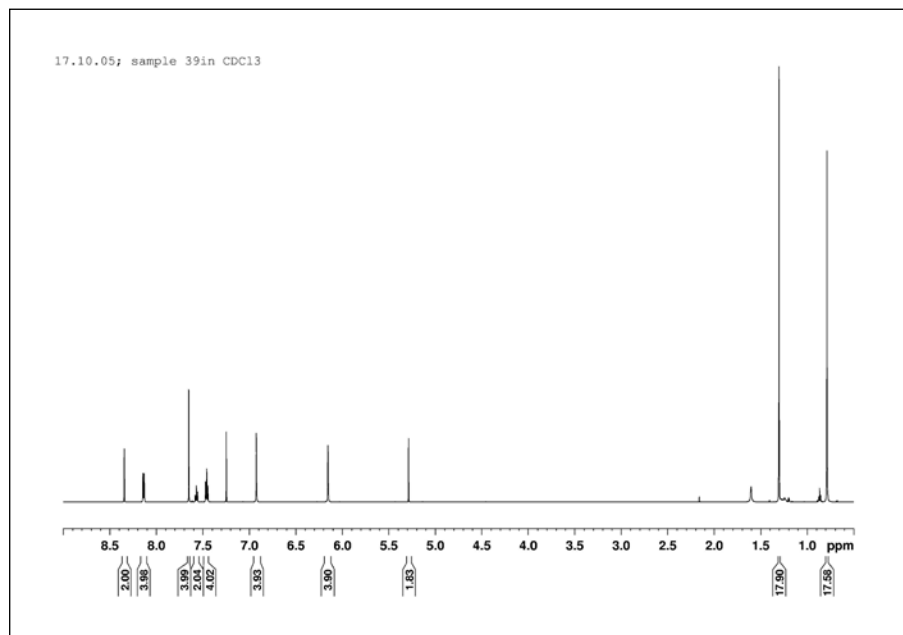
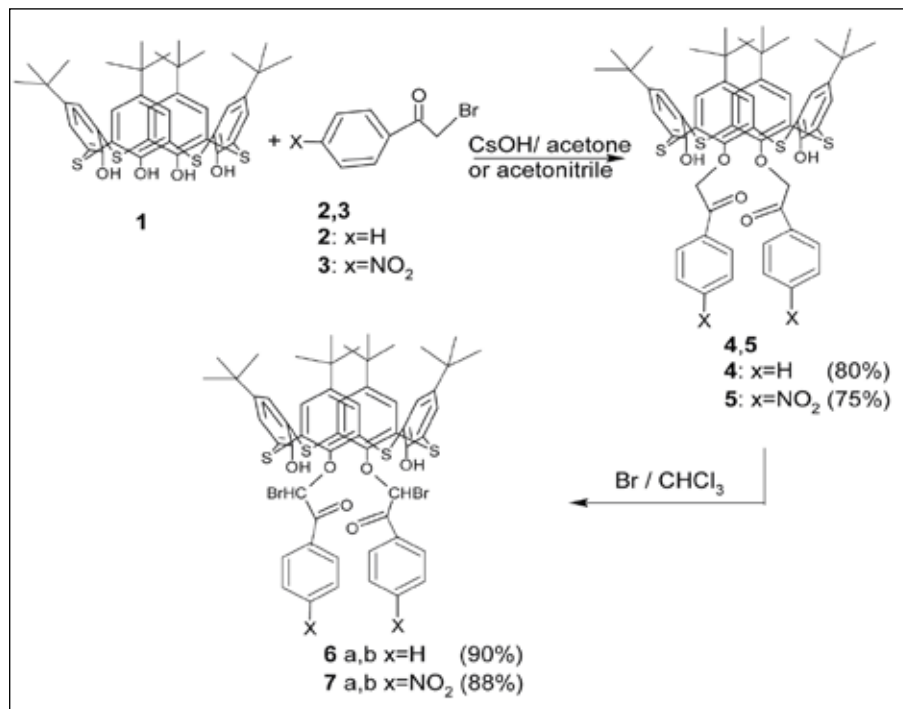
- The interaction of lawesson's reagent with thiactalixarenes, as a new route for phosphorylation of thiactalixarenes.
- The interaction of Diethyl bromomalonate with thiactalixarenes under different alkali metal ions.

In Addition to the above items from 1-3 there are also a few attempts for the thiactalixarenes derivatizations.

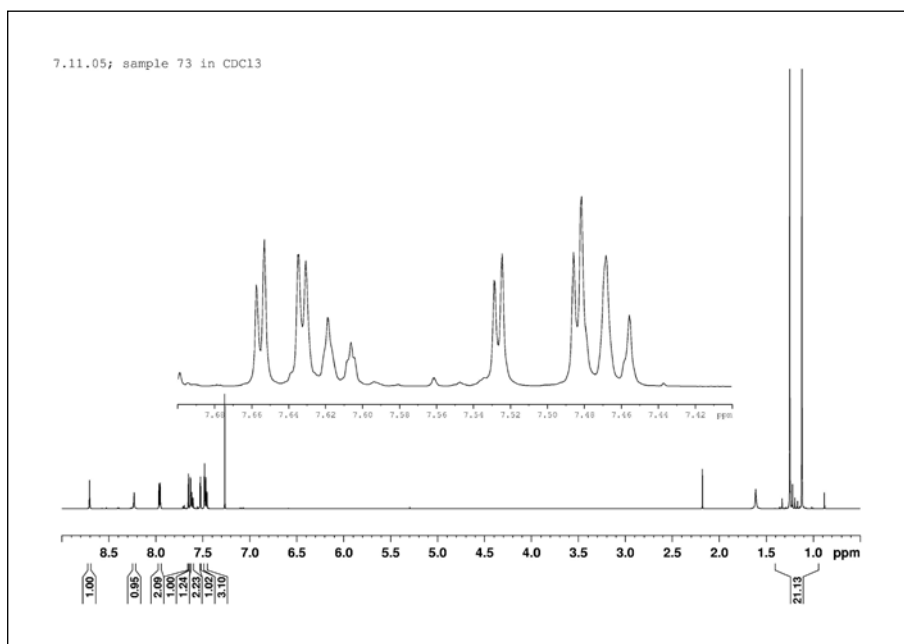
Again, I would like to thank the Bibliotheca Alexandrina for their financial support which allowed me to modify and continue my research.

Department. My great appreciation and deep gratitude to Prof. Dr. Kim L. Larsen for guiding me during my visit and for his cooperation.

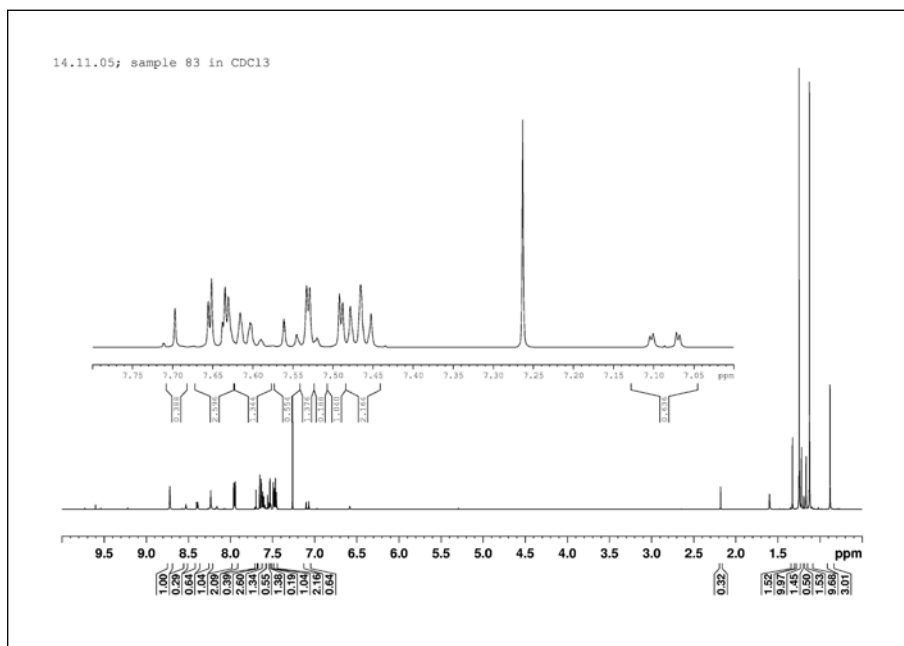
Appendixes

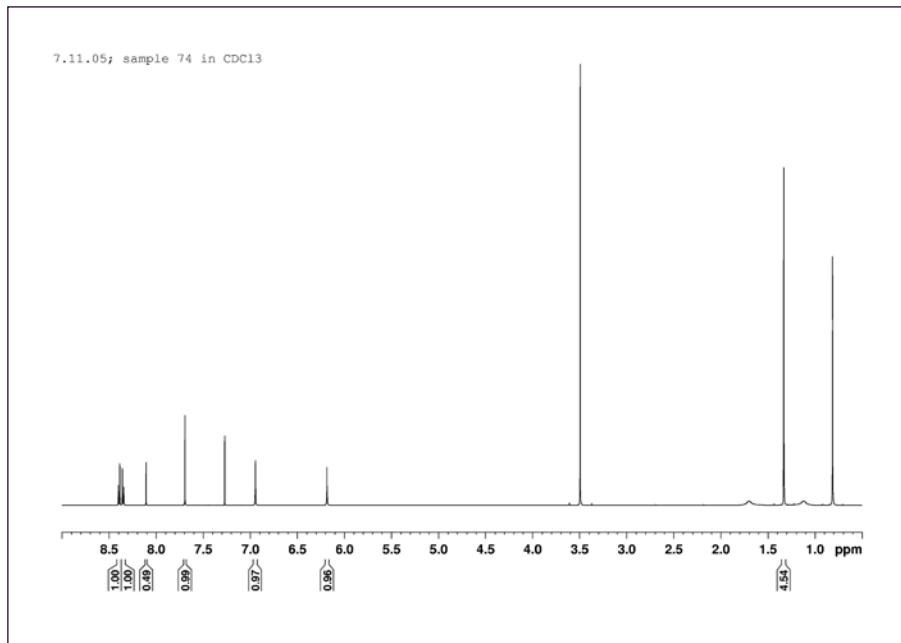
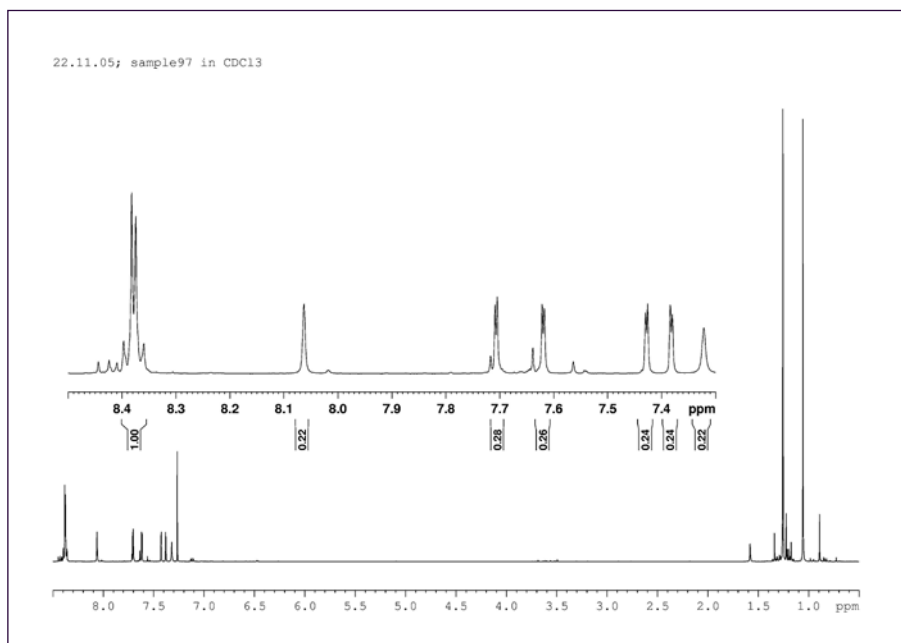


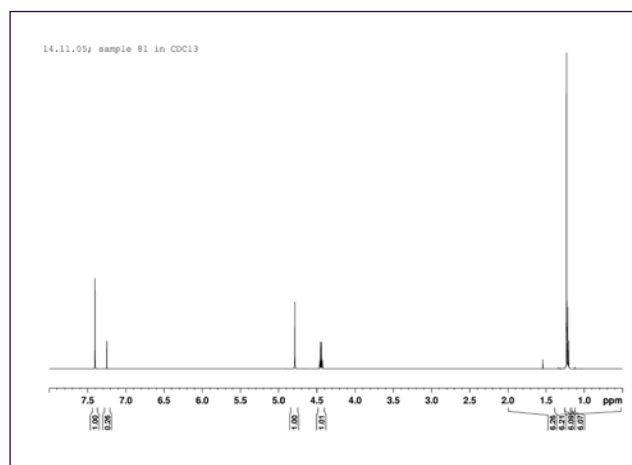
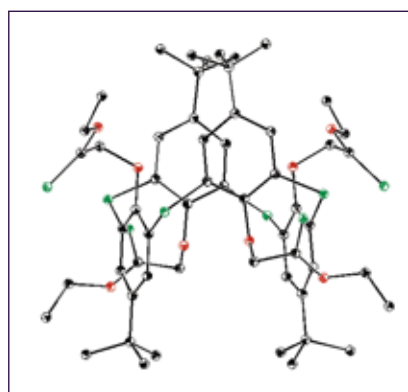
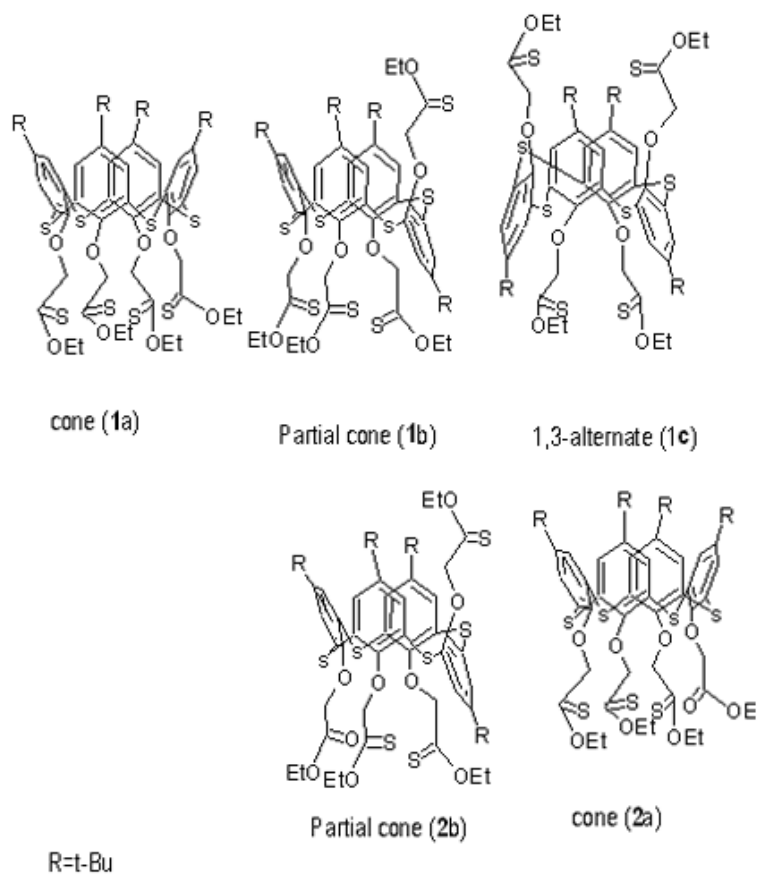
The ¹HNMR of the compounds 4



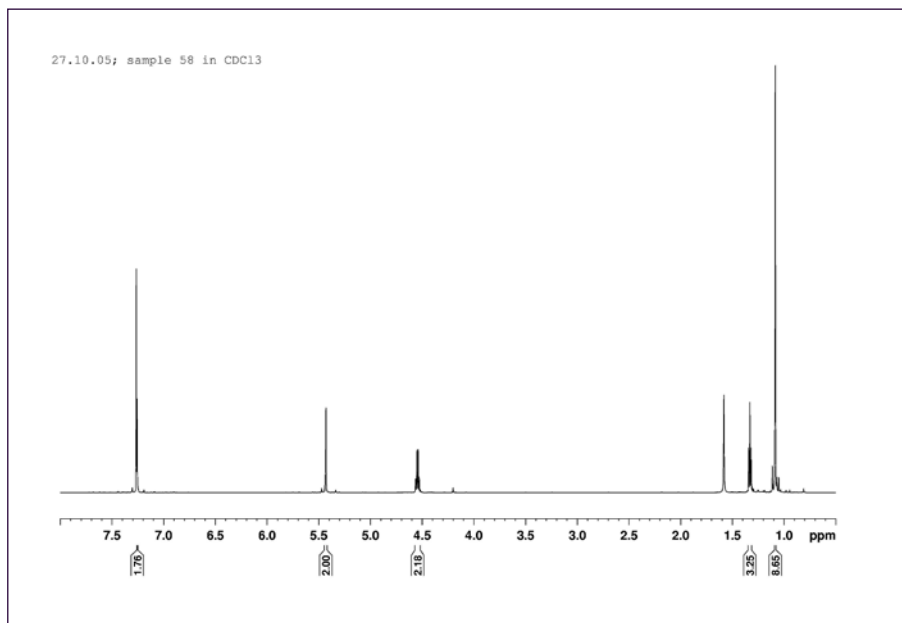
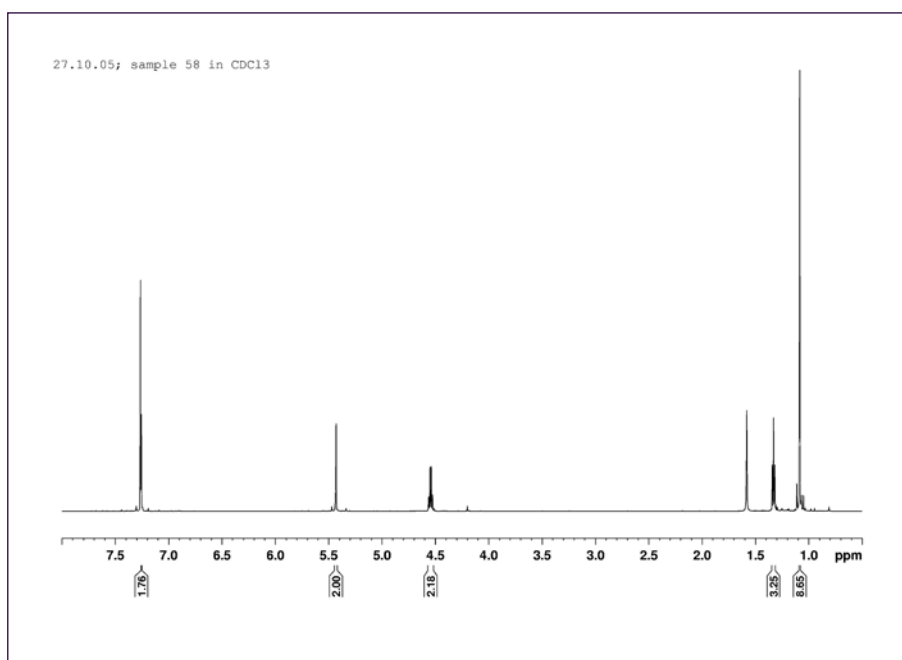
The ¹H NMR of the compounds 6a

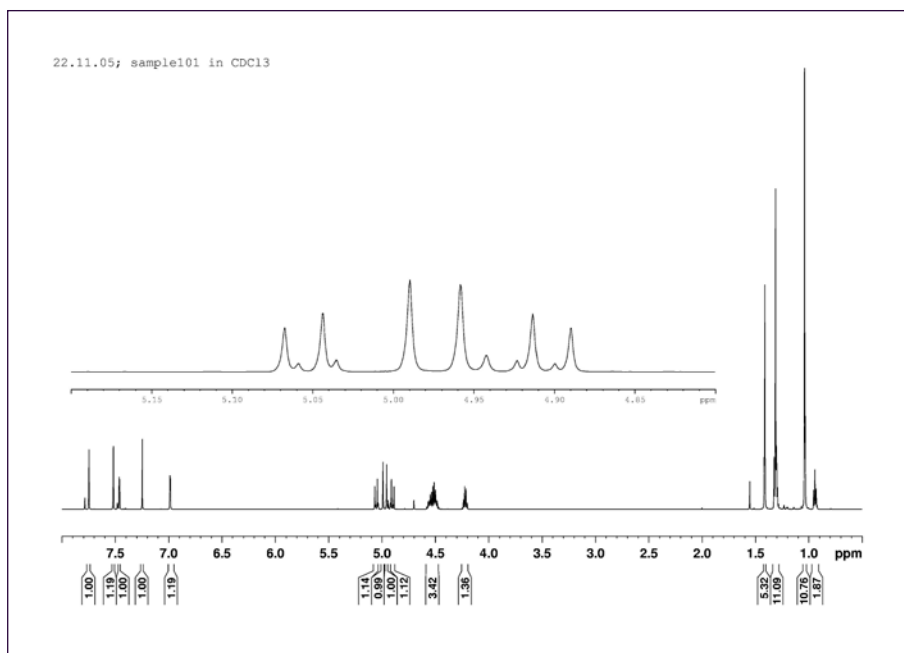


The ^1H NMR of the compounds 6bThe ^1H NMR of the compounds 5The ^1H NMR of the compounds 7a

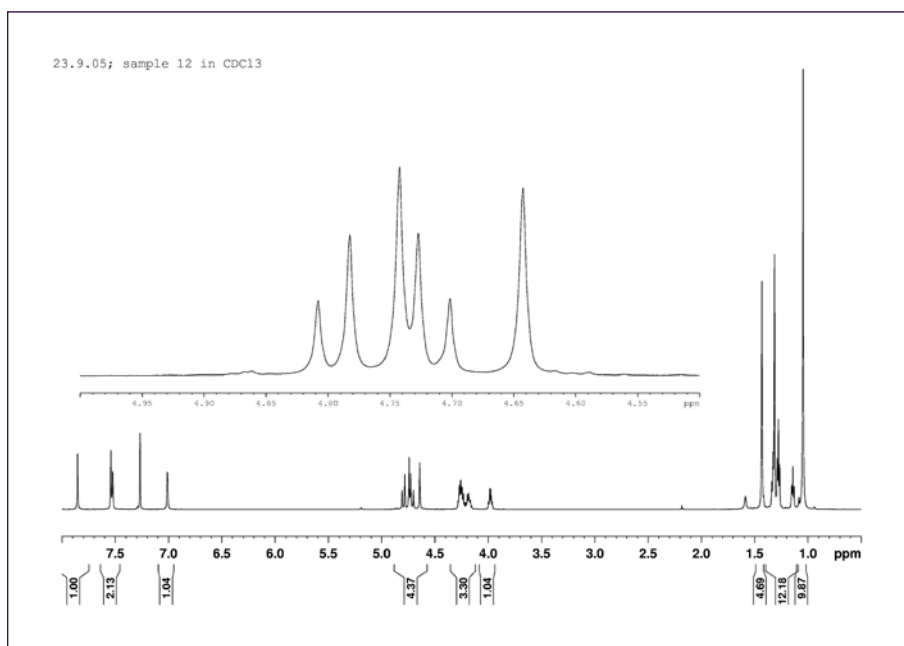


This is the ¹HNMR and X-ray of compound 1c

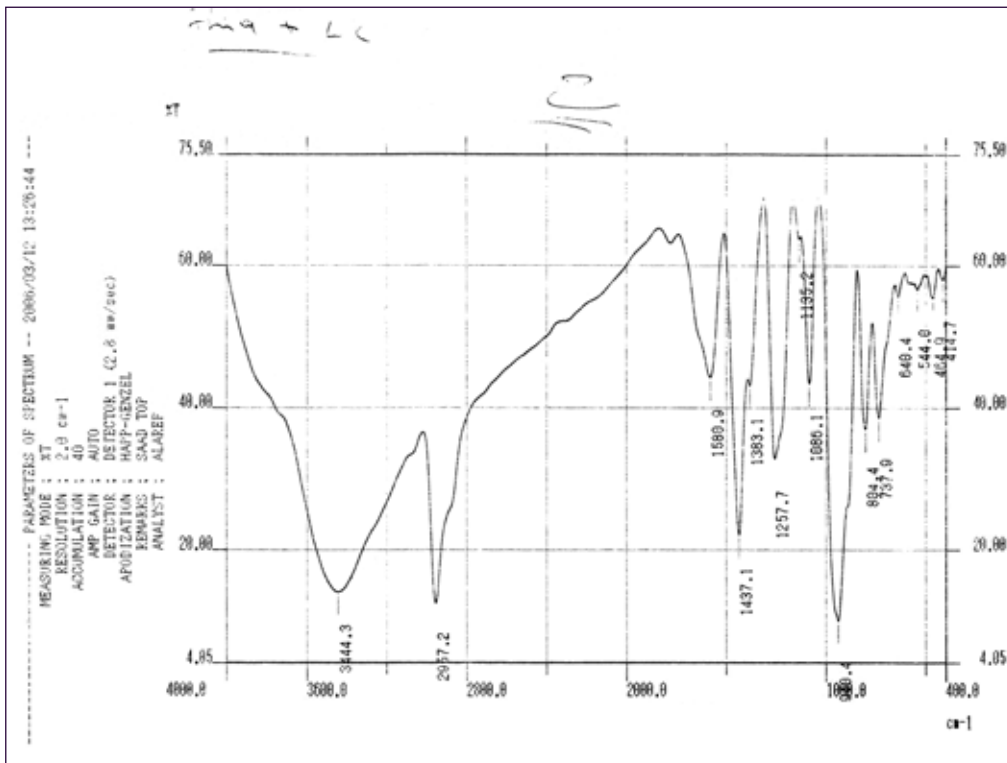
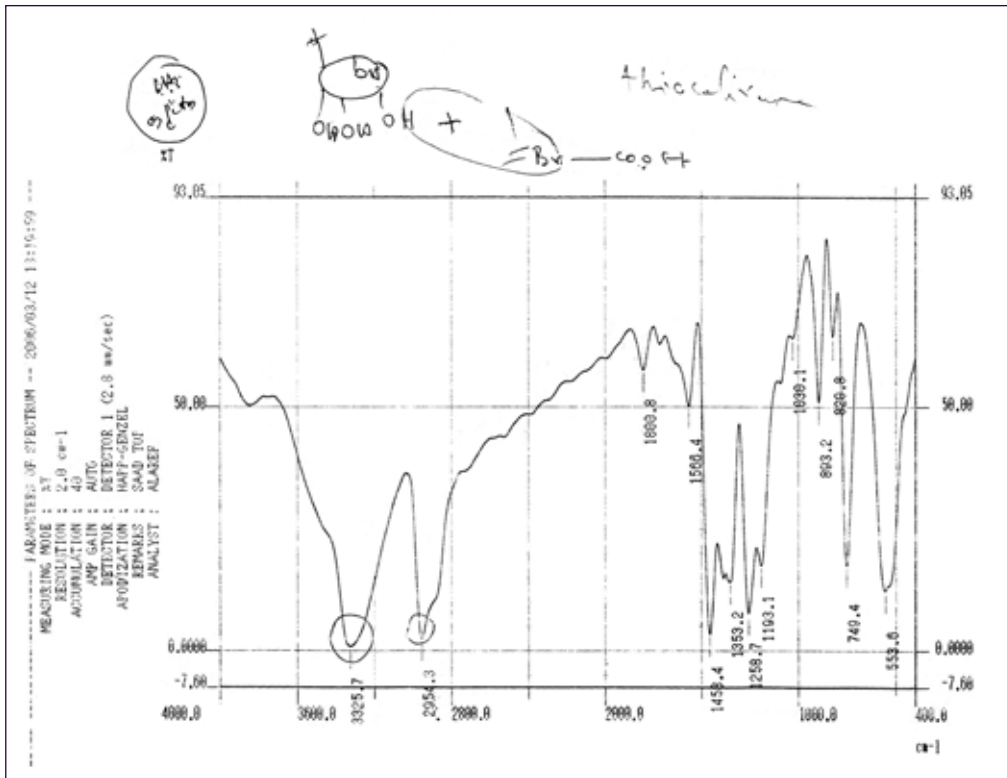
This is the ¹H NMR of compound 1aThis is the ¹H NMR of compound 2a

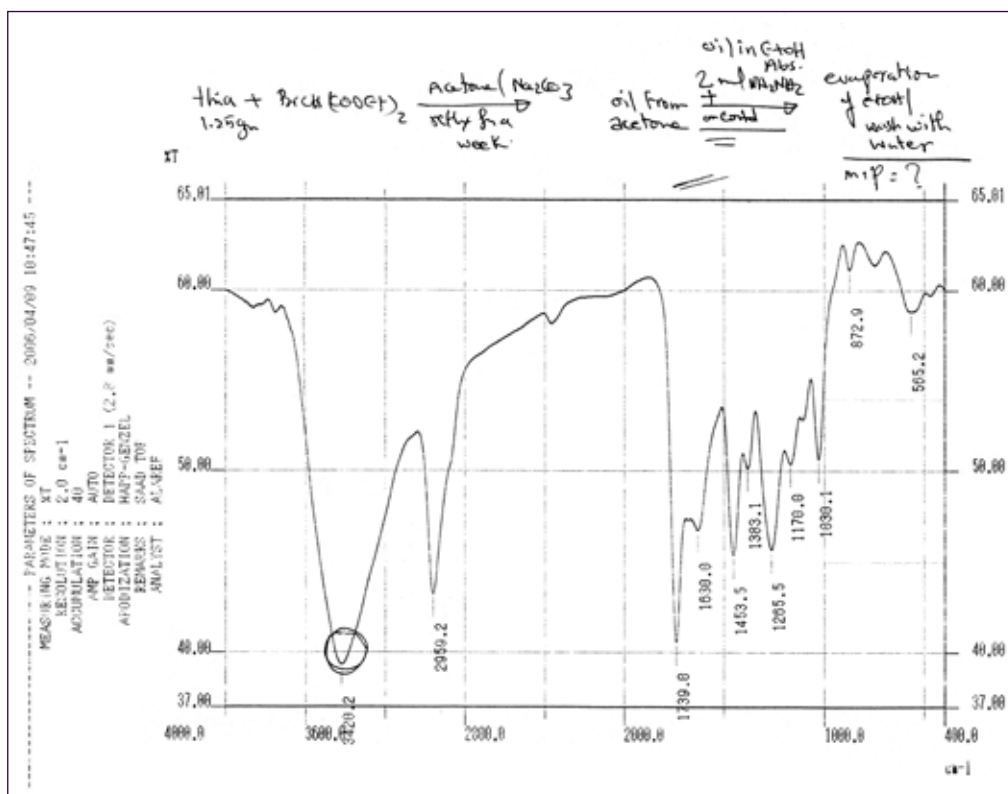
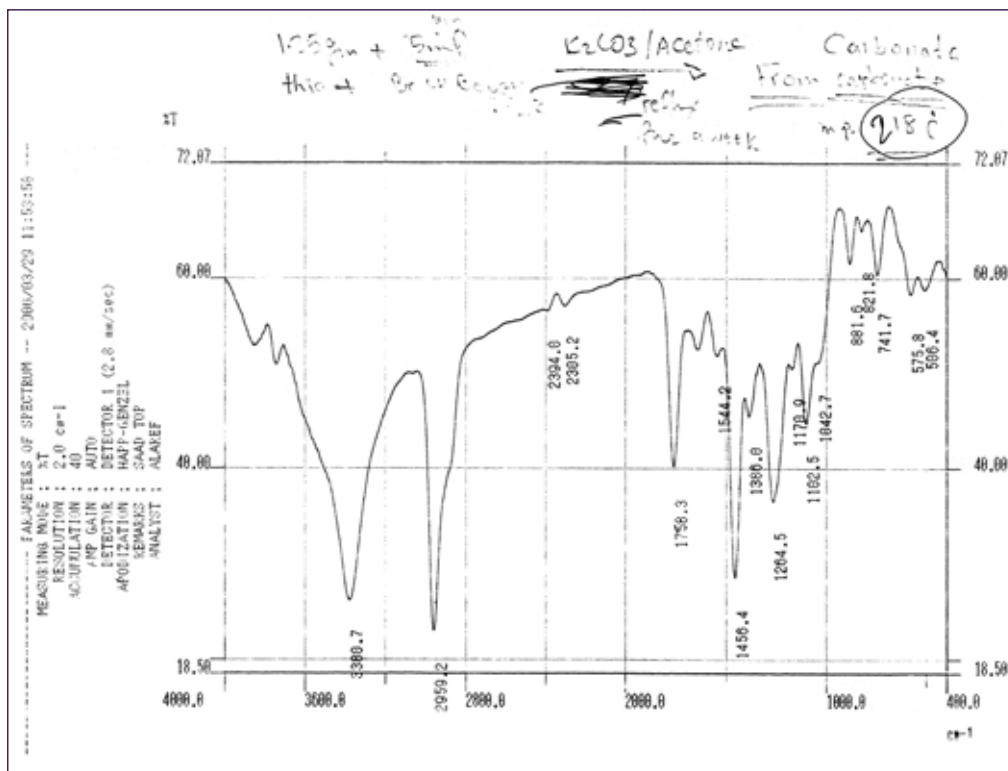


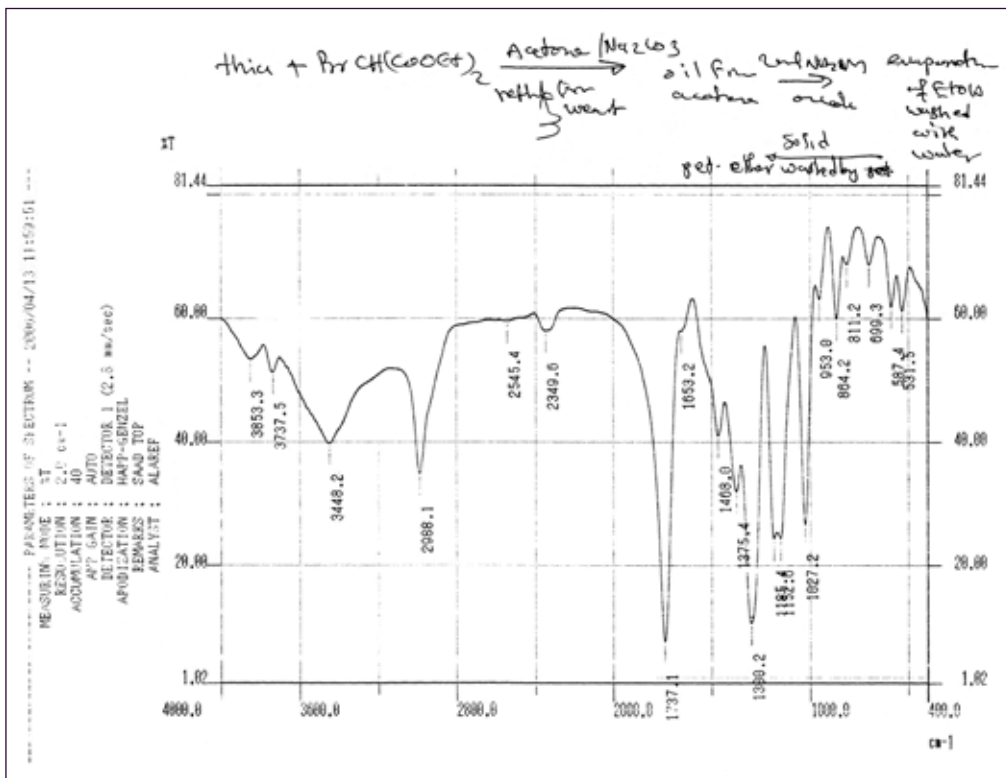
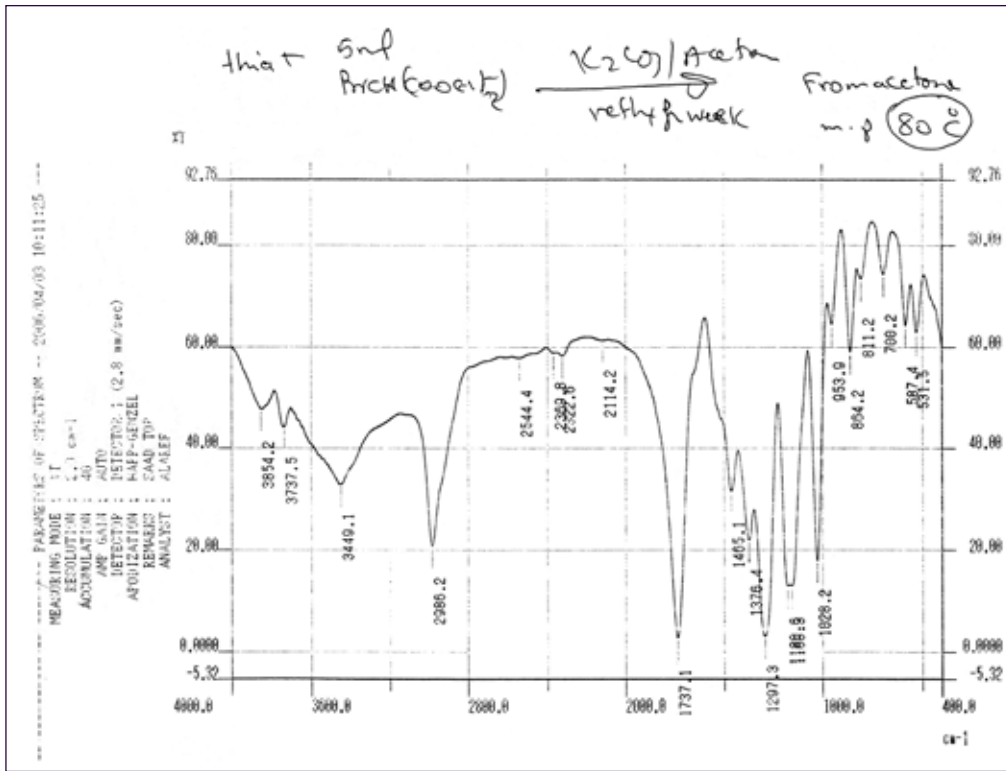
This is the ^1H NMR of compound 1b

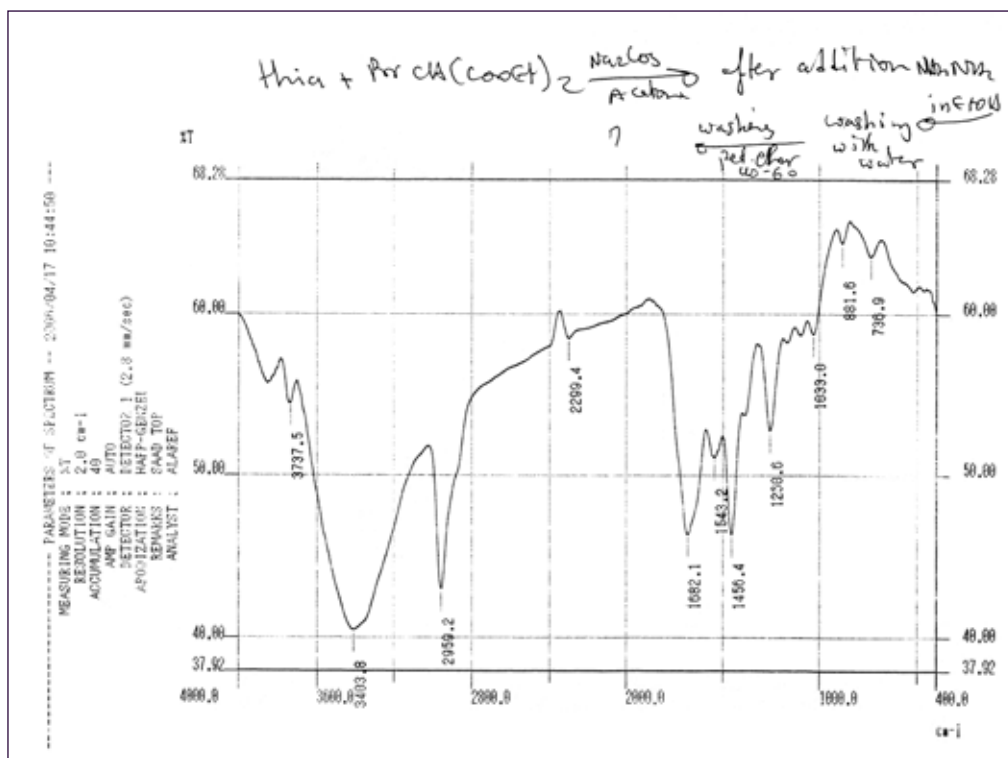


This is the ^1H NMR of compound 2b













Engineering Sciences



Ahmed Hassan Ghallab

Assistant professor at the Faculty of Engineering, Ain Shams University, Cairo, Egypt.

In June 1991, he graduated with a distinct degree, and has a considerable teaching experience as he lectured and demonstrated in a number of universities in Egypt and at the University of Leeds in the honor from the University of Ain Shams.

Four years later, in 1995, he obtained his Master's degree from the University of Ain Shams, and in 2001 he obtained his PhD from the University of Leeds, Leeds, West Yorkshire, England.

Apart from teaching, he has been involved in many different projects around Egypt that gained him more experience, in the field of concrete.

In 2004, he won the BA/CSSP Research Grants and he covered a full research on '*Strengthening Concrete Beams Using FRP as External Tendons*'.

Flexural Behavior of Externally Prestressed Continuous Concrete Beams

Ahmed Hassan Ghallab

Faculty of Engineering, Ain Shams University, Cairo, Egypt

ABSTRACT

Many bridges in the world are considered deficient and in need of rehabilitation or replacement. Some of them are deficient because their load-carrying capacity is inadequate for today's increased traffic load. To improve their efficiency and increase their load capacity, several methods can be used; one of them is the External Prestressing. In order to avoid corrosion problem that face this type of strengthening, Fiber Reinforced Plastics (FRP) can be used instead of steel tendons. Within the different types of FRP, Parafil rope was established to be well suited for the prestressing system, combining the benefits of light-weight, high strength, easy handling and efficient anchorage system. Nine continuous reinforced concrete beams, one with an ordinary steel reinforcement only and the rest with strengthened externally using Parafil Ropes Type G, were tested up to failure. Five factors were studied to investigate their effect on the behavior of strengthened beams. These factors are the value of the external prestressing force and its eccentricity, loading pattern, tendon profile and deviator positions.

Analytical investigations were also conducted to propose simple equations that could be used in the analysis of this beam type, regarding its deflection and flexural strength with an acceptable accuracy. The study indicated that external prestressing using Parafil rope is a very powerful system for strengthening or rehabilitation of continuous reinforced concrete structures. Moreover, providing external prestressing force by a moderate amount improves the stiffness and both the cracking and ultimate flexural strength of continuous reinforced concrete beams without significant reduction in ductility. The modifications made to the methods used to calculate deflection and ultimate moment of reinforced concrete, generalised these methods. These methods, after modification, were found to give fairly accurate results. Furthermore, the suggested modification to the flexural strength calculation methods as well as the proposed method made the analysis of the externally strengthened continuous beams under ultimate loads less complicated and with reasonable accuracy.

1. Introduction

External prestressing method is considered as one of the efficient strengthening methods used to increase the capacity of structural members especially in flexure and shear. However, the lack of data regarding the behavior of external prestressed concrete beams especially at ultimate can be considered the main obstacle against wider use of this system. This is because the behavior of externally prestressed beams not only differs from that of ordinary bonded prestressed beams due to the lack of bond between tendons and concrete, but it is also different from that of internal unbonded prestressed concrete beams, due to the reduction in the effective depth of the tendons during loading.

To overcome the corrosion problem that appears when using external steel tendons and reduce or eliminate the maintenance cost of the structures, FRP started, during the last decade, to replace steel as external tendons due to its high corrosion resistance and high strength. This adds another difficulty during the analysis of the prestressed concrete beams strengthened using FRP tendons, as the behavior of beams strengthened

using FRP tendons may differ from those strengthened using steel tendons especially at ultimate. This is because of the lower elastic modulus and the linear stress-strain relationship till failure of FRP that can change the failure type of the beam and affect the increase of the tendons' stress.

Although several researches were carried out to study the behavior of the beams strengthened using unbonded or external steel tendons and examine the factors affecting it (Harajli, 1990. Harajli and Kanj, 1992; Chakrabarti, 1995; Naaman and Alkhairi, 1991 part 1 and 2), few studies were carried out to study the behavior of beams strengthened externally using FRP tendons (Aravinthan *et al.*, 1997; Ghallab 2001). In addition, these studies focused mainly on the determinate structures, simple beams, whereas the application of the external prestressing in strengthening continuous beams, which are commonly seen in practice, has not been adequately addressed, and a few researches were conducted for this purpose.

1.1 Objectives of the Present Investigation

The objectives of this investigation can be summarized as follows:

- Study experimentally the influence of the following factors on the behavior of reinforced continuous concrete beams after being externally strengthened using Parafil rope type G with particular attention to crack formation, camber and deflection, losses in tendon's eccentricity, variation in internal and external prestressing force, and cracking and ultimate strengths.
 - Value of external prestressing force
 - Effective depth of the external prestressing force
 - Loading pattern
 - Tendon profile
 - Location of deviators
- Obtain simple equations that can be used to calculate the cracking and ultimate strengths and are less complicated and time consuming.
- Modify some of the existing methods of deflection calculation to externally prestressed continuous beams.

1.2 Outline of the Report

For a better understanding of the behaviors of externally prestressed simple and continuous beams and the difference between them, a review of literature related to the external prestressing system, FRP and Parafil rope was carried out and is presented in chapter 2.

Chapter 3 is concerned with the manufacture and testing of the specimens. Material characteristics, test equipment and test procedure are all incorporated. The behavior of test specimens and the test results are presented in chapter 4.

Chapter 5 presents an extensive discussion of the test results as well as relations between some parameters. A brief literature review of the analytical methods used to calculate deflection and ultimate moment of bonded and unbonded prestressed concrete beams is presented in chapter 6, which is then extended to describe the behavior of the reinforced concrete continuous beams after being externally strengthened.

Finally, chapter 7 includes a synopsis of the main observations and conclusions obtained from the experimental and analytical works, and a number of suggestions for further research.

2. Literature Review

Introduction

External prestressing system and behavior of externally prestressed beams with steel and fiber reinforced plastics (FRP) tendons are discussed in this chapter. Several types of the commercial fiber reinforced plastics used in prestressing are also compared and their properties are discussed. Finally, the properties of Parafil rope and its anchorage are presented and discussed.

2.1 External Prestressing

External prestressing is the form of prestressing in which the prestressing tendons are unbonded and are outside the concrete section, and their load is transferred to the concrete through end anchorages and deviators as shown in Fig. 2.1. Bruggeling (1990) mentioned some reasons for the development of this type of prestressing:

1. The demand for methods to repair prestressed concrete bridges with corroded prestressing tendons or to strengthen concrete bridges or other structures already in use, due to the increase of traffic loads.
2. The need for less complicated profile of prestressing tendons in the concrete structures. Simplifying tendon profiles has its effect on the concreting of the structure, the stressing of the tendons (friction problem) and the grouting of ducts (interaction between adjacent ducts).
3. The growing interest in methods in which the influence of workmanship on the overall quality of the realized concrete structures is reduced.
4. The need to maintain and repair concrete structures, especially bridges, without harming the use of the structure, e.g. by closing off the traffic on the bridge or viaduct. In such cases, the use of external cables offers a very good solution.
5. New development in bridge design and construction results in the use of external cable.

2.2 Method and System of Strengthening

External prestressing can be considered as one of the most efficient methods for strengthening. It requires a minimum of demolition and has only a minor impact on the overall structure with significant improvement in strength. This extends the life span of the structure at a very reasonable cost. Various components constituting the system of external prestressing include



a. Outside the box



b. Inside a box section



c. Transversal and longitudinal external prestressing for the reinforcement of the Raba bridge a Sarvar (Hungary) (Freyssinet, 2009)



d. Silos strengthened with external prestressing in Brej (PL) (Freyssinet, 2009)

Figure 2.1 External prestressing tendons layout

2.2.1 Tendons

Several types of tendons can be used to strengthen concrete members such as: steel, Carbon Fiber-reinforced plastic (CFRP), Aramid Fiber-reinforced plastics (AFRP), or Glass Fiber-reinforced plastics (GFRP), etc.

The main requirements of Reinforcement for Prestressed Concrete are:

- High tensile strength: Reinforcement used in prestressed concrete must have high tensile strength to enable it to counterbalance the high creep and shrinkage losses in concrete and have adequate residual stress to sustain the required prestressing force.
- Low relaxation: Stress relaxation in prestressing tendon is the loss of prestress when the wires or strands are subjected to essentially constant strain; so the smaller the relaxation, the higher the effective prestressing.
- High resistance to corrosion and deterioration of strands: Corrosion decreases the cross-sectional area of the tendon and hence increases the applied stress. This stress can increase becoming higher than the nominal strength of the tendons which leads to

premature failure of the tendons and failure of the structural system.

- Modulus of elasticity (Young's modulus): High modulus is needed to limit the extension of material during stressing, whereas the low modulus reduces losses due to creep and shrinkage of the concrete. During prestressing, the extension of tendons can be managed so using lower modulus will be an advantage.

The tendons mostly used for prestressing are:

2.2.1.1 Steel Tendons

There are three main types of tendons used in prestressed concrete: wires, strands (made of several wires), and bars. Fig. 2.2 shows typical stress-strain curves for prestressing steel compared with reinforcing steel. In prestressing steel, the yielding point is not well defined and because of this, the yield strength is determined according to strain criteria. There are different equations according to the building codes. Theoretically, the proportional limit is fixed to the point in which the stress-strain curve deviates from the linear trend; usually the proportional limit is determined by the stress corresponding to

a residual of 0.01%. The elasticity modulus of steel is essentially a constant, independent from strength.

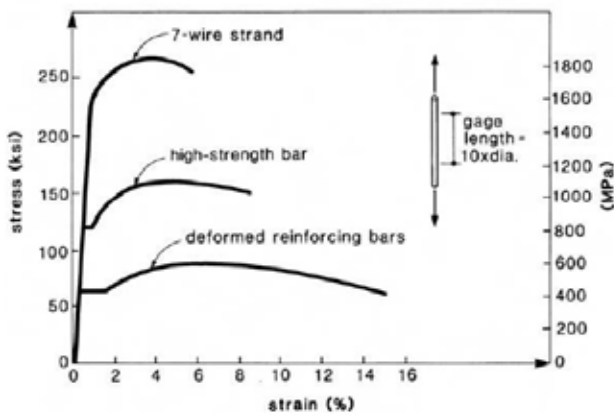


Figure 2.2 Stress-strain curves, (Collins and Mitchell 1991)

However, this modulus is smaller for the strands which are made with several wires.

The prestressing steel is more sensitive to corrosion than reinforcement steel bars (Collins and Mitchell 1991). This is because the diameter of tendons is relatively small and high-grade steel is more susceptible to corrosion compared to ordinary reinforcement steel. Even a small uniform corrosive layer or a corroded spot can substantially reduce the cross-sectional area of the steel. The exposition of unprotected steels to the environments, even for a few months, can produce a larger reduction of mechanical properties and of fatigue life. If unbounded tendons are used, they must be protected by anti-corrosive material such as asphalt, grease, oil or a combination of grease and plastic tubing.

2.2.1.2 FRP Tendons

Using steel as external prestressing tendons increases the chance of corrosion. This problem can be overcome by using fiber reinforced composites instead of steel as the external prestressing tendons. Composite materials typically consist of fibers and a matrix material. Several high strength fibers exist for possible use as non-metallic tendons in prestressed structures. The most popular fibers used for prestressing tendons are glass, aramid and carbon fibers. The selection of the fiber is primarily based on consideration of cost, strength, rigidity, and long-term stability. The fibers may be used individually, as rope (e.g. Parafil rope), or encased in a resin such as epoxy to form bars. The physical performance of the fiber reinforced composite depends on several factors such as fiber type, matrix type, adhesion between the fiber and the matrix, manufacturing techniques, etc.

The following are the most common types of FRP tendons used in prestressed concrete:

Glass Fibers (GFRP)

Glass fibers are the most common of all reinforcing fibers for FRP. Three main types of glass fibers are gen-

erally used: E-glass, which was developed for electrical applications; S-glass, which was developed for structural applications;

Z-glass with high resistance to alkalis. Young's modulus of glass fiber ranges between 72 and 85 GPa whereas its tensile strength ranges between 3400–4580 MPa (Vaughan, 1998).

Carbon Fibers (CFRP)

The production of commercial carbon fibers begins with organic precursors such as rayon, Polyacrylonitrile (PAN), isotropic and liquid crystalline pitches.

Depending on variables such as precursor heat treatment and degree of stretch during processing, the strength and elastic constants of carbon fibers can vary greatly (Bakis, 1993). Young's modulus of carbon fiber ranges between 230 and 830 GPa while its tensile strength ranges between 2200 and 5650 MPa (Lafdi and Wright, 1998). Carbon fibers, in general, are not affected by moisture, atmosphere, solvents, bases or weak acids at room temperature.

Aramid Fibers (AFRP)

Aramid is a generic term for 'Aromatic Polyamide Fibers'. Aramid is an organic, man-made fiber with a high degree of crystallinity. Aramid fibers have a highly anisotropic structure that leads to low longitudinal shear modulus, poor transverse properties, and low axial compressive strength. In addition, the interfacial bond strength between aramid fibers and epoxy resins is normally lower than experienced with carbon fiber composites (Jang, 1994). However, aramid has high fatigue resistance, static and dynamic, high specific strength, toughness and creep resistance combined with moderate cost. Young's modulus of aramid fiber range between 54 and 143 GPa while its tensile strength ranges between 2900 and 4590 MPa (Clements, 1998).

Fig. 2.3 shows typical stress-strain relationships for different types of FRP and high tensile steel whereas Table 2.1 shows a comparison between their properties.

It should be noted that when comparing the several commercial FRP bars with prestressing steel, the ratio of fiber volume must be taken into consideration.

Advantages of Fiber Reinforced Plastics (FRP) Compared to Steel (Arnold *et al.*, 1991; Erik and Rizkalla, 1993; Meier, 2000)

- High ratio of strength to mass density (10 to 15 times greater than steel).
- FRP reinforcement generally has a mass only one-seventh to one-fifth of steel reinforcement of equivalent diameter. The reduced dead weight of the deck allows the bridge to carry an increased traffic load.
- Carbon and aramid fibers have excellent fatigue characteristics.

- Excellent corrosion resistance and electromagnetic neutrality.
- Low axial coefficient of thermal expansion, especially for carbon fiber reinforced composite materials.

Disadvantages of FRP Reinforcement (Erki and Rizkalla, 1993)

- Higher cost than steel.
- Low modulus of elasticity when used in ordinary reinforced beams.
- Low failure strain.
- Special attention must be paid to anchorages when FRP reinforcement is used for prestressing.
- Long-term strength of FRP reinforcement can be lower than short-term static strength (e.g. the long-term strength of GFRP is approximately 70% of its short-term strength)
- Ultra-violet radiation can deteriorate FRP rods, but that is easily resolved by adding pigments to the polymer when it is constructed.

- Aramid fibers can deteriorate due to water absorption.
- The low durability in acidic or alkaline environments.

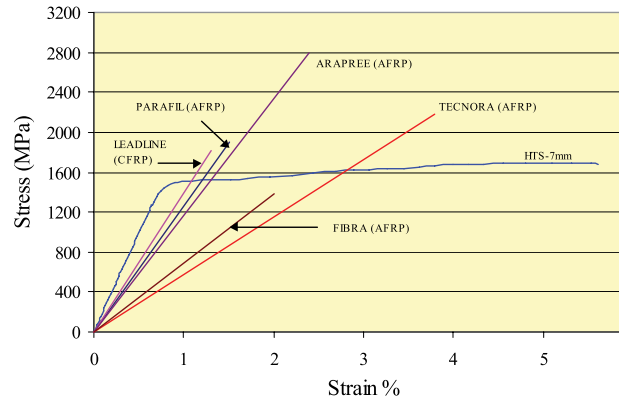


Figure 2.3 Stress-Strain curves of different types of FRP

Table 2.1 Comparison between GFRP, AFRP and CFRP

| Factor | GFRP | AFRP | CFRP |
|---|--|--|--|
| Types | <ul style="list-style-type: none"> • E-glass (good strength, electrical and weathering properties) • S-glass (more expensive than E-glass, but has a higher strength, Young's modulus and temperature resistance) • S-2 as S-glass but with different coating • T-glass (has higher strength, higher modulus, higher heat resistance and less thermal coefficient than E-glass, also has improved impact strength and electrical properties and improved thermal and chemical resistance) • R-glass (has higher tensile strength and modulus relative to E-glass, and gives beneficial results with higher resistance to fatigue, ageing, temperature and corrosion) | <ul style="list-style-type: none"> • Arapree: are fabricated from high modulus Twaron fibres with epoxy resin. • FIBRA: aramid fibres with flexible/ elastomeric and rigid resins. • Technora: are made from Poly-Para-phenylene-3, 4-Oxidiphenylene Terephthalamide (PPODTA) fibres and vinyl ester resin. | <ul style="list-style-type: none"> • Leadline: are pultruded using unidirectional carbon fibres at 65% fibre volume fraction with an epoxy resin • Carbon Fibre Composite Cable (CFCC): are made from PAN based carbon fibre in epoxy or bismaimide resins • Nippon Steel Advanced Carbon Fibre Composite (NACC): is made using both PAN and Pitch based carbon fibers. |
| Tensile strength | • 0.55–1.67 GPa | <ul style="list-style-type: none"> • Arapree: 2.8–3 GPa • FIBRA: 1.39 GPa • Technora: 2.18 GPa | <ul style="list-style-type: none"> • Leadline: 1.78–1.83 GPa • CFCC: 1.8 GPa • NACC: 0.79–2.02 GPa |
| Modulus of elasticity in longitudinal direction | <ul style="list-style-type: none"> • 41–55 GPa (approximately 25% of that of the steel). • The properties of glass fibres are isotropic. Thus, the axial and transverse modulus of elasticity are the same | <ul style="list-style-type: none"> • Arapree: 125–130 GPa • FIBRA: 68.6 GPa • Technora: 54 GPa • Properties are anisotropic | <ul style="list-style-type: none"> • Leadline: 147 GPa • CFCC: 137 GPa • NACC: 118–206 GPa • Properties are anisotropic |
| Ultimate strain % | • 3–5.5% | <ul style="list-style-type: none"> • Arapree: 2.4% • FIBRA: 2% • Technora: 3.8% | <ul style="list-style-type: none"> • Leadline: 1.5–1.7% • CFCC: 1.6% • 0.3 HM–2.0 LM |

| Factor | GFRP | AFRP | CFRP |
|--|--|--|---|
| Creep | <ul style="list-style-type: none"> Glass fibres have excellent resistance to creep. Creep rupture diminishes if (P sustained/P short term) 60% | <ul style="list-style-type: none"> Has lower creep resistance than steel, GFRP and CFRP | <ul style="list-style-type: none"> Has high resistance to creep (at 1000 hrs creep strain 0.006%) |
| Relaxation | <ul style="list-style-type: none"> Has a good resistance to relaxation (better than steel, but less than carbon) | <ul style="list-style-type: none"> Lower resistance to relaxation than steel. | <ul style="list-style-type: none"> Has an excellent resistance to relaxation |
| Fatigue (Dynamic behaviour) | <ul style="list-style-type: none"> GFRP's fatigue strength is lower than that of steel. GFRP bars do not fatigue when stressed to no more than 50% of their ultimate strength | <ul style="list-style-type: none"> AFRP has an excellent fatigue strength | <ul style="list-style-type: none"> CFRP has better fatigue strength than that of steel. |
| Transverse Shear strength | <ul style="list-style-type: none"> quite low in comparison with their longitudinal properties | | |
| Coefficient of Thermal Expansion (CTE) in the longitudinal direction | <ul style="list-style-type: none"> 6–12×10⁻⁶/°C | <ul style="list-style-type: none"> Arapree: 1.8×10⁻⁶/°C FIBRA: -5.2×10⁻⁶/°C Technora: -3×10⁻⁶/°C | <ul style="list-style-type: none"> Carbon fibre has low longitudinal and transverse CTE b 0.6×10⁻⁶/°C |
| Specific gravity (SG) t/m ³ | <ul style="list-style-type: none"> (1.5–2.0) | <ul style="list-style-type: none"> (1–1.5) | <ul style="list-style-type: none"> (1.5–2.2) |
| Effect of humid Environment | <ul style="list-style-type: none"> Glass fibres do not absorb water | <ul style="list-style-type: none"> Aramid fibres absorb water and can be deteriorated due to water absorption. | <ul style="list-style-type: none"> Carbon fibres have excellent moisture resistance |
| Magnetic permeability | <ul style="list-style-type: none"> Electro-magnetic neutrality. | <ul style="list-style-type: none"> As GFRP | <ul style="list-style-type: none"> Less than steel strand |
| Chemical attack | <ul style="list-style-type: none"> GFRP bars have high resistance to acids GFRP bars can deteriorate rapidly in an alkaline environment. | <ul style="list-style-type: none"> AFRP has excellent resistance to chlorides Due to chemical attack, AFRP strength (after 100 years) b 85% of the initial strength. | <ul style="list-style-type: none"> Carbon fibres exhibit a good resistance to both highly acid and highly alkaline environments. |
| Impact resistance | <ul style="list-style-type: none"> Less than AFRP | <ul style="list-style-type: none"> Has excellent impact resistance | <ul style="list-style-type: none"> Carbon fibres have a low impact resistance due to their low ultimate strain |
| Electrical conductivity | <ul style="list-style-type: none"> GFRP bars have excellent electrical insulating properties. | <ul style="list-style-type: none"> As GFRP | <ul style="list-style-type: none"> Can be highly conductive to electricity |
| Ultraviolet (UV) effect | <ul style="list-style-type: none"> Almost no deterioration | <ul style="list-style-type: none"> Aramid fibers are strong UV absorbers and deteriorate when exposed to ultraviolet light. | <ul style="list-style-type: none"> Almost no deterioration |
| Fracture | <ul style="list-style-type: none"> Almost completely brittle and fracture without any reduction in cross-sectional area. | <ul style="list-style-type: none"> Aramid fibres fracture in ductile manner, although the overall strain to failure is still small | <ul style="list-style-type: none"> As GF |
| Workability | <ul style="list-style-type: none"> Using thermosetting resins, bars cannot bend sharply (90° or 180°) in the field Can be cut easily in the field with portable saw | <ul style="list-style-type: none"> AFRP reinforcement made in the form of rods, tendons and ropes | <ul style="list-style-type: none"> CFRP reinforcement made in the form of rods, tendons and ropes |
| Cost | <ul style="list-style-type: none"> Some types are cheaper than steel | <ul style="list-style-type: none"> Higher than steel | <ul style="list-style-type: none"> Higher than aramid fibres |

* Clements, 1998. Karbhari, 1998. Vaughan, 1998.

2.2.2 Ducts and Tendon Geometry

The ducts form straight-line connections between the various 'fixed points' (anchorage and deviators) and are used to protect the tendons from environmental attack or vandalism. For steel tendons, high density polyethylene sheaths are suitable as ducts, due to their high resistance to atmospheric effects (Manjure, 1996).

2.2.3 Deviators

Deviators are provided for the geometric requirements of the tendon and to accommodate the considerable force imposed by change in direction, and to maintain the eccentricity of the tendon under ultimate bending conditions (McKenna and Chan, 1996). At deviation points, it is beneficial to provide a radius as large as possible. Excessively small radii of curvature should be avoided (Manjure, 1996).

To avoid unacceptable vibrations of the external tendons, the free length of the external tendons should be limited; a maximum distance of 7–8m between two deviation points of a tendon has been recommended (Bruggeling, 1990). To avoid second order effect due to beam deflection between the fixing points, BD58/94 (1995) suggested that the distance between the fixing points should not exceed 12 times the minimum depth of the beam. If the spacing between points where the tendons are held in position laterally exceeds 12m, checks shall be made to ensure that the first natural frequency of the tendons vibrating between fixing points is not in the range 0.8 to 1.2 times that of the bridge.

In order to reduce the stress concentration due to bending of the prestressing tendon at the deviators, BD58/94 (1995) suggested that the radius of curvature of tendons in the deviators is not less than 5 times the tendon diameter for wire, or 10 times the diameter for strand. The total angle of deflection should not exceed 15°. The deviators through which the tendons pass nominally straight are required to maintain the eccentricity of the tendon under ultimate bending conditions. The design forces on them are calculated by consideration of the angular change that will occur at failure of the beam as a whole (McKenna and Chan, 1996).

2.2.4 Anchorages and Diaphragms

Anchorage are used to transfer the tendon forces to the structure. Different types can be used depending on the type and number of tendons used in the prestressing. Fig. 2.4 shows the steel anchorages, while Fig. 2.5 shows anchorages of FRP. The difference between the

steel anchorages and the FRP anchorages are related to the difference in their properties.

Diaphragms are generally provided to transfer the imposed loads onto the bearing, and transfer the prestressing forces to the structure.

2.2.5 The Protection System

The external tendons, as they are located outside the concrete section, are more susceptible to atmospheric conditions than the internal tendons embedded in the concrete. To protect the tendons, outer ducts filled with protective material should be used. For steel tendons, these ducts should fulfil the following requirements (Bruggeling, 1990):

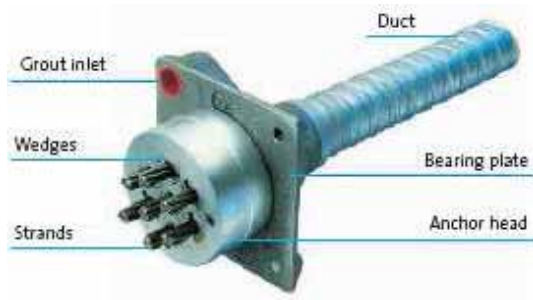
- Resistance against environmental attack, to provide a corrosion protection to the prestressing steel over the whole length.
- Waterproof.
- Compatibility with prestressing steel and its corrosion protection.
- Resistance against damage during construction and installation.
- Resistance against damage in service.
- Fireproof in cases where fire cannot be excluded.
- Controlled creep behavior of the materials of the duct.
- Resistance against transverse forces (deviations).
- Replaceability.

In case of external prestressing, grouting the external cables is easier to control because the ducts can be simply inspected as they are accessible. If some defects are determined they

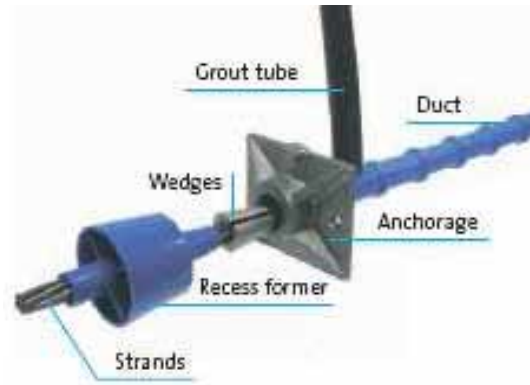
can be repaired because small holes can be drilled in the ducts to add new grout. The ducts used to protect steel tendons are commonly from steel with an internal cable sheathing made of polyethylene (Bruggeling, 1990).

For steel, several materials can be used to protect the tendons, such as cement grout, grease, wax, bitumen or plastics by injection in the ducts.

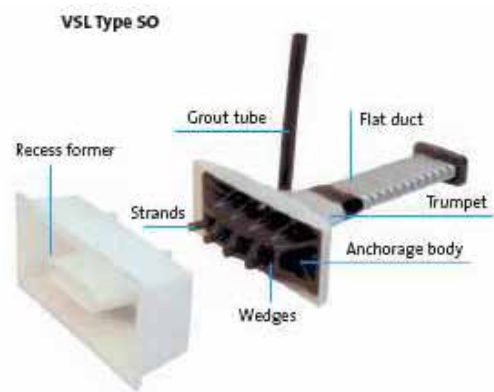
Experience has shown that the grouting of prestressing cables needs great care if later damage is to be avoided (Eibl, 1990). However, due to previous failure regarding external prestressing tendons protected by cement grout in contact with the tensile elements in France over the last few years, this type of protection is in fact no longer used for external prestressing tendons (Sétra and LCPC, 2008). The requirements of the protective sheath can be reduced when using FRP tendons due to their high resistance to corrosion.



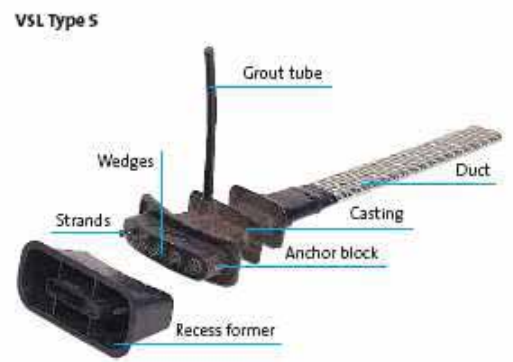
a Multi strands anchorage



b Single strand anchorage



c Several strands anchorage



d Bar system

Figure 2.4 Typical anchorages used in various steel prestressing systems (VSL, 2006)



Figure 2.5 Anchor components for different FRP tendons (Nanni et al, 1996)

2.2.6 Losses in Post Tensioned Prestressing

The loss of stress in external prestressing tendons is less than that in internal prestressing tendons, as friction will be, for external tendons, at the deviator, while being for internal tendons, along the tendon length accompanied by warping effect if the tendons are not straight. Table 2.2 shows the types of losses in both external and internal prestressing tendons and its stage of occurrence.

2.2.7 Advantages of External Prestressing

Compared to internal bonded post-tensioning, the external prestressing has the following distinct advantages (Structural System, 2009):

- a. The application of external prestressing can be combined with a broad range of construction materials such as steel, timber, concrete, composite structures and plastic materials. This can considerably widen the scope of the post-tensioning applications.
- b. Due to the location and accessibility of the tendons, monitoring and maintenance can be readily carried out compared to internal, bonded prestressing.

Table 2.2 Types and stage of occurrence of losses in external and internal prestressing tendons

| Type of prestress loss | Stage of occurrence | |
|--------------------------------|-----------------------|-----------------------|
| | Internal prestressing | External prestressing |
| Elastic shortening of concrete | At sequential jacking | At sequential jacking |
| Shrinkage of Concrete | After transfer | After transfer |
| Creep of Concrete | After transfer | After transfer |
| Relaxation of Tendons | After transfer | After transfer |
| Friction | At jacking* | At jacking** |
| Anchorage seating loss | At jacking | At jacking |

* (location: at deviator points and along the length of duct tube)

** (location at deviator points)

- c. Due to the absence of bond, it is possible to restress, destress and exchange any external prestressing cable, provided that the structural detailing allows for these actions.
- d. Improvement of the concrete placing due to the absence of tendons in the webs.

- e. Improvement of conditions for tendon installation which can take place independently from the concrete works.
- f. Reduction of friction losses, because the unintentional angular changes, known as wobble, are practically eliminated. Moreover, with the use of a polyethylene sheathing, the friction coefficient is drastically reduced compared to internal bonded prestressing using corrugated metal ducts.
- g. External prestressing tendons can easily (and without major cost implication) be designed to be replaceable, de-stressable and re-stressable.
- h. Generally, the webs can be made thinner, resulting in an overall lighter structure.
- i. Strengthening capabilities.
- j. Higher effective depth of prestressing tendons can be used.

As a result, better concrete quality can be obtained leading to a more durable structure.

2.2.8 Disadvantages of External Prestressing

Although external prestressing method has several advantages, it also has some disadvantages (Picard et al. 1995):

- a. External tendons are more accessible than internal ones and consequently, are more vulnerable to sabotage and fire.
- b. External tendons are subjected to vibrations and therefore, their free length should be limited.
- c. Deviation and anchorage zones are cumbersome additions to the cross section. These elements must be designed to support large longitudinal and transverse forces.
- d. In the deviation zones, high transverse pressure acts on the prestressing steel. The saddles inside the deviation zones should be precisely installed to reduce friction as much as possible and to avoid damage to the prestressing steel.
- e. In the case of internal grouted tendons, the long-term failure of anchor heads has limited consequences because prestressing may be transferred to the structure by bond. In the case of external tendons, the behavior of anchor heads is much more critical. Therefore, anchor heads should be carefully protected against corrosion.
- f. At ultimate limit states, the contribution of external tendons to flexural strength is reduced compared to internal grouted tendons. The stress variation between the cracking load and ultimate load cannot be evaluated at the critical section only, as is done for internal bonded tendons.
- g. At ultimate limit states, failure with little warning due to insufficient ductility is a major concern for externally prestressed structures.

2.3 Typical Applications for External Prestressing

Typical applications where external tendons are feasible, practical and economical are:

- Repair work and strengthening of all kinds of structures.
- Precast segmental construction.
- Simple and continuous spans.
- Under slung structures.
- Incremental launching procedure, in particular concentric prestressing.

2.4 Behavior of Externally Prestressed Simple Beam

The behavior of an externally prestressed beam not only is different from that of an internally bonded prestressed beam, due to lack of bond between the external tendons and the concrete, but is also different from that of an unbonded prestressed beam with internal tendons, due to the reduction in the tendon eccentricity especially at ultimate. However, the behavior of externally prestressed beams, prior to cracking, is similar to that of beams with conventional bonded tendons. While after cracking and as the load is increased, there is a tendency for one crack to open more than the others, which eventually leads to failure.

Thus, at failure, the externally prestressed beam can be analyzed by assuming that the beam consists of a pair of rigid blocks, with all the rotation concentrated in a single hinge at the center (Burgoyne et al. 1996).

Harajli (1993) made a comparison between the behavior of externally prestressed concrete beams and internally unbonded prestressed concrete beams. Harajli reported that in the case of a small area of prestressing tendon, the maximum moment strength of a prestressed beam with exterior cables is much less than that of interior cables. This is because the beam obtains a large deflection capacity, as the area of tension reinforcement is small. Moreover, the rotation of the beam, as the load increased, causes the tendon to move relative to the compression flange, thus reducing the lever arm of the tendon and lowering the load capacity of the beam. Final failure was caused by explosive failure of the concrete in the compression zone, leading to complete collapse of the structure. (Burgoyne *et al.* 1996. Clark and Toms, 1996).

After cracking and as failure approaches, the strain in unbonded tendons increases, but the increase is constant over the tendon length, or at least over the distance between deviators as shown in Fig. 2.6. This strain is less than that of bonded tendons and is less likely to reach yield. The lack of yield at failure means that the prestress in the tendons as well as the strength of the tendons has a significant effect on the strength of

the structure, so a partial safety factor should be applied to the prestress (Jackson, 1996).

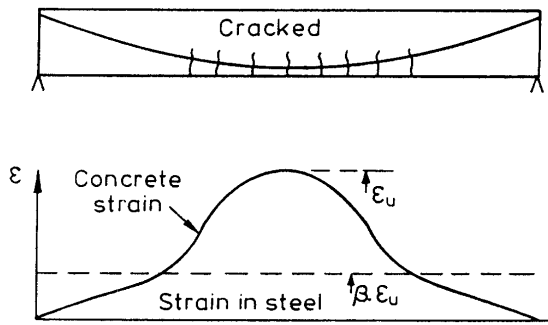


Figure 2.6 Strains in a cracked beam with an unbonded tendon

Yaginuma and Kitada (1988) studied the effect of (span/depth) ratio on the behavior of externally prestressed beams. Yaginuma and Kitada reported that for prestressed concrete beams with external tendons, the deflections up to maximum moment are similar to those of prestressed concrete beams with internal tendons regardless of supporting points (deviators) when (L/d) is small. However, when (L/d) is larger, the bending moment in externally prestressed concrete beams without supporting points tends to decrease greatly at all stages after the onset of cracking in comparison with other prestressed concrete beams.

Tan and Ng (1997) compared the behavior of externally prestressed concrete beam with draped tendons and identical beam with straight tendons, and they concluded that the beam with draped tendons has less stiffness, wider spread of cracks, greater tendon stress and more ductility at failure.

2.4.1 Effect of Loss of Tendon Eccentricity and Tendon Profile

The difference between the behavior of externally prestressed concrete beams and internally unbonded prestressed concrete beams, as mentioned before, is mainly caused by the secondary effect, namely 'Loss of tendon's eccentricity', induced by the large deflection of beam under bending load as shown in Fig. 2.7. An externally prestressed concrete beam with a large distance between deviators gives a significantly lower flexural strength than that of internal unbonded prestressed concrete beam. (Matupayont *et al.*, 1994)

An externally prestressed beam with a straight horizontal tendon profile is relatively less effective in increasing the flexural resistance as compared to a deviated profile, because of the progressive reduction of the depth of the straight external tendons with increasing member deformation as failure is approached (Harajli, 1993; Yaginuma and Kitada, 1988). In addition, tests carried out by Tan and Ng (1997) on beams with straight tendons and a span-depth ratio of 15 indicated that the provision of a single deviator at the section of

maximum deflection resulted in satisfactory service and ultimate load behavior.

Songkiat *et al.*, (1994) stated that 'It is found that the externally prestressed concrete beam possessing a proper arrangement of deviators to eliminate the loss of tendons eccentricity (that is, deviator at mid span in the simple beam) shows the same flexural behavior as that of the internal unbonded PC beam'.

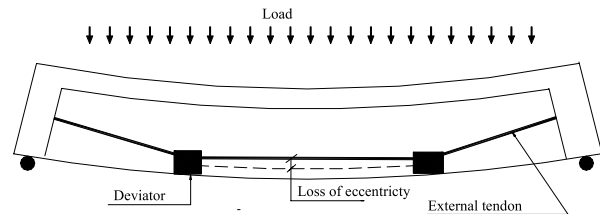


Figure 2.7 Loss of tendon eccentricity in external prestressed beam

Harajli *et al.*, (1999), studied the effect of deviators on the response of externally prestressed members, using a straight horizontal tendon profile having constant effective eccentricity. Three different configurations of deviators along the span were evaluated (tendon without deviators, tendons with one deviator at the mid-span and tendons with two deviators).

Three different values of external prestressing force for each configuration were applied. They reported that:

1. For a horizontal tendon profile, and in the presence of deviator(s), the influence of the second order effects on the response of externally prestressed members is minimal.
2. Single-draped profile (when using one deviator) produced lower nominal moment capacity and post elastic deflection than did the other draped profiles (when using two or more deviators).
3. With increasing distance between deviators, the nominal moment capacity increased up to $\alpha = L_d/L = 0.25$ where L_d = distance between the two deviators and L = effective span, then decreased depending on the extent of the second order effect. The undraped profile ($\alpha = 1.0$) produced the lowest nominal moment resistance.

Ghallab and Beeby (2005) studied the effect of several factors on the increase in the ultimate stress in external Parafil ropes as well as external steel tendons. These factors were related to the external prestressing system, internal prestressed and ordinary bonded steel, beam geometry and material properties. The accuracy of equations proposed by the Eurocode (EC2), ACI318 and BS8110 to calculate the ultimate stress in external steel and FRP prestressing tendons was also examined. The experimental and the analytical results showed that the studied factors had the same effect on both steel (up to yield) and Parafil ropes though this effect was greater

in case of steel tendons. Factors such as tendon profile (straight or deviated), high strength of the concrete, effective tendon depth, number of deviators should be taken into consideration when calculating the ultimate stress in the external tendons.

Ghallab (2006) tested four identical prestressed concrete I-beams strengthened externally using Parafil ropes to study the effect of the deviators locations and the distance between the deviators on the behavior of strengthened beams. All beams were strengthened using deviated tendons and loaded by two concentrated loads. The distances between loads varied between zero and $L/2$. Test results show that using two deviators to strengthen prestressed concrete beam subjects to two concentrated load at the third span or to uniform load is more efficient than using one deviator at the mid span. Furthermore, beam strengthened using two deviators within the flexural zone has higher external prestressing force and higher ultimate moment especially at ultimate stage than that strengthened using one deviator at the mid span

2.4.2 Effect of Steel Area

For an externally prestressed concrete beam with a straight horizontal profile or a deviated profile, providing the same prestressing force, the use of a larger tendon area gave similar service load behavior but a higher ultimate strength and less ductile behavior near failure (Tan and Ng, 1997).

2.4.3 Effect of Prestressing Force

Use of a smaller effective prestressing force leads to larger stress in external tendons, larger crack width, and service load deflections, but more ductile behavior at ultimate (Tan and Ng, 1997). Ghallab (2001) tested the effect of prestressing force value on behavior of externally prestressed simple concrete beams. Ghallab concluded that the increase in the external prestressing force had a negligible effect on both stiffness and deflection before cracking, while after cracking the increase in external prestressing force improved beam stiffness and reduced deflection.

2.4.4 Effect of Loading Type

Tests of prestressed beams with single deviator and without deviators under different type of loading (concentrated, two-third points and uniform loading) were investigated by (Harajli *et al.*, 1999). The results showed that, because a single concentrated load developed the smallest equivalent plastic hinge length at failure, they tended to mobilize the lowest post elastic deflection at failure in comparison with uniform load or third point loading. Since the nominal reduction in the tendons' depth is related to the ductility of the member, the difference in the nominal moment capacity acquired us-

ing tendons with or without deviators was least significant for concentrated loads.

2.4.5 External Prestressing and Fatigue

External prestressing causes a significant improvement in the fatigue life of the strengthened beams due to the lack of bond between concrete and tendons, which results in a decrease in the stress ranges and mean stress levels.

2.5 Prestressed Continuous Concrete Beams

Prestressed continuous beams are commonly used in cast-in situ structures with long spans, as it offers significant reduction in the required materials and a lower deflection compared to simple prestressed beams. However, continuous prestressed beams show different behavior compared to ordinary continuous reinforced concrete beams as additional phenomena and behaviors appear which should be carefully considered such as secondary moments, moment distribution, linear transformation and concordancy of tendons. The following are some details regarding the behavior of ordinary continuous prestressed beams:

2.5.1 Elastic Analysis for Continuous Prestressed Beams

Before cracking, continuous prestressed concrete beams have shown elastic behavior which can be applied with accuracy within the working range. As there are no cracks under working loads, the beam behaves as a homogenous elastic material. By making proper allowance for shrinkage and creep, the elastic theory can be applied for all practical purposes to compute the deflections, strains and stresses up to cracking.

2.5.2 Secondary Moments and Moments Redistribution

Secondary moments are the moments resulting from the reactions at intermediate supports preventing the continuous beam to deflect away from support under the effect of prestressing. During loading, the bending moments in a continuous beam can be predicted using a linear-elastic analysis, provided that the load level does not exceed the elastic limit. When the elastic limit is exceeded, at any particular load level, the bending moments in the beam will likely differ from those predicted by a linear-elastic analysis. The difference for a particular load level between the actual moment at a section and that determined by a linear-elastic analysis is referred to as redistribution of moment.

The failure load of a continuous prestressed concrete beam depends on the extent of redistribution of moment that occurs prior to failure. The extent of redistribution of moment can be full, partial, or nil, depending on a number of factors. Parametric studies conducted

in previous researches demonstrated that the stiffness of the span and the presence of secondary moments influence the extent of redistribution of moment; it has thus been recommended that overall structural ductility be considered in determining the amount of redistribution. The majority of current codes of practice bases the allowable amount of redistribution of moment on cross-sectional ductility at a critical section, and do not take secondary moments into account in determining the permitted amount of redistribution of moment. Design codes for concrete structures usually recommend the use of a linear-elastic analysis and either ignore the nonlinear effect or recognize it by applying a somewhat arbitrary adjustment to the design elastic moments (Campbell *et al.*, 1999).

Campbell and Kodur (1990) studied the different factors affecting the moment distribution of a continuous prestressed beam and proposed an approach for determining the percentage of redistribution of moment occurring at failure of continuous prestressed concrete beam. The approach was based on two parameters, the percentage of redistribution and the moment ratio (MR), and was developed using results from nonlinear finite element analyses of a large number of continuous prestressed concrete beams. In the proposed approach, the available redistribution of moment is based on the overall structural behavior rather than on the cross sectional behavior. It was concluded that:

- The extent of redistribution of moment increases with stiffness of the span, plastic hinge length, and secondary moment.
- An increase in the span-depth ratio L/d results in decreased redistribution of moment.
- The extent of redistribution of moment is influenced by the type of loading.
- The most important parameters affecting the redistribution of moment are the stiffness of the critical cross sections, cross-sectional shape, loading type, concrete strength, span-depth ratio, partial prestressing index, magnitude and nature of the secondary moments.

2.6 Externally Prestressed Continuous Concrete Beams

Behavior of externally prestressed continuous beams is different from that of ordinary prestressed continuous beams due to the lack of bond between the tendons and the concrete and due to the variation of tendon eccentricity during loading. Some factors that affect the behavior of externally prestressed continuous concrete beams are presented as follows:

2.6.1 General Behavior

Burns *et al.*, (1991) tested two specimens that had rectangular cross section and consists of two spans each

7.5 m. They concluded that the change in the tendon force was not significant until the stress in the extreme fibers of the critical section exceeds the tensile stress for concrete and that tendon stress calculated by the ACI was slightly near the actual values. Burns *et al.*, recommended that the prestress force used to calculate the service load stress, deflection and the cracking load should be the effective tendon force at the point in question. Harajli and Mabsout (2002) made experimental and analytical evaluations for the behavior and strength characteristics of continuous concrete beams prestressed using external tendons. The test variables included the areas of the external prestressing steel and the ordinary bonded reinforcement, configuration of the deviators, and the profile of the external tendons. Similarly to beams with internal unbounded tendons, the stress in the prestressing steel at nominal flexural strength was below or slightly exceeded yield. As a result of the change in tendon eccentricity with increasing beam deflection (second order effects), specimens with undeviated tendons mobilized relatively smaller load capacities and post-elastic deformations. Increasing the area of internal bonded reinforcement resulted in better crack distribution and, consequently, a more ductile mode of flexural failure.

2.6.2 Secondary Moments and Moments Redistribution

Aravinthan *et al.*, (1995) studied the influence of secondary moment on moment redistribution of continuous externally prestressed concrete beams loaded by symmetrical loading on both span and unsymmetrical loading. It was concluded that the amount of moment redistribution was affected by the tendon layout and loading pattern on each span. In symmetrically loaded beams, the moment redistribution decreased with the secondary moment in an almost linear manner. In case of unsymmetrical loading, however, moment redistribution was found to be insignificant

2.6.3 High Eccentricity External Tendons

Aravinthan and Mutsuyoshi studied the effect of high eccentricity external tendons on single-span and two-span continuous externally prestressed beams. The test variables included external tendon profile, loading pattern on each span, casting method, and confinement reinforcements. It was found that continuous girders with linearly transformed tendon profiles exhibited the same flexural behavior irrespective of tendon layout. The presence of confinement reinforcement enhanced the ductility behavior but did not increase the ultimate flexural strength.

Yielding of external tendons was observed in specimens with full loading on both spans. Tendon stress increased proportionally with midspan deformation until tendons yield. The rate of increase was influenced by

the type of loading arrangement; that is, the ultimate flexural strength of unsymmetrically loaded beams is approximately 20% less than that of symmetrically loaded beams.

Frictional effects at the deviators had some effect in the case of unsymmetrically loaded beams due to the large deviation angle of the external tendons. Furthermore, the stress increase in single-span beams was nearly the same as that of symmetrically loaded continuous beams.

2.6.4 Different Tendon Configurations

Tan and Tjandra (2007) carried out an experimental investigation to examine the flexural behavior of continuous beams externally prestressed with various tendons configurations. The research included the results of 12 two-span continuous T-beams strengthened using different external tendon types and profiles and subjected to third point loadings.

Test results indicated that an increase in ultimate strength with sufficient ductility could be achieved using short tendons located over the critical sections. Such a strengthening scheme led to a more ductile beam behavior compared to those with continuous tendons over both spans or with draped tendons within each span. Parabolic tendons anchored beyond the interior support however effectively strengthened the negative moment region with improved ductility at ultimate limit state. It was concluded that the provision of straight tendons anchored within beam spans represents a viable strengthening scheme with satisfactory beam performance in terms of ultimate load and ductility, and deflections under service loads. On the other hand, a parabolic profile, with tendons overlapping at interior support, effectively strengthened the positive and negative moment regions of the beam with improved ductility at ultimate. Anchoring parabolic tendons within the beam spans resulted in less ductile failure due to shear distress at the un-strengthened interior span regions.

2.6.5 Factors Which Affect the Performance of FRP When Used as Bonded Tendons

The performance of FRP tendons when used as internal bonded prestressing tendons is affected by several factors. Some of these factors are as follows:

2.6.5.1 Bond

FRP bars, in general, have shorter transfer length and higher bond stress than steel. This, in conjunction with a low cover value, may lead to splitting cracks along the FRP element (Rostasy, 1993). The bond between FRP bars and concrete, as previously mentioned, strongly depends on the matrix type and surface texture of the FRP element, and on the tensile and compressive strength of the concrete. Any deterioration in the

surface of FRP bars or in the bond between the fibers and the resin matrix will reduce the bond strength and hence, the efficiency of FRP bars as reinforcement to the concrete.

This deterioration could be due to moisture absorption, alkaline environments, cyclic loading, etc. The following subsections discuss some of the factors which may reduce the bond between FRP bars and concrete:

2.6.5.2 Moisture

Water acts as a plasticizer when absorbed by the matrix, softening the material and reducing some properties of the laminate. Moisture may also migrate along the fiber matrix interface, affecting the adhesion. Moisture in composites reduces matrix-dominated properties, such as transverse strength, fracture toughness and impact resistance. Debonding can occur due to formation of discontinuous bubbles and cracking in the matrix. Mechanical properties may be further reduced if heat is present or if the composite is under cured or has a large amount of voids. Moisture absorption is usually dependent on the matrix, but aramid fibers will also absorb water (Whitaker *et al.*, 1998).

After testing FRP bars conditioned in aqueous solutions for 14 and 84 days at a temperature of 80°C, Bank *et al.*, (1998) recommended that polyester resin should not be used for FRP bars due to its severe degradation. It was reported that radial and circumferential cracking was observed in the resin matrix. Circumferential cracking can lead to a failure phenomenon whereby the cores of unidirectional fibers are debonded from the outer surface of the rod which remains bonded to the concrete.

2.6.5.3 Cyclic Loading

Katz (2000) studied the effect of cyclic loading on the bond between FRP rods (with different resin matrices) and concrete immersed in water at 60°C and 20°C to accelerate deterioration effects.

Katz reported that the reduction in the bond strength was approximately 70% after loading. Three mechanisms of failure were identified:

1. Abrasion of the surface of the rod which, in the case of uniform resin throughout the rod, may lead to a reduction of 20–30% in the bond strength.
2. Delamination of the outer layer of the resin at the surface of the rod, which may lead to a reduction of up to 60% in the bond strength.
3. Abrasion of cement particles entrapped between the rod and the concrete, which serves as the main source of 'bond' for smooth rods.

2.6.5.4 High Temperature

FRP bars showed a reduction between 80% and 90% in the bond strength as the temperature increased

from 20°C to 25°C. While, in comparison, ordinary deformed steel bars showed a reduction of only 38% in the same temperature range. The reduction in bond strength of FRP bars was attributed to the polymer in the bar surface only and the reduction in concrete properties was not the cause of the loss of bond strength at high temperature (Katz *et al.*, 1999).

This severe reduction in bond strength at high temperature can lead to the failure of members.

2.6.5.5 FRP Tendon Strain

During the life of a structure, cracking of concrete can occur for several reasons, such as increase in concrete stress above its tensile strength and environmental attack, etc. When cracks occur on the tension face of a bonded prestressed concrete element, the tendons may be subjected to very high strains at the crack location. In case of steel tendons, local debonding between steel and concrete may occur and steel is able to deform locally in a ductile manner to lessen such localized high strain. This continues until the average strain along the debonded length of the bar is less than the high strain as shown in Fig. 2.8.

When using FRP as prestressing tendons, it should be noted that:

- FRP has a linear elastic response right up to failure with little or no ductility.
- FRP has a limited strain capacity which is less than steel (typically 0.015 or above).

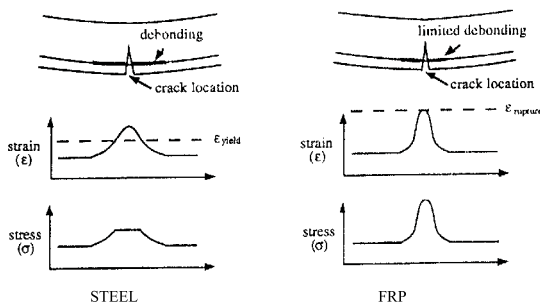


Figure 2.8 Strains and Stresses at the crack location

As FRP is expensive, it is preferred to use it close to its strain capacity, but during prestressing, much of the fiber strain capacity is absorbed in prestressing. This leaves the tendon very sensitive to additional strain induced by beam curvature or cracking of concrete, and may lead to failure of the concrete structure.

For unbonded tendons, when the beam is subjected to its ultimate load, and concrete strains increase to a very high value, the tendon will not see that peak strain, since it will continue to be subjected to an average value as shown in Fig. 2.9. Though this value is affected by contact between tendons and deviators (where some sizeable friction effects may arise), the tendon strain

will remain much lower than the local concrete strain (Burgoyne, 1993).

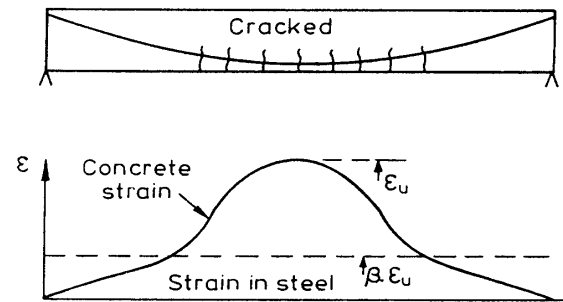


Figure 2.9 Strains in a cracked beam with an unbonded tendon

2.6.5.6 Coefficient of Thermal Expansion

FRP bars have two coefficients of thermal expansion CTE, one in the longitudinal direction and the other in the transverse direction. For most commercially produced FRP bars, the longitudinal coefficient of thermal expansion is generally closer to that of concrete, while the transverse coefficient of thermal expansion is higher than that of concrete and may be 10 times that of concrete.

In reinforced concrete, as both steel and concrete have the same coefficient of thermal expansion, internal strains due to temperature variation will not occur between steel and concrete. When using FRP bars, however, this problem appears, as the coefficient of thermal expansion of FRP is different from that of concrete. CFRP, for example, has a longitudinal coefficient of thermal expansion of almost zero. While GFRP and hardened concrete have the same longitudinal coefficient of thermal expansion, GFRP transverse coefficient of thermal expansion is over five times higher (Abdalla and Elbadry, 1997).

In addition, the longitudinal coefficient of thermal expansion of AFRP approaches zero (this leaves a difference from the surrounding concrete of approximately $12 \times 10^{-6}/^{\circ}\text{C}$) and its transverse coefficient of thermal expansion is about (4 to 5) times that of the surrounding concrete (Gerritse, 1993).

The difference between the longitudinal coefficient of thermal expansion of FRP bar and concrete at high temperature leads to internal slip between the concrete and FRP bars which results in a reduction of failure strength of the section. This difference results in a marginal change in prestressing force (dependent on the temperature variation), and should be taken into consideration especially at high or low temperatures (Gerritse, 1993).

The difference in the thermal expansion in the transverse direction may also cause significant bursting stress within the concrete around the bars under temperature increase, or separation of the bars from the concrete under temperature decrease (Abdalla and Elbadry, 1997).

2.7 Behavior of Prestressed Concrete Beams Strengthened by External FRP Post-Tensioned Tendons

Jerrett and Ahmad (1996) tested four (203×406×5490 mm) steel prestressed beams strengthened by external CFRP post-tensioned tendons. The beams were each prestressed with either one or two (13 mm) 7 wire steel prestressing strand and tested under four points loading. External post tensioning for strengthening was provided by two 8 mm diameter CFRP (Leadline) tendons, deviated by (4.8) degrees at each of two points.

Effective steel prestress of the beams varied from 985 to 1130 MPa. The post-tensioning stress in the CFRP tendons varied from 1240 to 1500 MPa. Due to the external prestressing, the average strength was increased by 115% for the beams with single steel strands and 46% for beams with double steel strands.

Saeki *et al.*, (1993), tested artificially cracked prestressed concrete beams externally strengthened using aramid ropes, under both static and repeated loading. Fatigue tests of strengthened beams were conducted under the condition of two million cycles, the stress level being up to 33% of the ultimate statical strength of beam and cable tension force being 34% of tensile strength. The change of rigidity of beam was found to be of no significant difference before and after fatigue tests and the ultimate bending strength of beams after fatigue test was nearly the same value as that of beams before testing.

2.8 Using FRP Materials in Prestressed Concrete Structures

Due to their lightweight, high tensile strength and excellent corrosion resistance FRP are used in a wide range of structures such as bridges, piers, radar stations, etc. FRP reinforcements have been used in pedestrian and road bridges. Bridge types range from simply supported slabs to the most sophisticated systems, such as cable-stayed bridges.

2.8.1 Application of CFRP in Post-Tensioned Prestressed Concrete Bridges

- CFRP strands were used as part of the tendons in a post-tensioned prestressed concrete highway bridge erected in 1991 in a German factory area. The bridge is approximately 80 m long and 11.2 m wide. Large capacity multi-cable of 19 CFRP strands of 12.5 mm diameter were used and anchored by a wedge system.
- CFRP rods were used as tendons in a simple two-span prestressed concrete highway bridge erected in 1989 in Kitakyusyu City in Japan. The bridge is 35.8 long and 12.3 wide. The tendons consisted of eight multi-cables bundled with eight CFRP rods of 8- mm diameter. A wedge- type steel anchorage was used for the multi-cables.

- CFRP stirrups as well as CFRP prestressing cables were used in Taylor Bridge in 1997. The bridge is located in Manitoba, Canada. The total length of the bridge is 165 m, divided into five equal spans. In addition, GFRP reinforces portions of the barrier walls.
- In the cable-stayed Storchen Bridge in Winterthur, Switzerland, two 35m long CFRP stay cables have been incorporated with 22 steel stay cables. The total length of this road bridge is 124m.
- In Denmark, the Herning cable-stayed Bridge, with a total length of 80m, is built with the exclusive use of CFRP stay cables. The bridge deck is post-tensioned with six CFRP tendons (12.5mm) seven wire strands from Tokyo Rope, and a 40m segment of the bridge deck is reinforced with CFRP bars and stirrups. The other 40m segment will be reinforced with a conventional steel and stainless steel reinforcement.

2.8.2 Application of AFRP in a Post-Tensioned Prestressed Concrete Bridges

- AFRP bands were used as tendons in a post-tensioned prestressed concrete suspended slab bridge, 54.5m long and 2.1m wide pedestrian bridge built in 1990 at a golf course in Mito City in Japan. The cross section of AFRP bands is 4.86×19.5 mm. Eight of the bands were combined to make a single cable, and 16 cables were used. Cables were anchored by inserting eight AFRP bands into a sleeve (material: SCM435) and filling it with expansive mortar. Cable bundling nine CFRP rods of 8 mm diameter was used for ground anchors.
- GFRP rods were used as multi-cables in the Ulenberg-Stasse Bridge. The bridge was built in 1986 in Dusseldorf in Germany. The bridge is a 2-span continuous girded highway bridge, one span is 21.3m long and the other is 25.6m long, both are 15m wide, 59 multi-cables consisting of 19 GFRP rods with a diameter of 7.5mm. The tendons are anchored by adhesion to a mortar containing quartz and polyester resin, which was injected to avoid alkali reaction of the glass fibers.
- The Schiessbergstrasse Bridge in Leverkusen, Germany was built in 1990. It is a three span, solid concrete slab bridge with two side spans of 16.3m each and a 20.4m middle span. The slab is 9.7m wide and the deck is 1.12m thick. Twenty-seven glass fibers prestressing tendons were used in a post-bonding process. Optical fiber sensors were also integrated for remote observation of the stress.
- GFRP use in construction of the Notsh Road Bridge in Karnten, Austria began in 1990. The bridge is very similar to the Schiessbergstrasse Bridge, but has different span lengths and was designed to be partially

prestressed using 27 glass fiber tendons. The side spans are 13m, the main span is 18m, and the slab thickness is 0.75m. The bridge is equipped with optical fiber sensors as well as chemical sensors

2.9 Parafil Ropes

Parafil ropes were the first products launched by Linear Composites Ltd. in 1969.

They consist of a closely packed core of high strength synthetic fibers lying parallel to each other, and encased in a tough and durable polymeric sheath. Fibers used in the core of Parafil rope differ from type to type as shown in Table 2.3 (LCL, 2008).

Table 2.3 Comparison between types of Parafil ropes

| Rope Type | Fibre Type | Sheath Type |
|-----------|-------------------------------------|--|
| Type A | Polyester | Different Type can be used with each rope |
| Type F | Standard modules aramid (Kevlan 29) | |
| Type G | High modules aramid (Kevlan 29) | <ol style="list-style-type: none"> 1. Polyethylene 2. Polyethylene-EVA copolymer 3. Polyester elastomer 4. Flame retardant |

The sheath is used to hold the fibers together, maintain the circular profile of the rope and protect the core from ultraviolet radiation and external abrasion. The especially formulated Polyethylene sheath is most commonly used and is perfectly satisfactory for most purposes, but the Polyethylene-EVA copolymer sheath is more flexible. Higher resistance to heat and abrasion can be obtained from the Polyester elastomer. The avoidance of twist and of fibers crossing each other enables maximum use to obtain from the tensile strength and stiffness of the fibers. It also avoids the complication and sometimes adverse properties of more formal rope structures e.g. high creep and low tension-tension fatigue performance (Kingston, 1988). Aligning the yarns parallel to each other has the added advantage that they do not rub over each other on loading, so no inter-yarn abrasion occurs within the main body of the rope. The only abrasion that occurs is within the termination, or where the path of the rope is deviated over a sheave (Burgoyne *et al.*, 1989).

2.9.1 Properties of Parafil Rope Type G

The structural behavior of Parafil rope depends mainly on the fibers due to the lack of bond between the fibers and the sheath. This enables the full benefit of Kevlar fibers and eliminates problems which appear when the fibers are held in a matrix as discussed before.

2.9.1.1 Short-term Properties

Tensile Strength

The stress-strain relationship for Parafil rope is shown in Fig. 2.10. The strength of Parafil rope exceeds that of

prestressing steel, while its elastic modulus represents approximately two thirds that of steel. However, tensile strength of the rope decreases with the increasing rope diameter. Parafil rope has a linear stress-strain relationship with a nominal strength of 1962 MPa and a strain at failure of about 1.5%.

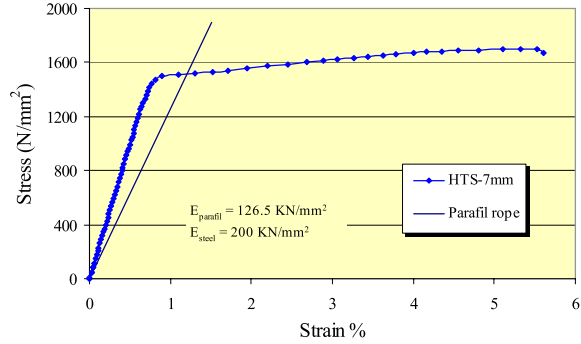


Figure 2.10 Stress-strain curves of Parafil rope and high tensiles

Effect of the Rope Length and Curvature

Tests carried out by Chambers (1988) on 6- tonne Type G ropes with lengths of 2.9m and 10.9m, revealed that the rope strength remained unaffected by length. Moreover, stretching the rope around a deflector with a deflection angle up to 15° and a radius of curvature of 50 times the diameter had no effect on their strength.

Effect of Rope Size

As discussed before, the strength of a group of fibers will be less than the strength of individual fiber, due to the bundle effect and the weaker fibers fail at a lower load than the stronger ones, leaving the total load-carrying capacity reduced. This process has to be applied twice in Parafil ropes; they are made as a bundle of parallel yarns, which are in turn made from about 1000 individual filaments. The filaments themselves have strengths of about 3500 MPa, the yarns have strength of about 2900 MPa, and the ropes have a minimum strength of about 1930 MPa (Burgoyne, 1993). Fig. 2.11 shows the relation between the tensile strength and rope size.

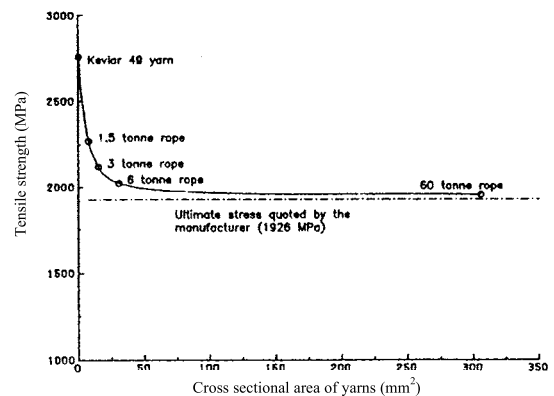


Figure 2.11 Effect of rope size on the tensile strength of Parafil rope type G

Effect of Temperature

Parafil based on aramid fibers which has been tested at temperatures between (-40°C) and ($+80^{\circ}\text{C}$) showed no detectable change in properties. Moreover, aramid fibers exposed to a temperature of 150°C for long periods of time showed no detectable change in residual strength when tested at normal temperatures.

Aramid fibres showed a strength loss of only 5% after 20 hours exposure at 200°C when tested at normal temperatures. While at a temperature of 250°C , the drop was much more accentuated, resulting in a residual strength of about 65% after 20 hours exposure. However, at about 460°C , the kevlar 49, which constitute the core of Parafil rope decomposed with a significant weight loss. Fig. 2.12 shows the relation between the percentage of tensile strength and the time of exposure, even though these results are for resin impregnated strands of kevlar, the results are broadly applicable to bare yarns. (Guimaraes, 1988).

The relation between the coefficient of thermal expansion (CTE) & the ratio (initial strain/ultimate strain) is linear for a stress level varying from 3% to 45% of the tensile strength of the yarns. At a ratio of 33% the coefficient of thermal expansion will be $-5.7 \times 10^{-6}/^{\circ}\text{C}$. The coefficient of thermal expansion also decreases as this ratio increases (Guimaraes, 1988).

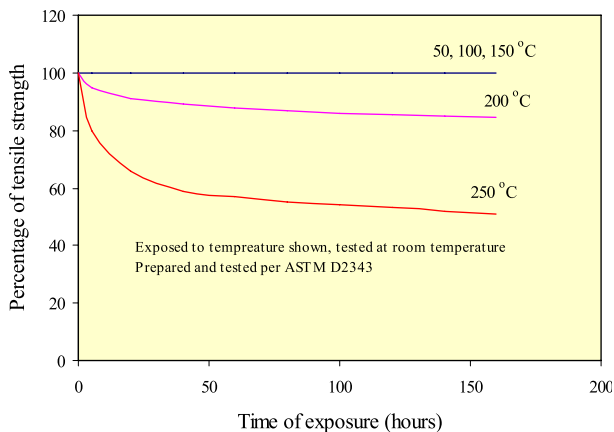


Figure 2.12 The effect of temperature on the tensile strength of resin impregnated strands of Kevlar 49 (DU PONT, 1981)

Bond

As there is no bond between the yarns that constitute the core of Parafil rope and the surrounding sheath, the bond between the sheath and the concrete, if it exists, will have a negligible effect on the core. Hence, the Parafil rope has to be considered only as unbonded tendons.

2.9.1.2 Long Term Properties

Since prestressing tendons are subjected to high permanent stress, the long-term time dependent properties are extremely important. The properties of prime significance are creep, stress-rupture and stress relaxation.

Creep

Parafil ropes will creep to failure at high stress level. Chambers (1988) investigated the behavior of 60 tonnes nominal breaking load (NBL) rope subjected to different sustained stress values (68%–95% of normal breaking stress). Chambers concluded that there is a linear relationship between applied stress and the logarithm of the “time to break” which leads to the prediction that a rope subjects to 50% of its NBL will fail after about 100 years.

The total creep strains are of the order of 0.13%, which can be compared with a rope extension when stressed to about 50% of its NBL of about 0.8%. Thus, we can expect to lose something like 16% of the initial prestress force in a Parafil tendon (Burgoyne, 1993). Guimaraes and Burgoyne (1992) studied the creep behavior of Parafil rope type G of 1.5 and 3.0 tonne NBL and reported that applying a pretensioning load to Parafil rope has the effect of reducing the creep strain of ropes in subsequent loading.

Stress-Relaxation

The stress-relaxation relationship of Parafil rope type G shows a linear relation.

Chamber (1988) studied the stress relaxation of Parafil rope type G of 60 tonne NBL and based on a numerical equation he calculated the predicted relaxation after 100 years as shown in Table 2.4 and Fig. 2.13.

Table 2.4 Predicted relaxation at 100 years

| Nominal initial stress %NBL | Predicted relaxation at 100 years %NBL |
|--------------------------------|--|
| 30 | 7 |
| 40 | 7.4 |
| 50 | 7.8 |
| 60 | 8.2* |
| 70 | 8.6* |

*at these stresses, over long periods of time, Parafil may fail due to stress-rupture

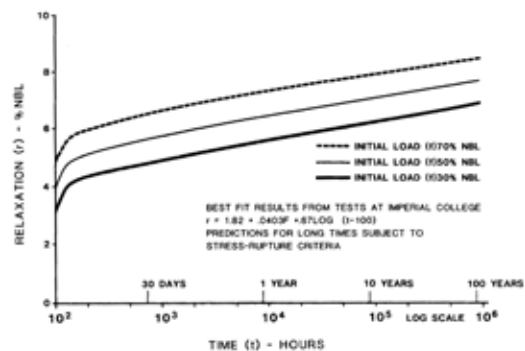


Figure 2.13 Stress-Relaxation of Parafil rope type G

It should be pointed out that the total loss of prestressing force in a member prestressed with Parafil is very similar to that in a beam prestressed with steel. This is because, whereas the losses due to the relaxation of the tendon are higher than steel, as explained above, the losses due to the elastic shortening, creep and shrinkage of the concrete are less because the Young's modulus of Parafil rope is lower than that of steel (about 2/3). Moreover, the anchorage system of Parafil rope does not cause any loss due to anchorage slip. Therefore, the total losses will be very similar (Chambers, 1988. Burgoyne, 1993).

Fatigue Performance

The fatigue characteristics of aramid fibers are very good. The resistance of Kevlar to tension-tension fatigue is better than that of steel. When fatigue failures of Kevlar do occur, they are normally due to fretting of fibers over one another. This can only occur at the terminations, or at loading points, and the variation in force in prestressing tendons, especially when unbonded, is extremely low. Thus, it is not believed that fatigue is a problem in prestressing applications (Burgoyne, 1993).

Resistance to Environmental Effects

The tendons can be expected to have high durability in normal environments. Kevlar is degraded by ultra-violet light, but this is shielded by the sheath and is not a problem. Kevlar fibers also suffer hydrolytic attack by strong acids and alkalis, but the tendons would not be bonded to the concrete, so the fibers will not come into contact with the alkaline concrete. In any event, the sheath will act as a barrier to ingress of chemicals.

DuPont reported that Kevlar is not degraded by either fresh or salt water at normal pH levels (Burgoyne, 1993).

2.9.2 Anchorages of Parafil Ropes

Parafil ropes are anchored by means of a spike and barrel fitting, which grips the fibers between a central tapered spike and an external matching barrel as shown in Fig. 2.14. This has the advantage that as the rope is loaded; the spike is drawn into the barrel, thereby clamping the rope even more tightly. To attach the termination, the end of the rope is passed through the terminal body, and the sheath is removed over the length of the spike. The yarns are then spread out evenly around the terminal then the spike is pushed in the center of the end of the rope while the rope itself is slowly pulled down until the cut end of the sheath is level with the back end of the termination. To reduce the creep losses, the rope should be pretensioned to a load in excess of that applied in practice.

This system has a number of advantages over wedge systems which grip the outside of a tension member (Burgoyne, 1993):

- The gripping force between the spike and the barrel has to pass through every fiber (Fig. 2.15) which means that each fiber can develop an equal friction force against its neighbours or the fitting. Thus there is no tendency for some of the fibers to carry a disproportionate amount of the load, which would cause early failure of those fibers, and hence the rope. Systems, which rely on external wedges, have a tendency to develop hoop compression around the outside of the tension member, leaving the inner fibers less well gripped.



Figure 2.14 Parafil rope and its anchorage and Installation procedure for Parafil rope

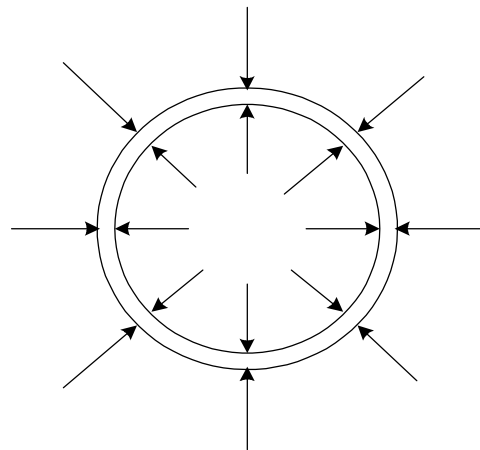


Figure 2.15 Gripping forces within termination

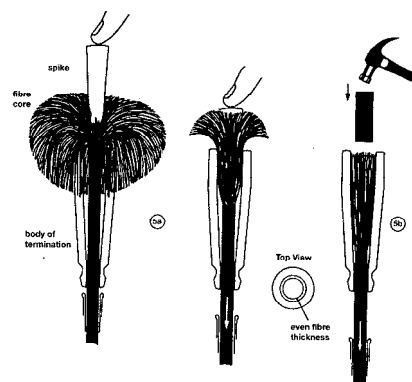


Figure 2.16 Installation procedure for Parafil Rope

- There is no resin in the system, which means that the effectiveness of the termination is not affected by temperature or creep.
- The system is easy to fit, on site if necessary.
- There are no side effects, terminations for large ropes are linearly scaled versions of the terminations for small ropes. The mechanics of operation remain the same.

The terminations can develop the full strength of the parent rope as shown from test results. The possibility to change the material of terminations, such as (aluminum, galvanized steel, stainless steel, etc.), makes it suitable for all environmental conditions.

3. Experimental Program

Introduction

To study the service and ultimate behavior of continuous beams externally prestressed using Parafil ropes type G, eight concrete beams were tested up to failure after externally strengthened over a period of nine months. All the beams were rectangular section (100mm×200mm) with two spans 2.5 m each.

An ordinary reinforced concrete beam with the same dimensions and steel reinforcement was also tested to compare its behavior with the strengthened beams. Some of the main factors affecting the flexural behavior of strengthened prestressed beams, during service and ultimate stages, were examined. These factors are:

- Value of external prestressing force
- Effective depth of the external prestressing force
- Loading pattern
- Tendon profile
- Location of deviators

3.1 Description of Test Beams

3.1.1 Test Beams

The basic considerations for the test beams were that they should be relatively small in size in order to overcome the practical problems associated with fabricating and testing beams in the laboratory. Considering the testing facilities available in the laboratory, the test beams were designed with an overall depth of 200mm, and two spans each 2.5m. Continuous beams were chosen as it is mostly used in construction of bridges. Dimensions and reinforcement details are shown in Figs. 3.1 and 3.2.

All beams were referred to by two letters and two numbers, the first letter P means prestressed concrete and the second C means continuous, while the first

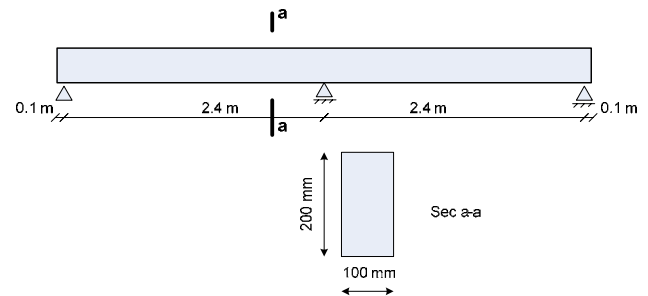


Figure 3.1 Beam dimensions

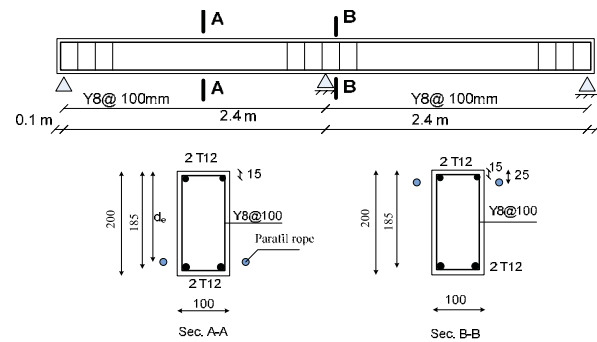


Figure 3.2 Beam reinforcement details

Table 3.1 Proportions of concrete mixes by weight

| Mix | I |
|---------------------|------|
| Cement | 1 |
| Dlomite | 2.86 |
| Sand | 1.94 |
| Water | 0.54 |
| Measured slump (mm) | 185 |

number is the group number and the second is the beam number in this group. For example, beam PC3–2 means prestressed continuous concrete beam, group three, beam number two in this group.

3.1.2 Mix Design

The concrete was designed to give nominal 28 days cube strength equals to 40 MPa, with a reasonable workability due to the narrow section. The ingredients of the mix were as follows:

- Cement: Ordinary Portland cement (OPC) with no additives was used throughout the whole series of tests
- Fine aggregate: Ordinary concreting sand having a maximum size of 0.5mm was used.
- Coarse aggregate: Crushed limestone (Dolomite) with 10 mm maximum size was used. The proportions of concrete mix are shown in Table 3.1.

3.1.3 Steel

3.1.3.1 Longitudinal Non-Prestressed Steel

Two 12mm high tensile steel bars were provided at the bottom and at the top of the beam as tensile reinforcement, and to facilitate the formation and location of the reinforcing cage. The results of tensile tests on sample bars are given in Table 3.2.

3.1.3.2 Shear Reinforcement

Shear reinforcement was provided by 8mm mild steel. They were used to hold the longitudinal steel in position. In each beam, shear reinforcement at a spacing of about 100mm was used throughout the two spans.

3.1.3.3 External Prestressing Tendons

External prestressing tendons were composed of two Parafil ropes Type G with a diameter of 11mm (Fig. 3.3). The properties of the Parafil rope are shown in Table 3.2.

Table 3.2 Properties of Steel and Parafil Rope

| | Stirrups | High Tensile Steel | Parafil Rope |
|--|----------|--------------------|--------------|
| Diameter (mm) | 8 | 12 | 11/(1.6)* |
| Area (mm ²) | 50.3 | 113.04 | 30.55** |
| Yield strength (N/mm ²) | 240 | 410 | --- |
| Young's modulus (KN/mm ²) | 200 | 200 | 126.5 |
| Ultimate strength (N/mm ²) | 550 | 650 | 1900 |
| Ultimate strain (ϵ_{ult} %) | 19 | 20 | 1.5 |



* Outside sheath diameter / fibers core diameter



** Based on area of fibers in the core

Figure 3.3 Testing of Parafil Rope

3.1.4 Manufacturing of Test Beams

3.1.4.1 Moulds

The moulds were constructed using wooden partitions, with height of 200mm and length of m, to cast more than one beam. Varnished wood sections were used to separate the beams as shown in Fig. 3.4.



Figure 3.4 Mould of test beams

3.1.4.2 Casting and Placing

Before placing the reinforcing cage in the mould, the sides of the mould were coated with mould oil then the reinforcing cage was located accurately by means of spacers at regular intervals to maintain the required concrete cover (10mm). For each concrete mix, all the constituent materials were weighed in the required proportions before being fed into a mixer of 250kg dry weight capacity. The materials were turned over for about a minute before the addition of the required quantity of water, which was followed by two minutes of mixing to ensure a uniform workable mix. Control tests comprising three 158mm cubes and two prisms (150×150×600mm³) were cast from each mix. The concrete was placed in the mould in layers and compacted by means of a vibrator at a frequency of 50Hz. Care was taken to ensure that the concrete flowed between the reinforcing bars. The exposed surface of the beams and specimens were then covered with wet burlap and plastic sheets, the former of which was watered daily.

3.1.5 Control Tests

Concrete strength was determined using three 158mm cubes, which were tested at the day of beam test. The average concrete compressive strength is given in Table 4.1.

3.2 FRP Wrapping at Anchorage Zones

In test beams with high prestressing force, high stress concentration at both ends of the beam can result in

cracking the end block. Hence, to avoid failure at end block zones, for PC1-1 and PC1-3 with prestressing force (48 and 60kN), respectively, a carbon fiber (CFRP) textile was used to confine the indicated areas in Fig. 3.5.

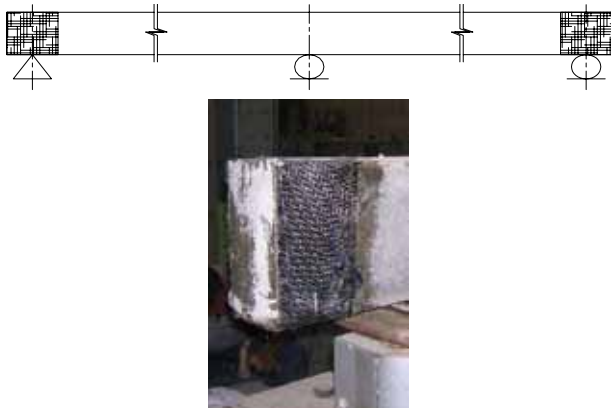


Figure 3.5 Details FRP wrapping

3.3 External Prestressing Procedure

3.3.1 Components of External Prestressing System

- Tendons: Parafil rope type G with diameter 11mm was used as external prestressing tendons.
- Ducts: Plastic tubes were used at the deviator locations to protect Parafil ropes from abrasion. Before external prestressing, the inside and outside surface of these tubes were greased to eliminate the friction between them and Parafil ropes and deviators during stressing.
- Deviators: Five steel deviators were used in this research. Components and dimensions are shown in Fig. 3.6.

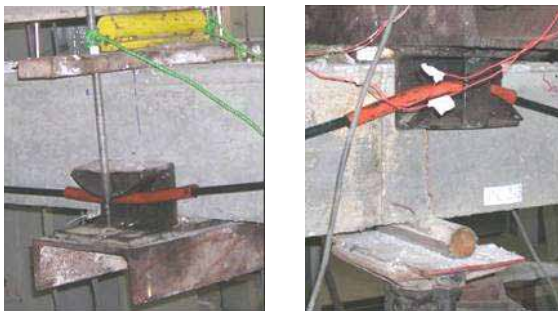
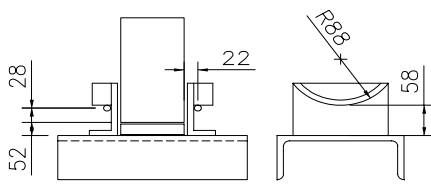


Figure 3.6 Details of upper and lower deviators

- Anchorages: Four aluminium anchors were used to transfer the rope forces to the end plates then to the beam. Details of anchorage method were discussed

in chapter two. Fig. 3.7 shows the details of anchorage-beam connection.



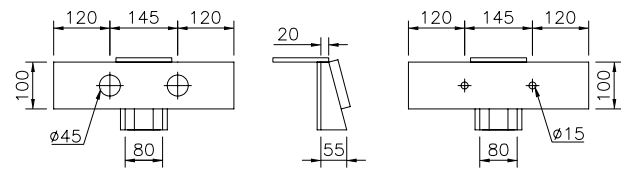
a. Live end at stressing jack



b. Dead end anchor

Figure 3.7 Live and dead ends

- End plates: Two steel end plates as shown in Fig. 3.8 were used to transfer the external prestressing force to the beam. Dimensions were selected to transfer and spread the force safely to the beam at the end blocks and to keep the ropes away from contact with the beam surface in order to eliminate any friction.



All Dimensions in mm

Figure 3.8 Dimensions of the end plates

3.3.2 External Prestressing Process

External prestressing was applied using two (11mm diameter) Parafil ropes type G, located at the same distance from the longitudinal axis of the beam as shown in Fig. 3.9. Before tensioning, the ropes were greased at the deviators to reduce the friction. The two ropes were tensioned simultaneously using two hydraulic jacks connected to the same pump. During prestressing, precautions were taken to prevent increasing prestressing

force in one rope relative to the other to avoid biaxial bending of the beam, by closing the connection of the higher force to the pump and increasing the force in the other rope

After reaching the required force, the ropes were locked by tightening the anchorage nuts against the end plate. The losses due to anchorage draw in were almost zero. After twenty-four hours, the ropes were re-tensioned to compensate for creep, and then the test was started. The external prestressing force during the prestressing process and testing was measured in both ropes using two 100kN load cells at the end of the ropes as shown in Figs 3.10–3.11.

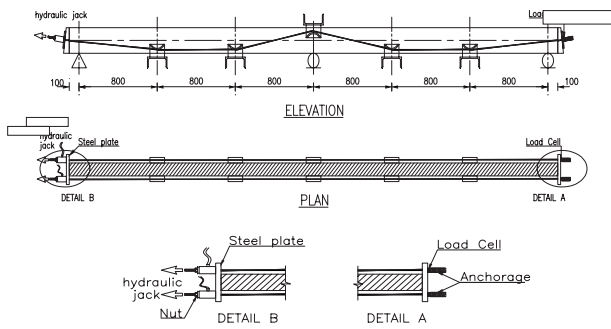


Figure 3.9 External prestressing layout



Figure 3.10 Load Cell used to measure prestressing force

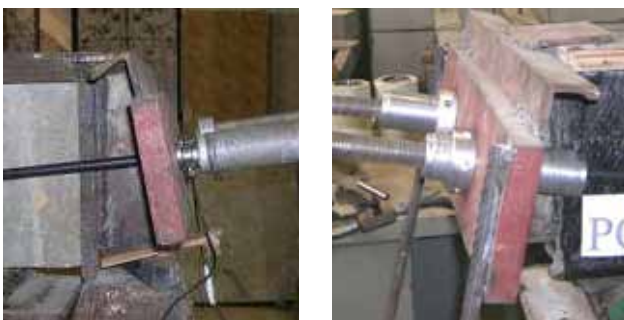


Figure 3.11 Details of Parafil rope connections at the beam ends

3.4 Instrumentation

3.4.1 Steel Strain Measurements

The strain on the nonprestressed steel was measured by six PL-5 electrical strain gauges, mounted on the steel

bars. The strain gauges and all the exposed electrical connections were covered with a layer of M-Coat that provided insulation against any possible electrical leakage and sealed the gauge from moisture and contamination.

The treated area was finally covered with silicon painting to ensure that the coating was well protected and isolated. Before testing, the strain gauges were connected to the data logging system

3.4.2 Load Cells

Two 100kN load cells with sensitivity of 0.01kN as shown in Fig. 3.10 were used to measure the prestressing force in each rope during external prestressing and test. Before usage, the load cells were calibrated, and then fixed at the rope end as shown in Fig. 3.11. Both load cells were connected to the same data logging system.

3.4.3 Deflection Measurement

During the external prestressing and testing process, seven linear voltage differential transducers (LVDT's) were used to measure the deflection, one at each mid-span, one at each deviator, and one at the intermediate support as shown in Figs. 3.12 and 3.13. All LVDT's were calibrated before use and connected to the data logging system.

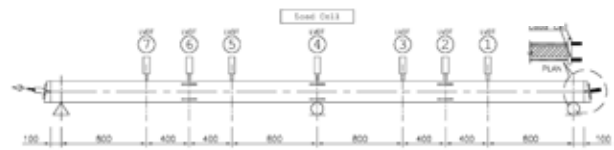


Figure 3.12 Arrangements of LVDT's for deflection measurements (back view)

3.4.4 Reactions Measurements

As the test beams are statically indeterminate, the actual bending moment forming in the beam cannot be calculated with the elastic theory as plastic hinges are expected to occur when approaching the ultimate load. Consequently, the bending moments will be affected and will vary from the elastic bending moments calculated from elastic theory.

In order to determine the actual bending moment at a certain applied load, two load cells were used at both external supports as shown in Fig. 3.13. The load cell

readings were observed and recorded manually at each load increment



Figure 3.13 Load cells at external supports

3.5 Beam Testing

3.5.1 Preparation of Beams for Testing

After about one month from casting, each beam was externally prestressed and loaded to failure. Before being externally prestressed, the beam was set up and carefully aligned in a test rig with the required effective spans, supported on three steel rollers designed to simulate hinged and roller supports. The deviators were then fixed in their positions. Three spreader beams were used to apply the required loading profile on the beams as shown in Fig. 3.14. Each spreader beam was supported on two supports; roller and hinged. The LVDTs were then adjusted vertically at their locations. The load cells, LVDTs, and steel strain gauges were then connected to the data logging system.

After beam set up and before applying the external prestressing force, the beam was inspected carefully for any cracks due to shrinkage or mishandling, and strain and deflection readings were taken; the beam was then externally prestressed. During and after applying the external prestressing force, steel and concrete strains, external prestressing force, as well as the deflection, were recorded. The following day, the external prestressing force was readjusted, the beam was carefully inspected for any cracks, and the strain and deflection readings were retaken. The hydraulic jack was carefully centered over the spreader beam as shown in Fig. 3.14.



Beam PC1-2



Beam PC4-2



Beam PC5-2

Figure 3.14 Loading system of the test beams

3.5.2 Data Logging System

The load cells, strain gauges and LVDT's were connected to the data logging system shown in Fig. 3.15.



a. Back face

b. Front face

Figure 3.15 Data logging system

3.5.3 Testing Procedure

Following external prestressing the specimens were subjected to an incremental load till failure. During loading, all measurements, such as beam deflections (at middle and at load positions), strains in internal tensile steel bars, and force in the external ropes were recorded at each increment.

Before cracking, the load was applied in increments 10kN until the first crack appeared, and then reduced to 5kN near failure. After each increment of load had been added, the cracking pattern was inspected and marked. In the higher loading range, the tendency of beam to creep was more noticeable and the load had to be maintained for a longer period of time to obtain reasonably steady strain and deflection readings. Load increments were added until failure took place. The time required to load the beam to failure was usually between three to four hours.

4. Test Results

Introduction

To understand the behavior of externally prestressed continuous concrete beams, and to determine the main factors affecting this behavior, eight continuous reinforced concrete beams after being externally strengthened using Parafil rope, were tested up to failure and compared with ordinary reinforced concrete beam. In this chapter, results obtained from experimental works are presented and compared.

4.1 Results of Test Beams

The beams were divided into five groups according to the studied factors as shown in Table 4.1 and Figs.

4.1–4.5. Table 4.2 shows the properties of beams at test day. The following are the experimental results of each group presented and compared.

Table 4.1 Studied factors and group number

| Group no. | Factors | Beam No. |
|-----------|--|-----------------------------|
| G1 | Value of external prestressing force | RC1, PC 1–1, PC 1–2, PC 1–3 |
| G2 | Effective depth of external prestressing force | PC 1–2, PC 2-2 & PC 2–3 |
| G3 | Loading pattern | PC 1–2 & PC 3–2 |
| G4 | Tendon Profile | PC 1–2 & PC 4–2 |
| G5 | Location of deviators | PC 1–2 & PC 5–2 |

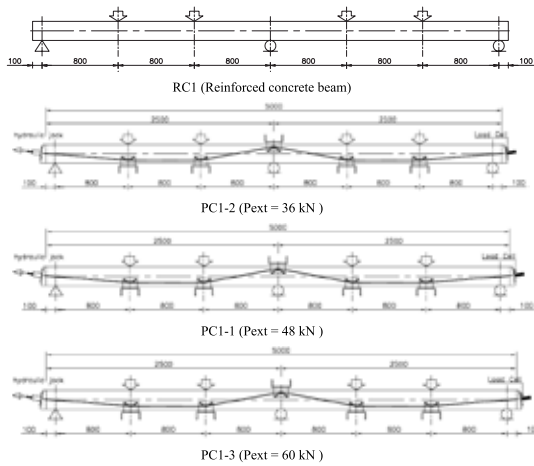


Figure 4.1 Beams in Group 1 (Value of external prestressing force)

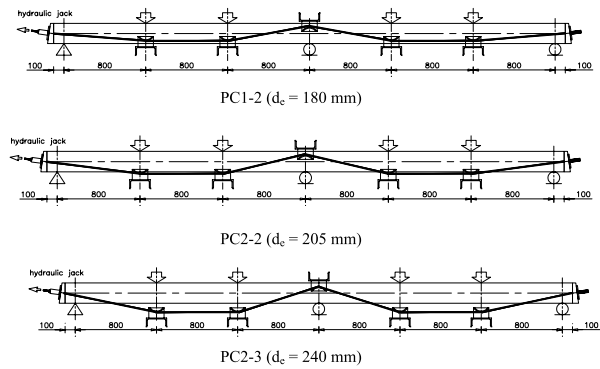


Figure 4.2 Beams in Group 2 (Effective depth of external prestressing force)

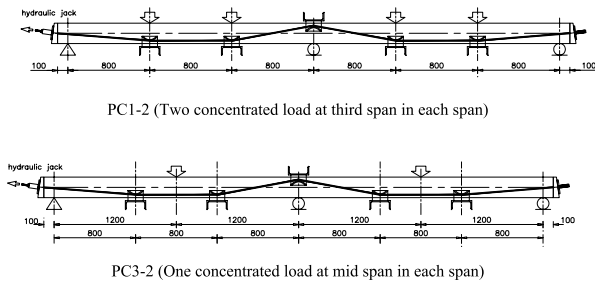


Figure 4.3 Beams in Group 3 (Loading pattern)

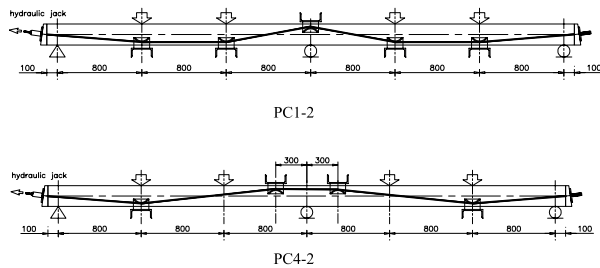


Figure 4.4 Beams in Group 4 (Tendon profile)

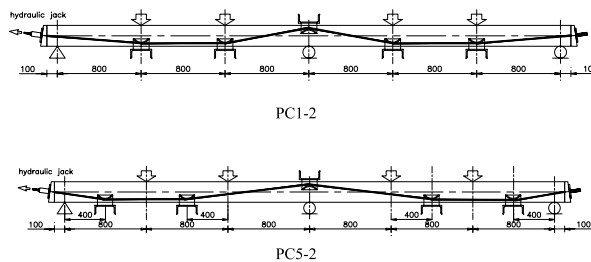


Figure 4.5 Beams in Group 5 (Location of deviators)

Table 4.2 Properties of test beams (at test day)

| Beam No. | Load Type | f_{cu} (MPa) | $(\frac{L}{h})^*$ | External Prestressing Force | | | | Number of deviators |
|----------|-----------|----------------|-------------------|-----------------------------|-----------------------------|--------------------------------|---------------------------------|---------------------|
| | | | | P_{ex}^{**} (kN) | $P_{ex}/P_{ult}^{\diamond}$ | $.d_c$ at midspan (mm) § | $.d_c'$ at Support (mm) § | |
| RC1 | | 39 | 12 | - | - | - | - | - |
| PC 1-2 | | 39 | 12 | 36 | 30% | 180 | 25 | 5 |
| PC 1-1 | 2-L/3 | 40 | 12 | 48 | 40% | 180 | 25 | 5 |
| PC 1-3 | | 40 | 12 | 60 | 50% | 180 | 25 | 5 |
| PC 2-2 | | 40 | 12 | 35 | 29.2% | 205 | 25 | 5 |
| PC 2-3 | | 40 | 12 | 34.2 | 28.5% | 240 | 25 | 5 |
| PC 3-2 | 1-L/2 | 39 | 12 | 35.2 | 29.4% | 180 | 25 | 5 |
| PC 4-2 | 2-L/3 | 39 | 12 | 36.1 | 30.1% | 180 | 25 | 4 |
| PC 5-2 | | 39 | 12 | 36.8 | 30.7 | 180 | 25 | 5 |

*L=effective span length **effective prestressing force P_{ult} = total ultimate breaking tendons load § measured from upper edge of beam



a Right span



b Internal Support



c Left span

Figure 4.6 Cracking pattern of reinforced concrete beam (RC1)



a Right span



b Internal Support

Figure 4.7 Typical cracking pattern of externally prestressed concrete

4.1.1. Cracking Patterns

In reinforced concrete beam, cracks appeared over the interior support and under the applied concentrated loads on both spans at almost the same load (about 35kN), then spread and extended towards the concentrated load. As the load increased, cracks became more obvious with significant increase in width.

Cracks on beam RC1-1 appeared earlier than those on the externally prestressed beams and its cracking pattern was characterized by larger number and wider width of cracks compared to that of externally prestressed beams. The cracks on beam RC1 were more distributed and extended faster than all other strengthened beams. In externally prestressed beams, cracks appeared over

the interior support and in only one span at almost the same load. Then flexural cracks on the bottom of the other span appeared at a higher load. As the load increased, additional cracks developed simultaneously at the interior support and at the mid-span sections and previous cracks extended. Near the ultimate load the cracks seem to concentrate on only one span (left or right) and the rate of increase of crack width at this section was greater than those on the other span.

Most of the tested beams failed in flexural mode by forming plastic hinges at both the interior support and the mid span regions. Figs. 4.6–4.7 show the typical cracking patterns of ordinary reinforced concrete beam and externally prestressed concrete beam at ultimate load.

To compare the cracking patterns of the externally prestressed beams, the load at which the cracks were visually observed is used. Generally, the following were noticed for all beams:

- Cracks between the concentrated loads were almost vertical, while those in the shear span were inclined due to the effect of shear stress.
- During loading and before yielding stage, there was no sign of concentration of deformation at a single crack location.
- Before failure, concrete crushed at the bottom fiber of the section at the interior support location due to high stress concentration at the support area (high bearing stress).

Group G1 (Value of the External Prestressing Force)

Fig. 4.8 shows the cracks pattern of beams in group (G1). The number and the distance between the flexural cracks of beams PC1-2, PC1-1 and PC1-3 ($P_{ex}=36$,

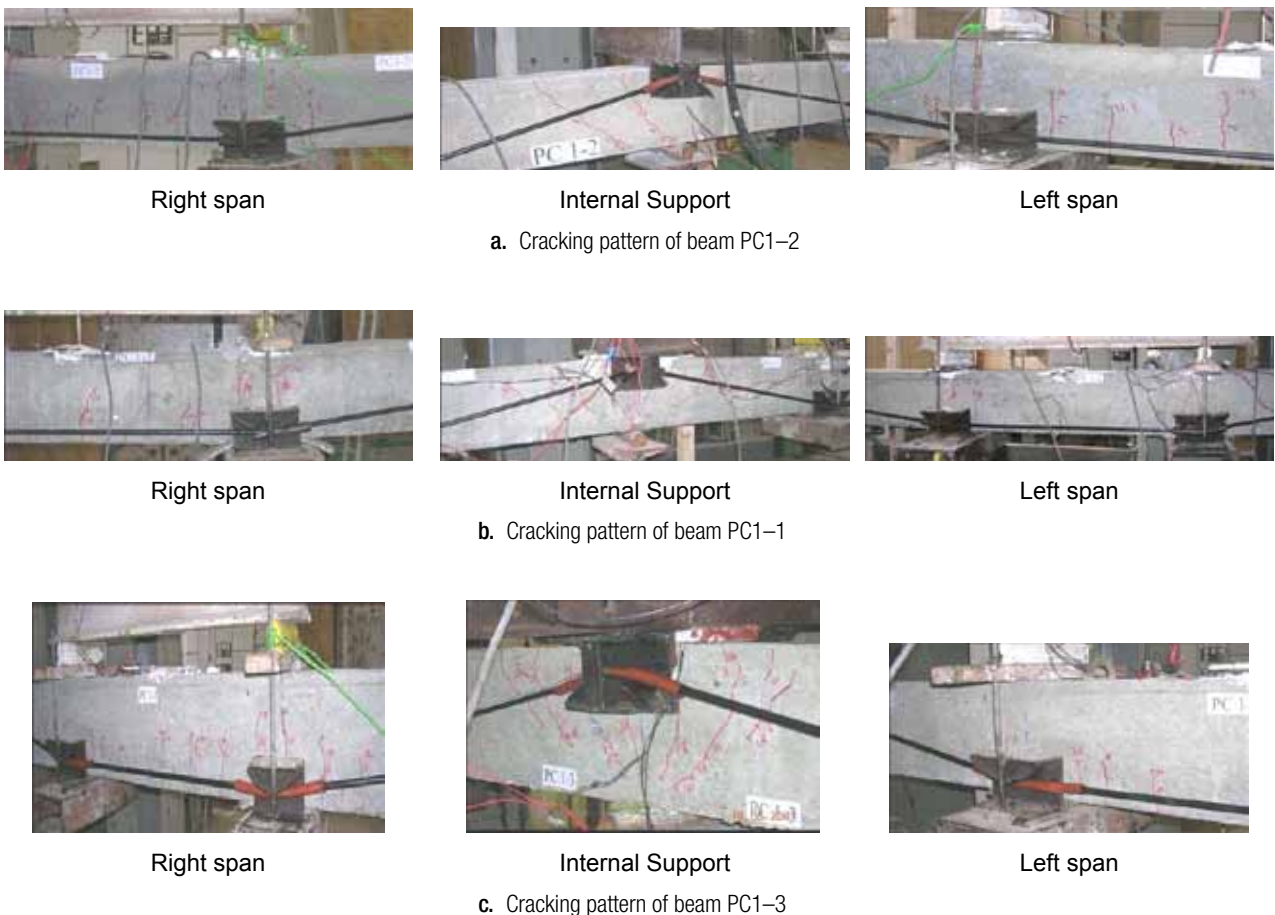


Figure 4.8 Cracking pattern of beams in group G1

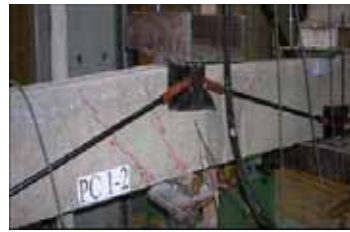
48 and 60kN, respectively) are slightly different. Flexural cracks of beam PC1–1 appeared at a load (117kN) higher than that of beam PG1–2 (100 kN) and lower than that of beam PG1–3 (128kN). During loading it was observed that as the external prestressing force increased, the cracks extension and the cracks widths (using visual observation) decreased. The difference between the cracks patterns on both spans was also significant at the higher prestressing values.

Group G2 (Effective Depth of the External Prestressing Force)

Fig. 4.9 shows the cracks distribution on beams in group (G2). Generally, the cracks patterns of beams PC1–2, PC2–2 and PC2–3 ($d/h=0.9, 1.025$ and 1.2), were almost the same. The flexural cracks on beams in this group appeared at almost the same load (about

100kN) but at different locations, top flexural cracks appeared first at the interior support on beam PC1–2 and on beam PC2–2, while bottom flexural cracks near to the concentrated load appeared first on beam PC2–3. Afterwards, several diagonal cracks at the top and vertical cracks at the mid span, near the outer concentrated load appeared. During loading, several diagonal cracks appeared on beam PC2–3 on the right shear span. Beam PC1–2 and beam P2–2 failed by compression at top fibers under the concentrated load near the outer support, while beam PC2–3 failed at the mid support.

Number of cracks on the right span of beam PC1–2 and beam PC 2–3 were greater than number of cracks on the left span. On beam PC2–2 cracks distributed on both spans and resulted in rapid reduction in its stiffness compared to beams PC1–2 and PC2–3. Be-



a. Cracking pattern of beam PC1–2



Right span

Internal Support

Left span

b. Cracking pattern of beam PC2–2



Right span

Internal Support

Left span

c. Cracking pattern of beam PC2–3

Figure 4.9 Cracking patterns of beams in group G2

fore failure, the major crack that resulted in failure of beam PC2-3 was at the mid support and not within the span as on beam PC1-2 and beam PC2-2. It was noticed that as the eccentricity of the cable increased, the number and width of cracks reduced, although the distance between cracks was almost the same in all beams.

Group G3 (Loading Pattern)

Fig. 4.10 shows the crack patterns of beams in group (G3). For beam PC 3-2 (loaded with one concentrated load at the midspan), cracks appeared on top fiber at

the interior support and on bottom fiber at the mid span at almost the same load (50kN). Cracks were concentrated at the applied loads in the mid span and at the interior support. As the load increased, cracks were extended towards the concentrated load, while for beam PC1-2 cracks appeared at load (100kN) and extended almost vertically, specially between applied loads. PC1-2 which was loaded with two-third point loading performed better cracks resistance with relatively smaller cracks width compared to PC3-2. The flexural cracks of PC1-2 at both sides of the internal support started at a distance shorter than that observed



a. Cracking pattern of beam PC1-2



Right span



Internal Support



Left span

b. Cracking pattern of beam PC3-2

Figure 4.10 Cracking pattern for group G3

in case of PC3-2. At the same loading level, bending moment due to one concentrated load is different from bending moment due to third point loading. Therefore, the two beams are compared at the same bending moment level (-ve moment at the interior support).

First crack of PC1-2 appeared at the internal support at (-12.8kN.m), whereas first crack at the interior support for beam PC3-2 appeared at (-11kN.m).

Group G4 (Tendon Profile)

Fig. 4.11 shows the cracks pattern of beams in group (G4). Cracks on beam PC4-2 (two deviators at interior

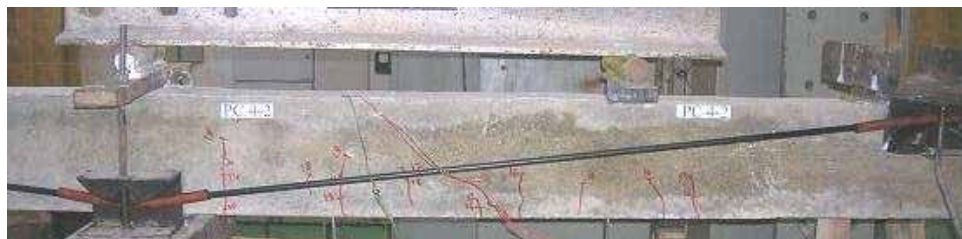
support) started to appear at the interior support at a lower load (70kN) than that of beam PC1-2 (one deviator at interior support), (110kN), and as the load increased, several cracks at the top of the interior support appeared. Vertical cracks between the two concentrated loads appeared at higher load (100kN). As the load increased, cracks at the top extended to the mid support and become wider. Before failure, several cracks between the concentrated loads appeared. Cracks spread on the bottom of beam PC4-2 more than spreading on beam PC1-2. Furthermore, top cracks at the interior support were concentrated in a region smaller than that



a. Cracking pattern of beam PC1-2



Right span



Internal Support



Left span

b. Cracking pattern of beam PC4-2

Figure 4.11 Cracking pattern for group G4

on beam PC1-2. Failure of beam PC4-2 was at the interior support while that of beam PC1 was at the span near the concentrated load

Group G5 (Location of Deviators)

First crack on beam PC1-2 appeared at the mid support region while those on beam PC5-2 (two deviators at outer applied load) appeared at top flange on the mid support and at the bottom flange under the outer con-

centrated load. Cracks on beam PC5-2 also appeared on the right span earlier than those on the left span and during loading, cracks spread in the flexural and shear spans. Cracks on beam PC5-2 appeared at a higher load compared with beam PC1-2 (110 and 100kN, respectively) and spread between the two concentrated loads wider than those on beam PC1-2. Cracks number on beam PC5-2 was higher than that on beam PC2-1 and extended higher as shown in Fig. 4.12.



a. Cracking pattern of beam PC 1-2



Right span



Internal Support



Left span

b. Cracking pattern of PC5-2

Figure 4.12 Cracking pattern for group

Table 4.3 Camber of tested beams

| Group Name | Beam No. | Camber at mid left span (mm) | Camber at mid right span (mm) | Average Camber (mm) |
|---|----------|------------------------------|-------------------------------|---------------------|
| Value of external prestressing force (G1) | PC 1-2 | -0.82 | -0.37 | -0.6 |
| | PC 1-1 | -0.90 | -0.46 | -0.68 |
| | PC 1-3 | -0.6 | -0.9 | -0.75 |
| Effective depth of external prestressing force (G2) | PC 1-2 | -0.82 | -0.37 | -0.6 |
| | PC 2-1 | -1.2 | -1.3 | -1.25 |
| | PC 2-3 | -3.0 | -2.2 | -2.6 |
| Loading Pattern (G3) | PC 1-2 | -0.82 | -0.37 | -0.6 |
| | PC 3-2 | -0.4 | -0.8 | -0.6 |
| Tendon Profile | PC 1-2 | -0.82 | -0.37 | -0.6 |
| | PC 4-2 | -0.3 | -0.1 | -0.2 |
| Location of deviators (G5) | PC 1-2 | -0.82 | -0.37 | -0.6 |
| | PC 5-2 | -0.9 | -2.7 | -1.8 |

4.1.2 Load Deflection Behavior During Prestressing

During the external prestressing process, camber increased (in both spans) as the prestressing force increased. After reaching the target prestressing force, the beams were loaded. So the effect of creep on concrete camber was not taken into consideration. Table 4.3 shows camber of tested beams while Fig. 4.13 shows a schematic drawing of camber distribution along the beam spans for group G2. In Table 4.3 Camber is given (-ve) sign while deflection is given (+ve) sign. As can be seen, both the eccentricity of the prestressing force and deviators locations had a significant effect on camber of the strengthened beams (beams PC2-3 and PC5-2 had the maximum camber), while the tendon geometry had a slight effect on camber of the strengthened beams (Group 4).

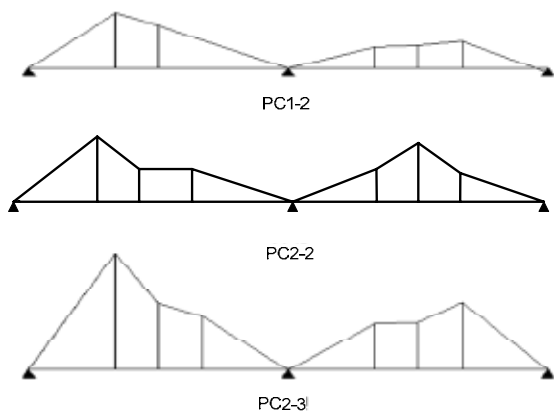


Figure 4.13 Schematic diagram of camber of beams in Group 2 after external Prestressing

During Loading

Generally, the relation between load and deflection for the continuous beams is characterized by three stages as shown in Fig. 4.14. Initially, the beam is uncracked and behaves elastically, with the maximum negative and positive moments, respectively, at the sections at the interior support and under the outer concentrated loads. The major crack at top and the major crack at bottom (Points B and C on the curve) were expected at these critical sections. The difference between the value of the top cracking and bottom cracking loads and the order of cracks appearance was dependent on the relative strengthening effects in the negative and positive moment regions.

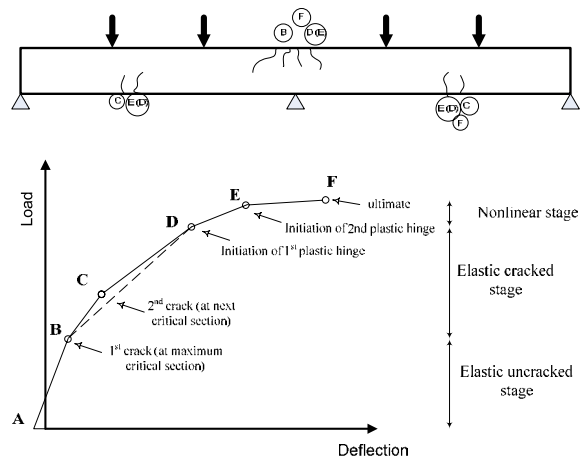


Figure 4.14 Typical load deflection curve of externally prestressed continuous beam

After cracking, the beams showed elastic behavior until the internal tensile steel reinforcement at one of the critical sections started to yield (Point D) and a plastic hinge was assumed to occur, and this was followed by the formation of the second plastic hinge at the other critical section (Point E). The ultimate flexural strength was reached when the extreme compressive concrete fiber at one of the critical sections attained its ultimate strain (Point F). It should be noted that the difference between the loads at points B and C and points D and E is mainly dependent on the cracking and ultimate strengths of the sections as well as the prestressing moment at these sections

In case of reinforced concrete beam RC1, the deflection was higher than that of all the strengthened beams. In addition, beam RC1 showed higher ductility, and better cracks distribution and plastic hinges clearly appeared on both spans before failure.

Fig. 4.15 shows maximum deflection of the test beams at different stages.

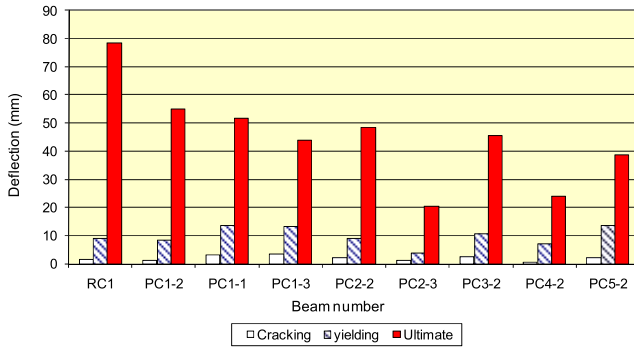


Figure 4.15 Maximum deflection of test beams at different stages

Group G1 (Value of the External Prestressing Force)

Fig. 4.16 shows the relation between load and deflection for beams PC1–2, PC1–1 and PC1–3 ($P_{ex}=36, 48$ and 60kN), respectively, along with the reinforced concrete beam (RC1), while Table 4.4 shows the value of maximum deflections at the mid span at each stage of loading. It can be seen that, as expected, the load deflection characteristics were almost similar up to the cracking load. Beyond yielding, beam PC1–3 registered a smaller deflection at any particular load than the other two beams, while beam PC1–2 had higher deflection at any load.

Comparing the beams before and after cracking, it can be seen that there was a slight improvement in the beam stiffness as the external prestressing force increased. As prestressing force increased, the ultimate beam strength increased; yet the beam ductility, represented in the maximum deflection, decreased.

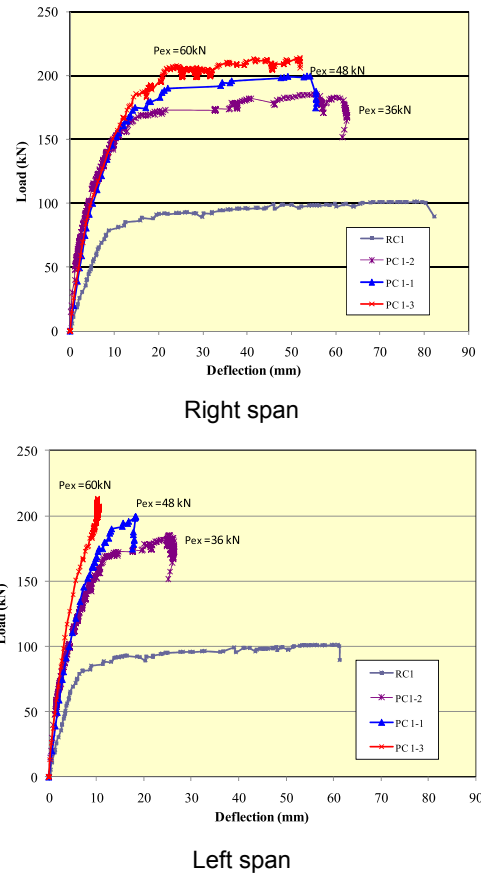


Figure 4.16 Load deflection curves of group G1

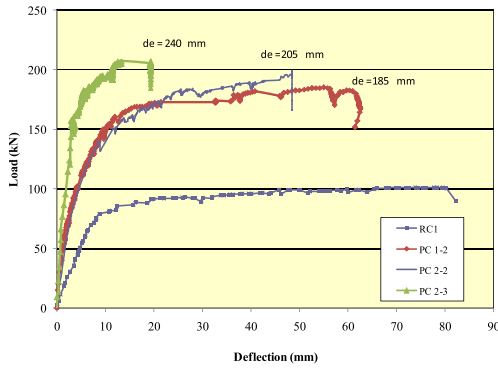
Table 4.4 Deflection at different load stages of group G1

| Beam no. | Deflection at Mid-span (mm) | | | |
|----------|-----------------------------|----------------|----------------|----------------|
| | External Prestressing | Cracking load* | Yielding load* | Ultimate load* |
| RC1 | 0 | 1.7 | 9.1 | 78.33 |
| PC1–2 | –0.6 | 1.41 | 8.35 | 55 |
| PC1–1 | –0.68 | 3.2 | 13.6 | 51.7 |
| PC1–3 | –0.75 | 3.6 | 13.2 | 44 |

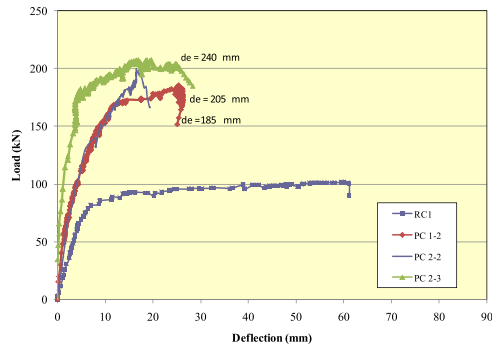
*Since applying load

Group G2 (Effective Depth of the External Prestressing Force)

Fig. 4.17 shows the relation between the load and deflection for beams RC1–1, PC1–2, PC2–2, and PC2–3 ($d/h=0, 0.9, 1.025$ and 1.2), respectively, while Table 4.5 shows the value of maximum deflections at the mid span at each stage of loading. Before cracking, deflections and stiffness of all beams were almost the same. After cracking, beam PC2–3 with the highest eccentricity had higher stiffness and lower deflection than the other beams. While after yielding, the rate of reduction in stiffness was reduced as the eccentricity increased. However, this was accompanied by less ductile behavior.



a. Right span



b. Left span

Figure 4.17 Load -deflection curves for group G2

Table 4.5 Deflection at different load stages of group G2

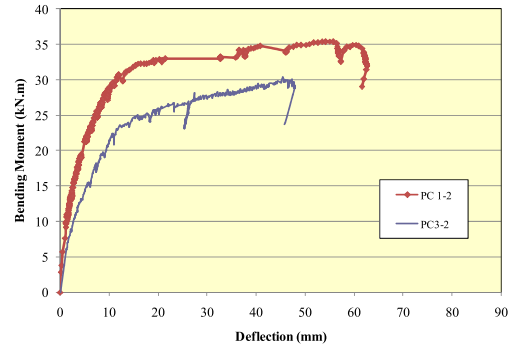
| Beam no. | Deflection at Mid-span (mm) | | | |
|----------|-----------------------------|----------------|----------------|----------------|
| | External Prestressing | Cracking load* | Yielding load* | Ultimate load* |
| RC1 | 0 | 1.7 | 9.1 | 78.33 |
| PC1-2 | -0.6 | 1.41 | 8.35 | 55 |
| PC2-2 | -1.25 | 2.3 | 9 | 48.5 |
| PC2-3 | -2.6 | 1.16 | 3.9 | 20.31 |

Group G3 (Loading Pattern)

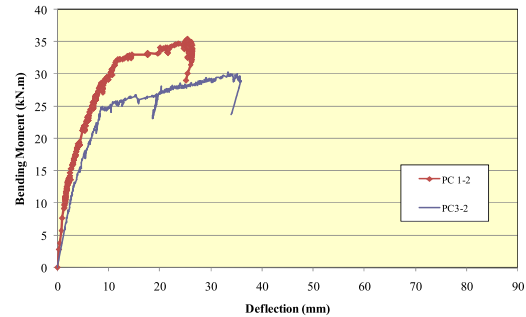
The relation between the (-ve) moment at the internal support and the deflection of beam PC1-2 (loaded by two concentrated load at the third span) and that of beam PC3-2 (loaded by one concentrated load at the mid span) are shown in Fig. 4.18 while Table 4.6 shows the value of maximum deflections at the mid span at each stage of loading.

As shown in Fig. 4.18, both beams had almost the same moment-deflection relation at early loading stages; however, as the applied load increased, beam PC3-2 showed a decrease in stiffness compared to beam PC1-2. Before yielding, beam PC1-2 had a higher

stiffness and less ductile behavior. However, after yielding, a sharp reduction in beam stiffness was observed unlike beam PC3-2 which showed a more gradual decrease in stiffness after yielding. Before failure, beam PC1-2 had a higher ductility and a higher moment resistance than PC3-2 which failed at lower moment.



a. Right span



b. Left span

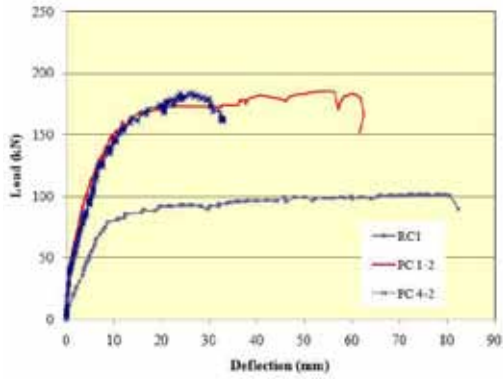
Figure 4.18 (-ve Moment – deflection) relation for G3

Table 4.6 Deflection at different load stages of group G3

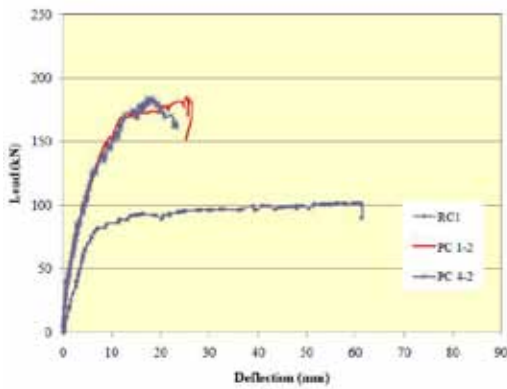
| Beam no. | Deflection at Mid-span (mm) | | | |
|----------|-----------------------------|----------------|----------------|----------------|
| | External Prestressing | Cracking load* | Yielding load* | Ultimate load* |
| RC1 | 0 | 1.7 | 9.1 | 78.33 |
| PC1-2 | -0.6 | 1.41 | 8.35 | 55 |
| PC3-2 | -0.6 | 2.5 | 10.6 | 45.4 |

Group G4 (Tendon Profile)

Fig. 4.19 shows the relation between load and deflection for beams RC1-1, PC1-2 (two bottom deviators at third span with one top deviator over interior support) and PC4-2 (one bottom deviator at mid span with two deviators at the top, each 300 mm from the interior support), while Table 4.7 shows the value of the deflection at the mid span at each stage. As can be seen, the relation between load and deflection of the two beams (PC1-2 and PC4-2) was largely similar up to yield. After yielding, beam PC1-2 showed a higher ductility and lower stiffness.

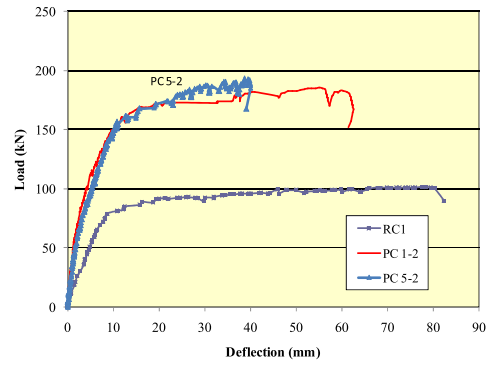


a. Right span

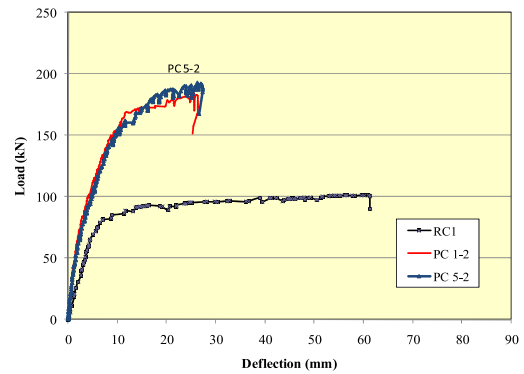


b. Left span

Figure 4.19 Load -deflection curves for group G4



a. Right span



b. Left span

Figure 4.20 Load -deflection curves for group G5

Table 4.7 Deflection at different load stages of group G4

| Beam no. | Deflection at Mid-span (mm) | | | |
|----------|-----------------------------|----------------|----------------|----------------|
| | External Prestressing | Cracking load* | Yielding load* | Ultimate load* |
| RC1 | 0 | 1.7 | 9.1 | 78.33 |
| PC1-2 | -0.6 | 1.41 | 8.35 | 55 |
| PC4-2 | -0.2 | 0.5 | 6.9 | 24 |

Group G5 (Location of Deviators)

Fig. 4.20 shows the relation between the load and deflection for RC1-1, PC1-2 (two deviators at third span) and PC5-2 (two deviators, each at 400mm from the point load near the outer support), while Table 4.8 shows the value of deflection at the mid span at each stage. As can be seen, beams PC1-2 and PC5-2 had a similar load- deflection relation before cracking, while after cracking, stiffness of beam PC5-2 was less than that of beam PC2-1. However, after yielding, beam PC1-2 showed lower stiffness and higher ductility than beam PC5-2.

Table 4.8 Deflection at different load stages of group G5

| Beam no. | Deflection at Mid-span (mm) | | | |
|----------|-----------------------------|----------------|----------------|----------------|
| | External Prestressing | Cracking load* | Yielding load* | Ultimate load* |
| RC1 | 0 | 1.7 | 9.1 | 78.33 |
| PC1-2 | -0.6 | 1.41 | 8.35 | 55 |
| PC5-2 | -1.8 | 2.4 | 13.4 | 38.7 |

4.2.3. Mode of Failure

Failure of reinforced concrete beam RC1 was ductile and accompanied by formation of plastic hinges at the interior support and at the concentrated load in both spans. While for the externally prestressed beams, the failure was destructive and accompanied by concrete spalling at the tension face, crushing at the compression face and buckling of the compression steel. However, the behavior of these beams was ductile and gave a good warning before failure, due to yielding of the nonprestressed tensile steel and the increase in deflection. Although few diagonal cracks appeared in the shear span on both sides, they did not cause failure in any of these beams.

Generally, the failure of externally prestressed beams started by forming a plastic hinge at the interior support, followed by forming a plastic hinge at the point of loading. Although the final failure tended to concen-



a. General view of beam RC1 at failure



b. At interior support



c. At right span



d. At left span

Figure 4.21 Failure of reinforced concrete beam RC1



a. At interior support



b. At span

Figure 4.22 Failure of beam PC1-2 at concentrated load



a. At interior support



b. At span

Figure 4.23 Failure of beam PC1-



a. At interior support



b. At span

Figure 4.24 Failure of beam PC1-3



a. At interior support



b. At span

Figure 4.25 Failure of beam PC2-2

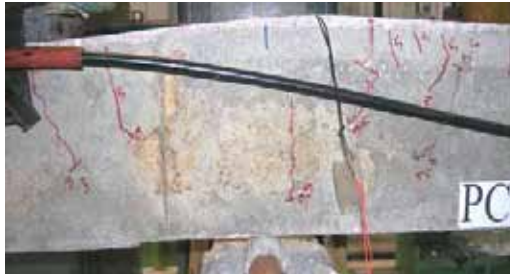


a. At interior support



b. At span

Figure 4.26 Failure of beam PC2-3



a. At interior support



b. At span

Figure 4.27 Failure of beam PC3-2



a. At interior support



b. At span

Figure 4.28 Failure of beam PC4-2



a. At interior support



b. At span

Figure 4.29 Failure of beam PC5-2

Table 4.9 Cracking, yielding and ultimate loads of tested beams

| Factor | Beam No. | Per (kN) | P_y (kN) | P_{ult} (kN) | Pult | | |
|--|----------|----------|------------|----------------|------|----------|-----------|
| | | | | | Per* | Per(RC1) | Pult(RC1) |
| unstrengthened | RC1 | 28 | 90 | 101 | 3.61 | 1.00 | 1.00 |
| External prestressing force value | PC1-2 | 51 | 146.6 | 185.3 | 3.63 | 1.82 | 1.83 |
| | PC1-1 | 70 | 160.8 | 199.2 | 2.85 | 2.50 | 1.97 |
| | PC1-3 | 84 | 175 | 208 | 2.48 | 3.00 | 2.06 |
| Effective depth of external prestressing force | PC1-2 | 51 | 146.6 | 185.3 | 3.63 | 1.82 | 1.83 |
| | PC2-2 | 66 | 140 | 199 | 3.02 | 2.36 | 1.97 |
| | PC2-3 | 76 | 153 | 207 | 2.72 | 2.71 | 2.05 |
| Loading pattern | PC1-2 | 51 | 146.6 | 185.3 | 3.63 | 1.82 | 1.83 |
| | PC3-2 | 44 | 125 | 142 | 3.23 | 1.36 | 1.41 |
| Tendon profile | PC1-2 | 51 | 146.6 | 185.3 | 3.63 | 1.82 | 1.83 |
| | PC4-2 | 38 | 125 | 184 | 4.84 | 1.36 | 1.82 |
| Location of deviators | PC1-2 | 51 | 146.6 | 185.3 | 3.63 | 1.82 | 1.83 |
| | PC5-2 | 62 | 160 | 193 | 3.11 | 2.21 | 1.91 |

*First Crack

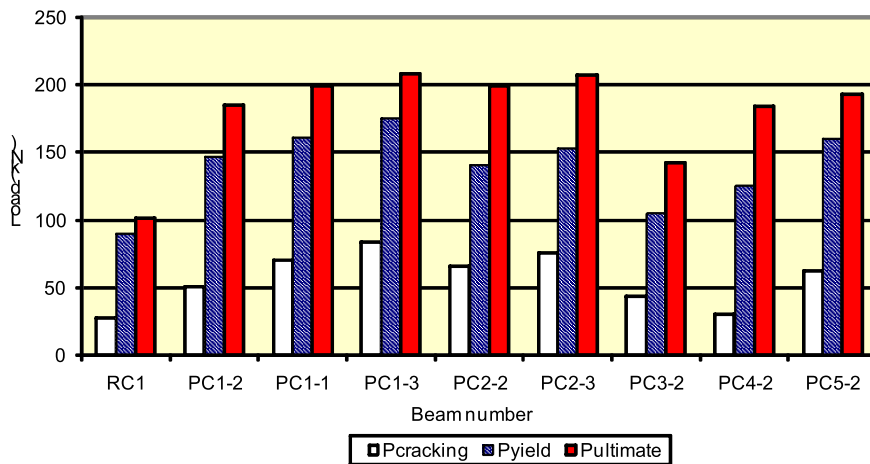


Figure 4.30 Cracking, yield and ultimate loads of test beams

trate at one of the two spans, the midspan deflections, the spread of plasticity, and the extent of cracking and crack growth can be considered approximately similar in both spans before yielding for most of the beams.

Failure for most of the beams occurred near the concentrated load location, or near to the middle, in the pure flexural zone as shown in Figs. 4.21–4.29. Except for beam PC2–3 and beam PC4–2, the failure occurred at the intermediate support. Plastic hinges also appeared on both sides of beam PC3–2 before failure occurred in the mid of left span.

Before failure occurred, considerable deflection and wide cracks were observed, giving ample warning of

impending failure. Ultimate moments were more than twice the cracking moments. Therefore, code requirements regarding the prevention of brittle failure after flexural cracking were satisfied (e.g. ACI 318–08)

4.2.4. Cracking and Ultimate Load Resistances

A significant increase in the cracking load of the beams after strengthening was observed as shown in Fig. 4.30. This increase depended on several factors such as value of the external prestressing force, the position of the deviator and the eccentricity of the external prestressing force. An appreciable increase in the ultimate strength was also obtained by the addition of

the external prestressing, although the external ropes did not reach their ultimate strength in any test. Table 4.9 shows the cracking, yielding and ultimate loads, and their ratios relative to those of beam RC1

Group G1 (Value of the External Prestressing Force)

Both cracking and ultimate loads increased as the external prestressing force increased. However, the increase in the cracking moment was higher than the increase in the ultimate moment. The cracking load of beams PC1-2, PC1-1 and PC1-3 ($P_{ext}=36, 48$ and 60kN) increased by 82%, 150%, and 200%, respectively, while the ultimate load increased by 83%, 97% and 106%, respectively, compared to the reinforced concrete beam. Comparing the beams PC1-1 and PC1-3 to beam PC1-2, it can be seen that the increase in the cracking load of PC1-1 and PC1-3 was 37% and 65%, respectively; whereas the increase in the ultimate loads was 8% and 12%, respectively.

Group G2 (Effective Depth of the External Prestressing Force)

Both cracking and ultimate load increased as the eccentricity of the Parafil Rope increased. However, the increase in the cracking load was slightly higher than the increase in the ultimate load. The cracking load of beams PC1-2, PC2-2 and PC2-3 ($d_e/h=0.9, 1.025$ and 1.2) increased by 82%, 135%, and 171%, respectively, while the ultimate load increased by 83%, 97% and 105%, respectively.

Moreover, it can be seen that increasing the eccentricity of PC2-2 by 13.9% (relative to that of PC1-2) increased the cracking load by 29% and the ultimate load by 7%, while increasing the eccentricity of PC2-3 by 33.3% (that of PC1-2) increased the cracking load by 49% and the ultimate load by 12%.

Group G3 (Loading Pattern)

Loading the strengthened beam by one concentrated load at the mid span (beam PC3-2) rather than two concentrated loads at the third span (beam PC1-2), resulted in a reduction in its ultimate strength and slightly affected its cracking strength. It should be noted that, although beams PC1-2 and beam PC3-2 cracked at loads equal to 51kN and 44kN, respectively, their corresponding cracking moments were approximately the same (about 9kN.m).

Group G4 (Tendon Profile)

Using only one deviator over the interior support and two deviators at the third span (PC1-2), show higher cracking and ultimate strengths than using two deviators over the interior support and only one de-

viator at the third span (PC4-2). The cracking load of beams PC1-2 and PC4-2 increased by 82% and 36%, relative to beam RC1, respectively, while the ultimate load increased by 83% and 82%, respectively, relative to the reinforced concrete beam.

Group G5 (Location of Deviators)

Both the cracking and ultimate strength of beam PC5-2 was higher than that of beam PC1-2. The cracking and ultimate load of beam PC5-2 increased more than those of beam PC1-2 by 22% and 4%.

4.2.5. External Prestressing Force (Parafil Rope Load)

The increase in the external prestressing force was measured using two load cells at the dead end of the ropes. Fig. 4.31 and Table 4.10 show the value of the external prestressing force at specific load stages, while Table 4.11 shows the ratio of increase in the external prestressing force at those load stages. The relation between the applied load and the external prestressing force showed a shape similar to that between the applied load and deflection.

During loading three stages were observed. Before cracking, the increase in the external prestressing force was linear and relatively low up to the flexural cracking moment. After cracking, the external prestressing force tended to increase as the applied load increased and the relation between the increase in the external prestressing force and the load was linear up to the yielding moment.

At ultimate, the rate of increase in the external prestressing force reached its maximum value as the external prestressing force tended to increase rapidly with any slight increase in the applied load. Fig. 4.31 shows a comparison between external prestressing force at different load stages.

Group G1 (Value of the External Prestressing Force)

Fig. 4.32 shows the relation between the applied load and the increase in Parafil rope load up to failure for beams PC1-2, PC1-1, PC1-3 ($P_{ext}=36, 48, 60\text{kN}$), respectively.

Before cracking, the increase in the rope load was small. After cracking there was a rapid increase in the rope load in all beams. The increase in rope load of test beams before cracking was significantly lower than that after cracking. At ultimate, the rate of increase in rope load increased as the initial external prestressing force decreased; whereas the ultimate rope load increased as the initial external prestressing force increased. The increase in rope load at ultimate relative to the breaking ultimate load of beams PC1-2, PC1-1 and PC1-3 was 60%, 66% and 71%, respectively.

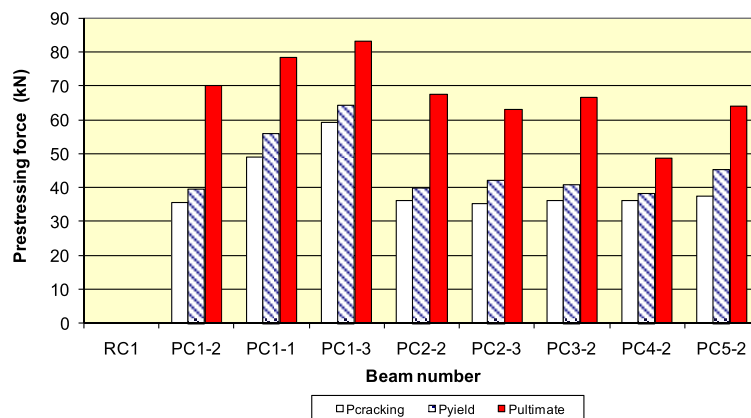
Table 4.10 External prestressing force value at different loads

| Factor | Beam No. | Initial rope load (kN) | Rope load different stages (kN) | | |
|--|----------|------------------------|---------------------------------|-------|-----------|
| | | | P_{er} | P_y | P_{ult} |
| External prestressing force value | PC1-2 | 36 | 36.72 | 40.46 | 71.42 |
| | PC1-1 | 48 | 48.5 | 56.1 | 78.6 |
| | PC1-3 | 60 | 60.84 | 66 | 85.62 |
| Effective depth of external prestressing force | PC1-2 | 36 | 36.72 | 40.46 | 71.72 |
| | PC1-1 | 35 | 36.33 | 40 | 67.65 |
| | PC1-3 | 34.2 | 35.51 | 42.27 | 63.18 |
| Loading pattern | PC1-2 | 36 | 36.72 | 40.46 | 71.42 |
| | PC3-2 | 35.3 | 36.15 | 40.91 | 66.53 |
| Tendon profile | PC1-2 | 36 | 36.72 | 40.46 | 71.42 |
| | PC4-2 | 36.1 | 36.24 | 38.26 | 48.73 |
| Location of deviators | PC1-2 | 36 | 36.72 | 40.46 | 71.42 |
| | PC5-2 | 36.8 | 37.35 | 45.46 | 64.16 |

Table 4.11 Percentage of the increase in the external prestressing force at different loads

| Factor | Beam No. | Rope load different stages%* | | | % of rope load to ultimate rope load [§] |
|--|----------|------------------------------|-------|-----------|---|
| | | P_{er} | P_y | P_{ult} | |
| External prestressing force value | PC1-2 | 2.0 | 12.4 | 98.4 | 60 |
| | PC1-1 | 1.0 | 16.9 | 63.8 | 66 |
| | PC1-3 | 1.4 | 10.0 | 42.7 | 71 |
| Effective depth of external prestressing force | PC1-2 | 2.0 | 12.4 | 98.4 | 60 |
| | PC1-1 | 1.2 | 14.7 | 91.1 | 56 |
| | PC1-3 | 4.0 | 23.8 | 85.1 | 53 |
| Loading pattern | PC1-2 | 2.0 | 12.4 | 98.4 | 60 |
| | PC3-2 | 2.5 | 16.0 | 88.6 | 55 |
| Tendon profile | PC1-2 | 2.0 | 12.4 | 98.4 | 60 |
| | PC4-2 | 0.4 | 6.0 | 34.9 | 41 |
| Location of deviators | PC1-2 | 2.0 | 12.4 | 98.4 | 60 |
| | PC5-2 | 1.5 | 23.5 | 74.3 | 53 |

*Relative to the initial external prestressing force; §Maximum rope load (at ultimate)/breaking rope load

**Figure 4.31** External Prestressing force at different load stages

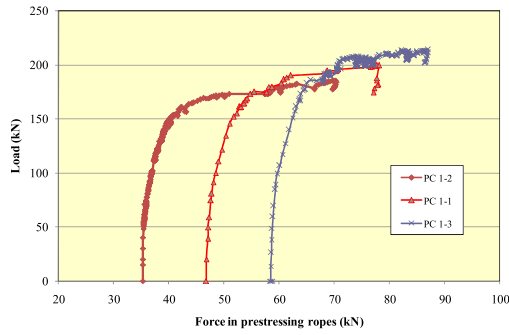


Figure 4.32 Relation between applied load and prestressing force of group G1

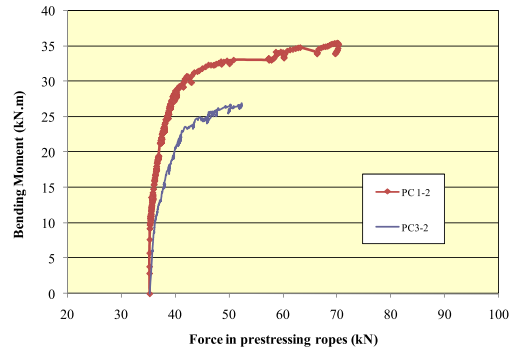


Figure 4.34 Relation between (-ve) moment and prestressing force of G3

Group G2 (Effective Depth of the External Prestressing Force)

Fig. 4.33 shows the relation between the applied load and the increase in Parafil rope load up to failure of beams PC1–2, PC2–2 and PC2–3 ($d_e/h = 0.9, 1.025$ and 1.2).

Behavior of all beams was similar up to the cracking load. After cracking the rate of increase in the rope force increased as the effective depth of the rope increased. However, at ultimate, the rate of increase in the rope force decreased as the effective depth of the rope increased.

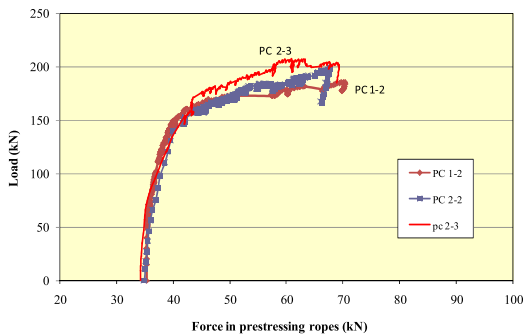


Figure 4.33 Relation between applied load and prestressing force of group G2

Group G3 (Loading Pattern)

Fig. 4.34 shows the relation between force in prestressing cables and negative bending moment at internal support for beams PC1–2 and PC3–2. During loading there was a relatively small increase in prestressing force and the rate of increase in external force was negligible at this stage. After cracking a difference in the rate of increase between the two beams is observed. The used load configuration with beam PC3–2 caused formation of yield point at lower bending moment compared to beam PC1–2. It can be seen that the force in ropes of beam PC3–2 started to increase rapidly at lower bending moment relative to beam PC1–2

Group G4 (Tendon Profile)

Fig. 4.35 shows the relation between the applied load and the increase in Parafil rope force up to failure for beams PC1–2 and PC4–2 (two deviators over the interior support). Both beams show a similar relation up to yielding of internal bonded steel. After yielding, beam PC1–2 exhibited higher increase in external prestressing force than beam PC4–2. The increase in the rope force before cracking for both beams was very small. After yielding of the internal bonded steel, the rate of increase in the rope force was very high. During this stage, beam PC4–2 showed a slow increase rate of rope force and lower values than PC1–2. The increase in rope load at ultimate relative to the breaking ultimate load of beams PC1–2 and PC4–2 was 60% and 41%, respectively.

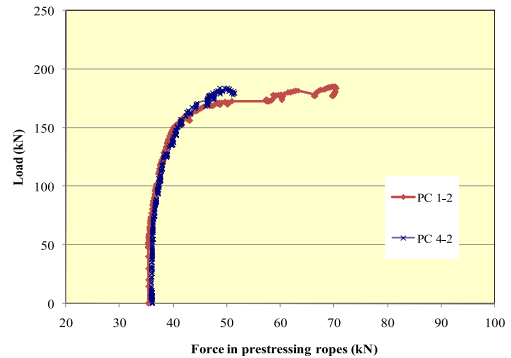


Figure 4.35 Relation between applied load and prestressing force of group G4

Group G5 (Location of Deviators)

Fig. 4.36 shows the relation between the applied load and the increase in Parafil rope force up to failure of beams PC1–2 and PC5–2. Before cracking, the increase in the rope load was almost the same for both beams. After cracking, the increase in the prestressing force was slightly higher in beam PC5–2 than in beam PC1–2. While after yielding, beam PC1–2 exhibited higher increase in prestressing force, at any load, than that of beam PC5–2. The increase in rope load at ul-

timate relative to the breaking ultimate load of beams PC1–2 and PC5–2 was 60% and 53%, respectively

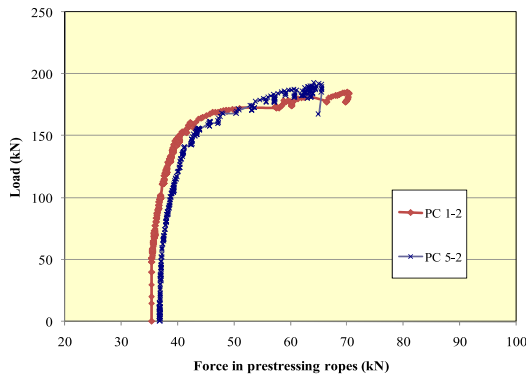


Figure 4.36 Relation between applied load and prestressing force of group G5

4.2.6. Total and Secondary Prestressing Moments

In continuous beams with nonconcordant tendon profiles, prestressing generally induces reactions at the supports. As a result, the supports exert reactions on the beam, causing the secondary moments ($M_{secondary}$). Total prestressing moment can be calculated using equivalent load method. Hence, secondary moment can be easily obtained from the following equation:

$$M_{total} = M_{primary} + M_{secondary}$$

Where $M_{primary}$ is the product of the prestressing force times its eccentricity from the center of gravity of the cross section of the beam. Table 4.12 shows the values of primary, secondary and ultimate moment of tested beams, while Figs. 4.37–4.41 show the distribution of the total, primary and secondary moments along the span of each beam. It can be seen that the total and the secondary moments increased as the prestressing force and the effective depth of the external prestressing force

Table 4.12 Primary, secondary and total prestressing moment

| Beam No. | prestressing moment (kN.m) | | | | | |
|----------|----------------------------|---------|-----------|-------------|---------|-----------|
| | At support | | | At mid span | | |
| | total | primary | secondary | total | primary | secondary |
| RC1 | | | | | | |
| PC1-2 | 4.31 | 2.95 | 1.03 | -2.46 | -2.95 | 0.50 |
| PC1-1 | 5.75 | 3.94 | 1.81 | -3.27 | -3.94 | 0.66 |
| PC1-3 | 7.18 | 4.92 | 2.26 | -4.09 | -4.92 | 0.83 |
| PC2-2 | 5.07 | 2.87 | 2.20 | -3.02 | -3.68 | 0.66 |
| PC2-3 | 5.90 | 2.80 | 3.10 | -3.67 | -4.79 | 1.11 |
| PC3-2 | 4.31 | 2.95 | 1.36 | -2.46 | -2.95 | 0.50 |
| PC4-2 | 1.30 | 2.98 | -1.68 | -1.37 | 1.49 | 0.12 |
| PC5-2 | 3.51 | 3.03 | 0.48 | -2.84 | -3.03 | 0.19 |

increased. The tendon profile and deviators locations can magnify or reduce the final prestressing moment. This effect was most significant in beam PC 4–2 and least visible in beam PC 5–2. This is attributable to the layout of the tendons in these beams; in beam PC 5–2, it was nearly concordant.

4.2.7. Strain for Normal Steel

The strain on the bonded steel bars was measured using six strain gauges fixed to the surface of the top and bottom reinforcement in three locations, at mid of each span and at the interior support. Figs. 4.42–4.48 show the relation between jack load and steel strain at mid-span of each beam. As can be seen from the graphs, the increase in strain in the tensile reinforcement with applied load showed a trend similar to the load-deflection response. The longitudinal reinforcement at top and bottom of beams was similar. While the tension reinforcement always yielded at advanced load stages, the compression reinforcement quite often developed only small stresses all the way up to beam failure

Before cracking, the increase in tension steel strain was linear and relatively low up to the flexural cracking load, but after cracking, the rate of increase in strain increased, and close to ultimate the rate rapidly increased. After cracking, different types of reading were observed depending on the crack locations relative to the strain gauge fixed on the bar surface. If cracks occurred on both sides of the strain gauge, its reading would decrease as the load increased and probably become (-ve) depending on the distance between the cracks and the strain gauge. If the strain gauge was near the crack, its reading would be very high.

This lead to a difficulty in comparing the results of strain gauges readings, however, it was beneficial during calculating cracking and yielding loads.

4.2.8. Changes in Rope Eccentricity (Second Order Effect)

Changes in rope eccentricity during external prestressing process and loading were calculated by measuring deflection at the middle and at the deviator locations; the increase or decrease in the rope eccentricity was determined from the difference between the deflection at the middle and the average deflection at the deviators.

During the external prestressing process, there was an increase in the eccentricity in the middle; while during loading, this eccentricity decreased as the load increased. Before cracking, the loss in rope eccentricity was small, but after cracking, it was increased as the load increased then rapidly increased at the ultimate stage. Before cracking, the deflection and the change in rope eccentricity were small; the measured values of losses in the rope eccentricity require more sensitive LVDTs to record more accurate measurements. How-

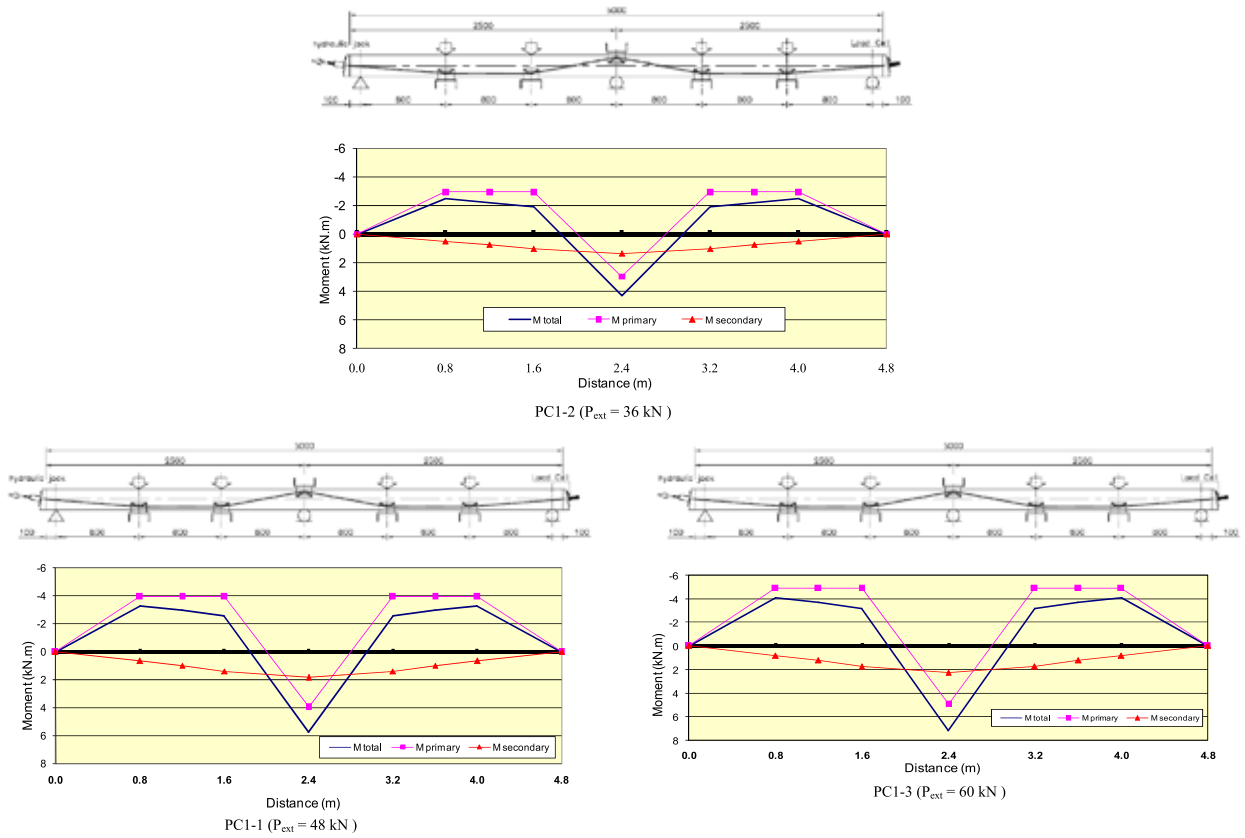


Figure 4.37 Total, Primary and Secondary prestressing bending moments Beams in Group 1 (Value of external prestressing force)

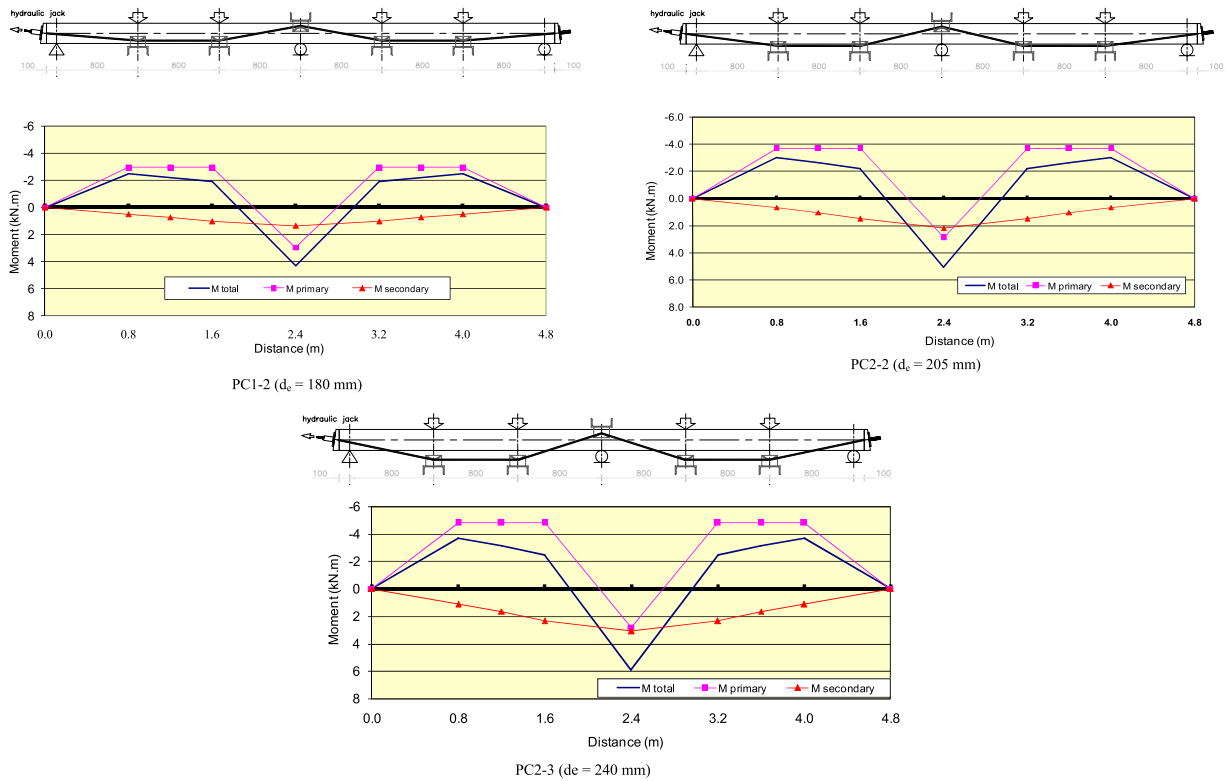
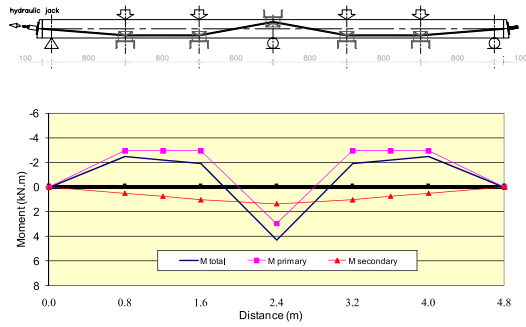
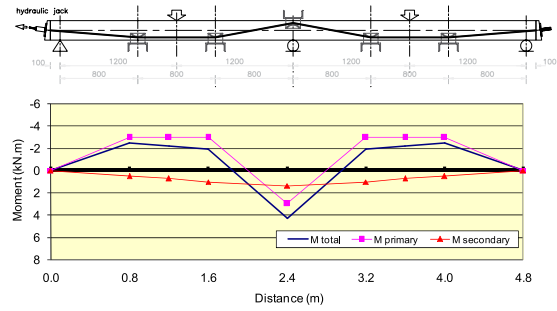


Figure 4.38 Total, Primary and Secondary prestressing bending moments Beams in Group 2 (Effective depth of external prestressing force)

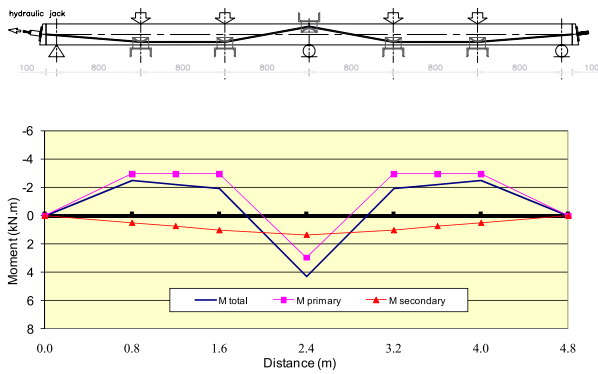


PC1-2 (Two concentrated load at third span in each span)

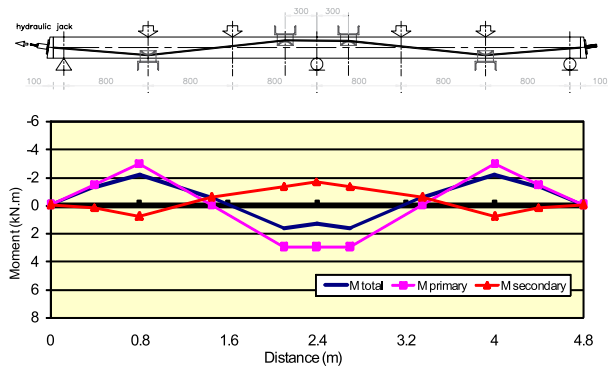


PC3-2 (One concentrated load at mid span in each span)

Figure 4.39 Total, Primary and Secondary prestressing bending moments Beams in Group 3 (Loading pattern)

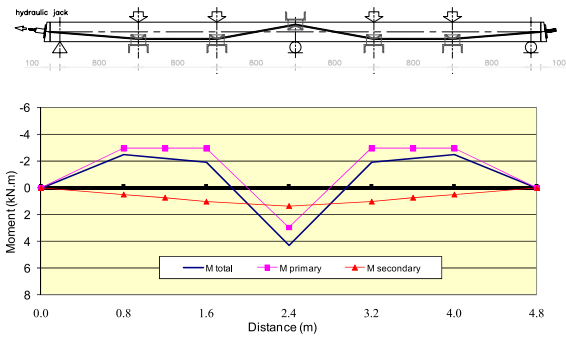


PC1-2 (Two concentrated load at third span)

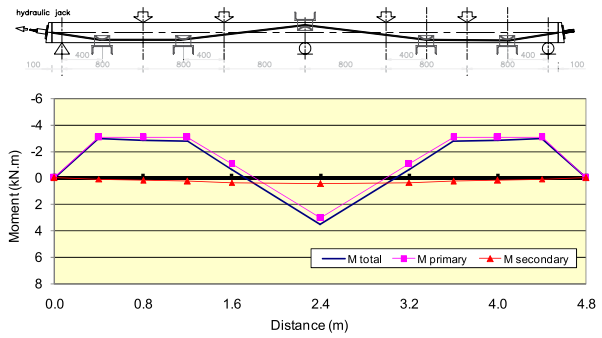


PC4-2 (two deviators at interior support)

Figure 4.40 Total, Primary and Secondary prestressing bending moments Beams in Group 4 (Tendon profile)



PC1-2 (Two deviators at third span)



PC5-2 (Two deviators under the outer applied load)

Figure 4.41 Total, Primary and Secondary prestressing bending moments Beams in Group 5 (Location of deviators)

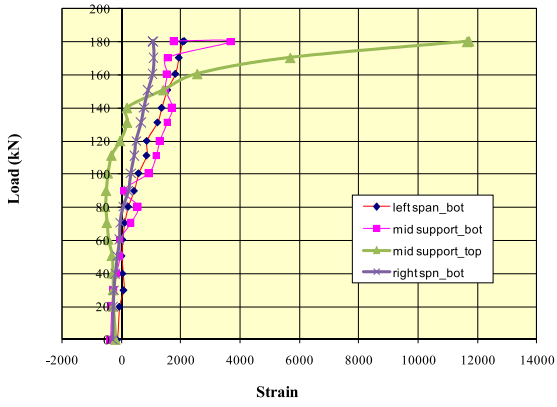


Figure 4.42 Relation between load and steel strain for beam PC1-2

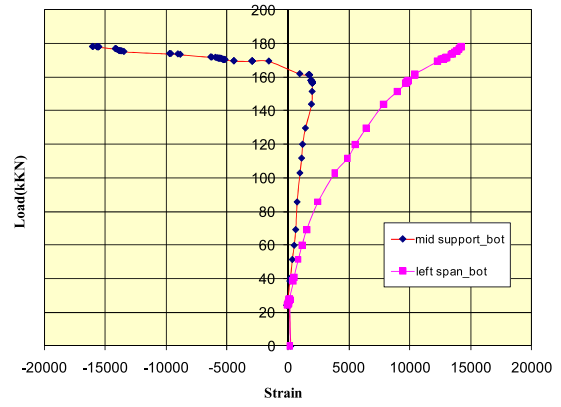


Figure 4.43 Relation between load and steel strain for beam PC1-1

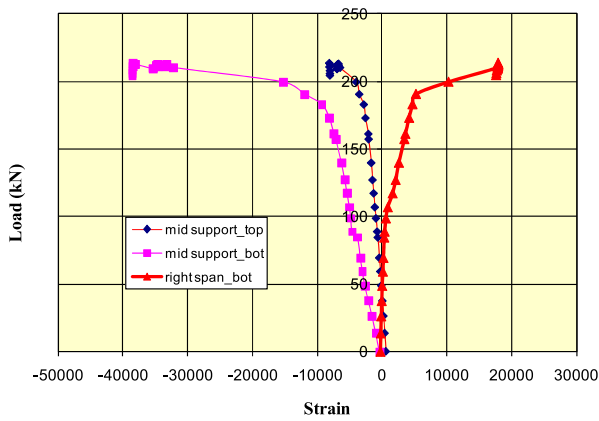


Figure 4.44 Relation between load and steel strain for beam PC1-3.

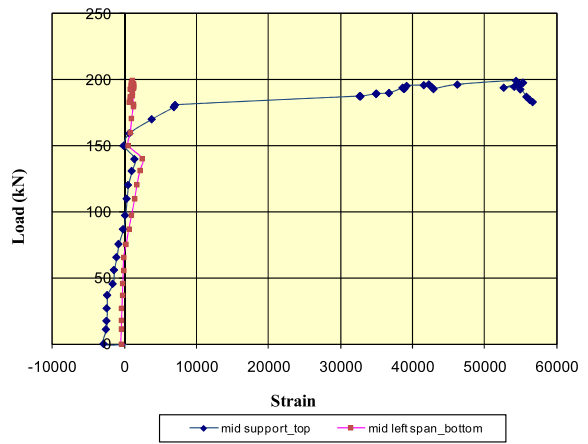


Figure 4.45 Relation between load and steel strain for beam PC2-2

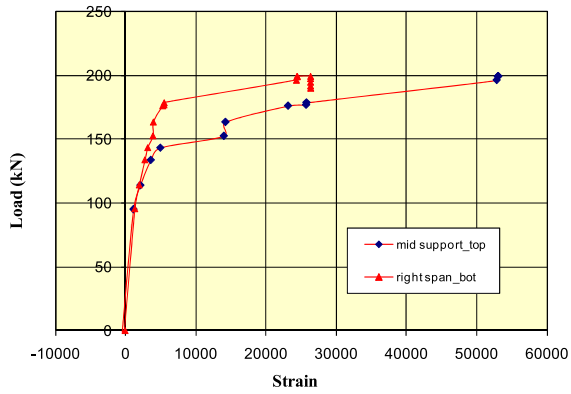


Figure 4.46 Relation between load and steel strain for beam PC2-3

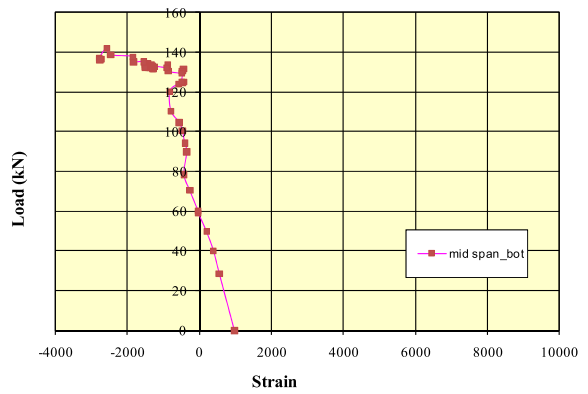


Figure 4.47 Relation between load and steel strain for beam PC3-2

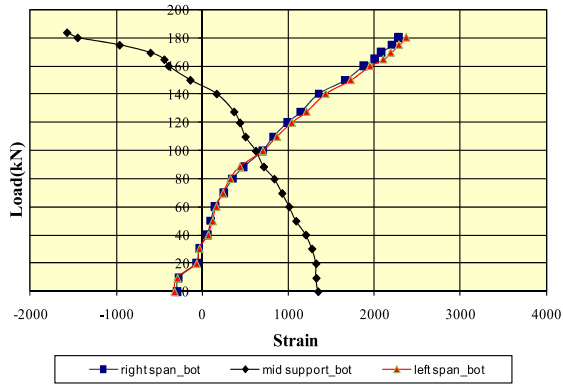


Figure 4.48 Relation between load and steel strain for beam PC4-2

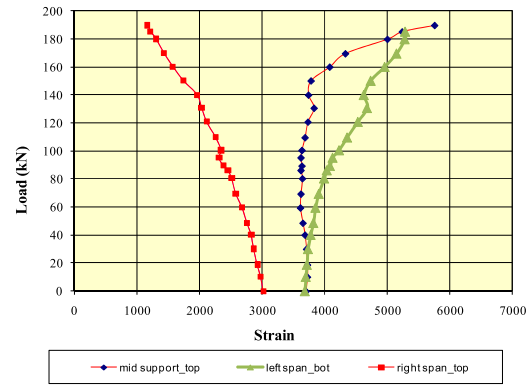


Figure 4.49 Relation between load and steel strain for beam PC5-2

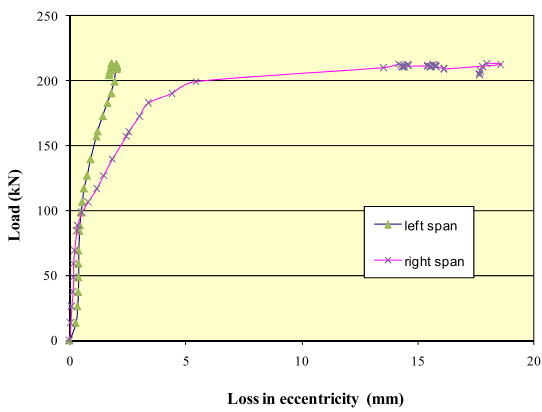


Figure 4.50 Relation between load and loss in rope eccentricity for beam PC1-3

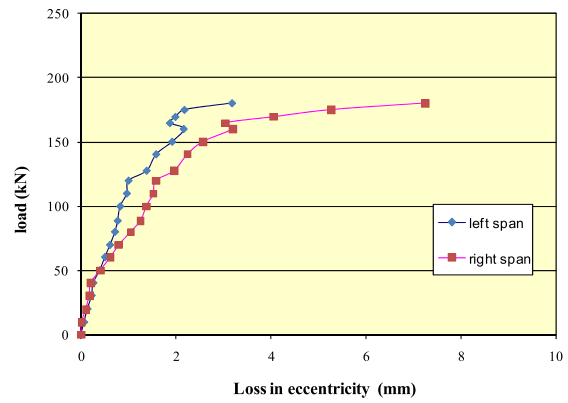


Figure 4.51 Relation between load and loss in rope eccentricity for beam PC4-2

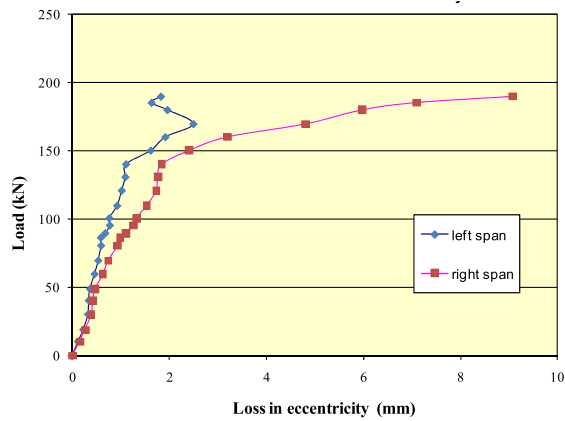


Figure 4.52 Relation between load and loss in rope eccentricity for beam PC5-2

ever, after cracking, the changes in the rope eccentricity were significant, especially at ultimate, hence, the sensitivity of the used LVDTs was sufficient.

Figs. 4.50–4.52 show the relation between load and losses in rope eccentricity of beam PC1–3, beam PC4–2 and beam PC5–2. Comparing all beams, it can be seen that the location of maximum deflection and maximum moment has a significant effect on the change in rope eccentricity; with the failure plane at the mid span or near to it, there was a significant loss in the rope eccentricity.

5. Discussion of Test Results

Introduction

Results of testing nine beams (one was ordinary reinforced concrete beam while the others were externally strengthened using Parafil Rope) were presented in the previous chapter. In this chapter, the effect of the studied factors on the behavior of tested beams are compared and discussed.

5.1 General Behavior

During loading, externally strengthened concrete beams showed well distributed cracks because of the presence of nonprestressed steel. However, cracks widths on the strengthened beams were smaller than on reinforced concrete beams as the presence of the compression force prevented cracks from opening. Cracks, in the shear span of reinforced concrete beams extended and distributed more than those on strengthened beams and their number was higher. This is because the vertical component of the external compression force reduced the shear force while the horizontal component reduced the principal tensile stress in the shear span.

Since almost all the tendons profiles were nonconcordant, reactions were induced at the supports due to the external prestressing. As a result, the supports exert reactions on the beam, causing the secondary moments.

During loading, the relation between load and deflection of the strengthened beams showed three stages, similar to reinforced concrete beam. In the first stage, this relation was linear and the increase in deflection was relatively small. After cracking, there was a reduction in stiffness and the rate of increase in deflection constantly changed. However, the stiffness of the strengthened beams was higher than the stiffness of reinforced concrete beams. This can be attributed to the slow propagation and extension of the cracks in the strengthened beams due to the external compressive force.

After formation of plastic hinges, stiffness of the strengthened beam was very small and the slope of the load-deflection curve was almost horizontal, even

though the stiffness of the strengthened beam was still higher than that of the non-prestressed beam at the same stage. In this stage, the internal reinforcement stress was in the inelastic range while the external rope did not reach its maximum strength. Both the cracking and ultimate moments of the strengthened beams were significantly higher than those of the reinforced concrete beam due to the effect of the additional compressive stress (produced by the external prestressing force) and the counter prestressing moment that reduced the effect of the applied moment.

During loading, there was an increase in the external prestressing force. Before cracking, the increase in external prestressing force was small due to the small deflection at this stage, while, after cracking, there was a more rapid increase in external prestressing force due to the more rapid increase in deflection. Therefore, it can be said that factors which affect the beam's deformation also have an effect on the increase in external prestressing force.

Furthermore, because the external ropes were not bonded to the concrete, there was a reduction in its effective depth during loading resulting in a reduction in the lever arm as the deflection increased. Since the loss of effective depth is these

simply equal to the deflection of the beam relative to the deflectors, it is obvious that the relation between loss and load will be similar to the relation between load and deflection and will depend on the same parameters. Therefore, factors which increase deflection are expected to increase the loss in rope effective depth as well. However, the effect of factors varies with the variation in tendon configuration.

Fig.5.1 shows schematic diagrams of the bending moment and shear force of the tested beams due to the applied load (third point loading and one concentrated load at midspan), and bending moment and shear force diagrams due to external prestressing. While Fig.5.2 shows the primary, secondary and total bending moments of the tested beams due to prestressing force.

Fig.5.2 shows that the total and secondary prestressing moments increased as the prestressing force and tendon eccentricity increased, and tendon profile and deviators locations had a significant effect on the total and secondary moments. Moreover, Fig. 5.2 shows that while the secondary moment reduced the moment at the support, it magnified the bending moment within the span which negatively affected the strength of the strengthened beam; while in case of beam PC4–2, the secondary moment reduced the prestressing moment at both the interior support and the mid span, hence reducing the resistance moment.

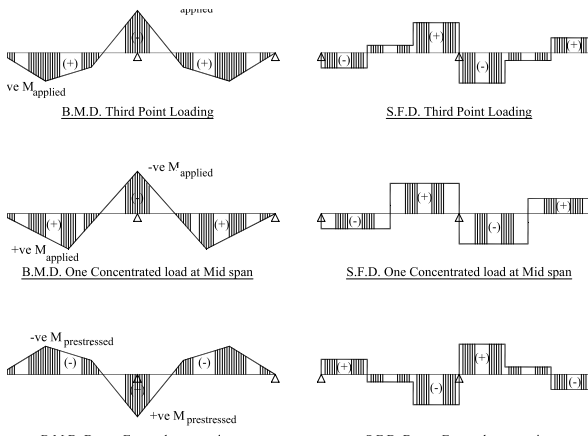
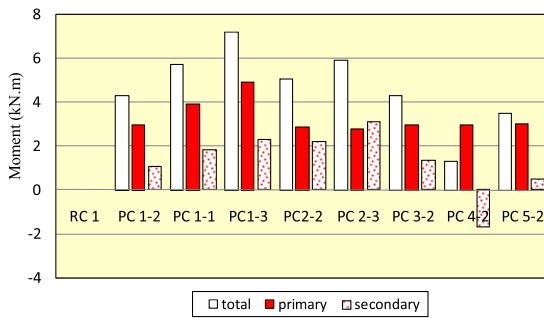


Figure 5.1 Bending moment and shear force diagrams of tested beams



a) Prestressing moment at the interior support

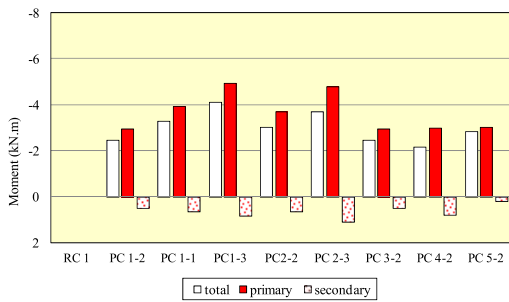


Figure 5.2 Total, Primary and Secondary prestressing bending moment diagrams for tested beams

5.2 Discussion of Results of Test Beams

The effect of each factor considered in this study on the behavior of the strengthened continuous beam is discussed as follows:

5.2.1 Effect of External Prestressing Force (Group G1)

Increasing the external prestressing force increased the resisting prestressing moment that counterbalanced the applied moment and improved the beam strength.

Increasing the external prestressing also increased the compressive stress at the tension side, hence, reducing the net tensile stress. This improved the cracking resistance of the beam and enabled the beam to resist higher load.

5.2.1.1 Cracking Patterns

Increasing the external prestressing force delayed the appearance of flexural cracks and decreased the rate of crack propagation. Increasing the external prestressing force increased its vertical component, hence, increased shear-cracking load and reduced number of diagonal cracks.

5.2.1.2 Load-deflection Behavior

As can be seen from Fig. 4.16 and Table 4.4, after cracking, deflection of beams in group G1 decreased as the applied external prestressing force increased, and its stiffness increased as the external prestressing force increased. This is because the increase of external prestressing force reduced the cracks widths and its propagation, hence reduced the reduction in the beam stiffness after cracking.

Fig. 5.3 shows that the increase in the external prestressing force has a negligible effect on the deflection, while, at ultimate, the deflection and ductility are inversely proportional to the external prestressing force.

The loss of ductility with increasing the prestressing force is associated mainly with a decrease in the ultimate deformation of the member. In turn, ultimate deformations are inversely proportional to the neutral axis depth at failure.

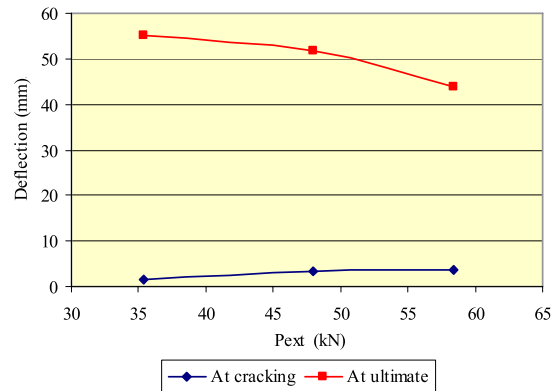


Figure 5.3 Deflection-External prestressing force relation

5.2.1.3 Cracking and Ultimate Loads

Increasing the external prestressing force increased the cracking load, as beam PC1-3 (Pext = 60kN) with the higher initial external prestressing force cracked at a higher applied load than PC1-1 (Pext = 48kN), and both were higher than beam PC1-2 (Pext = 36kN) which had the lowest initial prestressing force. This 67% increase in initial prestressing force improved the cracking load by 65% (comparing PC1-3 to PC1-2). This is due to the increase in external compression force in addition to the increase in prestressing moment that reduced the tensile stresses in the concrete section and consequently delayed cracking. However, the ultimate

strength of the strengthened beams is slightly affected by the increase in external prestressing force.

The ultimate loads of PC1–2, PC1–1 and PC1–3 were slightly different, and increasing the external prestressing force by 67% (PC1–3 compared to PC1–2) just increased the ultimate load by 12%. This is because the ultimate strength, which depends mainly on the prestressing tendons (areas and stresses) in tension and concrete in compression, was controlled by the concrete strength. The failure of the strengthened beams was due to concrete crushing, while the stress in Parafil rope never reached its ultimate strength.

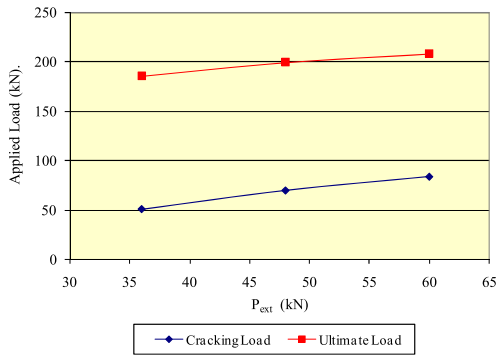


Figure 5.4 Applied load-External prestressing force relation

From Fig. 5.4 it can be seen that both cracking and ultimate loads vary linearly with the external prestressing force and the amount of increase in load at both cracking and ultimate loads are almost the same.

5.3.1.4 External Prestressing Force (Parafil Rope Load)

From Fig. 5.5, it can be seen that the value of the initial external prestressing force had a negligible effect on the increase in external prestressing force at cracking, while at ultimate the rate of increase in external prestressing force decreased as the initial prestressing force increased. This is because beam with higher prestressing force had higher stiffness and lower deflection, and thus had lower increase in external prestressing force.

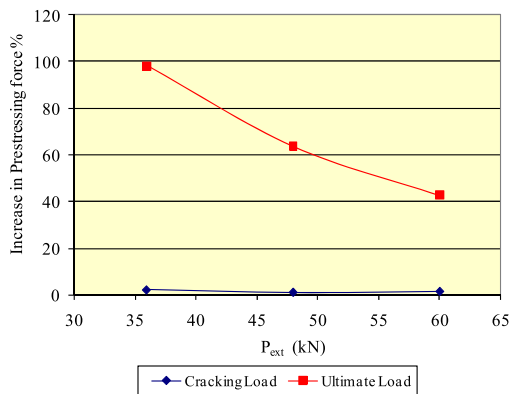


Figure 5.5 Relation between the increase in External prestressing force and the initial external prestressing force

5.2.2 Group 2 (Effective Depth of the External Prestressing Force)

Increasing the effective depth of the external prestressing force increased the prestressing moment and enabled the section to tolerate more loads. Increasing the effective depth also increased the prestressing compressive stress that prevented cracks from extending and decreased the reduction in inertia and stiffness after cracking. At the same time, as the effective depth increased the angle of deviation increased and the vertical component of the prestressing force increased. This resulted in reducing the shear force and improved the shear strength.

5.2.2.1 Cracking Patterns

From Fig. 4.9 it is shown that due to the increase in compressive stress, the flexural cracks on beam PC2–3 ($d_e/h=1.2$) appeared later and extended more slowly than the other beams. The same was observed when comparing the cracks on the shear span; those of PC2–3 ($d_e/h=1.2$) appeared at higher load and extended more slowly. This was attributed to the increase in the compressive stress as well as the increase in the external prestressing moment.

5.2.1.2 Load-deflection Behavior

After prestressing, the beam with higher effective depth had higher prestressing moment and higher camber as shown from Table 4.3 and Fig. 4.17.

After loading and until cracking, the effect of increase in the ratio of effective depth of the external prestressing force on stiffness and deflection was negligible as shown in Fig. 5.6. After cracking, the increase in effective depth of the prestressing force reduced the propagation of the cracks and improved the beam stiffness that resulted in lower deflection. At ultimate, the rate of increase in deflection significantly decreased as (d_e/h) increased, and beam with higher effective depth (PC2–3) had lower ductility than the beam with lower effective depth

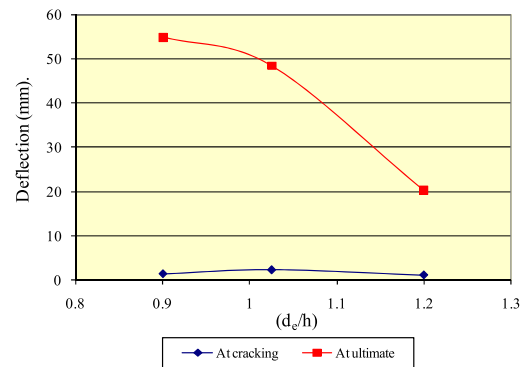


Figure 5.6 Deflection-(External prestressing force effective depth/depth) ratio Relationship

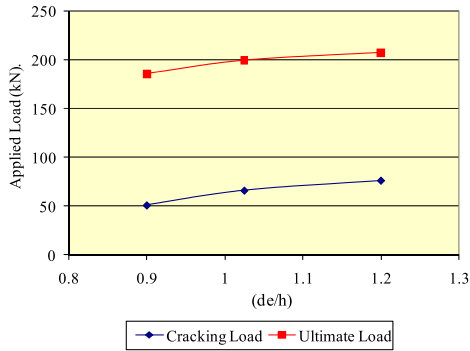


Figure 5.7 Applied load (effective depth/depth) ratio relationship

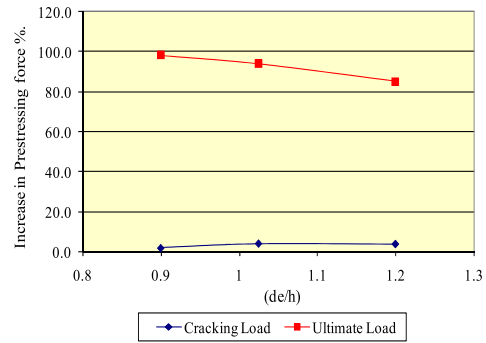


Figure 5.8 Relation between the increase in External prestressing force and (effective depth of the external prestressing force/ depth) ratio

5.2.2.2 Cracking and Ultimate Loads

The increase in the effective depth of the external prestressing force can be considered as one of the main factors affecting the increase in the cracking and ultimate moments. However, as shown in Fig. 5.7, although the rate of increase in both cracking load and ultimate load was almost similar, the increase in the cracking load was higher than the increase in the ultimate load. Increasing effective depth by 33% (PC2–3 compared with PC1–2) increased the cracking load by 49% and increased the ultimate load by 12% only. The increase in cracking load is attributed to the higher prestressing moment produced by higher effective depth, while the increase in ultimate moment can be attributed to the increase in the lever arm between the internal forces due to the increase in the effective distance of the prestressing tendons. The slight increase in the ultimate load compared to the cracking load may be explained by knowing that the ultimate load in all beams in this group was controlled by the concrete strength, and the failure of the strengthened beams was due to concrete crushing, while the stress in the Parafil Rope never reached its ultimate strength.

5.2.2.3 External Prestressing Force (Parafil Rope Load)

Fig. 5.8 shows the relation between the applied load and the increase in external prestressing force of beams PC1–2, PC2–2 and PC2–3 ($de/h = 0.9, 1.025$ and 1.2) at cracking and ultimate stages. The increase in the external prestressing force of beams in this group at cracking is almost negligible. After cracking, the rate of increase in the rope force increased as the effective depth of the rope increased.

This is because the change in the rope stress at this stage is relative to its distance from the neutral axis; the greater the distance the higher the stress. However, at ultimate, the rate of increase in the rope force decreased as the effective depth of the rope increased. This can be attributed to the low ductility of the beams as the effective depth of the tendon increased. The beam with higher effective depth had a larger angle of deviation which may increase the friction losses between the tendons and the deviators.

5.2.2.4 Change in Rope Effective Depth

The ratio of loss in effective depth decreases as the effective depth increases as shown in Fig. 5.9.

5.2.3 Loading Pattern (Group G3)

Using Loading pattern composed of one concentrated load at midspan (instead of two concentrated load at the third span) with two deviators at third point of the clear span resulted in concentrating the deformation under the concentrated load rather than distributing it between the two concentrated loads. This led to higher deflection, rapid increase in loss of effective depth of the external prestressing force especially at ultimate, and rapid failure, hence, reduced the beam strength, which in turn reduced the optimum utilization of the applied prestressing force.

5.2.3.1 Cracking Patterns

Applying one concentrated load at midspan PC3–2, compared to third point loading PC1–2 resulted in the following:

1. Cracks were concentrated at midspan with a tendency to deviate towards the concentrated load due to the effect of shear stress, while the cracks were almost vertical and extended from lower tension fibers to upper compression fibers in case of two point loads.
2. More cracks with wider distribution over the intermediate support were observed in case of one point loading compared to two points loading.
3. Significant increase in crack width at the same loading level was observed in case of one concentrated load.

This is can be attributed to the concentration of stresses at the midspan at the loading position that was accompanied by a higher rate of loss in effective depth (beam PC3-2). This decreased the ability of external prestressing force to counterbalance the applied load and to resist the propagation of cracks. Consequently, lower cracking resistance of beam PC3–2 was obvious compared to beam PC1–2, with early formation of cracks at intermediate support and midspan.

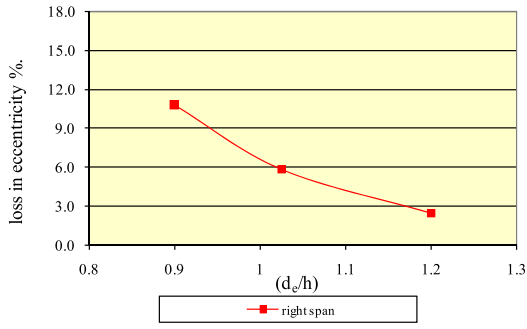


Figure 5.9 Relation between losses in ultimate Rope effective depth and (rope effective depth/depth) ratio

5.2.3.2 Load-deflection Behavior

From Fig. 5.10 it can be seen that at cracking, the maximum deflection was almost equal in both beam PC1–2 and beam PC3–2 as both beams had the same stiffness. After cracking, beam PC3–2 suffered a rapid loss in stiffness compared to beam PC1–2 as cracks concentrated under the applied load and rapidly extended towards the load. This resulted in a higher deflection and rapid formation of the plastic hinges. After yielding, cracks spread on the beam PC1–2 and rapidly extended. This resulted in a rapid loss in stiffness and a higher deflection at ultimate compared to beam PC3–2. In addition, from Fig. 5.10, it can be seen that the loading type seems to have no effect on deflection at cracking, while at ultimate the deflection is inversely proportional to the shear span (span between load and support).

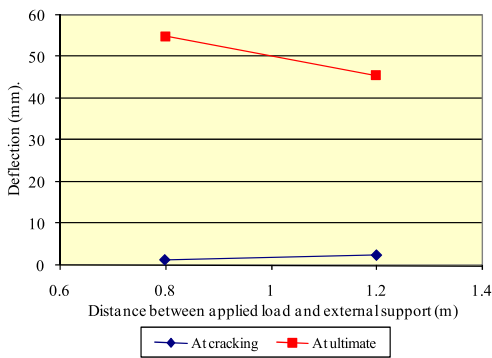


Figure 5.10 Deflection-Shear span relation

5.2.3.3 Cracking and Ultimate Loads

Although beam PC1–2 and beam PC3–2 cracked at loads equal to 51kN and 44kN, respectively, it should be noted that though these two loads are different in value, the corresponding cracking moments were approximately the same at approximately 9kN.m (Fig. 5.11). This is because both beams had the same eccentricity at the critical section. The ultimate load was approximately 185 and 142kN corresponding to moments of 35 and 30kN.m for beams PC1–2 and PC3–2, respectively. The difference in these moments is approximately 16%.

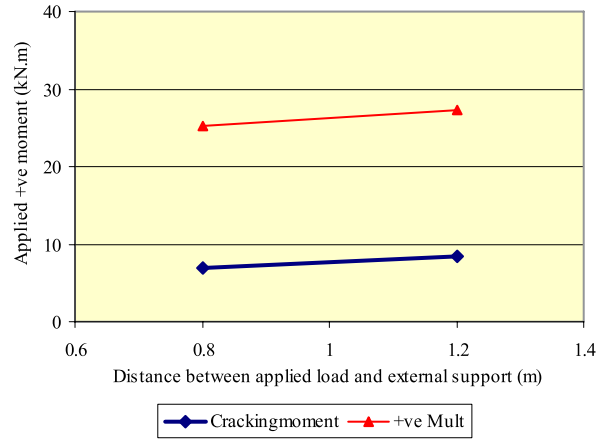
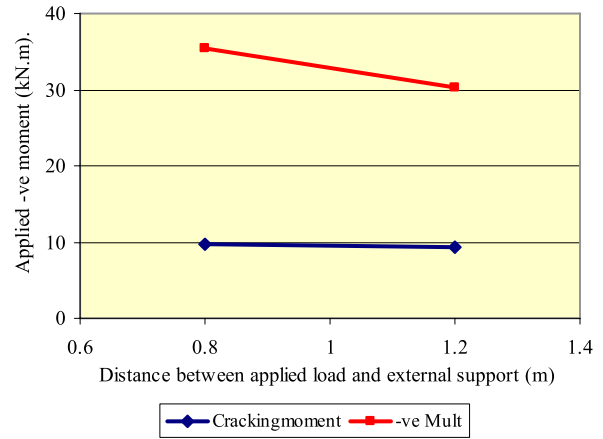


Figure 5.11 Bending moment-shear span relation

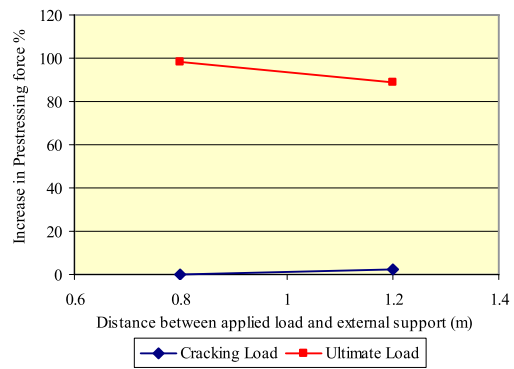


Figure 5.12 Relation between the increase in external prestressing force and the shear span

This is attributed to the rapid loss of eccentricity of beam PC3–2 at the critical section. From Fig. 5.11, it can be seen that the loading pattern has a negligible effect on the cracking moment, while the ultimate moment at support is inversely proportional to shear span contrary to the span ultimate moment which is proportional to shear span.

5.2.3.4 External Prestressing Force (Parafil Rope Load)

From Fig. 5.12, it can be seen that the value of shear span has a negligible effect on the increase of external prestressing force at cracking, while at ultimate load

the rate of increase in the external prestressing force decreased as the shear span increased. This is because the increase in external prestressing force depends on the deflection of the beam as mentioned earlier, and since the beam with less shear span (PC1–2) was more ductile; it had higher deflection at ultimate, and consequently higher increase in external prestressing force.

5.2.3.5 Change in Rope Effective Depth

Applying a concentrated load at midspan instead of applying loads at deviators location at third points of the span, results in a significant increase in the difference between the midspan deflection and average deflection at deviators, thus resulting in a significant increase in loss of rope effective depth. From Fig. 5.13, it can be seen that increasing the shear span and the applied load increased the loss in rope effective depth at ultimate load; on the other hand, at cracking load the shear span almost has no effect on the loss of rope effective depth.

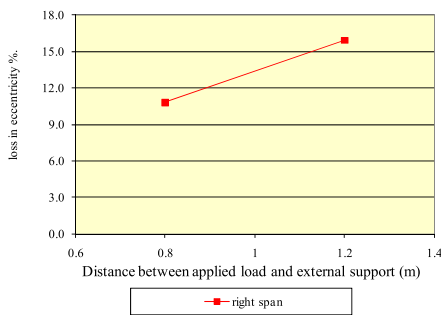


Figure 5.13 Relation between ultimate losses in Rope effective depth and distance between loads and external support

5.2.4 Group 4 (Tendon Profile)

The effect of the strengthened region was shown in this group. Due to location of deviators beam PC1–2 had a higher resisting prestressing moment at the mid support and at the third span than beam PC4–2, as shown in Fig. 5.2. While the secondary moment of beam PC2–1 improved the ultimate strength of the beam at the mid support, it negatively affected the ultimate strength of beam PC4–2 at the same support. This resulted in a reduction of the flexural strength.

5.2.4.1 Cracking Patterns

Cracks appeared at the top of intermediate support on beam PC4–2 earlier than that on beam PC1–2 due to the inverse effect of the secondary moment as previously discussed. Length of the top plastic hinge of beam PC4–2 was shorter than that of beam PC1–2, while the bottom cracks spread on a wider distance. This can be attributed to the higher effective depth and the higher compressive prestressing stress between the top two deviators and to the lower effective depth and compressive

prestressing stress at the bottom of beam PC4–2 compared to beam PC1–2.

5.2.4.2 Load-deflection Behavior

Fig. 5.14 shows that beams with different tendon configuration had almost similar deflections at cracking load. However, at ultimate, beam PC4–2 (Profile 2) was less ductile and had lower deflection than PC1–2 (Profile 1), as it had a shorter plastic hinge length. That made beam PC4–2 stiffer and less ductile at ultimate.

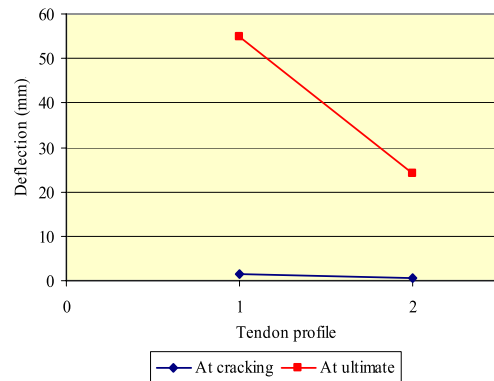


Figure 5.14 Deflection-Tendon Profile relationship

5.2.4.3 Cracking and Ultimate Moments

Strengthening the region over the interior support by two deviators resulted in decreasing the total prestressing moment, hence, reducing the cracking strength of the strengthened beam as shown in Fig. 5.15. While at ultimate, the ultimate strength of the strengthened beams was mainly affected by the prestressing force and its effective depth at the critical section, and slightly affected by the secondary moment due to its low value relative to the applied ultimate moment. Hence, both beams had almost the same ultimate strength.

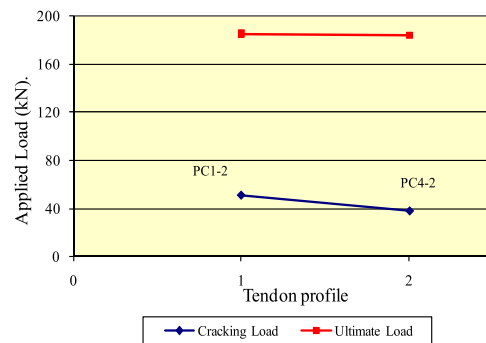


Figure 5.15 Applied load-Tendon profile relationship

5.2.4.4 External Prestressing Force (Parafil Rope Load)

As shown in Figs. 4.19 and 5.16 the increase in the external prestressing force before cracking was negligible in both beams due to the low deflection at this

stage. After cracking PC1–2 (Profile 1), had higher deflection which resulted in greater increase in the external prestressing force.

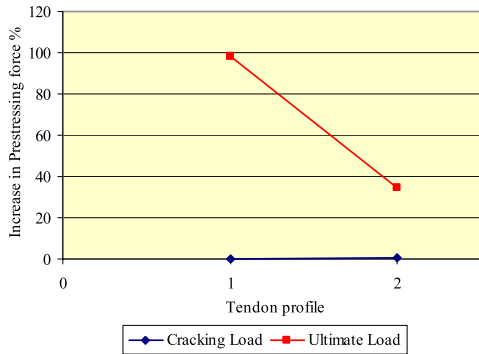


Figure 5.16 Relation between the increase in External prestressing force – Tendon Profile

5.2.4.5 Change in Rope Effective Depth

The loss in effective depth is simply a function of the deflection of the beam, therefore both beams PC1–2 (Profile 1) and PC4–2 (Profile 2) had very low loss in effective depth before cracking. After cracking and due to the ductility of PC1–2, it had slightly higher loss in effective depth compared to PC4–2.

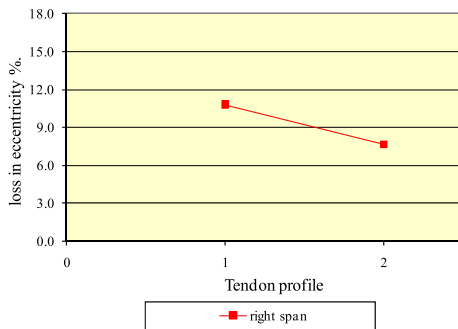


Figure 5.17 Relation between losses in Rope effective depth and Tendon Profile

5.2.5 Group 5 (Location of Deviators)

Providing the deviators at the critical sections of the beam enhanced its flexural strength capacity due to the higher prestressing moment that covered a wider length at the critical section.

5.2.5.1 Cracking Patterns

Cracks on beam PC5–2 appeared at a higher load and spread on a wider distance compared to that on beam PC1–2 due to its higher prestressing moment that covered the critical section and enhanced the cracking strength. During loading and due to the reduction in the eccentricities of the prestressing force and hence the prestressing moment at the inner concentrated loads, cracks appeared under both concentrated loads (external and internal). Cracks on beam PC1–2 appeared and concentrated under the external concentrated load

only due to the higher eccentricity and small applied moment at the inner concentrated load.

5.2.5.2 Load-deflection Behavior

As shown in Fig. 5.18, beam PC5–2 had higher deflection after cracking than beam PC1–2, which can be attributed to the spread of cracks over the span. While after yield, cracks on beam PC1–2 concentrated at the outer load and formation of the plastic hinges was faster in beam PC1–2 than in beam PC5–2 due to the loss in tendon eccentricity at the critical sections. This resulted in lower stiffness and higher deflection after cracking.

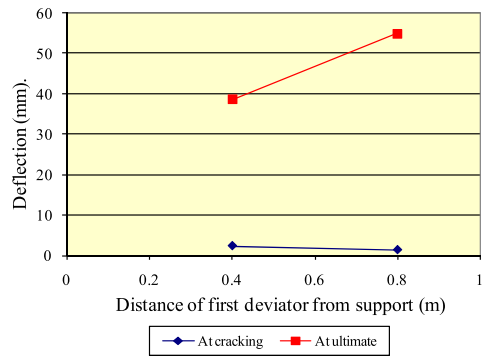


Figure 5.18 Deflection and distance of first deviator from support

5.2.5.3 Cracking and Ultimate Moments

As the location of deviators moved towards the critical section both the cracking and ultimate loads increased as shown in Fig. 5.19. The higher cracking strength of beam PC5–2 can be attributed to its higher prestressing moment and higher axial prestressing force at the mid support that enabled the section to tolerate higher load. While at ultimate, beam PC5–2 showed a slight higher ultimate strength than beam PC1–2 as beam PC1–2 suffered a higher loss of eccentricity of prestressing force at the mid span than beam PC5–2.

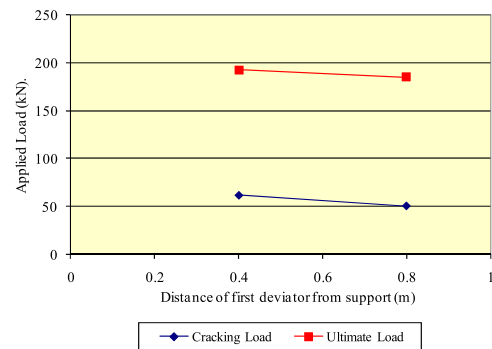


Figure 5.19 Applied Load and distance of first deviator from support

5.2.5.4 External Prestressing Force (Parafil Rope Load)

Fig. 5.20 shows the relation between the increase in the prestressing force of beam PC1–2 and beam PC5–2. Beam PC5–2 had higher increase in the prestressing

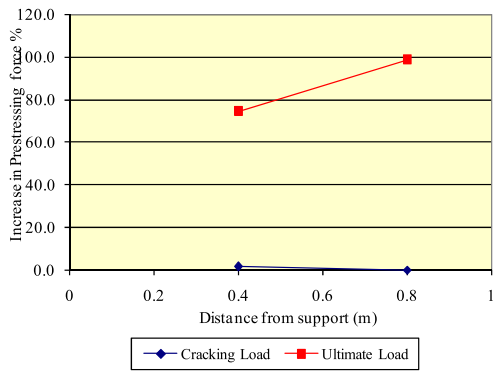


Figure 5.20 Relation between the increase in external prestressing force and distance of first deviator from support

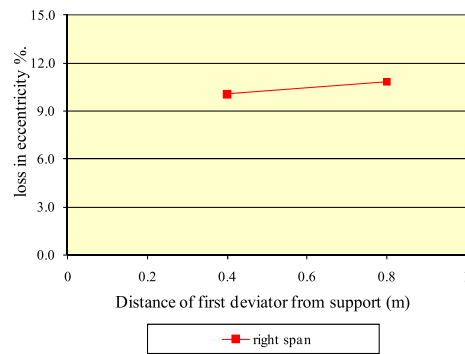


Figure 5.21 Relation between losses in rope effective depth and distance of first deviator from support

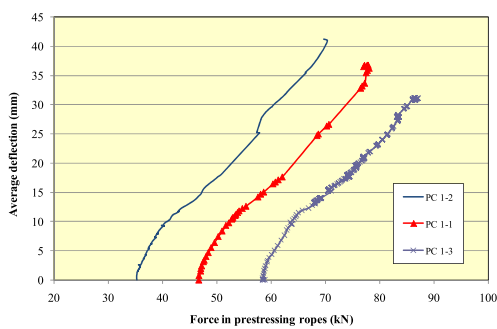


Figure 5.22 Relation between deflection and increase in external prestressing force for group G1

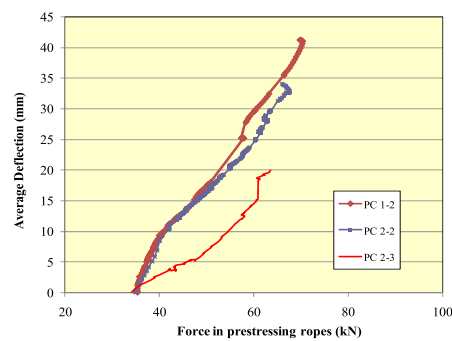


Figure 5.23 Relation between deflection and increase in external prestressing force for group G2

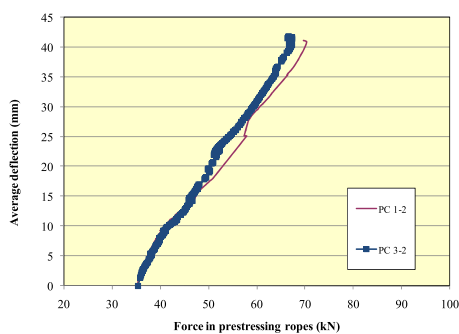


Figure 5.24 Relation between deflection and increase in external prestressing force for group G3 Before cracking, the slope of the relation

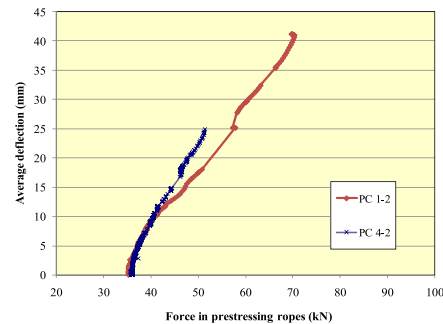


Figure 5.25 Relation between deflection and increase in external prestressing force for group G4

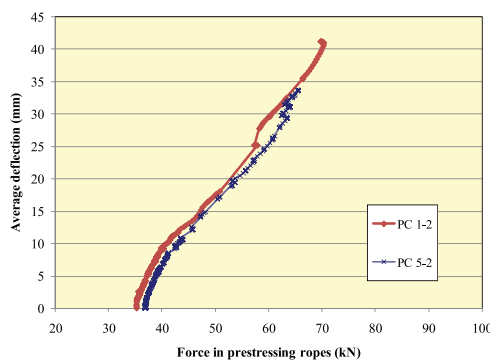


Figure 5.26 Relation between deflection and increase in external prestressing force for group G5

force at any load stage up to yield than beam PC1–2 due to its higher deflection. After yielding, beam PC1–2 had higher deflection and hence higher increase in the prestressing force

5.2.5.5 Change in Rope Effective Depth

As beam PC1–2 had higher ductility than beam PC5–2 thus, beam PC1–2 also had higher loss in rope eccentricity than beam PC5–2 as shown in Fig. 5.21.

5.2.5.6 Relation Between External Prestressing Force and Deflection

The increase in external prestressing force depends on deformation of the member. Hence, the change in external prestressing force is expected to be proportional to the deflection. Figs. 5.22–5.26 show the relation between deflection and external prestressing force up to failure. They show an approximate bilinear relation between deflection and external prestressing force for all beams, before and after cracking. Thus, it can be concluded that, the factors affecting the deflection similarly affect the external prestressing force between deflection and external prestressing force was higher than that after cracking; the increase in deflection was accompanied by a relatively small increase in external prestressing force. After cracking, the external prestressing force rapidly increased as the deflection increased and the relation between deflection and external prestressing force was almost linear up to failure.

As can be seen from the graphs, the relation between the increase in prestressing force and deflection is influenced by (de/h) ratio, deviators locations and tendon profile, while the prestressing force value and load configuration had a slight effect on this relation.

5.3 Ductility and Moment Redistribution of Tested Beams

5.3.1 Ductility

Ductility is defined as the capacity of a material, section (cross section of a structural member), or structure to undergo considerable plastic deformation without loss of strength capacity. Ductility is a measure of the energy absorption capacity. The best way to quantify ductility is through deformation, deflection, or rotation (Bernardo 1998), which is why the index of deformation ductility (μ) is characterized as follows:

$$\mu = \Delta_u / \Delta_y \quad (5.1)$$

Where (Δ_u) is the deformation at ultimate load, and (Δ_y) is the deformation at the onset of reinforcement yielding.

The concept of ductility is linked to the moment redistribution capacity and consequently, the safety of the structure. Designs based on nonlinear methods and plastic theories assume that structures must be able to adapt to the moment diagram used in the calculation at the ultimate limit.

The interest in studying the ductility and the moment redistribution in externally prestressed continuous concrete beams arises because the collapse of externally prestressed concrete beams is more explosive and fragile than that of bonded prestressed concrete beams or ordinary reinforced concrete beams. Table 5.1 shows a deflection of tested beams at different stages as well as its ductility factor.

5.3.2 Moment Redistribution in Continuous Beams

In continuous beams, a redistribution of moments can be expected after the critical section reaches the yield

Table 5.1 Ductility of tested beams

| Factor | Beam No. | Deflection (mm) | | Ductility |
|--|----------|-----------------|----------------|-------------------------|
| | | Δ_y | Δ_{ult} | Δ_{ult}/Δ_y |
| External prestressing force value | PC1–2 | 8.35 | 55 | 6.59 |
| | PC1–1 | 13.6 | 51.7 | 3.80 |
| | PC1–3 | 13.2 | 44 | 3.33 |
| Effective depth of external prestressing force | PC1–2 | 8.35 | 55 | 6.59 |
| | PC2–2 | 9 | 48.5 | 5.39 |
| | PC2–3 | 3.9 | 20.31 | 6.59 |
| Loading configuration | PC1–2 | 8.35 | 55 | 6.59 |
| | PC3–2 | 10.6 | 45.5 | 4.29 |
| Tendon profile | PC1–2 | 8.35 | 55 | 6.59 |
| | PC4–2 | 6.9 | 24 | 3.48 |
| Location of deviators | PC1–2 | 8.35 | 55 | 6.59 |
| | PC5–2 | 13.4 | 38.7 | 2.89 |

moment. If the beam behaves elastically, the variations in support reactions with load will exhibit linear behavior. Otherwise, moment redistribution may take place from the yielded section to the unyielded sections. To verify these phenomena, the support reactions were measured and used to calculate the maximum actual bending moment within the span and at the interior support. Changes in (+ve) moment and (-ve) moment with applied load at different stages are illustrated in (Figs. 5.27 and 5.31). It can be seen that behavior is nearly bilinear. The initial linear range reflects the elastic behavior of the structure, whereas the second part represents the nonlinear behavior. Up to the cracking moment, the stiffness along the beam length is almost constant and the moments are distributed according to the theory of elasticity.

In most of the beams loaded by two third loading, the beams were firstly cracked over the support. That resulted in reduction of the flexural stiffness of this section and caused a less rapid increase in the moment with further increase of loading. To maintain overall equilibrium, the moment in the span (stiffer section) grew faster. As load increased, this section cracked and its stiffness was reduced. For further increase of loading, the distribution of the moments depends entirely

on the stiffness distribution along the cracked member. Generally, after cracking the stiffness will be approximately proportional to the corresponding reinforcement ratio. The difference in stiffness will determine which of the critical sections first attains yielding. If strain hardening is neglected, no further increase of moment at the yielded section is predicted with further increasing load. In reality, the moment over the support will increase depending on the strain hardening ratio of reinforcing steel, a plastic hinge develops and starts to rotate. It was observed that the first plastic hinge was formed in the center support region in case of two third loading and deviators at the third span (except beam PC2-3). This is due to the fact that the ratio of moment capacity to applied moment was lower at the center support compared to the mid-span section. In beam with one concentrated load at the mid span (PC3-2), the first plastic hinge was observed at the mid span regions, then the moment was redistributed towards the center support (Fig. 5.29).

Two types of plastic hinges were observed; flexural crack hinge and shear crack hinge. The flexural crack hinge occurred in a mid span between the concentrated loads in which the bending moment is predominant,

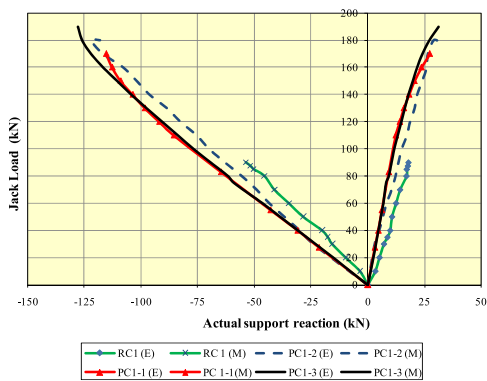


Figure 5.27 Jack load and actual support reaction relation (G1)

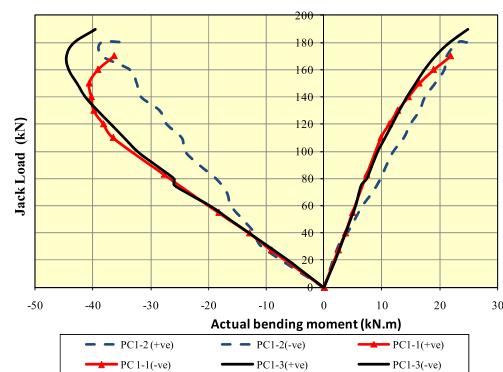


Figure 5.28 Jack load and actual bending moment relation (G1)

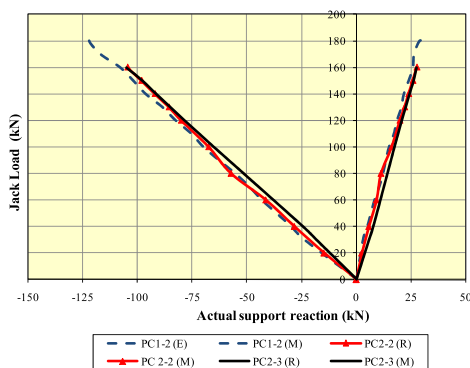


Figure 5.29 Jack load and actual support reaction relation (G2)

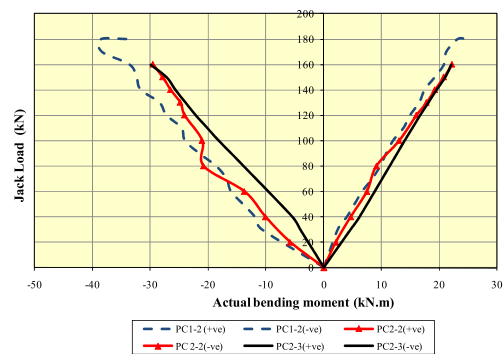


Figure 5.30 Jack load and actual bending moment relation (G2)

while the shear crack hinge developed at the interior support where in addition to a bending moment a considerable shear force was acting. Contrary to flexural crack hinges, where plastic deformations may concentrate in a single or few cracks so that their rotation capacity remains relatively low, shear crack hinge exhibit a significantly increased rotation capacity due to flexural-shear cracks, provided that the member possesses a sufficient shear capacity to avoid shear failure. This improvement of the behavior of the hinge is achieved

by the shift of the tensile force as a result of the inclination of the cracks thus enlarging the length of the plastic hinge. The value of shear stress governs not only the transition from one type of plastic hinge to the other, but influences the value of the rotation capacity for each type of plastic hinge as well (CEB-FIB, 1998).

Table 5.1 shows that the location of deviators, tendon profile and prestressing force value have the main influence on ductility index. While the eccentricity of the prestressing force and load configuration have less effect on the ductility of the strengthened beams.

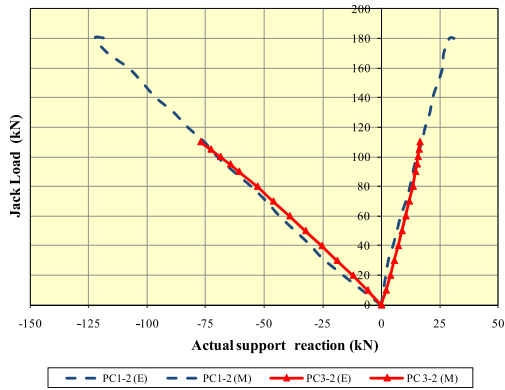


Figure 5.31 Jack load and actual support reaction relation (G3)

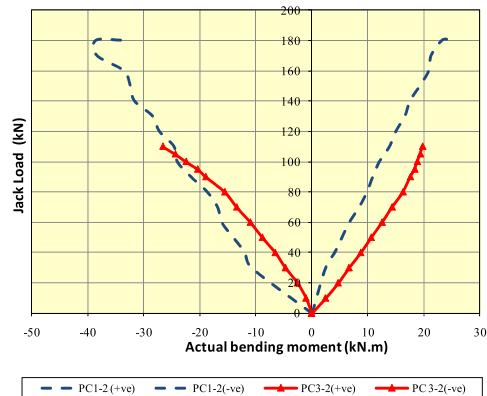


Figure 5.32 Jack load and actual bending moment relation (G3)

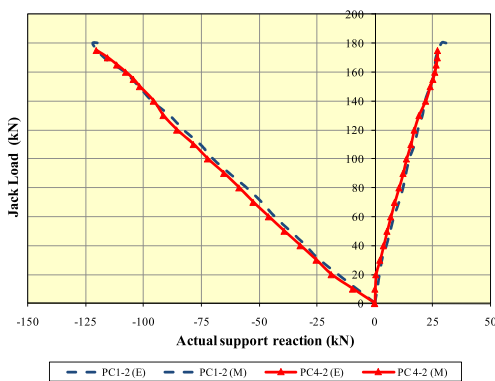


Figure 5.33 Jack load and actual support reaction relation(G4)

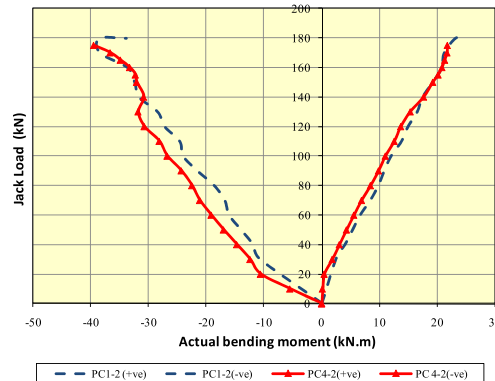


Figure 5.34 Jack load and actual bending moment relation (G4)

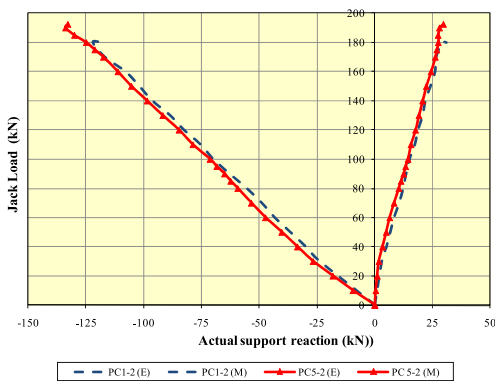


Figure 5.35 Jack load and actual support reaction relation (G5)

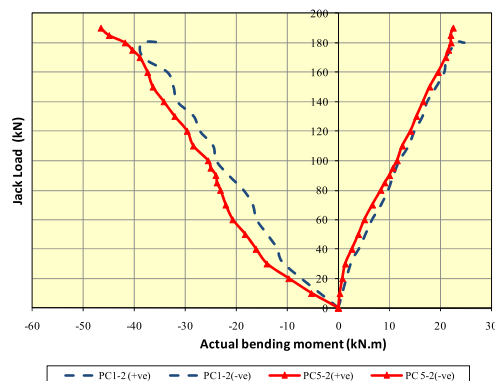


Figure 5.36 Jack load and actual bending moment relation (G5)

The reduction in ductility of the strengthened beams as the external prestressing force increased can be attributed to the low rate of reduction in stiffness of the beam as the prestressing force increased. While the reduction in ductility as the eccentricity of prestressing force increased, (G2) can be attributed to the low rate of reduction in stiffness and the higher vertical component of the prestressing force that reduced the shear force as the eccentricity of the external prestressing force increased.

6. Theoretical Analysis

Introduction

With the wide use of external prestressing in concrete structures, there is a need to examine the design and analysis in order to determine the behavior of the strengthened member, either for serviceability requirements (i.e. deflection) or for strength requirements (i.e. nominal strength). However, the analysis of externally prestressed concrete beams is more complicated compared with the analysis of conventional prestressed concrete beams (i.e. beams prestressed with bonded tendons), because the increase in stress of external tendons depends on the entire deformation of the member and the variation of eccentricity of external tendons under the additional load. In fact, calculating the cracking as well as the ultimate moments of such beams can be done using nonlinear analysis and numerical solution techniques, which are tedious and cumbersome. Moreover, several factors that affect the precision of the deflection calculation cannot be known with a high accuracy, especially in the field, such as the concrete strength, effect of creep and shrinkage, etc.

A simplified method or a prediction equation with more simplicity, reliability and accuracy is needed for guidelines and code purposes to determine the service and ultimate behaviors of strengthened flexural members. It should be done in a reasonably short time, replacing complicated equations especially in the design stage. Many prediction equations were proposed by various investigators. Nevertheless, they still doubt whether any of the proposed equations is generally consistent and applicable to continuous concrete beams externally prestressed using Parafil Ropes. In this chapter, available equations will be tested for their possible applicability to continuous beams, and will be extended to include the effect of the type of tendons.

6.1 Cracking Load

Before cracking, the increase in the external prestressing force and the reduction in the eccentricity of the external prestressing force are small and can be neglected.

$$f_r = -\left(\frac{P_{ex}}{A}\right) - \left(\frac{M_{ps}}{I}\right)y_b + \left(\frac{M_{cr}}{I}\right)y_b \tag{6.1}$$

OR

$$M_{cr} = f_r \frac{I}{y_b} + \left(\frac{P_{ex}}{A_c}\right) \frac{I}{y_b} + M_{ps} \tag{6.2}$$

Hence, the cracking moment can be calculated using the same equations used for bonded prestressed concrete beams considering the full section inertia in the calculation. The cracking moment can be calculated as follows:

Cracking load (P_{cr}) can be calculated from the elastic theory of analysis, where

- P_{ex} = effective external prestressing force
- A_c = area of the cross section = $Bh + (n-1)A_s + (n-1)A_s'$
- A_s = area of nonprestressed tensile steel
- A_s' = area of nonprestressed compressive steel
- I = inertia of the cross section = $\frac{Bh^3}{12} + (n-1)A_s(y_b)^2 + (n-1)A_s'(d-y_b-d')^2$
- n = modular ratio = E_s/E_c and
- y_b = the distance between the outer tension fiber and the neutral axis

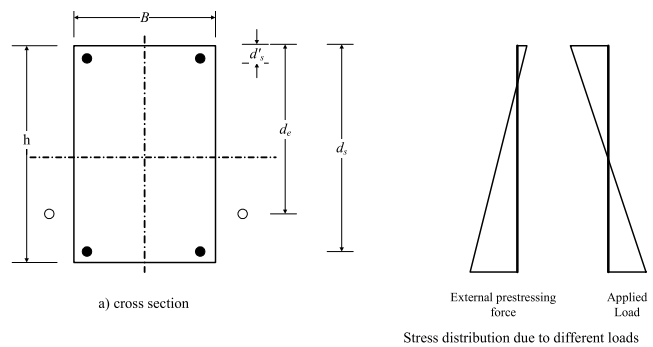


Figure 6.1 Stress distribution due to different loads

Table 6.1 shows the actual and calculated cracking load using concrete tensile strength as given in different code; f_{ctm} and f_r (mean value of axial tensile strength of concrete and modulus of rupture of concrete, respectively) of all beams, while Fig. 6.2 shows the relation between them. It can be seen that the calculated values are more conservative compared to the actual values. Generally, the calculated cracking moment was lower than the actual cracking moment. This is due to the difficulty in accurately determining the concrete tensile strength; in addition this may be attributed to the statically indeterminate behavior of the beams. It should be noted that neglecting the steel bars in calculating cracking load led to a 10–15% lower cracking moment as shown in Fig. 6.3. As can be seen, Euro code showed lower accuracy than ECP and ACI codes

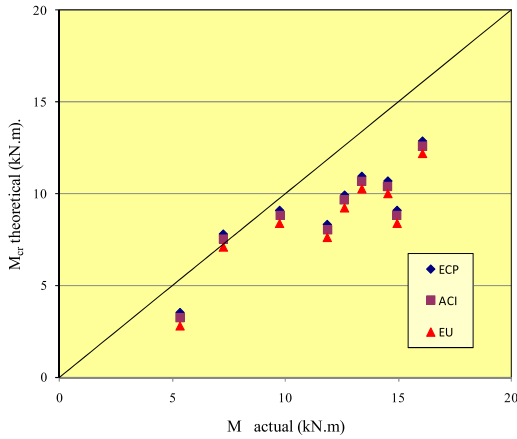


Figure 6.2 Comparison between the actual and the calculated cracking moments (considering effect of steel bar)

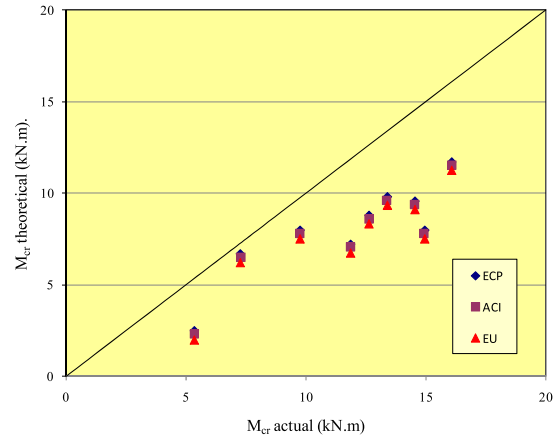


Figure 6.3 Comparison between the actual and the calculated cracking moments (neglecting effect of steel bar)

Table 6.1 Actual and calculated cracking moments

| Beam No. | Cracking moment (kN.m)* | | | | Ratio of actual to calculated M_{cr} | | |
|----------------------|-------------------------|-------|------------------|-------|--|---------|--------|
| | Actual | ECP* | ACI [†] | EU* | Act/ECP | Act/ACT | Act/EU |
| RC1 | 5.35 | 3.50 | 3.23 | 2.81 | 1.58 | 1.71 | 1.97 |
| PC1-2 | 9.75 | 9.08 | 8.81 | 8.39 | 1.11 | 1.14 | 1.20 |
| PC1-1 | 13.38 | 10.95 | 10.68 | 10.26 | 1.26 | 1.30 | 1.35 |
| PC1-3 | 16.06 | 12.87 | 12.60 | 12.18 | 1.29 | 1.32 | 1.36 |
| PC2-2 | 12.62 | 9.91 | 9.64 | 9.23 | 1.32 | 1.35 | 1.41 |
| PC2-3 | 14.53 | 10.68 | 10.41 | 10.00 | 1.41 | 1.44 | 1.50 |
| PC3-2 | 14.94 | 9.08 | 8.81 | 8.39 | 1.04 | 1.07 | 1.12 |
| PC4-2 | 7.27 | 7.78 | 7.52 | 7.09 | 0.97 | 1.00 | 1.06 |
| PC5-2 | 11.85 | 8.31 | 8.05 | 7.62 | 1.48 | 1.52 | 1.16 |
| Mean = | | | | | 1.27 | 1.32 | 1.40 |
| Standard deviation = | | | | | 0.20 | 0.23 | 0.28 |

* ECP ($f_{ctr} = 0.6 \sqrt{f_{cu}}$)

[†] ACI ($f_r = 0.62 \sqrt{f_c'}$)

• EU ($f_{ctm} = 0.3 (f_c')^{2/3}$)

6.2 Deflection

The deflection of prestressed concrete beams depends on several factors, such as concrete cracking strength, young's modulus of concrete, member shape, type and period of applied load and other factors that cannot be determined accurately especially in the field. So, the method used in the deflection calculation should not be too complicated or time consuming or give a false feeling of accuracy. Deflection of continuous prestressed concrete beams due to applied load can be calculated from the general equation as follows:

$$\Delta = K \frac{P_L L^3}{E_c I} \quad (6.3)$$

K = multiplier deflection factor depending on the load type

P_L = applied load

L = clear span

E_c = young's modulus of concrete

I = moment of inertia as a general (uncracked or cracked)

Before cracking, the gross moment of inertia (I_g) or more accurately the transformed moment of inertia, can be used to determine the deflection, though using the transformed moment of inertia does not result in a significant gain in accuracy. After cracking, the moment of inertia lies between the gross and fully cracked inertia depending on the value of applied moment relative to the cracking moment.

Several code methods have been developed taking in to consideration the effect of variation in stiffness caused by cracking along the span, some calculate the deflection from the effective moment of inertia, others use bilinear relation between load and deflection. In this chapter, a brief review of some code methods

that are used in deflection calculation is presented and discussed. However, methods that need iteration or integration are not included.

6.2.1 Deflection of Bonded Prestressed Concrete Beams

The equation for I_e (effective moment of inertia) originally proposed by Branson (1968) for reinforced concrete members, is expressed as follows:

$$I_e = \left(\frac{M_{cr}}{M_a}\right)^3 I_g + \left(1 - \left(\frac{M_{cr}}{M_a}\right)^3\right) I_{cr} \leq I_g \quad (6.4)$$

Where M_{cr} and M_a are the cracking and applied moment at the beam critical section, I_g and I_{cr} are the gross moment of inertia of uncracked (neglecting the steel) and cracked sections (neglecting concrete in tension), respectively.

Branson (1977) recommended the use of I_e for prestressed and partially prestressed cracked members using bonded or unbonded tendons after modification. Shaikh and Branson (1970), using the effective moment of inertia approach, suggested a simplified method to determine deflection of the prestressed concrete members based on computing the deflection increment due to the live load and adding this to the deflection due to the dead load and the prestress (Fig. 6.4). The effective moment of inertia is then calculated using Equation 6.4 with the cracking moment obtained from Equation 6.5.

$$M_{cr} = f_r \frac{I}{y_b} + \left(\frac{P_{ei}}{A}\right) \frac{I}{y_b} + p_i e_i - M_d \quad (6.5)$$

Branson and Trost (1982) suggested a unified formula for the effective moment of inertia for predicting the short-term deflection of cracked reinforced and prestressed concrete members. They suggested that the live bending moment is divided to two parts, $ML1$, the moment required to reduce the net camber due to prestressing and dead load to zero, and $ML2$, the moment producing deflection above zero (Fig. 6.4).

$ML1$ and $ML2$ can be calculated from the following equations:

$$M_{L1} = (\Delta_P - \Delta_D) \left(\frac{EI}{KL^2}\right) = \left(\frac{K_P}{K_L}\right) P_i e_i - \left(\frac{K_D}{K_L}\right) M_d \quad (6.6)$$

$$M_{L2} = M_L - M_{L1} \quad (6.7)$$

And the corresponding deflection

$$\Delta_{L1} = \Delta_P - \Delta_D = \frac{K_L M_{L1} L^2}{E_c I_g} \text{ (Produced by } M_{L1}) \quad (6.8)$$

$$\Delta_{L2} = \frac{K_L M_{L2} L^2}{E_c (I_e)_{L2}} \text{ (Produced by } M_{L2}) \quad (6.9)$$

The total deflection is then given by:

$$\Delta = -\Delta_P + \Delta_D + \Delta_{L1} + \Delta_{L2} = \Delta_{L2} \quad (6.10)$$

Where $(I_e)_{L2}$ is computed from equation 6.2 using M_{L2} for M_a and a modified cracking moment obtained from equation 6.11.

$$M'_{cr} = \frac{f_r I_g}{y_b} + \frac{P_i I_g}{A_c y_b} \quad (6.11)$$

Branson and Trost suggested using the same method for unbonded prestressed beams after replacing $(M_{cr}/M_a)^3$ by $(M'_{cr}/M_a)^4$ in Equation 6.4. Comparing the simplified method and the unified method with experimental results, Branson and Shaikh (1985) concluded that the results by the two I_e methods were shown to be in relatively close agreement

Harajli and Alameh (1989) proposed another equation to calculate the effective moment of inertia including the tension stiffening for partially prestressed concrete flexural members Fig. 6.4.

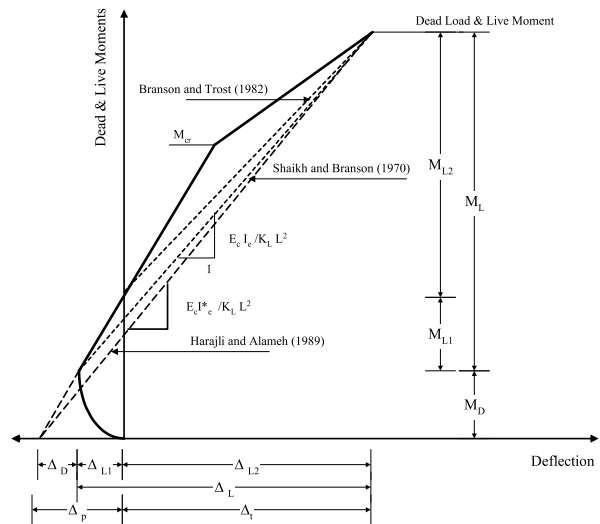


Figure 6.4 Idealization of load-deflection response of prestressed concrete beam (Shaikh and Branson, 1970 Branson and Trost, 1982. Harajli and Alameh, 1989)

They proposed calculating the deflection as follows:

$$\Delta_t = \frac{M_a K_L}{E_c I_e^*} \quad (6.12)$$

Where Δ_t is the total deflection due to the external applied moment (M_a),

$$I_e^* = I_g \quad \text{if } M_a < M_{cr} \quad (6.13)$$

$$I_e^* = \frac{I_{cra}}{1 - \frac{M_{cr}}{M_a} \left(1 - \frac{I_{cra}}{I_g}\right)} \quad \text{if } M_a \geq M_{cr} \quad (6.14)$$

$$M_{cr} = \frac{f_r I_g}{y_b} + \frac{P_i I_g}{A_g y_b} + P_i e_i \quad (6.15)$$

and I_{cra} is the inertia of the cracked section relative to the centroidal axis.

Comparing the calculated deflection using Harajli and Alameh method relative to the neutral axis and relative to the centroidal axis as suggested by Harajli and Alameh, Ghallab (2001) concluded “No significant improvement in accuracy was gained by using the inertia relative to the centroidal axis instead of relative to the neutral axis of the cracked section as suggested by Harajli and Alameh”

6.2.2 Deflection of Unbonded or External Prestressed Concrete Beams

Analysis of unbonded, prestressed or partially prestressed, concrete beams is more complex than the analysis of bonded tendons, as the stress in the tendons is assumed constant at all sections and must be determined from the analysis of the deformation of the entire structure. This is true for the elastic, inelastic, and ultimate limit states (Naaman and Alkhairi, 1991, parts 1 and 2).

However, Naaman (1990) proposed an approach whereby the unbonded tendons can be treated as bonded tendons using a bond or strain reduction coefficient (Ω). Thus, previous analytical solutions with bonded tendons could be used. The bond reduction coefficient for the elastic uncracked and elastic cracked stages can be determined as follows:

6.2.2.1 Elastic Uncracked Stage

For the elastic uncracked section analysis, the bond reduction coefficient Ω is defined as

$$\Omega = \frac{(\Delta \varepsilon_{psu})_m}{(\Delta \varepsilon_{psb})_m} = \frac{(\Delta \varepsilon_{psu})_{av}}{(\Delta \varepsilon_{cps})_m} \quad (6.16)$$

Where $(\Delta \varepsilon_{psu})_m$ is the strain increase in the unbonded tendons, $(\Delta \varepsilon_{psb})_m$ is the strain increase in the equivalent bonded tendon, and $(\Delta \varepsilon_{cps})_m$ is the strain increase in the concrete at the level of tendon beyond effective prestress, all taken at the section of maximum moment.

For simply supported beams with constant cross section, symmetrical loading, and symmetrical tendon profile, Ω can be calculated in general from:

$$\Omega = \frac{2}{M_{\max}(e_0)_{\max}} L \int_0^{L/2} M(x) e_0(x) dx \quad (6.17)$$

Where M_{\max} and $M(x)$ are the change in bending moment at the critical section and at any section (x) along the span, respectively, and $(e_0)_{\max}$ and $e_0(x)$ are the corresponding eccentricities of the tendons at these sections. It

is assumed that the change in the bending moment is taken with respect to a reference stage such as that corresponding to the effective prestress and dead load moment. The stress in the tendon at the reference stage is assumed known and equal to the effective prestress f_{pe} .

From equation 6.17, the value of Ω for the third point loading and deflected tendons at the third span equals $\Omega = (2 + e_s/e_c)/9$, where (e_s) is the eccentricity at end supports and (e_c) is the eccentricity at mid-span.

6.2.2.2 Elastic Cracked stage

After cracking and within the elastic cracked stage, the increase in strain, and hence stress, in the unbonded tendons can be calculated by introducing a bond reduction coefficient in the cracked stage Ω_{cr} . For simply supported beams with symmetrical loading and tendon profile and assuming a single crack occurs at the section of maximum moment, the value of Ω_{cr} can be calculated from the following general equation:

$$\Omega_{cr} = \Omega \frac{I_{cr}}{I_g} + \frac{2}{L} \left(1 - \frac{I_{cr}}{I_g} \right) \int_0^{L_c/2} \frac{M(x) e_0(x)}{M_{\max}(e_0)_{\max}} dx \quad (6.18)$$

Where L_c is the width of the crack, or the width of the smeared crack region. Values of Ω_{cr} were computed and given in detail by Naaman (1990) who suggested that if the value of L_c is small relative to the value of L , as is generally the case, Ω_{cr} can be taken as:

$$\Omega_{cr} \cong \Omega \frac{I_{cr}}{I_g} \quad (6.19)$$

Harajli and Kanj (1992), assuming the neutral axis is independent on the applied load and all beam sections follow a similar idealized moment-curvature relationship, suggested an approximate expression to calculate Ω_{cr} as follows:

$$\Omega_{cr} = \Omega - 0.5 \left(1 - \frac{L_o}{L} \right) \left(\frac{M_{cr}}{M_a} - \frac{1}{\left(\frac{M_{cr}}{M_a} - 1 \right) \frac{I_g}{I_{cra}} + 1} \right) \quad (6.20)$$

Where I_{cra} is calculated relative to the centroidal axis of the cracked section and Ω as given in equation 6.17.

Harajli and Kanj (1992) also concluded that the strain reduction coefficient Ω_{cr} did not differ significantly from its value before cracking. Hence, they suggested, in order to simplify the analysis of the partially prestressed unbonded members, that the strain reduction factor in the postcracking stage is equal to its value before cracking, and deflection due to the total applied load can be calculated as suggested by Harajli and Alameh (1989), (equations 6.15–6.18) by replacing A_p with ΩA_p or $\Omega_{cr} A_p$.

6.2.3 Code Methods for Deflection Calculations

6.2.3.1 Eurocode 2 (ENV 1992–1–1)

Two methods were suggested to calculate the deflection of both reinforced and prestressed concrete flexural members by Eurocode (EC2), one rigorous and the other more approximate. In the more rigorous approach, the curvature is calculated at a reasonable number of sections along the beam and then the deflection is calculated by numerical integration. In the approximate method, the deflection is calculated twice, assuming the whole member is in the uncracked or fully cracked conditions as shown in Fig. 6.5, the following equation is then employed:

$$\Delta = (1 - \zeta)\Delta_1 + \zeta\Delta_2 \quad (6.21)$$

Where

$$\zeta = 1 - B_1 B_2 (M_{cr}/M)^2 \quad (6.22)$$

B_1 is a coefficient which takes account of the bond properties of the bars:

- = 1 for high bond bars
- = 0.5 for plain bars.

B_2 is a coefficient which takes account of the duration of the loading or of repeated loading

- = 1 for a single short-term loading
- = 0.5 for sustained loads or many cycles of repeated loading

- Δ The deflection
- Δ_1 The deflection calculated on the basis of an uncracked section
- Δ_2 The deflection calculated on the basis of a cracked section
- I The inertia of either the cracked or the gross section relative to the bending moment.

Eurocode also suggested the following equation to calculate the young's modulus:

$$E_c = 9.5 (f_{ck} + 8)^{1/3} \quad (6.23)$$

(E_{cm} in kN/mm^2 ; f_{ck} in N/mm^2)

$$f_{ctm} = 0.30 f_{ck}^{2/3} \quad (6.24)$$

Where:

- f_{ctm} mean value of the tensile strength
- f_{ck} characteristic cylinder compressive strength of the concrete

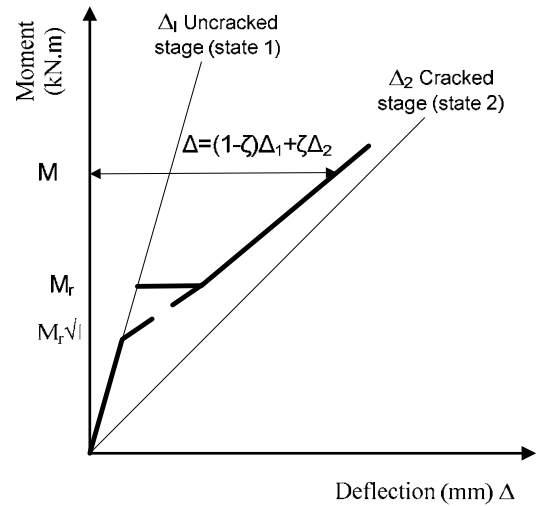


Figure 6.5 Moment versus deflection in a reinforced concrete member in flexure

Beeby *et al.* (2005) suggested that as the decay of tensile stress is relatively fast (i.e. a matter of hours), then B_2 should always be taken as 0.5.

For continuous beam, Beeby and Narayanan (1995) suggested that the critical section at which the curvature is calculated should be at the section with the maximum sagging moment, even though the hogging moment over the support may be bigger, because the positive moment had the higher effect on the total inertia of the beam.

Ghali *et al.*, (2002) suggested a similar equation to that in EC2 to calculate ζ . They only differed in the raised power; Ghali *et al.* suggested the term (M_{cr}/M) is raised to the power 1 instead of 2 as suggested by EC2.

6.2.3.2 ACI318 (2008)

After cracking, ACI318 requires that a bilinear moment-deflection relationship be used to calculate instantaneous deflections. When the magnitude of tensile stress in service exceeds $0.62\sqrt{f_c'}$, I_e is used to calculate the instantaneous deformation. The effective moment of inertia I_e is given as follows:

$$I_e = \left(\frac{M_{cr}}{M_a} \right)^3 I_g + \left(1 - \left(\frac{M_{cr}}{M_a} \right)^3 \right) I_{cr} \leq I_g \quad (6.25)$$

Where:

- M_{cr} = cracking moment based on $f_r = 0.62\sqrt{f_c'}$ MPa
- M_a = applied bending moment
- I_{cr} = moment of inertia of cracked section
- I_g = gross moment of inertia

For continuous members, ACI318 stipulates that I_e may be taken as the average values obtained from the critical positive and negative moment sections. Improved results for continuous prismatic members can,

however, be obtained using a weighted average as presented in the following equations:

$$I_e = 0.85 * I_e(\text{midspan}) + 0.15 * I_e(\text{sup port}) \quad (6.26)$$

6.2.3.3 ECP203 (2007)

The instantaneous deflection for beams can be calculated using effective moment of inertia I_e , which depends on the value of applied moment relative to the cracking moment using formula similar to equation 6.4, however M_{cr} should be calculated based on $f_{ctr} = 0.6\sqrt{f_{cu}}$.

In case of continuous beams ECP203 suggested using the average inertia of the sections subjected to higher positive and negative bending moments.

6.2.4 Deflection of Externally Prestressed Continuous Concrete Beams

To calculate deflection of externally prestressed continuous beams, the following concerns should be taken into consideration besides the factors covered in simple prestressed concrete beam:

1. Member continuity.
2. Secondary moment effect.
3. Depth and area of external prestressing tendons.

The previous methods have been modified taking in to consideration the effect of the mentioned factors as shown in table 6.2.

Figs. 6.6–6.13 show the relation between jack load and deflection (actual and theoretical) of tested beams while Figs. 6.14–6.26 show the relation between actual deflection and theoretical deflection calculated using the modified methods for all beams except beam PC2–3. All graphs show the deflection due to the applied load only (not due to prestress nor dead load), to compare the accuracy of the modified methods.

From these figures, it can be seen that for beams loaded with third point loading, ACI318 method gave conservative value for deflection while EC2 method and Branson and Shaikh method underestimated deflection of the tested beam especially at higher load level. The deflection calculated by EC2 and Ghali *et al.* methods is less estimated and less accurate than the other methods. Moreover, the difference between the deflection calculated by ACI38 method, using the average inertia for the critical positive and negative moment sections, and that using the relative inertia for the critical positive and negative moment sections is negligible. This may be because the critical positive and negative moment sections were slightly different in this study. However, further studies are needed in case of beam with different cross section shape.

Figs. 6.20–6.21 show that the gain in accuracy of deflection calculated using cracking moment based on

effective inertia of the cross section rather than that calculated using cracking moment based on gross moment of inertia, is negligible. It is worth noting that introducing bond reduction factor and depth reduction factor into the studied methods did not show improvement in deflection calculation.

Hence, neglecting effects of these factors during calculation will lead to less complicated calculation and less time consumption. All methods show a low accuracy when calculating deflection of beam PC2–3. This can be attributed to its unductile behavior and to the slow propagation of cracks, which results in a brittle failure. Further studies are needed to study the effect of high tendon eccentricity on the behavior of externally prestressed continuous beams

6.3 Nominal Moment Strength

For the analysis of reinforced continuous concrete beams after external strengthening using Parafil rope at ultimate, it is necessary to make certain assumptions and to know the stress-strain characteristics of concrete, steel, and Parafil rope. The following assumptions are generally made for prestressed concrete sections:

- Plane sections remain plane during bending and perpendicular to the neutral axis after bending. Consequently, the strain distribution is assumed linear.
- Perfect bond exists between concrete and the internal steel. Hence, the strain in steel is the same as the strain in surrounding concrete before cracking.
- Concrete is weak in tension and therefore neglected in the flexural analysis and the tension reinforcement is assumed to take the total tensile force.

6.3.1 Nominal Bending Moment Strength of Rectangular Section

For beam with rectangular cross section (R-Section), calculation of the nominal moment strength depends on the position of the neutral axis at failure as shown in Fig. 6.27.

From the equilibrium of the horizontal forces:

$$F_C + F'_s = T_s + T_e \quad (6.27)$$

Where:

$$F_C = 0.67 f_{cu} B(\beta_1 c) \quad (6.28)$$

$$F'_s = A'_s f'_s \quad (6.29)$$

$$T_s = A_s f_s \quad (6.30)$$

$$T_e = A_e f_{ps} \quad (6.31)$$

Substitute in Equation (6.7)

$$0.67 f_{cu} B * \beta_1 c + A'_s f'_s = A_s f_s + A_e f_{ps} \quad (6.32)$$

Table 6.2 Extending the calculation deflection methods to include the effect of external prestressing force

| Method | Cracking moment (M_{cr}) | Effective inertia (I_e) | Deflection |
|--|--|--|---|
| Shaikh & Branson (1970) Case (a&b) | $M_{cr} = f_r \frac{I_{gi}}{y_i} + \left(\frac{P_{ex}}{A_{gi}} \right) \frac{I_{gi}}{y_i} + M_{pi} - M_d$ using f_r in calculation | $I_e = \left(\frac{M_{cr}}{M_a} \right)^3 I_g + \left(1 - \left(\frac{M_{cr}}{M_a} \right)^3 \right) I_{cr} \leq I_g$ where M_a =live load moment (M_L) | $\Delta_L = \frac{K_L P_L L^3}{E_c (I_e^*)}$ |
| EC2 Case (a&b) | $M_{dec} = \frac{P_{ex} I_{gi}}{A_{gi} y_i} + M_{pi}$ $M_{cr} = \frac{f_{ctm} I_{gi}}{y_i}$ using f_{ctm} instead of f_r | $I =$ the inertia of the section at the maximum (+ve) moment either the cracked or the gross section relative to the bending moment M_L =total live load moment | $\Delta = \zeta \Delta_{II} + (1 - \zeta) \Delta_I$ $\Delta_I = \frac{K_L M_{L3} L^2}{E_c (I_g)}$ $\Delta_{II} = \frac{K_L M_{L3}}{E_c (I_{cr})}$ |
| EC2_dec Case (a&b) | $M_{dec} = \frac{P_{ex} I_{gi}}{A_{gi} y_i} + M_{pi}$ $M_{cr} = \frac{f_{ctm} I_{gi}}{y_i}$ using f_{ctm} instead of f_r | $I =$ the inertia of the section at the maximum (+ve) moment either the cracked or the gross section relative to the bending moment M_{L3} = part of live load moment after decompression | $\Delta = \zeta \Delta_{II} + (1 - \zeta) \Delta_I$ $\Delta_I = \frac{K_L M_{L3} L^2}{E_c (I_g)}$ $\Delta_{II} = \frac{K_L M_{L3}}{E_c (I_{cr})}$ |
| Ghali <i>et al.</i> (2005) Case (a&b) | $M_{dec} = \frac{P_{ex} I_{gi}}{A_{gi} y_i} + M_{pi}$ $M_{cr} = \frac{f_{ctm} I_{gi}}{y_i}$ using f_{ctm} instead of f_r | $I =$ the inertia of either the cracked or the gross section relative to the bending moment M_{L3} = part of live load moment after decompression | $\Delta = \zeta \Delta_{II} + (1 - \zeta) \Delta_I$ $\Delta_I = \frac{K_L M_{L3} L^2}{E_c (I_g)}$ $\Delta_{II} = \frac{K_L M_{L3} L^2}{E_c (I_{cr})}$ |
| ACI-08 Case (a&b) Case (c&d) | $\left(\frac{M_{cri}}{M_{ai}} \right) = \left(1 - \frac{f_{TL} - f_r}{f_L} \right)$ $f_{TL} = \frac{M_{ai} y_i}{I_{gi}} + \frac{M_{Di} y_i}{I_{gi}} - \frac{P_{ex}}{A_{gi}} - \frac{M_{pi} y_i}{I_{gi}}$ $f_L = \frac{M_{ai} y_i}{I_g}$ and $f_r = 0.62 \sqrt{f'_c}$ | $I_{ei} = \left(\frac{M_{cri}}{M_{ai}} \right)^3 I_{gi} + \left(1 - \left(\frac{M_{cri}}{M_{ai}} \right)^3 \right) I_{cri} \leq I_g$ where M_{cr} =maximum live load moment at i-section | $\Delta_L = \frac{K_L P_L L^3}{E_c (I_e^*)}$ |

• Subscript i in previous equation refer to section number

• In all methods, I_{cr} relative to the neutral axis was used

• Case (a): $I_{cr} = b_w c^3 / 3 + (B - b_w) h_f^3 / 12 + (c - h_f / 2)^2 + n_p A_{ps} (d_p - c)^2 + n_s A_s (d_s - c)^2 + n_e A_e (d_e - c)^2$

• Case (b): $I_{cr} = b_w c^3 / 3 + (B - b_w) h_f^3 / 12 + (c - h_f / 2)^2 + n_p A_{ps} (d_p - c)^2 + n_s A_s (d_s - c)^2 + \Omega n_e A_e (R_d d_e - c)^2$

• Case (c): using average inertia ($I_e = I_e(+ve) + I_e(-ve) / 2$)

• Case (d): using average inertia ($I_e = 0.85 I_e(+ve) + 0.15 I_e(-ve)$)

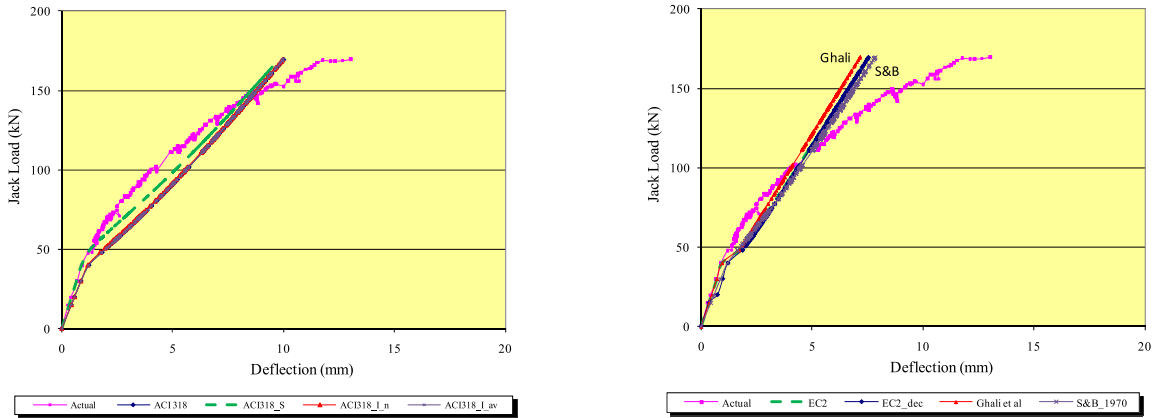


Figure 6.6 Comparison between actual and theoretical deflections of beam PC1-2

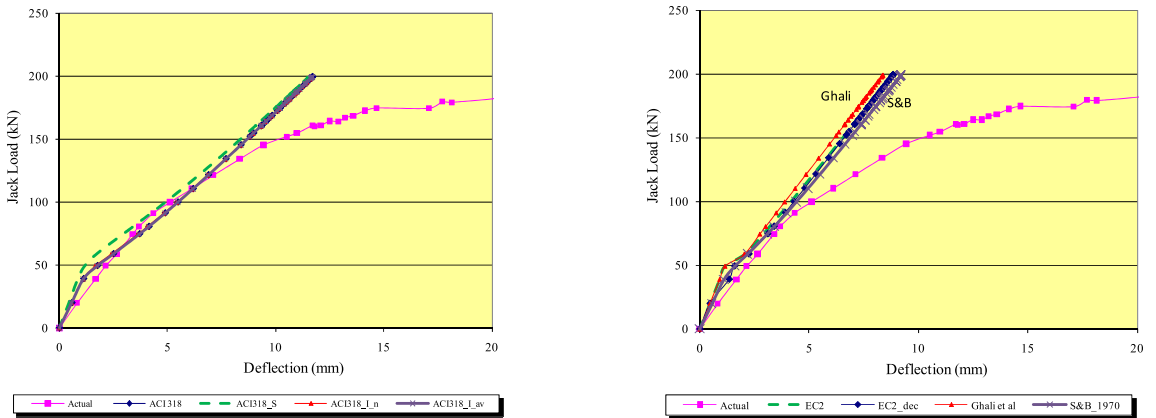


Figure 6.7 Comparison between actual and theoretical deflections of beam PC1-1

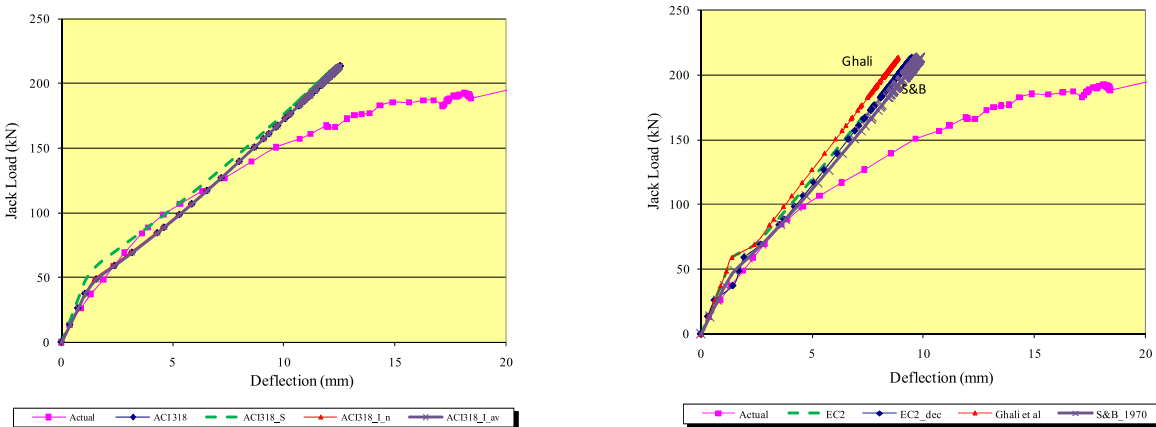


Figure 6.8 Comparison between actual and theoretical deflections of beam PC1-3

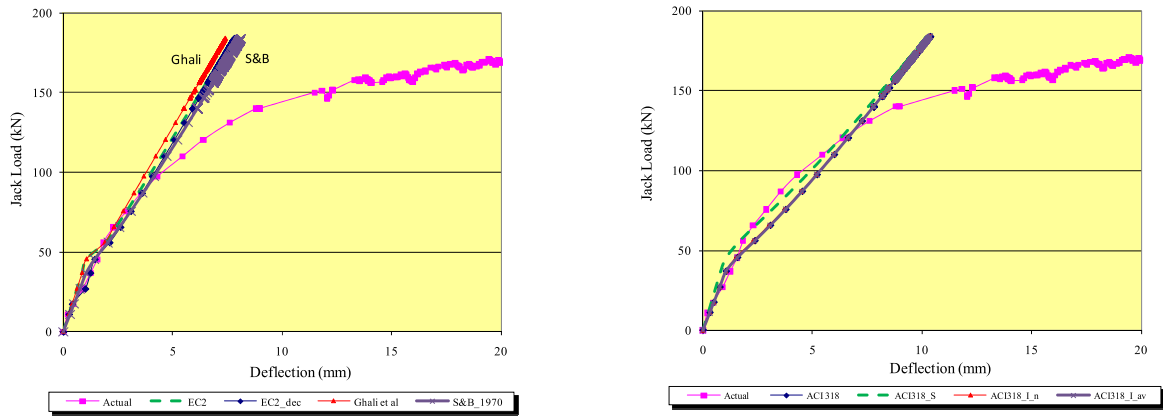


Figure 6.9 Comparison between actual and theoretical deflections of beam PC2-2

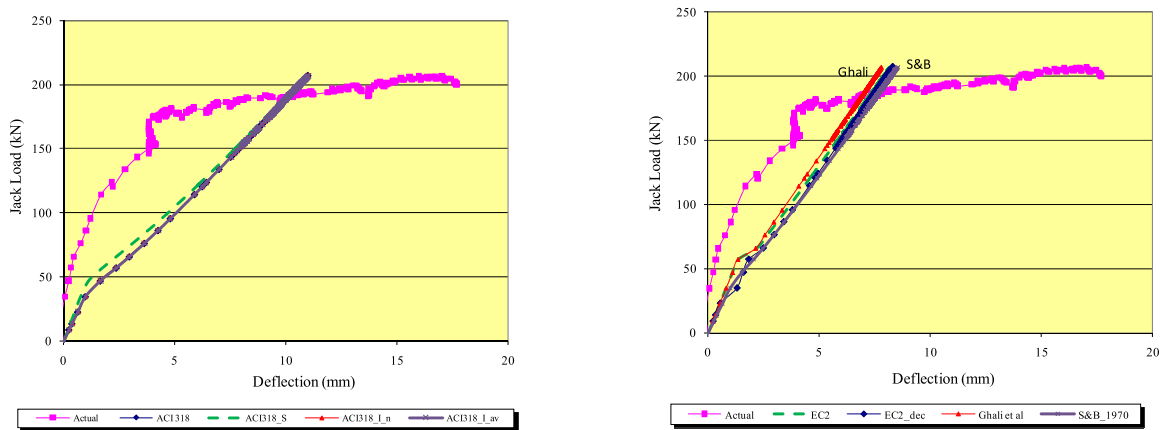


Figure 6.10 Comparison between actual and theoretical deflections of beam PC 2-3

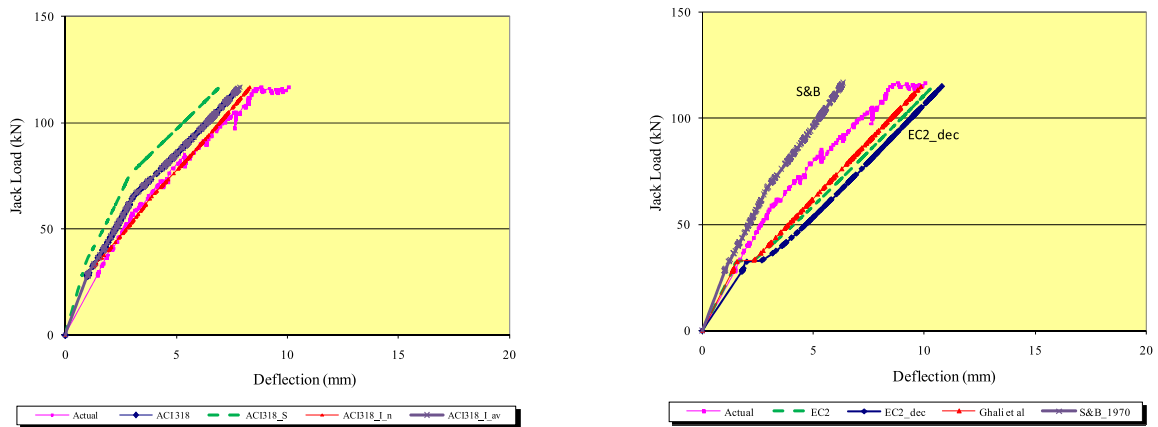


Figure 6.11 Comparison between actual and theoretical deflections of beam PC3-2

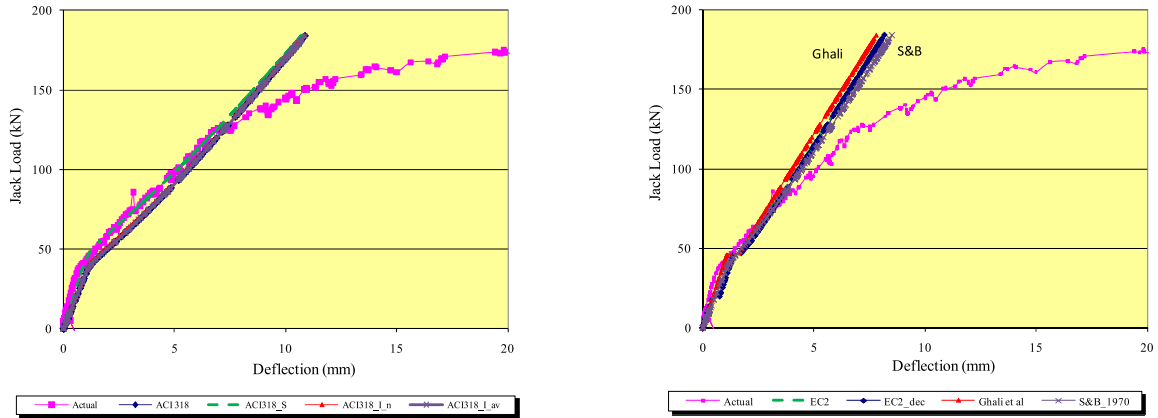


Figure 6.12 Comparison between actual and theoretical deflections of beam PC4-2

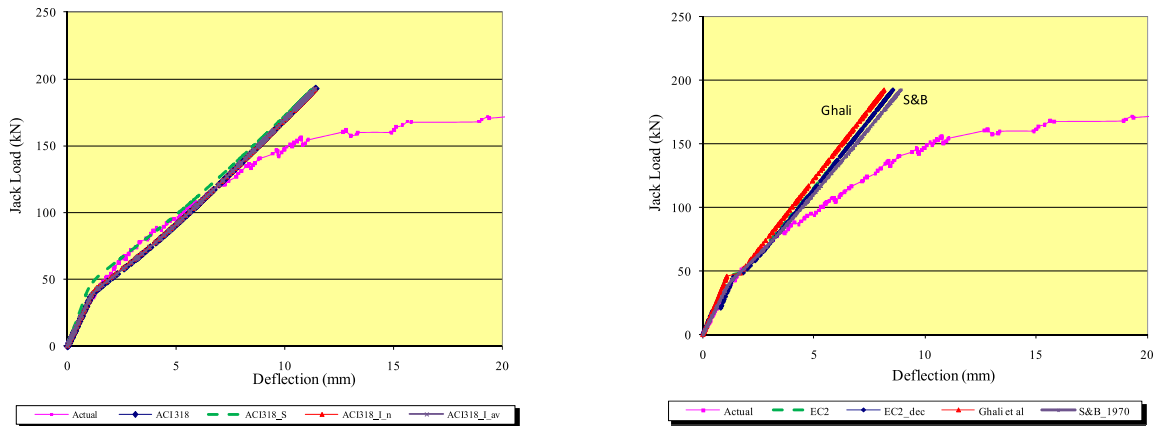


Figure 6.13 Comparison between actual and theoretical deflections of beam PC5-2

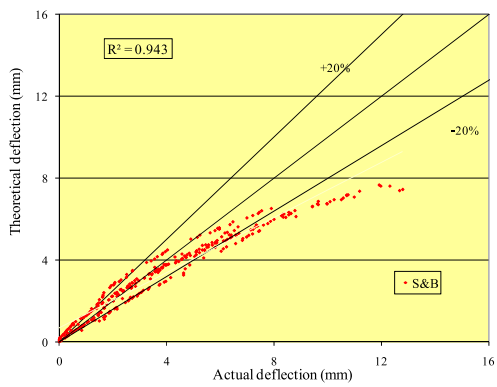


Figure 6.14 Relation between actual deflection and theoretical deflection using Shaikh and Branson (1970) method

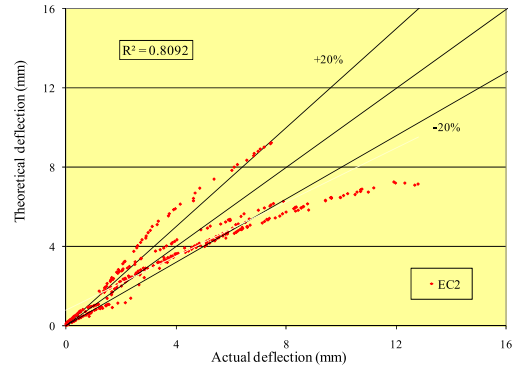


Figure 6.15 Relation between actual deflection and theoretical deflection using Eurocode (EC2) method

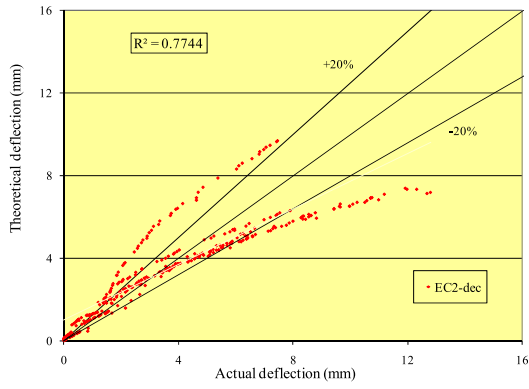


Figure 6.16 Relation between actual deflection and theoretical deflection using Eurocode (EC2)_decompression method

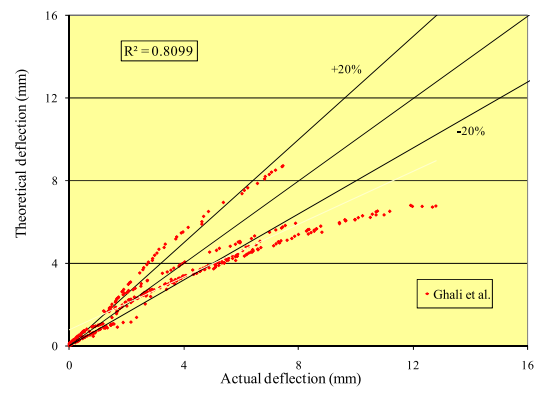


Figure 6.17 Relation between actual deflection and theoretical deflection using Ghali *et al.* (2005) method

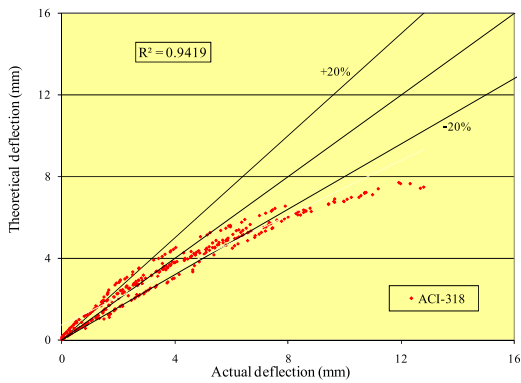


Figure 6.18 Relation between actual deflection and theoretical deflection using ACI (2008) _mid span Inertia method

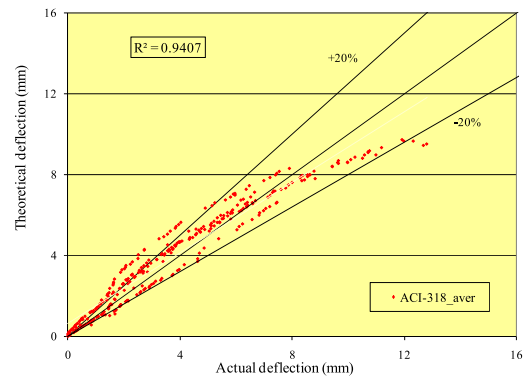


Figure 6.19 Relation between actual deflection and theoretical deflection using ACI (2008) _average Inertia method

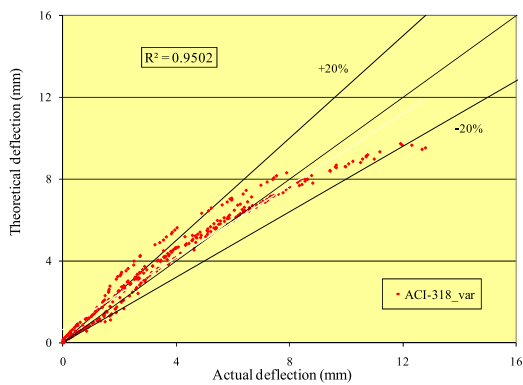


Figure 6.20 relation between actual deflection and theoretical deflection using ACI (2008) _variable Inertia method

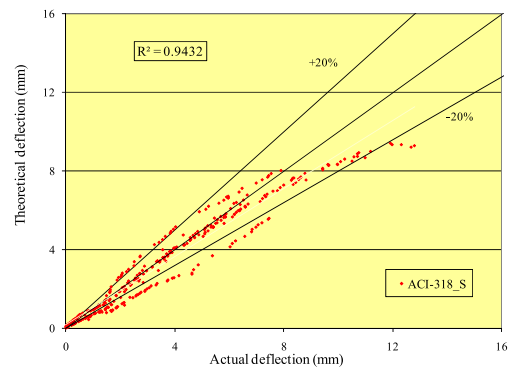


Figure 6.21 Relation between actual deflection and theoretical deflection usingb ACI318 (2008) _using effective inertia in calculated cracking moment

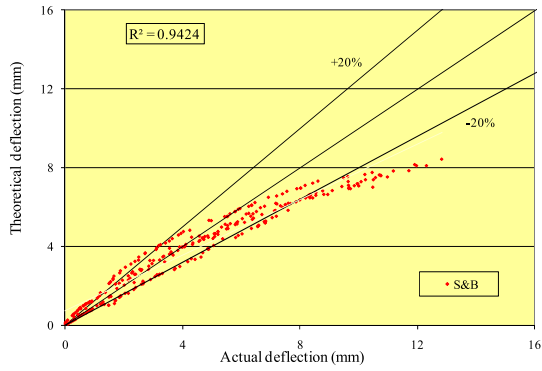


Figure 6. 22 Relation between actual deflection and theoretical deflection using modified Shaikh and Branson (1970) method

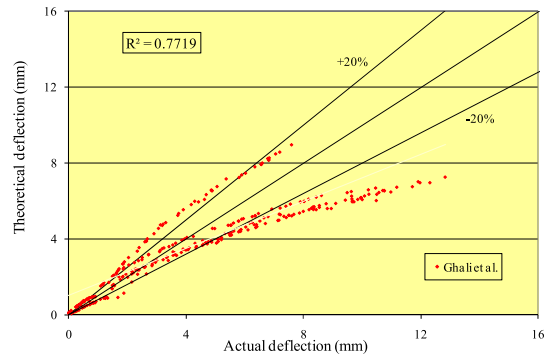


Figure 6. 23 Relation between actual deflection and theoretical deflection using modified Ghali *et al.* (2005) method

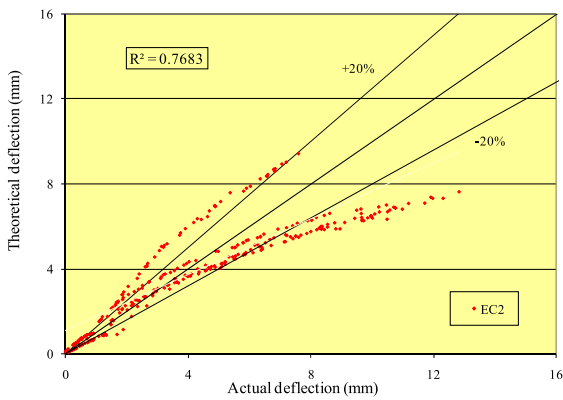


Figure 6. 24 Relation between actual deflection and theoretical deflection using modified EC2 (2008) method

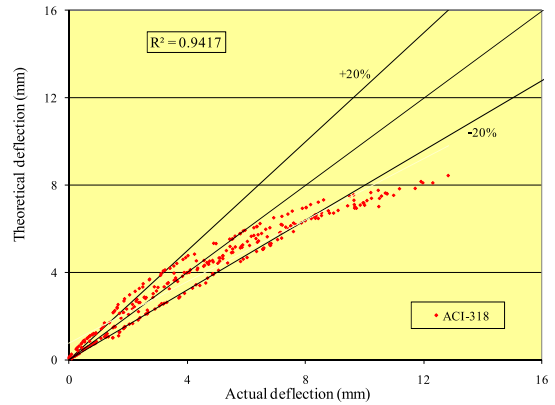


Figure 6. 25 Relation between actual deflection and theoretical deflection using modified ACI (2008) method

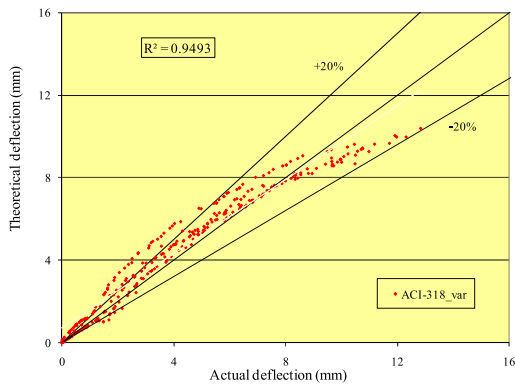


Figure 6. 26 Relation between actual deflection and theoretical deflection Using modified ACI (2008)_variable Inertia method

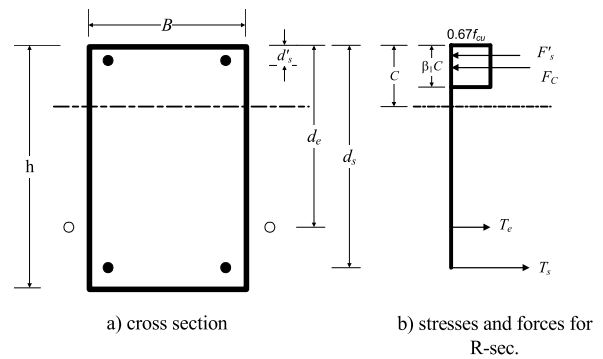


Figure 6. 27 Possible stresses and forces at ultimate stage for R-sec

For which:

$$c = \frac{A_s f_s + A_e f_{ps} - A'_s f'_s}{0.67 f_{cu} B \beta_1} \quad (6.33)$$

And

$$M_n = A_e f_{ps} \left(d_e - \frac{\beta_1 c}{2} \right) + A_s f_s \left(d_s - \frac{\beta_1 c}{2} \right) - A'_s f'_s \left(d'_s - \frac{\beta_1 c}{2} \right) \quad (6.34)$$

As can be seen from the previous equations, several unknowns should be determined first to calculate the nominal beam strength, namely:

- **Stress in the bonded tensile steel reinforcement:** That can be taken as yield stress of the steel.
- **Stress in the compression steel reinforcement:** This stress can reach the yield stress or less, depending on its position and strain value in the concrete at failure.
- **Stress in external prestressing tendon:** Under loading, the increase in strain in the unbonded tendons is averaged (as no bond exists) over the whole length of the tendon, and thus it is much smaller than the increase in strain of the bonded tensile steel taken at the section of maximum moment.
- **Effective depth of the external tendon:** As there is no bond between the rope and the concrete and the rope is attached to the concrete at the deviator points, its effective depth varies as the deflection increases.

Several investigations were made to determine the stress in the unbounded external prestressing strands. A brief review of some of these equations can be found in the following.

6.3.2 Stress in Unbonded Tendons

6.3.2.1 Codes Equations

In order to simplify calculations, several empirical equations were suggested by different codes to calculate the stress in unbounded tendons.

Some of these equations are briefly discussed.

- ACI318 (2008)

ACI318 suggested the following equation to determine stress in unbounded tendons depending on the span to depth ratio as approximate values.

For a span-to-depth ratio of 35 or less:

$$f_{ps} = f_{pe} + 70 + \frac{f'_c}{100 \rho_p} \leq f_{py} \quad (6.35)$$

$$\text{OR } (f_{pe} + 420) \text{ MPa}$$

For a span-to-depth ratio greater than 35:

$$f_{ps} = f_{pe} + 70 + \frac{f'_c}{300 \rho_p} \leq f_{py} \quad (6.36)$$

$$\text{OR } (f_{pe} + 200) \text{ MPa}$$

Where $\rho_p = \frac{A_{ps}}{Bd}$ and f_{pe} : effective prestressing

- BS8110

BS8110 suggested the following equations to determine f_{ps} and c by taking $\epsilon_{cu}=0.0035$ and $E_s=200\text{kN/mm}^2$

$$f_{ps} = f_{pe} + \frac{7000}{L/d} \left(1 - 1.7 \frac{f_{pu} A_{ps}}{f_{cu} B d} \right) \leq 0.7 f_{pu} \quad (6.37)$$

Where f_{cu} is the strength of concrete taken from cube tests, L is the length of the tendon between end anchorages, and the length of the plastic zone at ultimate is assumed equal to $10c$, where c is the depth of the neutral axis.

- ECP203 (2007)

The Egyptian code of practice suggested equations to predict the force in unbounded external tendons, depending on the span to depth ratio.

For a span-to-depth ratio of 35 or less:

$$f_{ps} = f_{pe} + 70 + \frac{0.8 f_{cu}}{125 \mu_p} \leq f_{py} \quad (6.38)$$

$$\text{or } (f_{pe} + 420) \text{ MPa}$$

For a span-to- depth ratio greater than 35:

$$f_{ps} = f_{pe} + 70 + \frac{0.8 f_{cu}}{375 \mu_p} \leq f_{py} \quad (6.39)$$

$$\text{or } (f_{pe} + 200) \text{ MPa}$$

Where $\mu_p = \frac{A_{ps}}{Bd}$ and f_{pe} effective prestressing stress.

- Eurocode 2004 (EC2)

For calculating stress of unbounded tendons at ultimate EC2 states that it is generally necessary to take the deformation of the whole member into account when calculating the increase of the stress in the prestressing steel. If no detailed calculation is made, it may be assumed that the increase of the stress from the effective prestress to the stress in the ultimate limit state is Δ_{ps} . The recommended value of Δ_{psult} is 100 N/mm².

6.3.2.2 Bond Reduction Method

Analysis of unbonded, prestressed concrete beams is more difficult than that with bonded tendons, as the stress increase in the tendons beyond the effective prestress due to external loading which is member-dependent (depends on the deformation of the whole member) instead of being section-dependent. Thus, the increase in stress in unbonded tendons is assumed uniform at all sections and must be determined from the analysis of the deformation of the entire structure. This is true for the elastic, inelastic, & ultimate limit states (Naaman and Alkhairi, 1991 parts 1 & 2).

Unbonded tendons can be treated as bonded tendons using a simple modification (a bond or strain reduction coefficient) as suggested by Naaman (1990). The concept of bond reduction coefficient for ultimate stage is briefly discussed next. Stress in the unbonded tendons f_{ps} at ultimate can be predicted using the following equation:

$$f_{ps} = f_{pe} + \Delta f_{ps} \quad (6.40)$$

Where, f_{ps} is the ultimate stress in cables, f_{pe} is the effective prestressing force and Δf_{ps} is the total increase in cables stress

Naaman and Alkhairi (1991, part 1) made an evaluation of the above equation to predict the stress in unbonded tendons. Then they concluded that there is a room for improvement not only in terms of accuracy but particularly in accounting for the variables that are found to influence mostly the value of f_{ps} .

Based also on previous work made by Naaman (1990), a new equation was proposed by Naaman and Alkhairi (1991, part 2) to predict the stress in unbonded tendons at ultimate.

Strain in unbonded tendons at ultimate can be obtained from the strain increase in bonded tendons using a bond reduction coefficient (Ω_u) defined as:

$$\Omega_u = \frac{(\Delta \varepsilon_{psu})_m}{(\Delta \varepsilon_{psb})_m} \quad (6.41)$$

Where $\Delta \varepsilon_{psu}$ is the increase in strain for unbonded prestressing tendon and $\Delta \varepsilon_{psb}$ is the increase in strain for the equivalent bonded tendon at section with maximum strain increase.

Strain increase in the unbonded tendon at the critical section can be treated as bonded tendons and calculated from the strain distribution at that section assuming perfect bond between concrete and steel then multiplied by bond reduction coefficient (Ω_u). From Fig. 6.28 the increase in strain can be calculated from equation 6.42:

$$(\Delta \varepsilon_{psb})_m = \varepsilon_{ce} + (\Delta \varepsilon_{cps})_m = \varepsilon_{ce} + \varepsilon_{cu} \left(\frac{d_e}{c} - 1 \right) \quad (6.42)$$

Assuming the value of Ω_u was known, so the strain increase in the unbonded tendon could be determined from:

$$(\Delta \varepsilon_{psu})_m = \Omega_u \varepsilon_{ce} + \Omega_u \varepsilon_{cu} \left(\frac{d_e}{c} - 1 \right) \quad (6.43)$$

Assuming the stress in the unbonded tendon remains in the elastic stage, the stress change in unbonded tendons at nominal moment resistance can be obtained from:

$$(\Delta f_{psu})_m = E_{ps} (\Delta \varepsilon_{psu})_m = \Omega_u E_{ps} \varepsilon_{ce} + \Omega_u E_{ps} \varepsilon_{cu} \left(\frac{d_e}{c} - 1 \right) \quad (6.44)$$

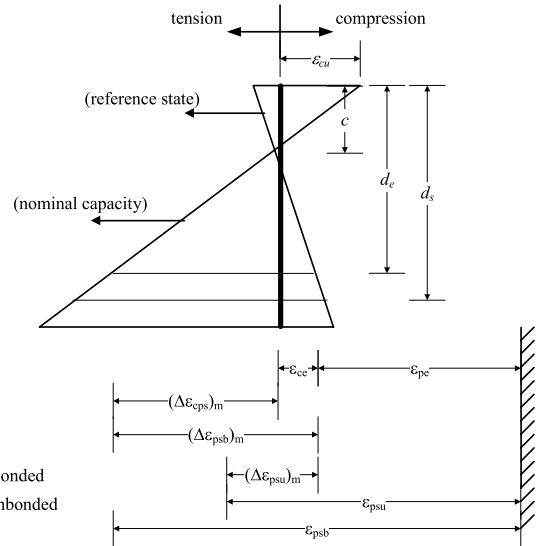


Figure 6.28 Strain distribution along section of maximum moment

The corresponding stress in the unbonded tendon is thus given by:

$$f_{ps} = f_{pe} + (\Delta f_{psu})_m = f_{pe} + \Omega_u E_{ps} \varepsilon_{ce} + \Omega_u E_{ps} \varepsilon_{cu} \left(\frac{d_e}{c} - 1 \right) \quad (6.45)$$

Generally, the value of ε_{ce} is negligible compared to the other terms and can be neglected. Hence, the previous equation becomes:

$$f_{ps} = f_{pe} + (\Delta f_{psu})_m = f_{pe} + E_{ps} \Omega_u \varepsilon_{cu} \left(\frac{d_e}{c} - 1 \right) \quad (6.46)$$

If the value of Ω_u can be determined, and by substituting the value of f_{ps} in the equation of force equilibrium, then the neutral axis depth (c) can be determined.

Based on the data collected from 143 beam tests carried out by various investigators, the value of Ω_u was proposed as follows:

$$\Omega_u = \frac{2.6}{L/d_p} \quad \text{for one-point loading} \quad (6.47)$$

$$\Omega_u = \frac{5.4}{L/d_p} \quad \text{for third-point or uniform loading} \quad (6.48)$$

For code purpose, Naaman and Alkhairi suggested the following equations:

$$f_{ps} = f_{pe} + (\Delta f_{psu})_m = f_{pe} + E_{ps} \Omega_u \varepsilon_{cu} \left(\frac{d_p}{c} - 1 \right) \frac{L_1}{L_2} \leq 0.94 f_{py} \quad (6.49)$$

$$\Omega_u = \frac{1.5}{L/d_p} \quad \text{for one-point loading} \quad (6.50)$$

$$\Omega_u = \frac{3.0}{L/d_p} \quad \text{for third-point or uniform loading} \quad (6.51)$$

Where:

- L_1 = length of loaded span or sum of lengths of loaded spans, affected by the same tendon
 L_2 = length of tendon between end anchorages
 L = clear span

The limitation of $0.94 f_{py}$ was selected to ensure that the stress in the steel remains as close as possible to the linear elastic range assumed in the analysis.

1. Mutsuyoshi *et al.* (1995)

Mutsuyoshi *et al.* firstly introduced a depth reduction factor, R_d , in order to account for the second order effects. They also modified the bond reduction coefficient as proposed by Naaman and Alkhairi for computing the tendon stress at the ultimate flexural strength of externally prestressed concrete beams. They proposed the following equation:

$$f_{ps} = f_{pe} + E_{ps} \Omega_u \varepsilon_{cu} \left(\frac{d_{pu}}{c} - 1 \right) < f_y \quad (6.52)$$

Where d_{pu} is the depth from the extreme compressive fiber to the centroid of prestressing tendon at the ultimate state, and can be determined from multiplying the depth reduction factor (R_d) with the initial tendon depth as follows:

$$d_{pu} = R_d d_{ps} \quad (6.53)$$

And Ω_u is the bond reduction coefficient which can be expressed for general case of beams subjected to two symmetrically concentrated loads as follows:

$$\Omega_u = \frac{1.47 + 10.3 \left(\frac{L_d}{L} \right)}{L/d_e} - 0.29 \frac{L_d}{L} \frac{S_d}{L} \quad (6.54)$$

Where

- L_d = is the distance between the concentrated loads
 S_d = is the distance between deviator

The depth reduction factor, R_d , can be defined as the following equation for third-point loading:

$$R_d = 1 - 0.022 \left(\frac{L}{d_e} - 5 \right) \left(\frac{S_d}{L} - 0.2 \right) + 0.0186 \frac{L}{d_s} q_s \quad (6.55)$$

Where:

- d_s = is the depth of tension reinforcement
 d_e = the depth from extreme compressive fiber to the centroid of prestressing tendons
 q_s = is the non-prestressed reinforcement index

$$q_s = \frac{A_s f_y}{b d_s f_c} \quad (6.56)$$

The depth reduction factor for one-point loading at midspan, R_{d1} , is defined as:

$$R_{d1} = 0.71 + 0.29 R_d \quad (6.57)$$

Where R_d is the depth reduction factor as taken from equation 6.54.

2. Naaman *et al.* (2002)

Two approaches were suggested to modify equation 6.51 and extend it to FRP tendons. The first approach was a conservative approach while the second was a refined one

- Conservative approach: Naaman *et al.* recommended the following equation for code use in case of steel or FRP tendons:

$$f_{ps} = f_{pe} + \frac{E_{pr} L_1}{1866 L_2} \geq f_{pe} + \frac{E_{pr}}{3732} \quad (6.58)$$

- Refined approach:

$$f_{ps} = f_{pe} + (\Delta f_{psu})_m = f_{pe} + E_{pr} \Omega_u \varepsilon_{cu} \left(\frac{d_p}{c} - 1 \right) \frac{L_1}{L_2} \leq 0.94 f_{py} \quad (6.59)$$

Where E_{pr} is the young's modulus of steel or FRP tendon

3. Ng (2003)

In his proposal, Ng (2003) developed a new modification based on the concept that the span-to-depth ratio was considered to have insignificant effect on the stress increase in external tendons at the ultimate flexural strength. Ng also applied a parameter (s_d/d_e) for controlling second order effects, and modified the bond reduction coefficient; Ω_u , as follows:

$$\Omega_u = \frac{d_e}{h} \left(0.895 - 1.364 \frac{L_s}{L} \right) - K_s \quad (6.60)$$

$$\text{Where } K_s = 0.0096 \frac{S_d}{d_e} \quad \text{if } \frac{S_d}{d_e} \leq 15 \quad (6.61)$$

$$K_s = 0.144 \quad \text{if } \frac{S_d}{d_e} > 15 \quad (6.62)$$

Where h is the height of the beam, L_s is the shear span (distance between support and applied load), K_s is a coefficient for controlling the second order effects.

4. Sivaleepunth *et al.* (2006)

Studying the applied load geometry as a major parameter affecting the tendon stress, the parameter L_d/L was introduced to account for the load geometry as well as the parameter S_d/d_e to account for the second order effect.

The bond reduction factor Ω_u was modified as follows:

$$\Omega_u = 0.3 \frac{L_d}{L} + 0.01 \frac{S_d}{d_{es}} + 0.1 \quad (6.63)$$

Where L_d is the distance between the applied loads, and S_d is the distance between deviators

Alternative New Method

Based on the relation between deflection and the increase in external prestressed force, Ghallab and Beeby (2004) proposed a simple method to calculate the stress in external or internal unbonded tendons (f_{pr}) in simple prestressed concrete beam at any loading stage (If $f_{pe} \geq 0.4f_{py}$). The stress in external tendons can be calculated from the following equation:

$$f_{pr} = f_{pe} + \frac{\Delta L}{L_t} E_{pr} \leq f_{py} \quad (6.64)$$

Where L_t is the total tendon length and ΔL is the increase in the total tendon length at any load and can be calculated as a function in the deflection from the geometry of the deflected tendon. Deflection during the working stage can be calculated using the effective moment of inertia.

While at ultimate, deflection (ΔL) at the critical section, e.g. mid span of uniformly loaded simply supported beam, can be calculated from the relation between deflection and curvature as follows:

$$\Delta_L = K \phi_u L^2 = K \frac{\epsilon_{cu}}{c} L^2 \quad (6.65)$$

Where

- K is the multiplier deflection factor depending on the load type
- L is the beam length,
- ϵ_{cu} is the ultimate concrete compressive strain
- c is the neutral axis depth of a fully cracked section.

Based on comprehensive study, Ghallab (2006) suggested the use of ultimate concrete strain equal to 0.003 in the previous equation. To simplify analysis, he suggested calculating neutral axis depth assuming yielding in both bonded steel and external tendons:

$$c_u = \frac{A_s f_y + A_{ps} f_{py} - A_s' f_y}{0.67 f_{cu} b (\beta)} \quad (6.66)$$

This method can be easily extended to externally prestressed continuous beams. From Fig. 6.29 and considering formation of plastic hinges at ultimate, the deformation can be assumed concentrated at the failure locations (critical sections). Hence, continuous beam can be considered as two simple beams, and deflection at any section can be assumed proportional to that at the critical section (Fig. 6.23), for example, deflection at section 3 equals:

$$\Delta_{3u} = \Delta_{4u} \frac{L_4}{L_4 + L_5} \quad (6.67)$$

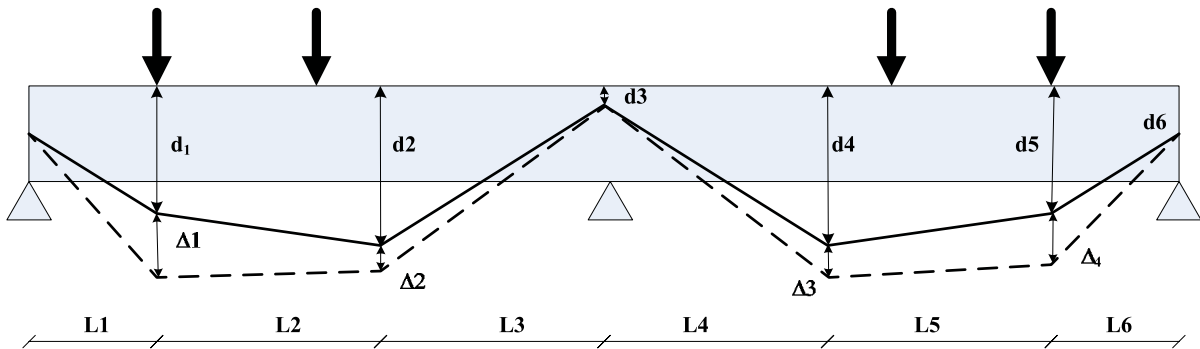


Figure 6.29 Deflected shape of external prestressing tendons due to loading

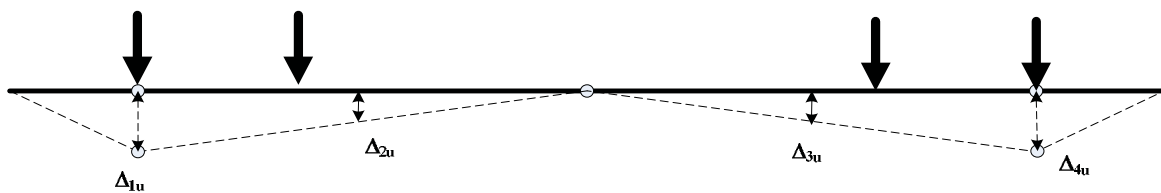


Figure 6.30 Failure shape of externally prestressed continuous beam at ultimate

Knowing deflection at each deviator, ultimate stress of the external prestressing tendons can be calculated from the deflected shape as follows:

$$\text{Increase in tendon length at ultimate} = \Delta L = L_{total}^* - L_{total} \tag{6.68}$$

$$\text{Increase in tendon strain} = \varepsilon_{cu} = \Delta L / L_{total}$$

$$\text{Ultimate tendon stress} = f_{pr} = f_{pe} + \varepsilon_{cu} E_{pr} = f_{pe} + \frac{\Delta L}{L_{total}} E_{pr} \leq f_{py} \tag{6.69}$$

$$\text{Where Initial total rope length} = L_{total} = l_1 + l_2 + l_3 + \dots \tag{6.70}$$

$$l_1 = \sqrt{L_1^2 + (d_1 - d_o)^2} ,$$

$$l_1 = \sqrt{L_2^2 + (d_2 - d_1)^2} ,$$

$$l_1 = \sqrt{L_1^2 + (d_2 - d_3)^2} \quad \text{etc,}$$

and Total length of the deflected tendon =

$$L_{total}^* = l_1^* + l_2^* + l_3^* + \dots$$

$$l_1^* = \sqrt{L_1^2 + [(d_1 + \Delta_1) - (d_o)]^2} ,$$

$$l_2^* = \sqrt{L_2^2 + [(d_1 + \Delta_1) - (d_2 + \Delta_2)]^2} ,$$

$$l_3^* = \sqrt{L_3^2 + [(d_2 + \Delta_2) - (d_3)]^2} \quad \text{etc.}$$

Table 6.3 shows a comparison between the studied methods while Fig. 6.31 shows a comparison between the experimental and analytical results at ultimate. As can be seen, results obtained by BS showed higher accuracy than the other codes, while Ghallab method yielded the best accuracy

6.4.3 Analysis of Test Beams

All test beams were analyzed using the previous discussed methods. A comparison between the actual and the analytical results are shown in Figure 6.32 and Table 6.4 while Table 6.5 shows the ratios of calculated and actual bending moments. The graphs show that code equations (ACI318, BS8110 and ECP03) underestimated the ultimate moment strength of externally prestressed beams while the other methods overestimated the ultimate moment strength of tested beams. Ghallab's method showed higher accuracy than the other suggested methods.

Table 6.3 Factors included in reviewed equations

| | External prestressing effect | | | | Tendon profile | | | Internal bonded steel | | | Beam properties and loading pattern | | | |
|----------------------------|------------------------------|------------|----------|-------|----------------|-------|---------|-----------------------|----------|-------|-------------------------------------|-----|----------|---|
| | f_{pe}^1 | f_{pe}^2 | A_{pe} | d_e | Shape | N_d | S_d/L | A_{ps} | f_{ps} | A_s | f_{cu} | L/h | L/ d_e | P |
| BS8110_97 | — | ■ | ■ | — | — | — | — | — | — | — | ■ | ■ | — | — |
| ACI318_08 | ■ | — | ■ | — | — | — | — | — | — | — | ■ | ■ | — | — |
| ECP-203_07 | ■ | — | — | — | — | — | — | — | — | — | ■ | ■* | — | — |
| Ghallab | ■ | — | ■ | ■ | ■ | ■ | ■ | ■ | ■ | ■ | ■ | ■* | ■* | ■ |
| Sivaleepunth <i>et al.</i> | — | — | — | — | — | — | ■ | — | — | — | — | — | ■ | ■ |
| Naaman <i>et al.</i> | ■ | — | — | ■ | — | — | — | ■ | ■ | ■ | ■ | ■ | — | ■ |

$f_{pe}^1 = \Delta f_{pe}$ not influenced by f_{pe} ; $f_{pe}^2 = \Delta f_{pe}$ influenced by f_{pe} ; N_d = number of deviators; S_d = distance between deviators; L= span length, P= loading pattern.

*This factor is not directly included in the equation

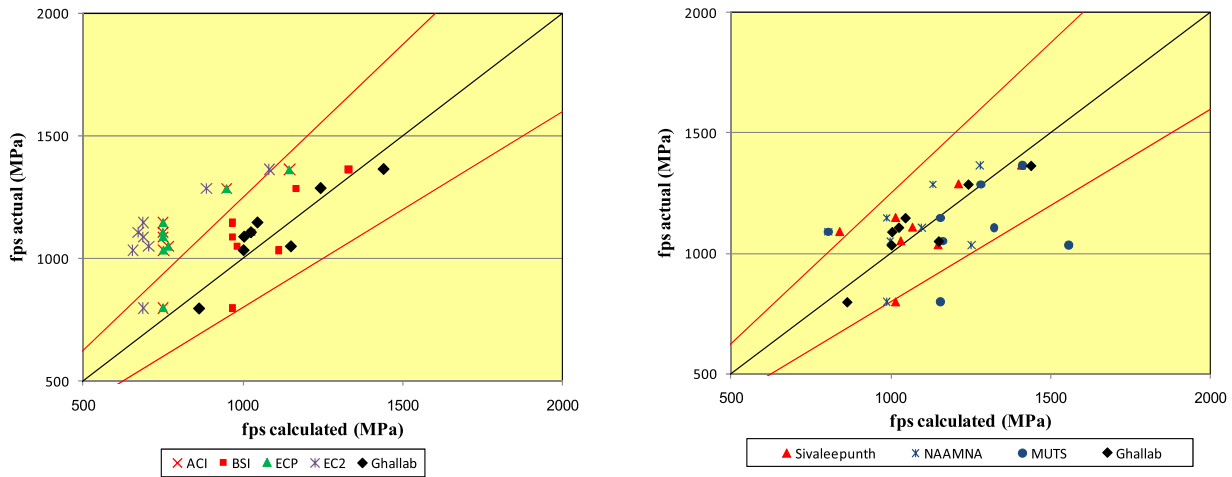


Figure 6.31 Comparison between actual and calculated tendon stress at ultimate.

Table 6.4 Actual and calculated ultimate moments (kN.m)

| beam no. | Actual | ACI318 | BS | ECP203 | Niwa | Naaman et.al | Muts. | Chee | Ghallab |
|--------------------|--------|--------|------|--------|------|--------------|-------|------|---------|
| P1-2 | 1.00 | 0.96 | 0.96 | 0.96 | 1.07 | 1.06 | 1.12 | 1.13 | 1.06 |
| PC1-1 | 1.00 | 0.97 | 0.96 | 0.97 | 1.07 | 1.04 | 1.09 | 1.10 | 1.05 |
| PC1-3 | 1.00 | 0.99 | 0.99 | 0.99 | 1.09 | 1.04 | 1.08 | 1.09 | 1.08 |
| PC2-2 | 1.00 | 0.94 | 0.94 | 0.94 | 1.08 | 1.09 | 1.19 | 1.21 | 1.03 |
| PC2-3 | 1.00 | 0.96 | 0.96 | 0.96 | 1.17 | 1.21 | 1.38 | 1.41 | 1.06 |
| PC3-2 | 1.00 | 0.87 | 0.87 | 0.87 | 0.90 | 0.89 | 0.89 | 0.92 | 0.94 |
| PC4-2 | 1.00 | 0.97 | 0.97 | 0.97 | 1.08 | 1.07 | 1.13 | 1.14 | 0.99 |
| PC5-2 | 1.00 | 0.93 | 0.93 | 0.93 | 1.03 | 1.02 | 1.08 | 1.09 | 1.05 |
| average | 1.00 | 0.95 | 0.94 | 0.95 | 1.06 | 1.05 | 1.12 | 1.14 | 1.03 |
| Standard deviation | 0.00 | 0.04 | 0.04 | 0.04 | 0.08 | 0.09 | 0.13 | 0.14 | 0.04 |

Table 6.5 Ratios of calculated to actual ultimate moment

| beam no. | Actual | ACI318 | BS | ECP203 | Niwa | Naaman et.al | Muts. | Chee | Ghallab |
|----------|--------|--------|-------|--------|-------|--------------|-------|-------|---------|
| P1-2 | 185.3 | 178.5 | 177.7 | 178.5 | 197.8 | 196.5 | 207.9 | 209.9 | 195.7 |
| PC1-1 | 199.2 | 192.5 | 191.6 | 192.4 | 212.6 | 206.4 | 216.4 | 218.2 | 209.8 |
| PC1-3 | 208 | 205.7 | 205.1 | 205.7 | 227.4 | 215.9 | 224.5 | 226.1 | 223.9 |
| PC2-2 | 199 | 187.2 | 186.1 | 187.2 | 215.5 | 217.3 | 237.3 | 241.0 | 205.8 |
| PC2-3 | 207 | 199.4 | 197.8 | 199.4 | 243.2 | 250.4 | 284.9 | 291.5 | 219.8 |
| PC3-2 | 142 | 123.9 | 123.4 | 123.9 | 128.2 | 127.0 | 126.6 | 130.1 | 133.8 |
| PC4-2 | 184 | 178.5 | 177.7 | 178.5 | 197.8 | 196.5 | 207.9 | 209.9 | 182.7 |
| PC5-2 | 193 | 179.7 | 178.9 | 179.6 | 199.0 | 197.2 | 208.5 | 210.4 | 203.2 |

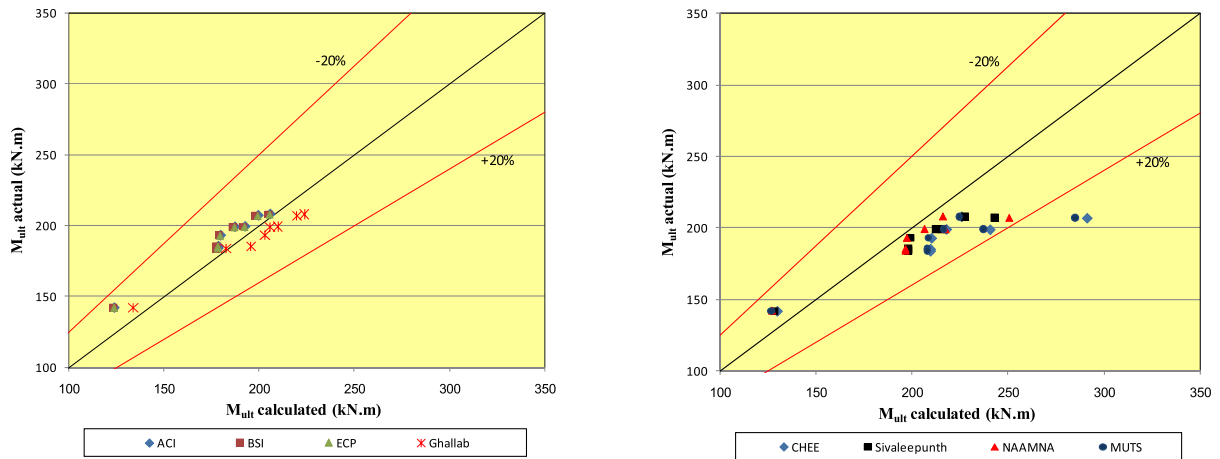


Figure 6.32 Relation between calculated and actual ultimate moment strength

7. Conclusions and Future Work

Introduction

Strengthening reinforced concrete members by the use of external tendons is becoming more popular worldwide. External prestressing may be defined as a prestressing introduced by tendons located outside a section of a structural member, only connected to the member through deviators and end-anchorage. The main advantages of using this technique are: higher utilization of small sectional areas, the speed of installation, low friction losses, direct monitoring of the tendons and ease in their replacement. This type of prestressing system can be applied to both new and existing structures that need to be strengthened due to changes in use, deficiencies in design or construction phase and structural degradation.

External prestressing tendons made of FRP materials are an alternative to steel tendons. Good durability properties and a first-rate behavior in creep and relaxation have given very good results so far. Within the different types of FRP, Parafil Rope was established to be well suited for prestressing system, combining the benefits of lightweight, high strength, easy handling and efficient anchorage system.

Recent literature shows that there have been a lot of researchers on external prestressing in the last few years. Yet most of these researches discussed external prestressing of single span structures, which have a different behavior than the externally prestressed continuous beams, due to the effect of secondary moment and moment distribution on the behavior of externally prestressed continuous beams.

The effect of several factors on the behavior of continuous prestressed concrete beams after being externally strengthened using Parafil rope Type G was ex-

perimentally investigated. Nine continuous reinforced concrete beams, eight of which were strengthened externally using Parafil Ropes type G, were tested up to failure. Five factors were studied to investigate their effect on behavior of strengthened beams.

These factors are:

- Value of external prestressing force.
- Effective depth of external prestressing force.
- Loading pattern.
- Tendon profile.
- Location of deviators.

Analytical investigations were also conducted to verify different methods that are used in the analysis of this beam type, regarding its deflection, tendon stress and flexural strength.

The main conclusions of the experimental and analytical studies as well as suggestions for future work are presented in the following sections.

Conclusions

Based on the results of the experimental and analytical investigations, the following conclusions were obtained:

7.2.1 General Conclusions

1. External prestressing using Parafil rope is a powerful system for strengthening or rehabilitation of continuous concrete structures, as it improves the stiffness and both cracking and ultimate flexural strengths of continuous concrete beams without a significant reduction in ductility.
2. Parafil rope Type G is an excellent alternative to steel tendon for strengthening or rehabilitation of concrete structures, due to its light weight and flexibility, which make installation easy. Its corrosion resistance is also highly beneficial.

3. The error resulting from using the effective external prestressing force in flexural strength calculations during the uncracked stage can be neglected since the increase in the prestressing tendon force before cracking is very small.
 4. Secondary moments and moment redistribution play a great role in the behavior of continuous externally prestressed concrete beams.
 5. Secondary moment due to external prestressing can be tolerated to improve the beam strength capacity.
 6. Providing external prestressing force by a moderate amount improves the stiffness and both cracking and ultimate flexural strength of prestressed concrete beams without a significant reduction in ductility.
 7. The camber of strengthened beams is slightly affected by an increase in the external prestressing force, loading pattern and tendon profile, while the increase in tendon effective depth and location of deviators had a significant effect on camber of strengthened beams .
 8. Although ductility of reinforced concrete beam is reduced after being externally strengthened, structural cracking gives ample warning of structural distress.
 9. The loss in ductility is affected by the prestressing force, effective depth of the prestressing force and deviators locations.
 10. Tendon stress increases proportionally with midspan deformation until yield. The rate of increase is influenced by the type of loading arrangement, eccentricity of external tendons and value of prestressing force.
 11. Considering moment redistribution, midspan sections showed a negative redistribution, while the support section exhibited a positive value in most of the strengthened beams. The amount of moment redistribution was affected by the prestressing force value, tendon layout and loading pattern on each beam.
 12. Including ordinary bonded steel in cracking strength calculations slightly improves the results.
4. The external prestressing force significantly increases both the cracking and ultimate moments compared to those before strengthening. However, the gain in the ultimate moment due to the increase in external prestressing force is relatively small.
 5. The value of the initial external prestressing force has a negligible effect on the increase in external prestressing force at cracking, while at ultimate the rate of increase in the external prestressing force decreases as the initial prestressing force increases.
 6. Losses of eccentricity of the external prestressing force significantly increases as the initial external prestressing force decreases.
 7. Both the primary moment and secondary moment increase as the prestressing fore increases.
 8. The loss of ductility with increase of prestressing force is associated mainly with a decrease in the ultimate deformation of the member.

7.2.3 Effect of Depth of the External Prestressing Force

1. Increasing the eccentricity of the external prestressing force results in reducing cracks propagation, higher stiffness after cracking and less ductile failure
2. Increasing eccentricity of the external prestressing force increased both cracking and ultimate load; hence increasing the eccentricity of the prestressing force can be useful in cases where cracking is not allowed. Moreover, it can be considered as one of the main factors which significantly increased beam strength.
3. The camber of strengthened beams significantly increases as the eccentricity of the external prestressing force increases.
4. The change in the effective depth of external prestressing force had a negligible effect on the prestressing force value up to cracking. While at ultimate the rate of increase in external prestressing force decreased as effective depth increased.

7.2.2 Effect of External Prestressing Force

1. The increase in the external prestressing force results in:
 - Reducing crack propagation
 - Improving stiffness after cracking and reducing deflections
2. Increase in the external prestressing force has a negligible effect on both stiffness and deflection before cracking while after cracking the increase in external prestressing force improves beam stiffness and reduces deflections (less ductile behavior).
3. Increase in the external prestressing force can change the behavior of strengthened beams at ultimate from ductile behavior to brittle behavior. Hence, the external prestressing force should be limited to avoid brittle failure.

7.2.4 Effect of Load Pattern

1. Before cracking, load pattern has almost no effect on beam stiffness (ductility) while after cracking stiffness of strengthened beams loaded using two concentrated loads at the third points of the span is higher than that loaded using one concentrated at the middle. In addition, at ultimate it showed higher ductile failure.
2. The loading pattern has a negligible effect on the cracking moment because the loss in effective depth at cracking load is small and has an insignificant effect. While the ultimate moment is inversely proportional with shear span
3. Because of the significant progressive reduction in the eccentricity of the tendons when loading with one concentrated load at the mid span, this loading

configuration caused a decrease in the flexural resistance of strengthened beams, compared to strengthened beams loaded with two concentrated loads at third points of the span.

4. Before cracking, the position of the applied load has no significant effect on the increase of the rope load. But after cracking, using two concentrated loads at the third points of the span increases the external prestressing force at ultimate and hence increases the ultimate moment.
5. Load pattern should be taken into consideration when analysing and designing externally prestressed continuous beams.

7.2.5 Effect of Tendon Profile

1. Choosing a proper tendon profile leads to a better service and ultimate behaviour of continuous beams.
2. Strengthening negative moment regions more than positive moment regions negatively affects the cracking and yield moments, however, it has a slight effect on the ultimate moment.
3. Before cracking, tendon profile has almost no effect on the increase of the rope load. But after cracking using two lower deviators increase the external prestressing force in the cables more than using two upper deviators.
4. Strengthening negative moment regions on wide length decreases the ductility of the beams and the percentage of moment redistribution that is transferred to the positive moment region.

7.2.6 Effect of Deviators Location

1. Changing the location of deviators (by translation towards the critical section) enhanced the cracking pattern, cracking strength, ultimate moment resistance, and stiffness of the beam.
2. By adapting the deviator location, the beam strength can be increased and can tolerate higher load especially at ultimate.

7.2.7 Analytical Investigation

7.2.7.1 Analytical Methods of Deflection Calculations

- a. Most methods can predict deflection of the externally prestressed beams with a reasonable accuracy up to the formation of the first major crack. However, after formation of the second major crack, they show less accuracy.
- b. ACI318 method shows higher accuracy among the studied methods. Using Equation (6.25) to calculate the effective inertia of the beam rather than using the

average inertia of sections at maximum positive and negative moments slightly improved accuracy.

- c. The unbonded method suggested by Ghali et al. and the Eurocode method are less accurate than the other methods.
- d. ACI318 method was conservative in most cases while Eurocode method was underestimated in most cases.
- e. Different code equations used for steel tendons are suitable for Parafil ropes after modifications.
- f. The suggested modification for all the reviewed methods used in calculating deflection of bonded or unbonded prestressed concrete beams, which is to calculate the deflection of prestressed concrete beams containing steel or FRP external prestressing tendons was found to give a fairly accurate results. This modification generalized these methods.
- g. Inertia of the section at the mid span can be only used in deflection calculation of continuous beam. Considering effect of inertia of section at the mid support had a slight effect on values of calculate deflection.

7.2.7.2 Analytical Methods of Cracking and Ultimate Moment Resistance Calculations

- a. All codes equations show a reasonable accuracy when calculating the cracking strength of externally prestressed continuous concrete beams. Neglecting steel reinforcement and parafil rope in cracking calculation slightly affect the results.
- b. Analytical methods need further investigation when used with eccentricity higher than the total beam height.
- c. The code equations for calculating the ultimate strength is less complicated and time consuming and gives fairly accurate results.
- d. ACI318 and EC2 methods underestimated values of the ultimate tendon stress.
- e. Different code equations used for steel tendons are suitable for Parafil ropes.
- f. Using bond reduction factor (λ_u) and depth reduction factor (R_d) as suggested by previous researches in ultimate strength calculations, showed no improvement in the results.
- g. New equations for bond reduction factor (λ_u) and depth reduction factor (R_d) should be adopted taking into consideration the location of deviators and the beam.
- h. British standard method showed the best accuracy among the other codes to calculate the ultimate tendon stress.
- i. The proposed method to calculate the ultimate strength showed good agreement with actual results, thus it can be used in continuous externally prestressed beams for any type of loading or tendon profile.

- j. ACI318, ECP203 and BS8110 underestimated the ultimate moment strength of externally prestressed continuous beams.

7.3 Recommendations

1. From the economic point of view, it is better to use moderate external prestressing force. This leads to using a lower capacity hydraulic jack and speeds the strengthening process.
2. The shape of deviated tendons are preferred to be selected relative to the load pattern as the ultimate flexural strength of concrete beams is very sensitive towards load pattern.
3. From the economic point of view, it is better to use highly eccentric tendons (higher than the section depth) to reduce the prestressing force and improve the serviceability of the strengthened member.
4. The shape of deviated tendons should be carefully selected to yield better results.
5. Deviator locations should be at the expected critical sections (i.e. mid span) so as to have higher flexural strength.

7.4 Future Work

The results of this study suggest several factors, which affect the behavior of strengthened beams where further research is needed, these are:

1. Behavior of the strengthened beams under long-term loading.
2. Effect of non-prestressed steel (type, percentage)
3. Effect of shear force and/or torsion moments on behavior of externally prestressed beams.
4. Effect of highly eccentric tendons of continuous beams on secondary moments and moment redistribution.
5. Effect of friction between tendons and deviators on the behavior of strengthened beams.
6. Effect of tendons materials (GFRP, CFRP, etc.).
7. Effect of using different tendons profile (straight-parabolic) on the behavior of beams.
8. Effect of loading and unloading span on the behavior of beams

References

1. Abdalla, H. A. and Elbadry, M. M. (1997) Temperature Effect on Concrete Members Reinforced with FRP Reinforcement. Proceeding of Annual Conference of Canadian Society of Civil Engineering. Sherbrooke, 27-30 May, 6, pp. 171-180.
2. ACI 318 (2008) Building Code Requirements for Structural Concrete and Commentary. American Concrete Institute, Michigan, USA.
3. Aravinthan T., Mutsuyoshi H., Matupayont S. and Machida A. (1995) "Moment Redistribution in Prestressed Concrete Continuous Beams with External Tendons", Transactions of the Japan Concrete Institute, v 17.
4. Aravinthan, T, Witchukreangkrai, E. and Mutsuyoshi, H. Flexural Behavior of Two-Span Continuous Prestressed Concrete Girders with Highly Eccentric External Tendons. *ACI Structural Journal* May-June 2005.
5. Aravinthan, T. Mutsuyoshi, H., Fujioka and A. Hishiki Y. (1997) Prediction of the Ultimate Flexural Strength of Externally Prestressed PC Beams. Transactions of the Japan Concrete Institute, 19, pp 225-230.
6. Arnold, C. A. Hergenrother, P. M. and Mcgrath, J. E. (1991) An Overview of Organic Polymeric Matrix Resins for Composites. In Composite Application: The Role of Matrix, Fiber, and Interface. Vigo, T. L. and Kinzig, B. J (eds). New York Cambridge, VCH, pp 3-30.
7. Bakis, C. E. (1993) FRP Reinforcement: Materials and Manufacturing. In Fiber-Reinforced-plastic (FRP) Reinforcement for Concrete Structures: Properties and Applications. Nanni, A. (ed.). Elsevier publishers B.V., pp 13-57.
8. Bank, L. C. Puterman, M. and Katz, A. (1998) Effect of Material Degradation on Bond Properties of Fiber Reinforced Plastic Reinforcing Bars in Concrete. *ACI Materials Journal*, 95 (3), pp 232-243.
9. BD 58/94 (1995) The Design of Concrete Highway Bridges and Structures with External Unbonded Prestressing. In Design Manual for Roads and Bridges. 1, section 3, part 9. Highways agency. HMSO. London, 10pp.
10. Beeby A. W. and Narayanan R. S. (1995) Designers' handbook to Eurocode 2. Part 1.1: Design of concrete structures. Thomas Telford Publisher, London.
11. Beeby, A. W., Scott, R. H., and Jones, A. E.K. (2005) Revised Code Provisions for Long-term Deflection Calculations. Proceedings of the institution of civil engineers, Structures and Buildings.
12. Branson D. E (1968) Design Procedures for Computing Deflections. *American Concrete Institute Journal and Proceedings*. NO 9, pp. 730-742.
13. Branson, D. E. and Shaikh, A. F. (1985) Deflection of Partially Prestressed Members. In Deflections of Concrete Structures. SP-86. American Concrete Institute. Detroit, MI, USA pp. 323-363.
14. Branson, D. E. and Trost, H. (1982) Application of the I-effective Method in Calculating Deflections of Partially Prestressed Members. *PCI Journal*, 27(5), pp 62-77.
15. Branson, D. E. and Trost, H. (1982) Unified Procedures for Predicting the Deflection and Centroidal Axis Location of Partially Cracked Nonprestressed and Prestressed Concrete Members. *ACI Journal*, 79(2), pp 119-130.

16. Branson, D. E. (1977) Deformation of Concrete Structures. McGraw-Hill. New York London. British Standards Institution (1997). BS8110 Structural Use of concrete, Part 1: Code of Practice for Design and Construction. BSI, London. UK.
17. Bruggeling, A. S. G. (1990) External Prestressing – a state of the art. In *External Prestressing in Bridges*. American Concrete Institute SP-120. Naaman, A. and Breen, J.(eds). Detroit, MI, USA, pp 61-81.
18. Burgoyne, C. J. (1993) Parafil Ropes for Prestressing Tendons. In *Alternative Materials for the Reinforcement and Prestressing of Concrete*. Clarke, J. L. (ed.). Blackie Academic and Professional. London, pp102-126.
19. Burgoyne, C. J. (1993). Should FRP be Bonded to Concrete!?. *International Symposium on Fiber-Reinforced-Plastic Reinforcement for Concrete Structures*. ACI SP-138. Nanni, A. and Dolan C. W. (eds), pp. 367-380.
20. Burgoyne, C. J. Campos, C. M. and Guimaraes, G. B. (1996) Behavior of Beams with External Tendons. *FIP Symposium on Post-Tensioned Concrete Structures*, London, 2, pp 865-871.
21. Burgoyne, C. J. Hobbs, R. E. and Strzemiecki, J. (1989) Tension Bending and Shear Bending Fatigue of Parallel Lay Ropes. Eighth International Congress on Offshore Mechanics and Arctic Engineering. The Hague, pp 691-698.
22. Burns, N. H., Helwig, T. and Tsujimoto, T. (1991) Effective Prestress Force in Continuous Post-Tensioned Beams with Unbonded Tendons. *ACI Journal*, 88(1), pp 84-90.
23. Campbell, T. I. and Kodur, V. K. (1990) Deformation Controlled Nonlinear Analysis of Prestressed Concrete Continuous Beams. *PCI Journal*. September-October. pp. 42-55.
24. Campbell, T. I., Kodur, V. K., Lopes, S. M.R. and Harrop, J. A. E.(1999) Study of Moment Redistribution in Prestressed Concrete Beams. *Journal of Structural Engineering*, Volume 125, Issue 3, pp. 351-352.
25. CEB-FIB, 1998 “Ductility of Reinforced Concrete Structures” Bulletin d’ Information No. 242.
26. Chakrabarti, P. R. (1995) Ultimate Stress for Unbonded Post-Tensioning Tendons in Partially Prestressed Beams. *ACI Structural Journal*, V. 92, No. 6, November-December, pp. 689-697.
27. Chambers, J. J. (1988) *Long term properties of Parafil. Symposium on Engineering Applications of Parafil Ropes*. Burgoyne C. J. (ed.). Department of civil engineering, Imperial College of science and technology. London, pp 21-27.
28. Clark, L.A. and Toms, S. (1996) Shear Strength of Beam with Unbonded or External Tendons. *FIP Symposium on Post-Tensioned Concrete Structures*, London, 2, pp 796-803.
29. Clements, L. L. (1998) Organic Fibers. In *Hand book of composites*. Peters, S. T.(ed.). Chapman and Hall. London. 2nd edition, pp 202-241.
30. Collins, M. and Mitchell, D. (1991) Prestressed Concrete Structures. Prentice Hall Publisher. *Englewood Cliffs, NJ*.
31. DU PONT (1981) Characteristics and Uses of Kevlar 49 Aramid High Modulus Organic Fiber, Bulletin NO. K-5, September, 12pp. (Guimaraes, G. B. (1988) Short Term Properties of Parafil. *Symposium on Engineering Applications of Parafil Ropes*.
32. Burgoyne, C. J. (ed.), Department of civil engineering, Imperial College of science and technology. London, pp 13-19.
33. ECP 203 (2007) Egyptian Code of Practice for Design and Construction of Concrete Structures. Cairo, Egypt.
34. Eibl J. (1990) Externally Prestressed Bridges. In *External Prestressing in Bridges*. American Concrete Institute SP-120. Naaman, A. and Breen, J. (eds). Detroit, MI, USA pp 375-388.
35. Erki, M. A. Rizkalla, S. H. (1993) A sample of the international production, FRP Reinforcement for Concrete Structures. *Concrete International*, 15(6), pp 48-53.
36. Eurocode 2 (2004) “Design of Concrete Structures. Part 1: General Rules and Rules for Buildings”, British Standards Institution BSI, London, UK.
37. Faza, S. S. and GangaRao, H. V. S. (1993) Glass FRP Reinforcing Bars for Concrete. In *Fiber-Reinforced-Plastic (FRP) Reinforcement for Concrete Structures: Properties and Applications*, Nanni, A. (ed.). Elsevier publishers B.V, pp. 167-188.
38. Freyssinet. http://www.freyssinet.be/4DCGI/an_struct_rehabi.htm. visisted 5/4/2009
39. Gerritse A. (1993) Aramid-based Prestressing Tendons. In *Alternative Materials for the Reinforcement and Prestressing of Concrete*. Clarke, J.L. Blackie Academic and Professional. London, pp172-201.
40. Ghali, A., Favre, R. and El-Badry, M. (2002) Concrete Structures: Stresses and Deformations. 3rd edition, Spon Press . London.
41. Ghallab A. and Beeby A. W. (2004) “Calculating Stress of External Prestressing Tendons”. Proceedings of institution of civil engineers- structures and buildings 2004, vol. 157; issue 4, p. 263-278.
42. Ghallab A. and Beeby A. W. (2005) “Factors Affecting the External Prestressing Force in Externally Strengthened Prestressed Concrete Beams”. *Cement and Concrete Composites*, vol. 27; number 9-10, pp 945-957.
43. Ghallab, A. (2006) Effect of Deviators Locations on Behavior of External Prestressed Concrete Beams. *Scientific Bulletin of Faculty of Engineering, Ain Shams University*, vol. 41, No. 3, pp. 33-51.
44. Ghallab, A. Strengthening Prestressed Beams Using Parafil Ropes as External Tendons. Ph.D. thesis. School of civil engineering, Leeds University (2001).
45. Guimaraes, G. B. and Burgoyne, C. J. (1992) Creep Behavior of a Parallel-lay Aramid Rope. *Journal of materials science*, 27, pp 2473-2489.

46. Guimaraes, G. B. (1988) Short Term Properties of Parafil. Symposium on Engineering Applications of Parafil Ropes. Burgoyne C. J. (ed.). Department of civil engineering, Imperial College of Science and Technology. London, pp 13-19.
47. Harajli M. H. (1993) Strengthening of Concrete Beams by External Prestressing. *PCI journal*, 38(6), pp 76-86.
48. Harajli, M. H. and Alameh, A. S. (1989) Deflection of Progressively Cracking Partially Prestressed Concrete Flexural Members. *PCI journal*, 34(3), pp. 94-127.
49. Harajli, M. H. and Kanj, M. Y. (1992) Service Load Behavior of Concrete Members Prestressed with Unbonded Tendons. *Journal of Structural Engineering*, 118(9), pp. 2569-2589.
50. Harajli, M. H. (1990) Effect of Span-deth Ratio on the Ultimate Steel Stress in Unbonded Prestressed Concrete Members. *ACI structural journal*, 87(3), pp 305-312.
51. Harajli, M. Khairallah, N. and Nassif, H. (1999) Externally Prestressed Members: Evaluation of Second-Order Effects. *Journal of Structural Engineering*, 125(10), pp. 1151-1161.
52. Jackson, P. (1996) Criteria for External and Unbonded Post-tensioning in Design and Strengthening. FIP Symposium on Post-Tensioned Concrete Structures, London, 2, pp865-871.
53. Jang B. Z. (1994) Advanced Polymer Composites. ASM International. Materials Park, OH, pp12-13.
54. Jerrett, C. V. and Ahmad, S. H. (1996) Behavior of Prestressed Concrete Beams Strengthened by External FRP Post-tensioned Tendons. In Proceeding of Advanced Composites Materials in Bridges and Structures. El-Badry, M. (ed.). Canadian Society for Civil Engineering, Montreal, pp. 305-312.
55. Karbhari, V. M. (1998) Use of Composite Materials in Civil Infrastructure in Japan. International Technology Research Institute. World Technology (WTEC) division. <http://www.itri.loyola.edu/compce/toc.htm> (Visited 2/2/01, 3/4/01).
56. Katz, A. (2000) Bond to Concrete of FRP Rebars after Cyclic Loading. *Journal of Composites for Construction*, 4(3), pp 137-144.
57. Katz, A. Berman, N. and Bank L. (1999) Effect of High Temperature on Bond Strength of FRP rebars. *Journal of Composites for Constructio*, 3(2), pp 73-81.
58. Kingston, D. (1988) Development of Parallel Fiber Tensile Members. Symposium on Engineering Applications of Parafil Ropes. Burgoyne C. J. (ed.). Department of civil engineering, Imperial College of Science and Technology. London, pp. 9-10.
59. Lafdi, K. 7 Wright, M. (1998) Carbon Fibers. In Hand book of Composites. Peters S. T. (ed.). Chapman and Hall. London. 2nd edition, pp. 169-201.
60. Linear Composite Limited (2007). Parafil Ropes: Technical Note PF1. Issue 1.UK.
61. Manjure, P. Y. (1996) Use of External Prestressing Technique - An Indian Experience. FIP Symposium on Post-Tensioned Concrete Structures. London, 2, pp.885-892.
62. Matupayont, S. Tsuchida, K. Mutsuyoshi, H. and Machida, A. (1994) Loss of Tendon's Eccentricity in Externally Prestressed Concrete Beam. Transactions of the Japan Concrete Institute, 16, pp. 403-410.
63. McKenna, C. J. and Chan, K. M. (1996) Externally Post Tensioned Bridges Route 3 Country Park Section-Hong Kong. FIP Symposium on Post-Tensioned Concrete Structures, London, 2, pp. 828-835.
64. Meier, U. (2000) Composite Materials in Bridge Repair. *Applied Composite Materials*, 7 (2), pp75-94.
65. Mutsuyoshi, H. Tsuchida, K. Matupayont, S. and Machida, A. (1995) Flexural Behavior and Proposal of Design Equation for Flexural Strength of Externally PC Members. Proceedings of JSCE, 26(508), pp 67-77 (in Japanese).
66. Naaman, A. E. and Alkhairi F. M. (1991) Stress at Ultimate in Unbonded Posttensioning Tendons: Part 2- Proposed Methodology. *ACI Structural Journal*, 88(6),pp.683-692.
67. Naaman, A. E. and Alkhairi, F. M. (1991) Stress at Ultimate in Unbonded Posttensioning Tendons: Part 1- Evaluation of the State-of-the-art. *ACI Structural Journal*, 88(5), pp.641-651.
68. Naaman, A. E. and Harajli, M. H. (1985) Evaluation of the Ultimate Steel Stress in Partially Prestressed Flexural Members. *PCI Journal*, 30(5), pp 54-81.
69. Naaman, A. E. (1990) New Methodology for the Analysis of Beams Prestressed with External or Unbonded Tendons. In External Prestressing in Bridges. American Concrete Institute SP-120. Naaman, A. and Breen, J. (eds). Detroit, MI, USA pp. 339-354.
70. Naaman, A. E., Burns, N., French, C., Gamble, W. L. and Mattock, A. H. (2002) Stresses in Unbonded Prestressing Tendons at Ultimate, Recommendation. *ACI Structural Journal*, V. 99, No. 4, July-August.
71. Naani, A. Bakis, C. E. O'Neil, E. F. and Dixon, T. O. (1996) Performance of FRP Tendon-anchor Systems for Prestressed Concrete Structures. *PCI Journal*, 41(1), pp 34-43.
72. Ng, C. (2003) "Tendon Stress and Flexural Strength of Externally Prestressed Beams" *ACI Structural Journal*, September-October, pp 644-653.
73. Picard A., Massicotte B. and Bastien J. (1995) Relative Efficiency of External Prestressing. *Journal of Structural Engineering*, Vol. 121, No. 12, December 1995.
74. Rostasy, F. S. (1993) FRP Tensile Elements for Prestressed Concrete- State of the Art, Potentials and Limits. International Symposium on Fiber-Reinforced-Plastic Reinforcement for Concrete Structures. ACI SP-138. Nanni, A. and Dolan, C. W. (eds), pp.347-365.
75. Saeki, N. Horiguchi, T. and Ikeda T. (1993) Strengthening of Damaged Concrete Beams by External Prestressing of Aramid Fiber Cable. International Symposium on Fiber- Reinforced-Plastic Reinforcement

for Concrete Structures. ACI SP-138. Nanni, A. And Dolan, C. W. (eds), pp. 913-932.

76. Sétra and LCPC (2008) "Information Note to Raise Awareness of Existing Structures with External Prestressing Protected by Cement Grout in Contact with the Tensile Elements". http://www.setra.equipement.gouv.fr/IMG/pdf/US_NI_OA_029_GB.pdf (visited January, 2008).
77. Shaikh A. F. and Branson, (1970) D. E. Non-tensioned Steel in Prestressed Concrete Beams. *PCI Journal*, 15, NO.1, pp. 14 –36.
78. Shaikh, A. F. and Branson, D. E. (1970) Non-tensioned Steel in Prestressed Concrete Beams. *PCI Journal*, 15(1), pp. 14 –36.
79. Sivaleepunth, C., Niwa, J., Diep, B., Satoshi tamura, S. and Hamada; Y. (2006) Prediction of Tendon Stress and Flexural Strength of Externally Prestressed Concrete Beams. *Doboku Gakkai Ronbunshuu e*, vol. 62, no. 1, pp. 260-273.
80. Songkiat, M. Hiroshi, M. Kazuteru, T. and Atsuhiko, M. (1994) Loss of Tendon's Eccentricity in Externally Prestressed Concrete Beam. *Transactions of the Japan Concrete Institute*.16, pp. 403-410. Structural system, 'prestressing technology'. http://www.structuralsystems.com.au/ssl/tech/docs/broch/2007/2007_ExternPTbroch.pdf. visited on 25/3/2009
81. Tadros, M. K. and Sulieman, H. (1983) Comments on Application of the I-effective Method in Calculating Deflections of Partially Prestressed Members. by Branson D. E. and Trost H. (1982). *PCI Journal*, 28(6), pp.131-136.
82. Tadros, M. K. Ghali, A. and Meyer, A. W. (1985) Prestresses Loss and Deflection of Precast Concrete Members. *PCI Journal*, 30(1), pp.114-136.
83. Tan K. And Tjandra R.A. (2007) "Strengthening of RC Continuous Beams by External Prestressing" *ASCE structural Journal*, Volume 133, Issue 2, February. 2007, pp. 195-204.
84. Tan, K. and Ng, C. (1997) Effects of Deviators and Tendons Configuration on Behavior of Externally Prestressed Beams. *ACI Structural Journal*, 94(1), pp. 13-22.
85. Vaughan, D. J. (1998) Fiberglass Reinforcement. In *Hand book of Composites*. Peters S. T. (ed.). Chapman and Hall. London. 2nd edition, pp. 131-155.
86. VSL International Ltd (2006) *Construction Systems*, Switzerland, p. 43.e.
87. Whitaker, A. F. Finckenor, M. M. Dursch, H. W. Tennyson, R. C. and Young, P. R. (1998) Environmental Effects on Composites. In *Hand Book of Composites*. Peters S.T. (ed.). Chapman and Hall. London. 2nd edition, pp. 810-821.
88. Yaginuma, Y. and Kitada, Y. (1988) Influence of Span on Behavior of Partially Prestressed Concrete Beams with Exterior Cables. *Transactions of the Japan Concrete Institute*, 10, pp. 409-416.

Notations

| | | |
|-----------|---|--|
| A_c | = | cross-sectional area of concrete. |
| A_e | = | area of external prestressing tendons. |
| A_s | = | area of nonprestressed tensile steel. |
| A_s' | = | area of nonprestressed compressive steel. |
| B | = | width of the web. |
| c | = | depth from concrete extreme compressive fiber to neutral axis. |
| D_e | = | depth from concrete extreme compressive fiber to centroid of external prestressing rope. |
| d_{cu} | = | depth from concrete extreme compressive fiber to centroid of external prestressing rope at ultimate. |
| d_s | = | depth from concrete extreme compressive fiber to centroid of nonprestressed tensile steel. |
| d_s' | = | depth from concrete extreme compressive fiber to centroid of nonprestressed compressive steel. |
| E_c | = | elastic modulus of concrete in compression. |
| E_{pp} | = | modulus of elasticity of Parafil rope. |
| E_{pr} | = | modulus of elasticity of steel or FRP tendons. |
| E_s | = | modulus of elasticity of nonprestressing steel. |
| f'_c | = | cylinder strength of concrete. |
| f_{ck} | = | characteristic cylinder compressive strength of the concrete. |
| f_{ct} | = | ultimate tensile strength of concrete. |
| F_{ctm} | = | mean value of axial tensile strength of concrete. |
| f_{cu} | = | cube strength of concrete. |
| f_L | = | calculated stress due to live load. |
| f_p | = | effective prestress in Parafil rope. |
| f_{ps} | = | ultimate stress in prestressing steel. |
| f_{pu} | = | ultimate strength of prestressing steel. |
| f_{py} | = | yield strength of prestressing steel. |
| f_r | = | modulus of rupture of concrete (MPa). |
| f_{TL} | = | total calculated stress in member. |
| f_y | = | yield strength of nonprestressed tensile steel. |
| h | = | total height of cross section. |
| I | = | inertia of the cross section. |
| I_e | = | effective moment of inertia. |

| | | | |
|----------------------|---|--------------------------|--|
| I_g | = moment of inertia of uncracked cross section (neglecting the steel). | Δ_p | = deflection calculated on the basis of a cracked section. |
| I_{cr} | = moment of inertia of cracked cross section (neglecting concrete in tension). | Δ_D | = deflection of midspan due to dead load. |
| I_{cra} | = inertia of the cracked section relative to the centroidal axis. | Δ_L | = deflection of midspan due to live load. |
| L | = clear span. | Δ_p | = deflection of midspan due to prestressing force. |
| L_1 | = length of loaded span or sum of lengths of loaded spans, affected by the same tendon. | $\Delta_{f_{ps}}$ | = tendon stress increase = $f_{ps} - f_{se}$ |
| L_2 | = length of tendon between end anchorages. | $\Delta_{\epsilon_{ps}}$ | = increase in strain in prestressing steel above effective prestress. |
| K | = multiplier deflection factor depending on the load type. | $\Delta\epsilon_{cps}$ | = the strain increase in the concrete at the level of tendon beyond effective prestress. |
| $K_D, K_L,$ K_p | = multiplier deflection factors of dead load, live load and prestressing force. | $\Delta\epsilon_{psb}$ | = the strain increase in the equivalent bonded tendon. |
| L | = span length between end anchorages. | $\Delta\epsilon_{psu}$ | = the strain increase in the unbonded tendons. |
| L_o | = equivalent plastic region length. | ϵ_{cc} | = strain in concrete at level of prestressing steel due to f_{se} . |
| L_p | = width of plastic zone. | ϵ_{cu} | = ultimate concrete compression strain in top fiber. |
| M_a | = applied moment. | ϵ_{ps} | = strain in prestressing steel at ultimate. |
| M_{cr} | = cracking moment. | ϵ_{pu} | = ultimate strain in prestressing steel. |
| M_{cr}^* | = net positive moment required to crack the section. | ϵ_s | = strain in nonprestressed tensile steel at ultimate. |
| M_d | = moment due to dead load. | ϵ_{se} | = effective prestrain in prestressing steel. |
| M_{dec} | = decompression moment (moment lead to zero stress on precompressed concrete extreme fibers). | ρ_p | = ratio of prestressing steel (A_{ps}/B_{dp}). |
| M_L | = moment due to live load. | ρ_s | = ratio of nonprestressed tensile steel (A_s/B_{ds}). |
| $M_{primary}$ | = the product of the prestressing force times its eccentricity from the center of gravity of the cross section of the beam. | Ω | = bond reduction factor before cracking. |
| $M_{secondary}$ | = moment caused by support reaction due to prestressing force. | Ω_{cr} | = bond reduction factor after cracking. |
| ne | = Parafil rope modular ratio. | Ω_{cr} | = bond reduction factor at ultimate. |
| n | = steel modular ratio. | | |
| P_i | = initial internal prestressing force. | | |
| P_L | = applied load. | | |
| P_x | = initial external prestressing force. | | |
| P_{ex} | = effective external prestressing force. | | |
| R_d | = depth reduction factor. | | |
| S_d | = distance between deviators. | | |
| y_b | = distance from neutral axis to bottom fiber of the section. | | |
| y_t | = distance from neutral axis to top fiber of the section. | | |
| β_1 | = concrete compression block reduction factor. | | |
| Δ | = deflection at midspan of the beam. | | |
| Δ_1 | = deflection calculated on the basis of an uncracked section. | | |



Ehab Mahmoud Abd El-Fattah El-Kassas

Professor of Structural Engineering, Assistant Dean for Technical Affairs, College of Engineering and Technology, Arab Academy for Science and Technology and Maritime Transport . He obtained his Bachelor of Science in Civil Engineering, June 1991, Alexandria University then; Master of Science in Civil Engineering, June 1996 Alexandria University; Doctor of Philosophy in Civil Engineering, June 2001, University of Dundee, Dundee, Scotland, United Kingdom.

He won many grants and awards in the United Kingdom and Egypt. He won the Overseas Research Students Award (ORS) in the United Kingdom for three consecutive years (1998, 1999, and 2000). Followed by Dr. Angus A Fulton Postgraduate Prize for the best research thesis examined in the academic year 2001, University of Dundee, UK, 2001. His first Grant was the BA/CSSP Research Grant, Egypt, 2005 which paved the way to two more prizes: the National Encouragement Award, Egypt, 2006 and Al-Shorouk Academy's Scientific Innovation Prize in the field of Civil and Architecture Engineering, Egypt, 2008.

Deployable Structures

Ehab Abdel Fatah El-Gazzaz

College of Engineering and Technology, Arab Academy for Science and Technology and Maritime Transport

ABSTRACT

The purpose of this report is to introduce the concept of deployable structures, and investigate the potential for using different types of them and the methods of their modelling and analysis. First, the report starts with an introduction to define the meaning of deployable structures, their characteristics and use. The main types of these systems and their applications in both civil field and aerospace industry are also given. Next, it describes the method of analysing these structures, and introduces the new deployable structure with continuous compression member and the numerical model for the canopy system. A new deployable arch and the model of proposed restraining systems are then introduced. In addition, this report describes how this process has been carried out and presents an assessment of the results.

Finally, concluding remarks and comments on the new types of deployable structures and recommendation for future work are given in the last section.

Introduction

Deployable structures are structures capable of large configuration changes in an autonomous way. These structures are used for easy storage and transportation and when required, they are deployable into their service configuration.

Deployable structures have many potential applications both on earth and in space. In civil engineering, temporary or emergency structures have been used for a long time. More recent applications are retractable roofs of large stadium, exhibitions and theatres. These structures are characterized by their rapid deployment and easy folding. In space, there is a growing need for erectable structures to be assembled there. Therefore, deployable structures are the only practical way to construct large, lightweight structures for remote locations in space. Recent development of deployable structures based on the tensegrity concept for applications in space, such as deployable masts and reflector antennas used for small satellites has been achieved.

The key step in the design of tensegrity structures is the form-finding analysis (finding the initial prestressed configuration). From the deployability point of view, tensegrity structures are very interesting since the compressive elements are disjointed. This provides the possibility to fold these members and hence the structure can be compactly stowed.

Many concepts for large deployable space structures have been developed over the last years. Space antennas and reflectors for telecommunications and earth sensing, or multipurpose earth orbiting space platforms are the main applications for these structures.

The idea to construct structures that include a large number of bi-stable elements (struts) and to exploit the

two stable states to set up different configurations of the structure, has been proposed and investigated to be used in many potential applications that include robotic manipulator arms, surfaces that control ventilation in building and active facades that control the sunlight entering a building. The bi-stable snap-through strut is based on the mises truss (the mises truss is a three-pin-arch constructed from two struts of equal length).

One of the most basic and dominating deployable systems is the deployable scissor structure. It is a deployable bar structure that consists of units where each unit is composed of a pair of bars. The unit is called a scissor unit, which consists of two straight bars connected to each other at an intermediate point with a pivotal connection, and hinged at their end nodes to end nodes of other units, allowing a compact and deployed configuration. Many applications of these structures have been proposed, ranging from civil engineering field to aerospace industry. A simple two-dimensional foldable structure can be made from two sets of parallel straight rods connected by pivots at the intersection points.

Recently, a new type of deployable systems has been proposed which is currently developed. This system consists of a very flexible compression member which is stiffened by additional vertical struts and diagonal wires. This stiffening is activated through prestressing a main tension cable till the desired deployable curved shape. Another similar idea was proposed to get an arched deployable structure, where bending a linear flexible compression member and holding it into the desired shape by the use of a fabric web derive the form. Prestressing of the web produces a form that is well suited to cope with environmental loadings. This idea was successfully applied to a military shelter.

Analysis of Deployable Structures

During the last few years, a new type of space deployable structures has been developed. The Scissor-Like Elements (SLEs), are assembled in such a way that they form a structural unit with plan view of normal polygons. Each side and each diagonal of the polygon is a SLE. The polygons can be equilateral triangle, square or hexagon. By combining many of these normal polygonal units, structures of various flat and curved geometric configurations can be created. This new deployable structure is stable and stress-free in both the folded and deployed configuration. During the deployment process, geometric incompatibility causes the occurrence of strains and stresses in the members. The geometric incompatibility of this type of structures can be well observed through the deployment process of a pentagonal unit. In the stage of deployment, the structural behaviour is characterized by highly geometric nonlinearity and a snap-through that locks the structure in the deployed configuration with stable state.

Analysis in the Deployed Configuration

The analysis of deployable structures in the deployed configuration is relatively straightforward where the behaviour is linearly elastic. There are three possible failure modes: strength, stiffness and buckling. Strength failure happens when stresses are higher than the defined allowable stresses. Stiffness failure is associated with deflections larger than a given limit. Both failure modes can be investigated with simple linear analysis. With respect to the buckling failure, a linearized buckling analysis gives very accurate results for the buckling loads and buckling modes, if they are compared with the results of geometrically nonlinear analysis. The accuracy of a linearized buckling analysis is expected because the prebuckling behaviour is characterized by small displacements. It is fair to say that the strength and buckling are more critical for smaller number of units, while stiffness is more critical for larger number of units, i.e. longer spans.

Analysis During Deployment

As previously mentioned, the structural behaviour of deployable structures during deployment is highly nonlinear. Experimental observations lead to the conclusion that the stress occurring in this phase is very sensitive to any small changes in geometry or member properties. This may result not only in expensive solutions, but also in making the feasibility of these structures during the deployment process questionable. Therefore accurate evaluation of stresses occurring during deployment

constitutes an integral part of the deployable structure design.

New Deployable Structures with Flexible Continuous Compression Member

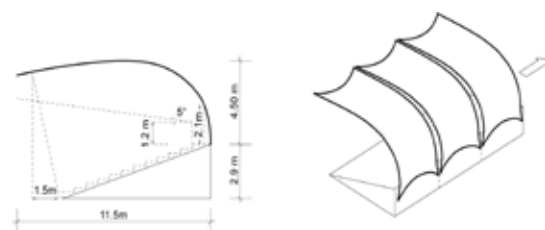
New types of deployable structures that consist of a flexible continuous compression member are stiffened with additional vertical and diagonal members, by prestressing the system through an active tension cable which sustains the system at the desired deployed curved shape. In the folded shape the continuous compression member becomes stress-free, where the diagonal wires and the active tension cable become slack.

The Canopy System

This system consists of ribs connected with membrane and prestressed with vertical tie to generate anticlastic curvature to this membrane. The rib, which can be deployed and folded, consists of the following:

- Two lower continuous compression flexible members made of aluminium and of cross section ($E = 70000 \text{ N/mm}^2$, $\sigma_y = 300 \text{ N/mm}^2$).
- Upper tension cable made of a compact strand of area 113 mm^2 , made of steel ($E = 120000 \text{ N/mm}^2$, $\sigma_y = 1200 \text{ N/mm}^2$).
- Diagonal elements made of wires each of area 12.6 mm^2 , made of steel ($E = 80000 \text{ N/mm}^2$, $\sigma_y = 1200 \text{ N/mm}^2$).
- Vertical elements made of A-frames, each leg of a circular tube $R = 15 \text{ mm}$ and $t = 3 \text{ mm}$, made of aluminium.
- Rung elements made of tubes of $R = 25 \text{ mm}$ and $t = 3 \text{ mm}$, made of aluminium.
- Vertical tie element made of wire of area 201 mm^2 , made of steel ($E = 80000 \text{ N/mm}^2$ and $\sigma_y = 1200 \text{ N/mm}^2$).

The canopy rib consists of 13 panels of length 1182 mm , where the panel is the spacing between A-frames. The average rise of A-frame is 700 mm . Spacing between ribs is 5.5 m . The canopy rib is supported with two hinged supports at the two ends of the last panel.



Numerical Model for the Canopy Rib

- The two lower compression members are modelled with beam elements.
- The upper tension cable is modelled with 2 truss elements for each segment between A-frames, to allow the cable slackness during folding/deployment process.
- The diagonal elements are modelled with truss elements.
- The vertical elements, A-frames, are modelled with beam elements but hinged with other elements.
- The rung elements are modelled with beam elements.
- The vertical tie element is modelled with two truss elements, to allow the slackness of this tie during the folding/deployment process.

A contact master surface is used to model the ground for the folded configuration stage.

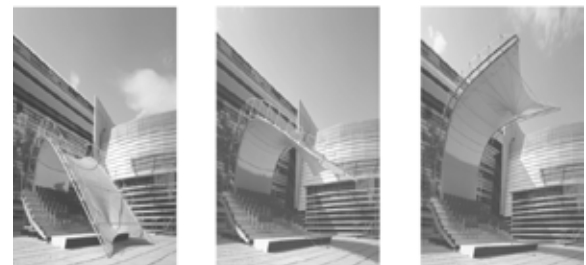
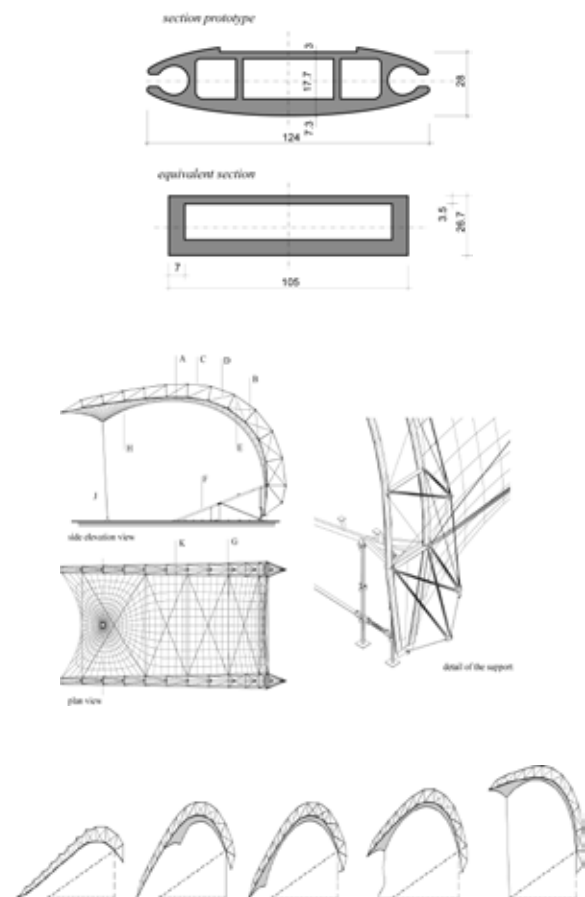
Nonlinear geometrical and material analysis was with ABAQUS software. The nonlinear carried out equilibrium path and the limit points were traced using the Riks iterative method.

Numerical Studies

The canopy rib was studied in the deployed configuration under gravity loads in addition to increasing concentrated load near the tip. Though the tension force in the upper tension cable is less than the compression force in the lower members, the horizontal component of the tension force is bigger than the horizontal component of the compression force at the critical panel, just before the last panel, where the slope of the tension member is less than the slope of compression member. The difference between these horizontal components is equilibrated by the horizontal component of the diagonal members causing compression force in these diagonals and in turn their slackness, as they are wires. Therefore, the dimensions and geometry of rib must be carefully determined and optimized.

The canopy has been studied under dead loads, snow and cases of wind loads. It has been found that under a certain case of wind loads, several diagonal wires are subjected to compression forces and become slack. To overcome this problem, it was proposed to use x-wire diagonals where one diagonal would be subjected to compression force and the other to tension force.

New technology developed to create a temporary structural system that can be deployed from the ground to cover large spans. The technology revolves around building a simple structure on the ground in a flat configuration. Complete control of the structure, either to increase its curvature or to lower it down for disassem-



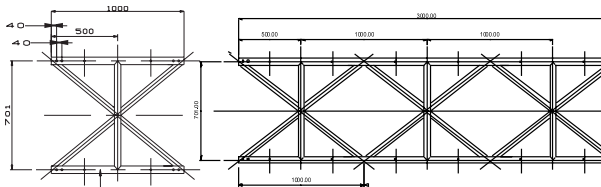
New deployable Arch

bly, is maintained all the time from ground level. This is necessary to avoid putting workers at risk and to speed up operations. Cross-sectional optimization has been completed considering the various combinations of straining actions expected in arch structures. Analysis of arch structures with different cross-sectional geometries has been conducted to determine straining actions values and distribution in addition to a complete study of the effect of using arch restraining systems on overall structural efficiency.

The Arch system

This system consists of small panels of beams either 1 m or 3 m connected with high tensile bold at the two ends of each panel to generate curvature. These beams

are fabricated using aluminium scaffold tube (48.3 mm dia×4.47 mm wall) for the main chords and uprights and a special 40 mm×21 mm×3.5 mm wall oval section for the diagonals. The average rise of beams is 700 mm. The spacing between uprights is 500 mm. The arch is supported with two hinged supports at the two ends of the last panel.



Numerical Model for the Arch

All elements are modelled with truss elements. Eight different shape of panels are used during the development process of optimum section to carry the applied loads due to enlargement of span.

- Case 1: Linear model composed of one beam.
- Case 2: Triangular model composed of three beams shaped as triangular section.
- Case 3: Box model composed of four beams shaped as box section.
- Case 4: Box model composed of four beams with double upper beam.
- Case 5: Box model composed of four beams with double lower beam.
- Case 6: Box model composed of four beams with double upper and lower beams.

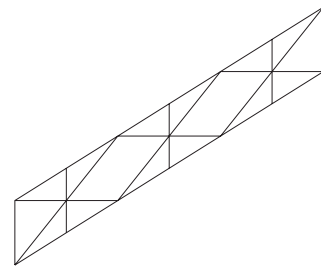
Nonlinear geometrical and material analysis has been done with ABAQUS software. The nonlinear equilibrium path and the limit points have been traced using the Riks iterative method.

Numerical Studies

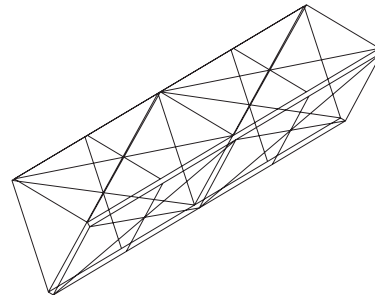
The arch was studied in the deployed configuration under gravity loads in addition to increasing concentrated loads and moments near the end of each panel. The arch was studied under dead loads, snow and cases of wind loads. It is evident that varying the section area has direct influences on the resistance capacity. However, this is not the only factor that improves this capacity, the member effective buckling length proved to have a direct influence on the section capacity to applied loads.

Structural Modeling of Arch Restraining Systems

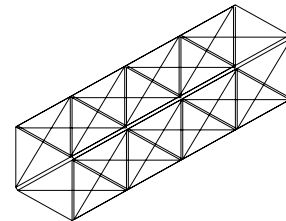
Arch construction is one of the oldest means of spanning rivers and forming the roofs of large buildings. An arch is a curved line forming a structural member



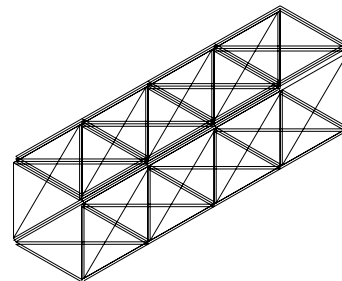
Case 1



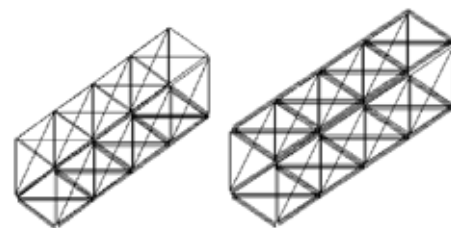
Case 2



Case 3



Case 4



Case 5

Case 6

that spans between two points. The common image of an arch is that of a structure composed of separate wedge-shaped pieces that retain their position by mutual pressure induced by the load. The exact shape of the curve and the nature of the loading are critical determinants as to whether the resultant assembly is stable

since the behaviour of an arch is strongly influenced by its boundary conditions. The work presented herein is a numerical parametric study that involves loading to failure a large number of unrestrained and arches restrained arches with tension cables while monitoring their behaviour. The variety of restraining systems enables the assessment of the effect of the number of restrained points on the arch chord (between two to six), and whether the restraining provided is direct or indirect. All arches are circular with hinged bases. They vary in rise/span ratio covering a range between 0.05 (very shallow arches) to 0.50 (semi circular arches). All structures are subjected to two basic loading conditions; a uniform load covering the whole length of the arch and a uniform load covering only the left half of the arch length.

Conclusion

The work described in this report is the first step of a project that aims to develop a large-span deployable structure. From the work presented, it can be seen that deployable structure with flexible continuous compression member and the large span arch system is a new type of deployable system. It seems to be very promising, though it is still under development; with further development, the technology would be suitable for industrial exploitation.

Furthermore, the following conclusions can be drawn from the work conducted and presented herein:

- Varying the section area has direct influences on the resistance capacity.
- The effective buckling length of the member has a direct influence on the section capacity.
- Implementing a restraining system that resists the sway movement of the arch is likely to lead to notable improvements in behaviour. By increasing the buckling load, and hence reducing the effective buckling length which delays failure.
- Providing more restraint to sway movement through preventing the displacement of more points on the arch chord meant higher strength.
- Reducing the number of restrained points on the arch chord to one per side, remains an effective yet inefficient solution.
- The strength increase in the former case over the unrestrained arch is between 60% and 240% depending on the location of the restrained points.
- The study shows as an example that, as the angle between the tie members increases, the efficiency of the restraining system decreases, leading to overall smaller strength improvements.

Recommendation for Future Work

The work presented indicates that it is feasible to produce a large span deployable structure. The following are some ideas for future work in this field

- The range of types covered should be extended to cover more types.
- New types should be separately analysed to assess their performance in different working conditions with different aspect ratio and boundary conditions.
- The work could be extended to include members under combined axial force and bending moment.

References and Bibliography

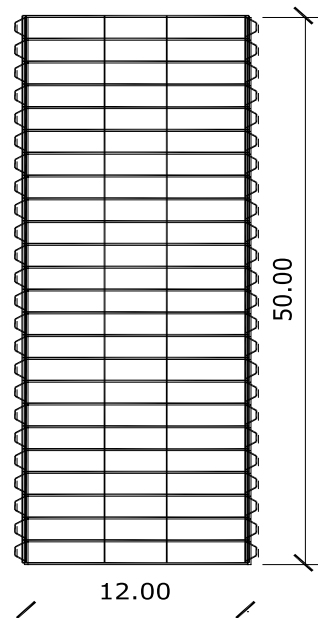
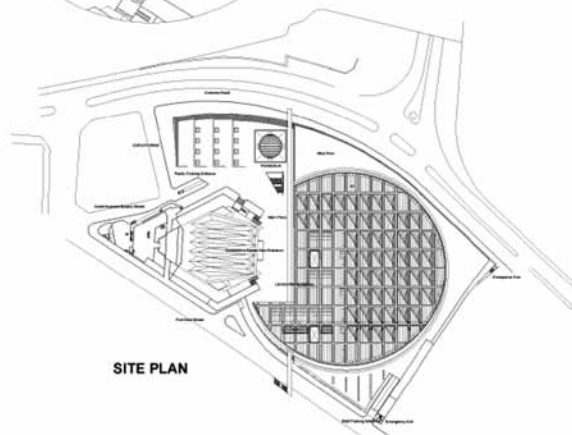
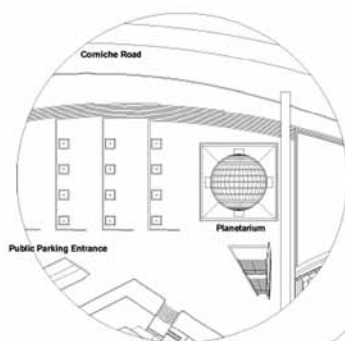
1. Arena Project, "A Deployable Membrane Canopy", Lightweight Structures Unit, Department of Civil Engineering, Dundee University, Dundee, Scotland, UK. March, 2001- 2002.
2. Argyris, J.H. and Scharpf, D.W., "Large Deflection Analysis of Prestressed Networks", *Journal of the Structural Division*, ASCE, 106(ST3), 1972-633-654.
3. Burford, N. and Smith, F., "Developing A New Military Shelter: A Case Study in Innovation", *Building Research and Information*, 27(1), 1999, 35-55.
4. Escrig, F., "Expandable Space Structures", *International Journal of Space Structures*, (1), 1985, 79-91.
5. Gantes, C. and Connor, J., "Combining Numerical Analysis and Engineering Judgment to Design Deployable Structures", *Computers and Structures*, Vol. 40, No. 2, 1991, 431-440.
6. Gantes, C. and Connor, J., "Structural Analysis and Design of Deployable Structures", *Computers and Structures*, Vol.32, No.3/4, 1989, 661-669.
7. Gantes, C. and Giakoumakis, A., "Symbolic Manipulation as Tool for Design of Deployable Domes", *Computer and Structures*, Vol. 64, No. 1-4, 1997, 865-878.
8. Gantes, C. and Logcher, R., "Geometric Design of Deployable Structures With Discrete Joint Size", *International Journal of Space Structures*, Vol.8, No.s 1 and 2, 1993, 107-117.
9. Gantes, C., Connor, J., and Logcher, R., "Simple Friction Model for Scissor Type Mobile Structures", *Journal of Engineering Mechanics*, ASCE, 119(3), 1993, 456-475.
10. Gantes, C., "Deployability Conditions for Curved and Flat, Polygonal and Trapezoidal Deployable Structures", *International Journal of Space Structures*, Vol. 8, No.s. 1 and 2, 1993, 97-106.
11. Hanaor, A, "Double-Layer Tensegrity Grids as Deployable Structures", *International Journal of Space Structures*, 8(1and2), 1993, 135-143.
12. Hanaor, A, and Liao, MK., "Double-layer Tensegrity Grids: Static Load Response. I-Analytical Study",

- Journal of Structural Engineering*, ASCE, 117(6), 1991, 1660-1674.
13. Hanaor, A., "Double-layer Tensegrity Grids: Static Load Response. II- Experimental Study", *Journal of Structural Engineering*, ASCE, 117(6), 1991, 1675-1684.
 14. Hanaor, A., "Design, Analysis and Response of Double-layer Tensegrity Grids," in Developments in Structural Engineering, Proc. Fourth Rail Bridge Centenary Conference, Topping H.Y. ed., E.and F.N. Spon, Chapman and Hall, London, August 1990, V I, 579-590.
 15. Hibbitt, Karlsson and Sorensen, Inc ABAQUS- Standard Users Manual. Detroit, MI, 2001.
 16. Kwan, A, and Pellegrino, S., "Matrix Formulation of Macro Elements for Deployable Structures", *Computers and Structures*, Vol. 50, No. 2, 1994, 237-254.
 17. Kwan, A. and Pellegrino, S., "A New Concept for Large Deployable Space Frames", *International Journal of Space Structures*, 9(3), 1994, 153-162.
 18. Langbecker, T., "Kinematic Analysis of Deployable Scissor Structures", *International Journal of Space Structures*, Vol. 14, No. 1, 1999, 1-15.
 19. Riks E., "The Application of Newton's Method to the Problem of Elastic Stability". *Journal of Applied Mechanics*, 39, 1972, 1060-1066.
 20. Rosenfeld, Y., et al., «A Prototype Clicking Scissor-Link Deployable Structure», *International Journal of Space Structures*, Vol. 8, Nos. 1and2, 1993, 85-95.
 21. Schioler, T. and Pellegrino, S., "Multi- Configuration Space Frames", In Proc. 45th ASAA/ In Proc. 45th AIAA/ ASME/ ASCE/ AHS/ ASC Structures, Structural Dynamics and Materials Conference, 19-22 April 2004, Palm Springs, CA AIAA 2004-1529.
 22. Soykasap, G., Watt, A. and Pellegrino, S., "New Deployable Reflector Concept", In Proc. 45th AIAA/ ASME/ASCE/AHS/ASC Structures, Structural Dynamics and Materials Conference, 19-22 April 2004, Palm Springs, CA AIAA 2004-1574.
 23. Tan, L. and Pellegrino, S., "Ultra Thin Deployable Antennas", In Proc. 45th AIAA/ ASME/ ASCE/ AHS/ ASC Structures, Structural Dynamics and Materials Conference, 19-22 April 2004, Palm Springs, CA AIAA 2004-1730.
 24. Tibert, G. and Pellegrino, S., "Deployable Tensegrity Masts", In Proc. 44th ATAA/ASME/ASCE/AHS/ ASC Structures, Structural Dynamics and Materials Conference, 7-10 April 2003, Norfolk, V A AIAA 2003-1978
 25. Tibert, G., "Deployable Tensegrity Structures for Space Applications", Doctoral Thesis, Department of Mechanics, Royal Institute of Technology, Stockholm, 2002.
 26. Tibert, G., 'Numerical Analysis of Cable Roof Structures', Department of Structural Engineering, Royal Institute of Technology, SE- 10044 Stockholm, Sweden, 1999 (ISSN 1103-4270).
 27. Vilnay, O., "Design of Tensegric Shells", *Journal of Structural Engineering*, ASCE, 117 (7), 1991, 1885-1896.
 28. You, Z. and Pellegrino, S., "Foldable Bar Structures", *Int. J. Solids and Structures*, Vol 34, No. 15, 1997, 1825-1847.

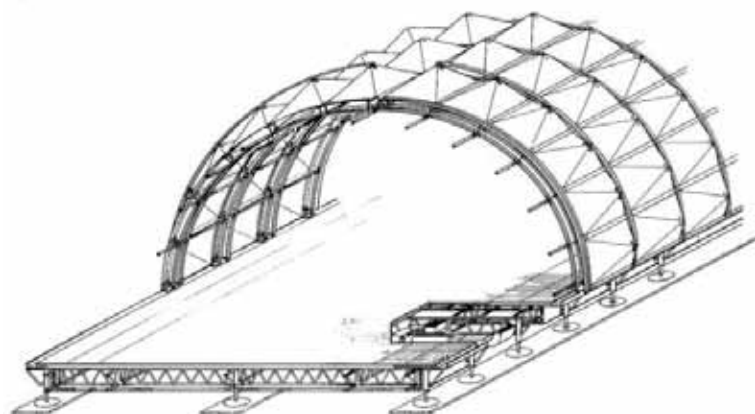
Appendix A

Proposed Model for a Temporary Exhibition Pavilion for the Bibliotheca Alexandrina

The Pavilion building is especially designed to be easy to demount, transport and retract. It is entirely clad in a transparent plastic, which also doubles up as part of the structure. The plastic is moulded into units which are stackable, light and pyramid-shaped for strength. The whole building including air conditioning equipment can be transported in container trucks and erected in a few weeks. The system consists of steel Arches or Arches are fabricated using aluminium scaffold tube. The suggested area of the Pavilion is (12m×50m). The span of the Pavilion is 12m while the spacing between arches is 5m.



Plan View



Isometric View

Appendix B

Structural Modeling of Arch Restraining Systems

ABSTRACT

Arch construction is one of the oldest means of spanning rivers and forming the roofs of large buildings. An arch is a curved line forming a structural member that spans between two points. The common image of an arch is that of a structure composed of separate wedge-shaped pieces that retain their position by mutual pressure induced by the load. The exact shape of the curve and the nature of the loading are critical determinants as to whether the resultant assembly is stable, as the behaviour of an arch is strongly influenced by its boundary conditions. The work presented herein is a numerical parametric study that involves loading to failure. A large number of unrestrained and arches restrained with tension cables while monitoring their behaviour. The variety of restraining systems enables the assessment of the effect of the number of restrained points on the arch chord (between two to six), and whether the restraining provided is direct or indirect. All arches are circular with hinged bases. They vary in rise/span ratio covering a range between 0.05 (very shallow arches) to 0.50 (semi circular arches). All structures are subjected to two basic loading conditions; a uniform load covering the whole length of the arch and a uniform load covering only the left half of the arch length.

Keywords: *Arches, modeling, restraining systems*

Introduction

Arch construction is one of the oldest means of spanning rivers and forming the roofs of large buildings. It is appropriate that this set should start with illustrations of a number of historic arches, including Roman and Medieval. It was inevitable that the arch form should dominate the early history of buildings as without the availability of a material capable of taking significant tensile stresses, a predominantly compressive system was the only means of forming large spans. Hence, early structural and architectural forms were primarily based on columns, arches, and domes. With the advent of steel and the ability to cast in concrete, there was a revolution in arch design, with a dramatic increase in possible spans.

An arch is a curved line forming structural member that spans between two points. The common image of an arch is that of a structure composed of separate wedge-shaped pieces that retain their position by mutual pressure induced by the load. The exact shape of the curve and the nature of the loading are critical determinants as to whether the resultant assembly is stable. When shapes are formed by simply stacking rigid block elements, the resultant structure is functional and stable only when the action of the load is to induce in plane forces that cause the structure to compress uniformly.

Constructing an arch bridge can be tricky, since the structure is completely unstable until the two spans meet in the middle. One technique is to build elaborate scaffolding, or “centring,” below the spans to support them until they meet. A new method supports the spans using cables anchored to the ground on either side of the bridge. In situations where there is an active

water or roadway below, this method allows contractors to build without disrupting traffic.

The work presented herein is a numerical parametric study that involves loading to failure a large number of unrestrained arches and arches restrained with tension cables while monitoring their behaviour. The objective of this paper is to determine the behaviour of unrestrained and restrained arches subjected to vertical loading, and the work will be extended to include other cases of loading. After presenting the parametric study in this paper, its results will be assessed.

Parametric Study

The present numerical parametric study involves loading to failure a large number of unrestrained arches and arches restrained with tension cables joining the supports with different points along the arch length while monitoring their behaviour. The arches, shown in Fig. 1, include an unrestrained Arch A, and Arches B to F restrained with five different restraining systems. The variety of restraining systems enables the assessment of the effect of two factors:

- The number of restrained points on the arch chord (two in Arches B and D, three in Arch F and six in Arches C and E)
- whether the restraining provided is direct (as in arches D, E and F) or indirect (in Arches B and C).

All arches are circular with hinged bases. They vary in rise/span ratio covering a range between 0.05 (very shallow arches) to 0.50 (semi circular arches). All structures are subjected to two basic loading conditions; a uniform load covering the whole length of the arch and

a uniform load covering only the left half of the arch length, (Fig. 2). In case of full uniform load, symmetry was deliberately removed by making the load on the left half of the structure 4% higher than that on the right half. This load variation is introduced to allow potential unsymmetrical buckling modes to develop.

For consistency, all arches have a 30 m span and two hinged supports. The rise varies between 1.5 m and 15 m as described before. An arch with rise/span ratio of 0.20 and a single tie connecting the two support nodes (in this case with a hinged support and a roller support) has been designed under a uniform load of 7.5 kN/m', and the resulting member sizes have been used in all cases to enable direct comparison of the results. The design specifications of BS5950, Part 1¹ have been used in designing the arch. The cross-sections used are: Circular Hollow Section 193.7×16 mm in the arch chord and solid bar with 50mm diameter in the tie

members. Steel grade S355 ($F_y = 355 \text{ N/mm}^2$ and $E = 205 \text{ N/mm}^2$) is used throughout.

All arches have been non-linearly analysed using the finite element software package Abaqus², which is well known for its accuracy and reliability. The analyses consider both geometric non-linearities due to change of joint coordinates and material non-linearities due to yielding. The arch chord is modeled as a series of 16 two-nodded beam elements with three degrees of freedom per node including displacements in the span and rise directions and rotation in the plane of the arch. Out-of-plane deformation is prevented as the arch is assumed to be fully restrained in the lateral direction by stiff inter-arch panels. The ties are modeled using single two-nodded tie elements capable of transmitting tension loads only. The "no compression" option in Abaqus is used in the material definition of the ties to indicate their ability to carry tension only.

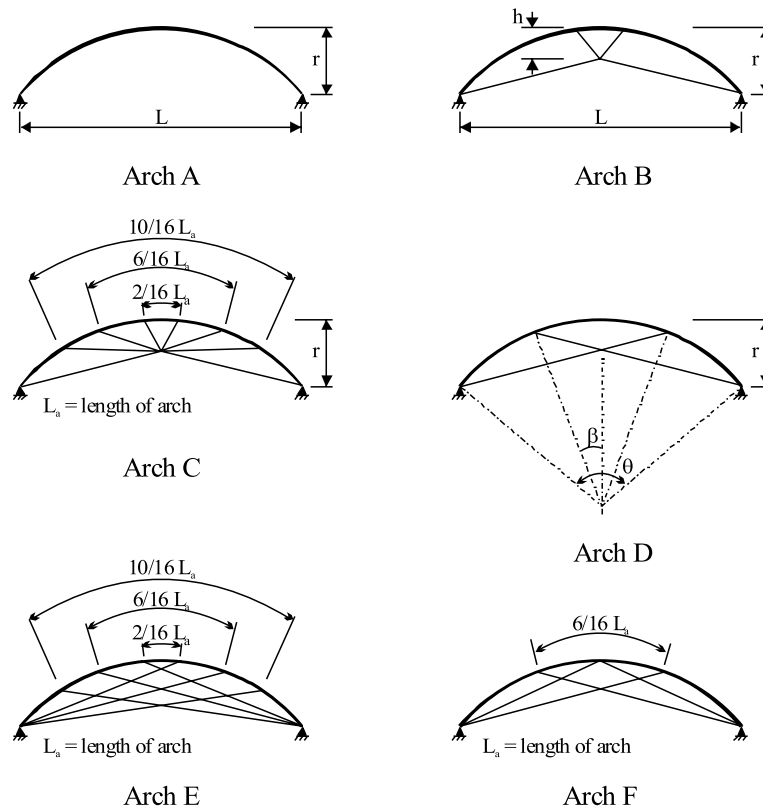
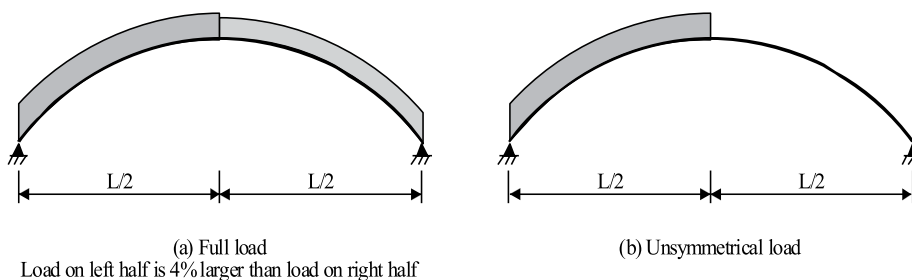


Figure 1 Restrained and unrestrained arches involved in the parametric study



(a) Full load
Load on left half is 4% larger than load on right half

(b) Unsymmetrical load

Figure 2 Arch loading cases

In tracing the nonlinear behaviour under loading, Riks method³ is adopted. In this method, load increments vary according to the current stage of overall behaviour, and are controlled automatically such that a solution is obtained even if the structure forms a mechanism and becomes unstable. The next section of the paper presents the results obtained from analysing the restrained arches. The analyses have been carried out in order to assess the effect of using different restraining systems on the overall strength, stiffness and behaviour of the arch.

Analytical Results

The study starts with the unrestrained arch for benchmarking the behaviour and strength of all other arches. The load central sagging behaviour of the unrestrained arches (thereafter called Arches A) under both symmetrical and unsymmetrical loads and the deformed shapes in both conditions are shown in Fig. 3. In all cases, the arches experience an overall buckling mode of the form depicted in Fig. 3, although this mode is more clearly pronounced under unsymmetrical loads. Under full loading, the behaviour is almost linear until buckling takes place. As buckling develops, nearly the right quarter point experiences rapidly increased bending and soon after localised yielding (in effect creating a plastic hinge) leads slowly to the collapse of arches. This process is less dynamic under unsymmetrical loading where the loading condition inevitably creates high bending moments in the arch and hence the bending at nearly the right quarter point develops gradually as the loading progresses until a plastic hinge is created. Although the behaviour under full load is controlled by the expected sudden buckling, yet it is dominated by a gradual bending action under unsymmetrical load. Comparing the cases with different rise/span ratios reveals that the best overall performance in terms of both strength and stiffness is associated with rise/span = 0.20. This ratio will be given more attention when studying the other restrained arches treated hereafter.

Arch B

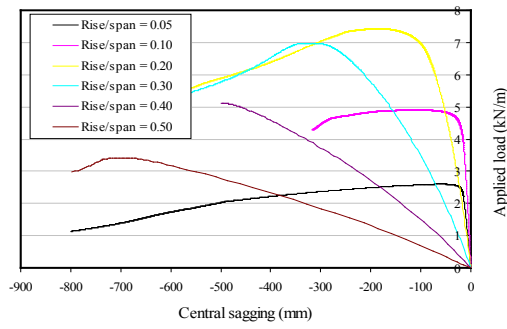
The first restrained arch to be covered is Arch B with four tie members connected to the two support nodes and meeting at a point below the arch center by distance, h , (see Fig. 1). This arrangement essentially provides a restraint against lateral movement at two points near the centre of the arch, and is therefore expected to help resist the failure mode experienced in unrestrained arches. The load deflection performance of Arches B under both loading conditions is shown in Fig. 4 and it is clear that the restraining system is able to produce a small improvement in both strength and stiffness. For

cases with $h/\text{rise} = 0.75$, the strength is increased by an average of 12.4% under full load and 3.6% under unsymmetrical load. The corresponding improvement in stiffness is marginal at 0.5%. There is also no notable change in the deformation pattern under full and unsymmetrical loads as can be seen in Fig. 4.

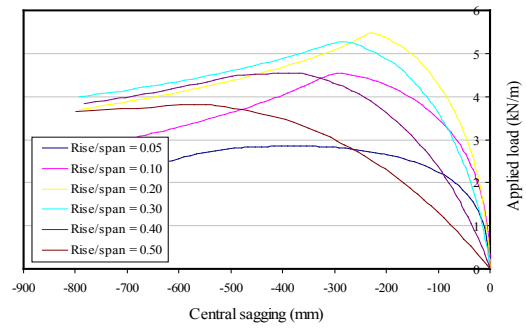
However, the efficiency of this restraining system can be improved by changing the distance h as can be seen in Fig. 5 where the ratio of h/rise varies between 0.0 and 1.0. Notice that with the ratio being 0.0, the system reduces to one with two tie members connecting the support nodes to the arch centre, while, with the last ratio, 1.0, the two outer tie members become horizontal. This latter case is clearly not expected to lead to a much improved performance due to the large angle between each two tie members connecting a point near the arch centre to an opposite support node. The improvement in strength in this case compared to the unrestrained arch is 2.4% under full load and 2.2% under full unsymmetrical load. As the tie connection point is raised, the connection between the arch centre and the support nodes becomes more direct. For instance, in the case with $\text{rise}/\text{span} = 0.20$, the angle between the two tie members connecting the arch centre to a support node decreases from 64.7° to 54.7° , 40.1° and 17.2° as h/rise reduces from 1.0 to 0.75, 0.50 and 0.25, respectively. The corresponding increases in strength compared with the unrestrained Arch A are 2.4%, 7.5%, 21.9% and 60.2%. This clear association between establishing a direct connection between the arch centre and a support node (or creating a direct restraint at the arch centre) is an important finding and will form the basis for a number of restraining systems that are to be studied hereafter. However, before moving on, it would be prudent to test a modified and a more promising form of Arch B in the next section.

Arch C

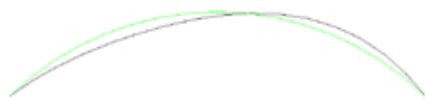
Arch C is restrained in a similar fashion to Arch B with the addition of two new tie members on each side of the arch. These tie members are expected to provide more restraint to sidesway movement of the arch in the form depicted in Fig. 1, and hence delay its sway buckling mode. By restraining the arch at six points, rather than two, it is expected that the effect will cause pronounced improvements in strength under both loading conditions. As can be seen in Fig. 6, the only case studied has a rise/span ratio of 0.20. Significant improvements in strength are evident compared with corresponding Arch B cases where the sway buckling mode prevails. Under full load, the strength grows by 161.3%, 263.1%, 276.7% and 206.2% for the cases with $h/\text{rise} = 0.25$, 0.50, 0.75 and 1.0, respectively, and similar values are obtained for cases under asymmet-



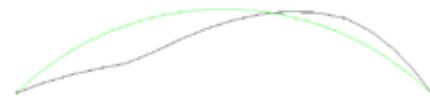
a Load central sagging behaviour under full load



b Load central sagging behaviour under unsymmetrical load

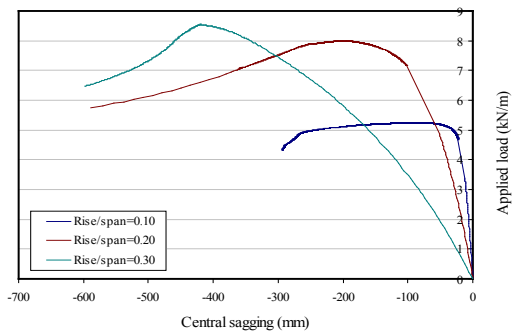


c Deformation under full load

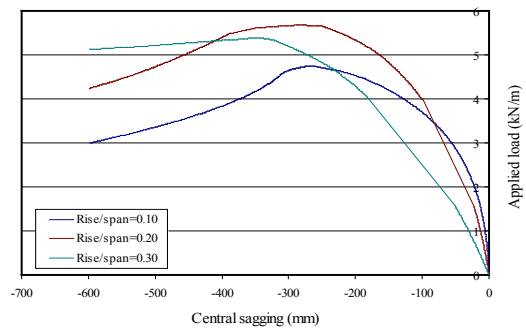


d Deformation under unsymmetrical full load

Figure 3 Behavior of unrestrained arches under full load



a Load central sagging behaviour under full load



b Load central sagging behaviour under unsymmetrical full load

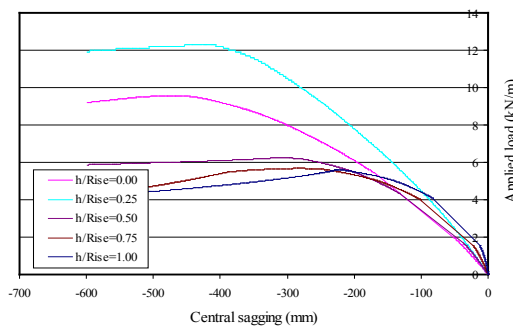


c Deformation under full load

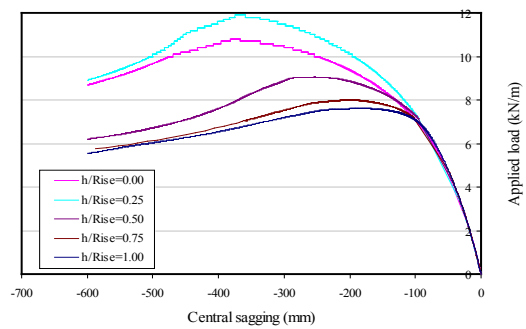


d Deformation under unsymmetrical full load

Figure 4 Behaviour of restrained Arches B under full load

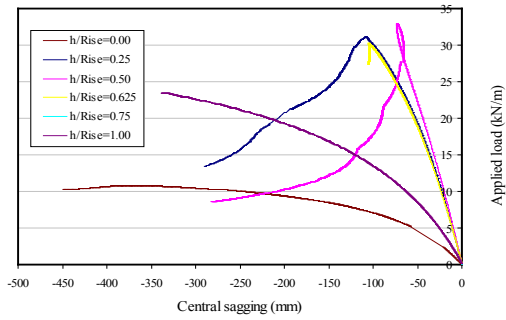


a Load central sagging behaviour under full load

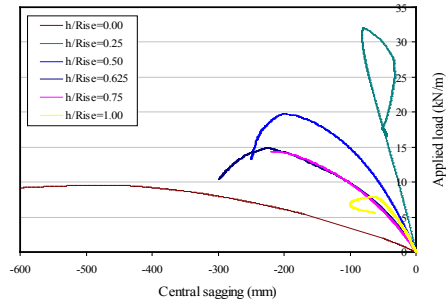


b Load central sagging behaviour under full unsymmetrical load

Figure 5 Behaviour of restrained Arches B with different h/rise ratios and with rise/span ratio=0.20



a Load central sagging behaviour under full load



b Load central sagging behaviour under full unsymmetrical load

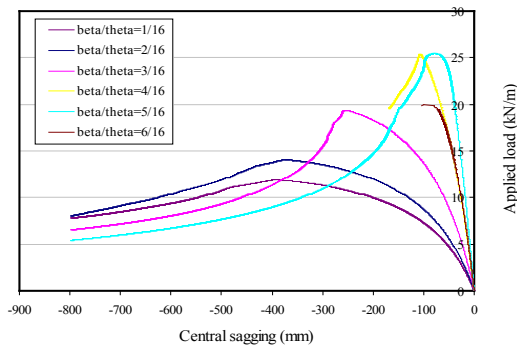


c Deformation under full load (h/rise = 0.625)

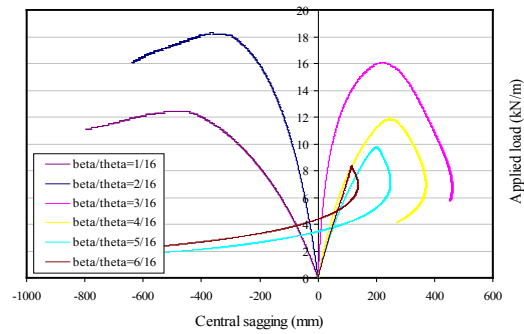


d Deformation under full unsymmetrical load (h/rise = 0.625)

Figure 6 Behaviour of restrained Arches C with different h/rise ratios and with rise/span ratio= 0.20

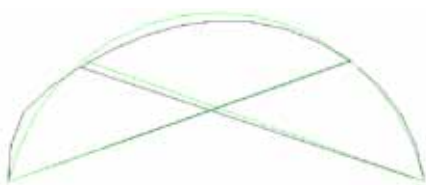


a Load central sagging behaviour under full load



b Load central sagging behaviour under full unsymmetrical load

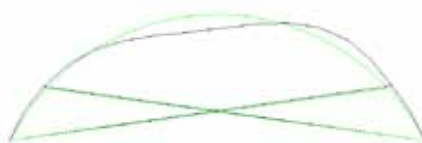
Figure 7 Behaviour of restrained Arches D with different beta/theta ratios and with rise/span ratio = 0.20



a Deformation under full load



b Deformation under full load (rise/span = 0.20, beta/theta = 5/16)



c Deformation under full load (rise/span = 0.30)

Figure 8 Deformation of restrained Arches D with different beta/theta and rise/span ratios

rical load. In addition to this considerable growth in strength, it is also evident that with more tie members providing more distributed restraint to the arch, there is now a wider range of locations where the tie connection points could be positioned while still benefiting from a significant strength improvement due to the non-sway buckling mode which will cause an increase in the ultimate load. This feature provides commended flexibility in the architectural design of the arch structure.

The deformed shape of the arch shown in Fig. 6 casts further light on the effect of the restraining system used. While the sides way movement is still dominant, one can see that the outward movement on the right side has been much reduced by the additional tie members, while most of the deformation took place on the left side in the form of inward deflection, which cannot be resisted by ties.

Arch D

Following on from Arch B, Arch D has two tie members directly connected to points near the arch center with the support nodes. The study is extended to allow the tie members to connect two different points on the arch chord. The variable used to define the location of the connection points is the ratio between angles beta and theta, Fig. 7. The ratio beta/theta ranges between 1/16 and 6/16, and the resulting behaviour for an arch with rise/span = 0.20 under both full load and unsymmetrical load is shown in Fig. 7. Under full load and with beta/theta increasing from 1/16, 2/16 to 6/16, the strength is found to be higher than the corresponding values of Arch A by 60.2%, 88.4%, 159.8%, 241.8%, 243.2% and 169.2%, respectively. Note that as the restrained points approach the quarter points of the arch, (where the highest sway movement takes place), the strength improvement increases. Similar findings are obtained under asymmetrical loads. Compared with Arch B, Arch D with its direct connection between the restrained points and the supports proves to be much more efficient. Arch D with beta/theta = 5/16, which has the highest strength, is stronger than Arch B with h/rise = 0.25 (the most efficient case) by 114.3%. This finding is another clear evidence of the importance of the direct restraint as that created in Arch D.

The deformation patterns shown in Fig. 8 depict another effect of the restraining system used in Arch D. Instead of the overall buckling mode experienced in earlier systems, the direct restraint in Arch D forced higher-order buckling modes. Notice also with a small b/q ratio, buckling is seen in the outer parts of the arch chord and not in the middle part. As the ratio b/q increases, the middle part also experiences buckling which becomes progressively clearer. It is now recommended to further extend this study to test arches re-

strained with more than one direct restraint on each side as in Arch E.

Arch E

Arch E has a restraining system similar to Arch D in terms of the direct connection between the restrained points on the arch chord and the opposite support nodes. In addition, Arch E has three, not one direct tie members on each side. This restraining system, while possibly viewed as restricting the usability of the space under the arch, is intended to provide efficient direct restraining against sway movement and buckling, and hence produce a large improvement in strength. The behaviour of Arches D with rise/span ratio between 0.10, 0.20, ...0.50 is depicted in Fig. 8. Compared with the unrestrained Arch A, the strength improvement under full load is 202.0%, 334.2%, 248.1%, 26.6% and 196.2%, respectively. Compared with Arch D, in the case with rise/span = 0.20 and beta/theta = 5/16 (the strongest case), the strength of Arch E is higher by 24.3%. It is also interesting to see that the deformation pattern of Arch E is different from all others. In this case, the resistance to sway movement is so substantial that the arch is forced to deform according to the more symmetric form depicted in Fig. 9.

Arch F

The final restraining system covered in this study is intermediate between those used in Arches D and E. In this case, two tie members are used to provide a direct restraint to points on the arch chord, 3/16L away from the centre in addition to two tie members providing another connection between the arch centre and both supports. As expected, the efficiency of this system is intermediate between Arches D and E. The strength improvement associated with arches with rise/span ratios ranging between 0.10 and 0.50 and compared with the unrestrained arches are 114.3%, 80.3%, 43.3%, 27.5% and 29.9%. The deformed patterns depicted in Fig.10 show further evidence of the efficiency of this restraining system in preventing the sway movement of the arch under full load and forcing a quasi symmetrical distribution of deformation.

Discussion

The behaviour of the unrestrained arch is evidently dominated by the liability to experience an overall buckling mode involving an anti-symmetric sway movement of the arch. Even under full load, this mode of failure is most likely to develop provided that the symmetry of the arch, whether caused by geometrical or loading effects, is incomplete. Under asymmetrical

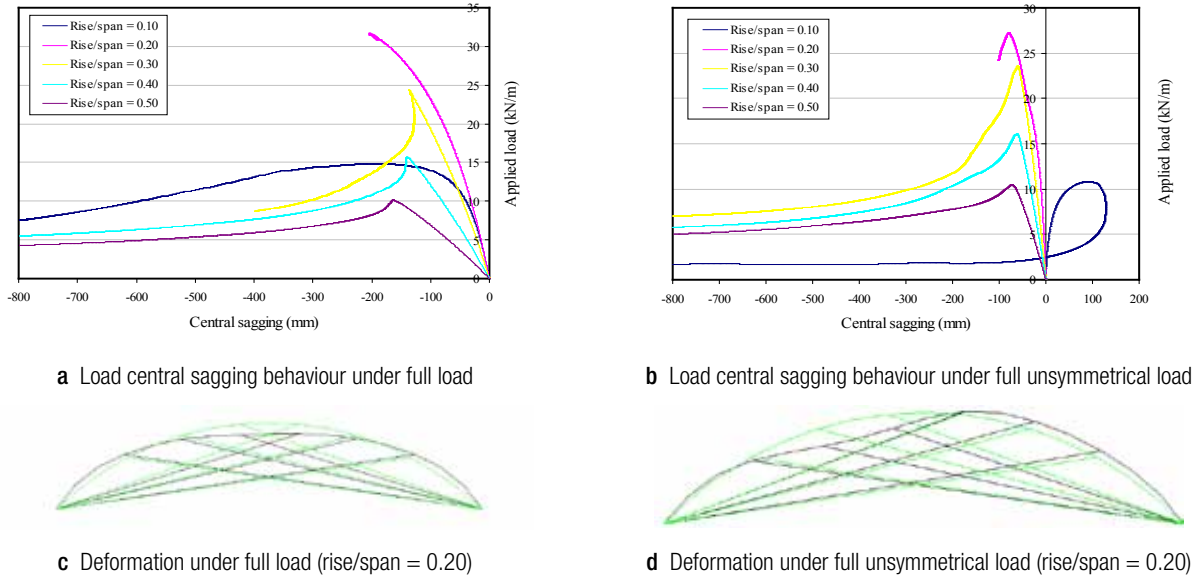


Figure 9 Behaviour of restrained Arches E with different rise/span ratio

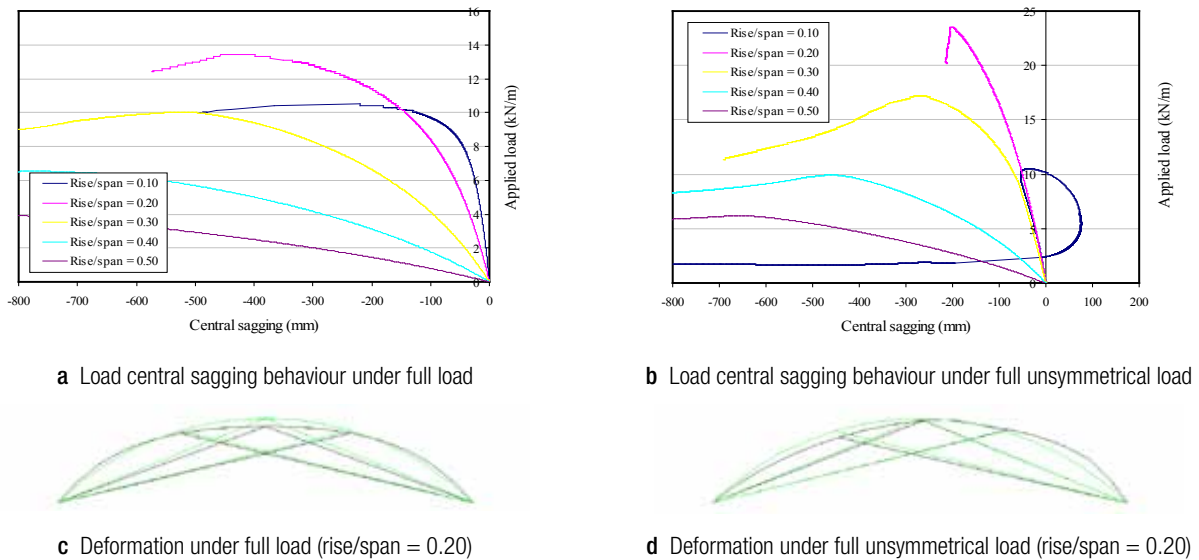


Figure 10 Behaviour of restrained Arches F with different rise/span ratios

load, the buckling failure mode becomes more pronounced and its effect can be seen from the outset. For this reason, implementing a restraining system that resists the sway movement of the arch is likely to lead to notable improvements in behaviour by increasing the buckling load or in other words reducing the effective buckling length and hence delaying failure.

The present study has found evidence that providing more restraint to sway movement through preventing the displacement of more points on the arch chord meant higher strength. Arch E with three points on each side of the arch chord restrained against lateral outward displacement has the best performance with strength increases in the order of 200–350% over the unrestrained arch. Reducing the number of restrained

points on the arch chord to one per side, as in arch D, remains an effective solution, but not as efficient as with Arch E. The strength increase in the former case over the unrestrained arch is between 60% and 240% depending on the location of the restrained point. The relative efficiency of Arch E in resisting the overall sway buckling mode is evident in the eventual mode of failure, which involves a quasi symmetrical form of vertical deformation not seen in any of the other less restrained, arches.

The efficiency of the restraint itself is another important factor. The most efficient solution, as would be expected, is to provide a restraint through a direct connection between a point on the arch chord and a support node. Examples of this direct restraint are in

the restraining systems of Arches D and E, with the resulting high strength increases reported above. The less efficient restraint used in Arches B and C involves the use of two tie members to create a connection between a point on the arch chord and a support node. When these tie members are not aligned, the connection loses stiffness and becomes less effective. The study shows as an example, that as the angle between the tie members increases, the efficiency of the restraining system reduces, leading to overall smaller strength improvements. Apart from making the connection to the support node straight or direct, another solution could be to restrain more points on the arch chord. In this case, providing restraint to more points, although not highly efficient, results in reasonable strength improvements. For example, the restraining system in Arch C, which restrains three points on each side of the arch chord, provides strength increases in the order of 160–270% compared with 10–60% achieved with Arch B in which only one point on each side of the arch is restrained.

Conclusion

The work presented herein is a numerical parametric study that involves loading to failure, a large number of restrained and unrestrained arches while monitoring their behaviour. All arches have been non-linearly analysed; the analyses consider both geometric and material non-linearities. The behaviour of the unrestrained arch is evidently dominated by the liability to experience an overall buckling mode involving a quasi anti-symmetric sway movement of the arch.

Furthermore, the following conclusions could be drawn from the work conducted and presented herein:

1. Implementing a restraining system that resists the sway movement of the arch is likely to lead to notable improvements in behaviour by increasing the buckling load and hence reducing the effective buckling length which delays failure.
2. Providing more restraint to sway movement through preventing the displacement of more points on the arch chord meant higher strength.
3. Reducing the number of restrained points on the arch chord to one per side, as in arch D, remains an effective solution, but not as efficient as with Arch E.
4. The strength increase in the former case over the unrestrained arch is between 60% and 240% depending on the location of the restrained points.
5. The study shows as an example, that as the angle between the tie members increases, the efficiency of the restraining system reduces, leading to overall smaller strength improvements.

Acknowledgements

This material is based on work supported by the Bibliotheca Alexandrina, Center for Special Studies and Programs under grant no. (040060933).

References

1. Alexander Chajes, "Structural Analysis", Prentice-Hall Inc., second edition, 1990.
2. Arbabi F., "Structural Analysis and Behavior", Mc Graw Hill Inc., 1991.
3. Bedenik B. and Colin Besant, "Analysis of Engineering Structures", Horwood Publishing Limited, 1999.
4. British Standards Institution, "BS5950 - Structural Use of Steelwork in Building", Part 1: Code of Practice for Design – Rolled and Welded Sections, BSI, 2000.
5. Buchholdt H. A., "An Introduction to Cable Roof Structures", Thomas Telford, second edition, 1999.
6. Frank Durka, "Structural Mechanics", Longman, fifth edition, 1996.
7. Hibbitt, Karlsson and Sorensen, Inc, "Abaqus – Standard Users Manual", Detroit, USA, 2001.
8. John F. Fleming, "Analysis of Structural Systems", Prentice-Hall Inc., 1997.
9. Mario Como and Antonio Grimaldi, "Theory of Stability and Continuous Elastic Structures", CRC Press Inc., 1995.
10. Megson T. H. G., "Structural and stress Analysis", Elsevier, second edition, 2005.
11. Ray Hulse and Jack Cain, "Structural Mechanics", Antony Rowe Ltd, second edition, 2000.
12. Riks E., "The Application of Newton's Method to the Problem of Elastic Stability", *Journal of Applied Mechanics*, 39, 1972, 1060





Information Technology



Amir Farouk Zeid

Assistant Professor in the American University in Cairo. His professional career started since 1989 until today. He was born on 8th of May 1969. He finished his Bachelor of Science at the American University in Cairo in 1989 in Computer Sciences, with a distinct GPA grade of 3.8 (Scale 4). In 1994, he started working on his PhD at the University of Carleton, Canada, with a thesis entitled 'AgenTINA; An Agent-based Architecture for TINA-compliant Systems'.

He was awarded different prizes in both Canada and Egypt. In addition he participated in organizing workshops and conferences and chaired a couple of them. In 2004, he won the BA/CSSP Research Grant which enabled him to accomplish his research entitled '*Towards A Metrics Suite for Agent-Based Programming*'. It is worth mentioning that his publications outnumbered 30 papers and are distributed around the globe.

Towards Engineering Web-Services and Agent Oriented Applications

Amir Farouk Zeid

Computer Sciences, American University in Cairo, Cairo, Egypt

ABSTRACT

Service Oriented Computing (SOC) is the new emerging paradigm for distributed computing and e-business processing that is changing the way software applications are designed, architected, delivered and consumed. Services are autonomous platform-independent computational elements that can be described, published, discovered, orchestrated and programmed using standard protocols for the purpose of building agile networks of collaborating business applications distributed within and across organizational boundaries. Engineering and modeling service-oriented architectures need extensions to existing modeling techniques and methodologies. In this paper, we propose a UML profile for service-oriented architectures. We consider this a step towards properly engineering web-services.

Keywords: *Engineering Web-services, UML profiles.*

1. Introduction

Service-oriented architectures can be considered the natural evolution of component based development. In recent years, web-services have become a field of interest for both academia and industry. For an industry to gain momentum and evolve as a scientific discipline, software engineering best practices have to be applied. Very few research activities were devoted to software engineering for service-oriented architectures. In this research we illustrate our efforts in developing a UML profile for service-oriented architectures.

2. Background

OMG has published the UML for Object Oriented Analysis and Design. OMG has published extension mechanisms for UML so that any organization can define new notations that will serve in a new domain of interest; this extension mechanism is called the UML Profiles[1].

2.1 Unified Modeling Language (UML)

The Unified Modeling Language (UML) is a language for specifying, visualizing, constructing, and documenting the artifacts of software systems, as well as for business modeling and other non-software systems. The UML represents a collection of engineering practices that have proven successful in the modeling of large and complex systems. The UML is a language, not just a notation for drawing diagrams. The UML is not a process; it provides a modeling language without enforcing a lifecycle. The UML can be extended to model new elements using the concepts of stereotyping and tagged values.

Stereotypes

Stereotypes are mechanisms for introducing new types of modeling elements. Stereotypes are strings enclosed in (<< >>), preceding the name of an element. They may have an associated graphic icon or graphic marker. The new modeling elements that can be introduced using stereotypes must be subclasses of existing modeling elements.

Service Oriented Architecture (SOA) is an architecture composed of loosely coupled discrete functions. Each function can be considered an independent service that can be used in many scenarios. The SOA is not a new architecture but it has been the talk of the hour because of the emergence of the web services technology. After all the attention the SOA has taken, it became a clear demand that UML profiles are required to model SOA. In this paper we propose a UML profile to model SOA.

3. SOA Profiles

Recently the web service architecture working groups have published a new web service architecture document [2] where they introduced four models for modeling service oriented architectures. The four models are: the service oriented model, the message oriented model, the resource oriented model and the policy model. Based on these models we have introduced five UML profiles for modeling service oriented architecture in UML. Four of these models are mapping for these architectural models:

Service Profile, the Resource Profile, the Message Profile, and the Service Policy profile. We propose an additional profile for agents dealing with services. An agent may be a provider or a user of the service. The rest

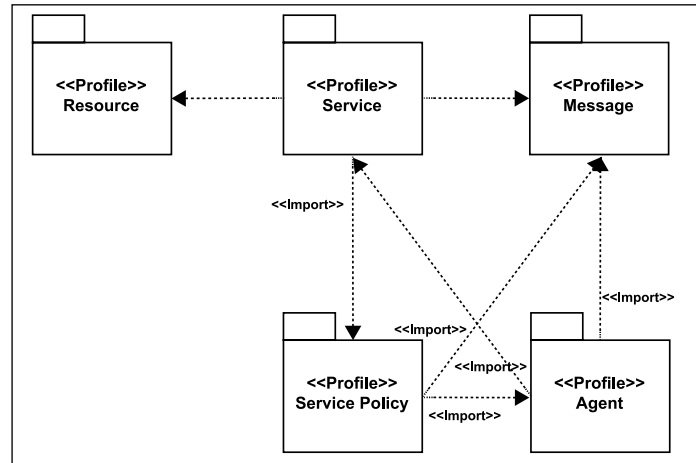


Figure 1 SOA Profiles

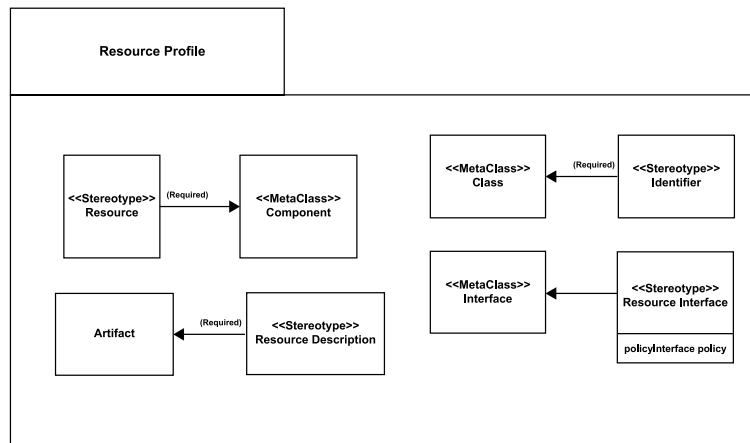


Figure 2 Resource Profile

of this section contains a description of our proposed profiles.

3.1 UML Profiles

Our SOA profiles consist of five profiles:

- The resource profile which is intended for modeling any resource by identifying a main key of the resource (identifier) (i.e. URI or QName).
- The service profile describes how to model a service with its internal components and describes how to compose and model the discovery service.
- The message profile describes how each message exchanged by the service should be modeled.
- The service policy profile describes the modeling of the policies that should be applied on the service usage.
- The agent profile shows how to introduce the agents dealing with the service into the model.

Table 1 Notations

| Resource Profile Stereotype | Notation |
|-----------------------------|---|
| Resource | <<resource>> |
| Identifier | <<identifier>> |
| Resource Interface | <<resourceInterface>> |
| Resource Description |  |

3.2 Resource Profile Description

The resource profile is mainly composed of resource component. This component contains a key class denoting the identifier of this resource which can be, for instance, URI or QName. The resource component exposes its functionality through a resource interface and describes its functionality through a machine readable resource description artefact. Fig. 2 illustrates the resource profile and Table 1 contains a summary of the used notations.

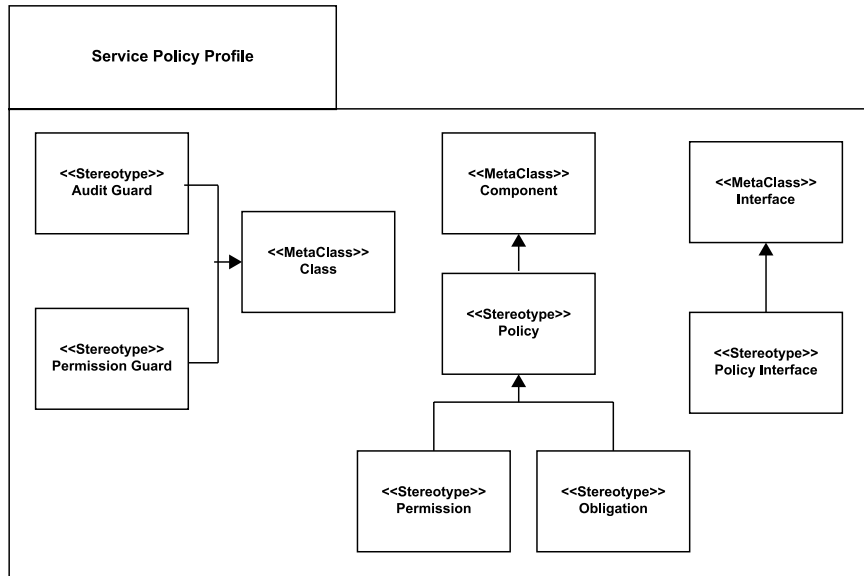


Figure 3 Service Policy Profile

Table 2 Notations

| Stereotype | Notation |
|------------------|---------------------|
| Audit Guard | <<auditGuard>> |
| Permission Guard | <<permissionGuard>> |
| Policy | <<policy>> |
| Permission | <<permission>> |
| Obligation | <<obligation>> |
| Policy Interface | <<policyInterface>> |

3.3 Service Policy Profile Description

The service policy profile is a Meta Model for modeling the policies to be used in the domain of the service oriented architectures. The profile is divided into two main areas: the permission, which represents a permission to do certain action or an obligation, which represents an obligation for a certain entity to do certain action. The policy component has a controller that controls the execution of the policy which is the permission guard for the permission and the audit guard for the obligations. Fig. 3 illustrates the service policy profile and Table 2 contains a summary of the used notations.

3.4 Message Profile Description

The Message Profile contains two components: the Message and the Message Transport. The Message Component contains the Message Contents, which are represented in the envelope that contains two main

classes: the body and the header. The Message Component also contains the Message controller which is a controller class. Finally, the Message Component is exposed through a message interface. The Message Transport Component should contain the logic responsible for transporting the message using the network

Layer. The Message Transport contains the address which is used for both the sender and the receiver and is dependent on the Message Transport Technology. The Message Transport component exposes its functionality through a message transport interface.

The Message Policy is controlled by a Service Policy Component which is represented as the service policy interface property in the Message Controller. Fig. 4 illustrates the Message Profile and Table 3 contains a summary of the used notations.

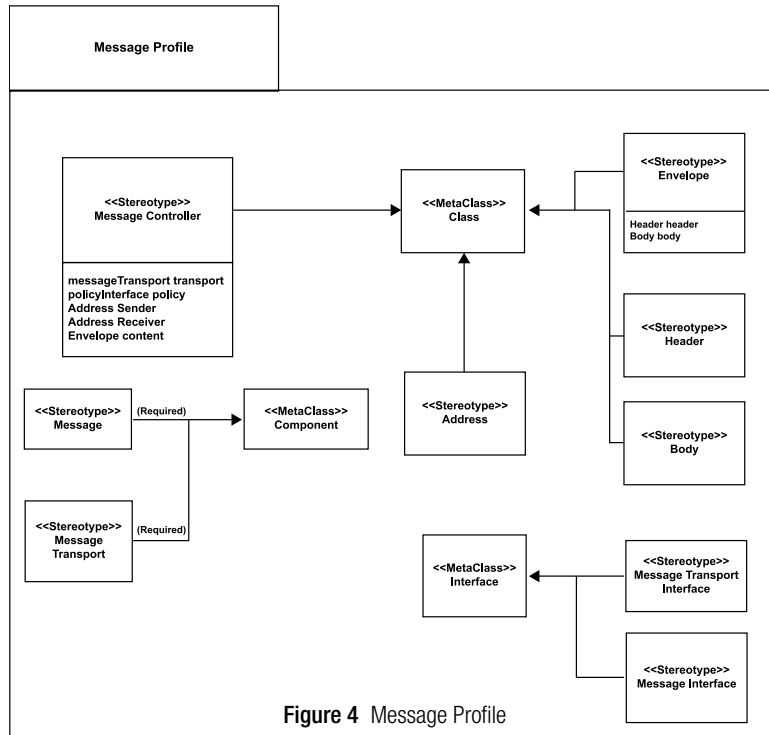


Figure 4 Message Profile

Table 3 Notation

| Message Profile Stereotype | Notation |
|-----------------------------|-------------------------------|
| Message Transport | <<messageTransport>> |
| Message Interface | <<messageInterface>> |
| Message Transport Interface | <<messageTransportInterface>> |
| Message Controller | <<messageController>> |
| Message | <<message>> |
| Address | <<address>> |
| Envelop | <<envelop>> |
| Body | <<body>> |
| Header | <<header>> |

3.5 Service Profile Description

The Service Profile represents the main profile for modeling a service. It explains modeling of the service in terms of components. The Service Profile contains two component types: the service and the service task. The Service Component contains a main controller class which is the Service Manager.

The Service Component exposes its functionality through the service interface which contains all the exposed functionality of the service. The Service Component ports a machine readable description of its functionality through the service description which is a kind of resource description. The task of the service is represented through the service task component which represents the actions of the service. The service tasks expose their functionality through the Service Task In-

terface. The Service Manager orchestrates the service task interfaces to compose the service functionality.

Finally, the Discovery Service is a kind of service which exposes its functionality through the Discovery Service Interface. It accomplishes two main tasks: publishing and searching.

The Discovery Service contains a main object, the Service Template. The Service Template contains some semantic values of the service to be used in indexing of the services in the publishing operation to be matched with those supplied in search operation.

Fig. 5 illustrates the service profile and Table 4 contains a summary of the used notations.

3.6 Agent Profile Description

The Agent Profile represents modelling of the actors of the service. The Agent Profile contains a main Agent

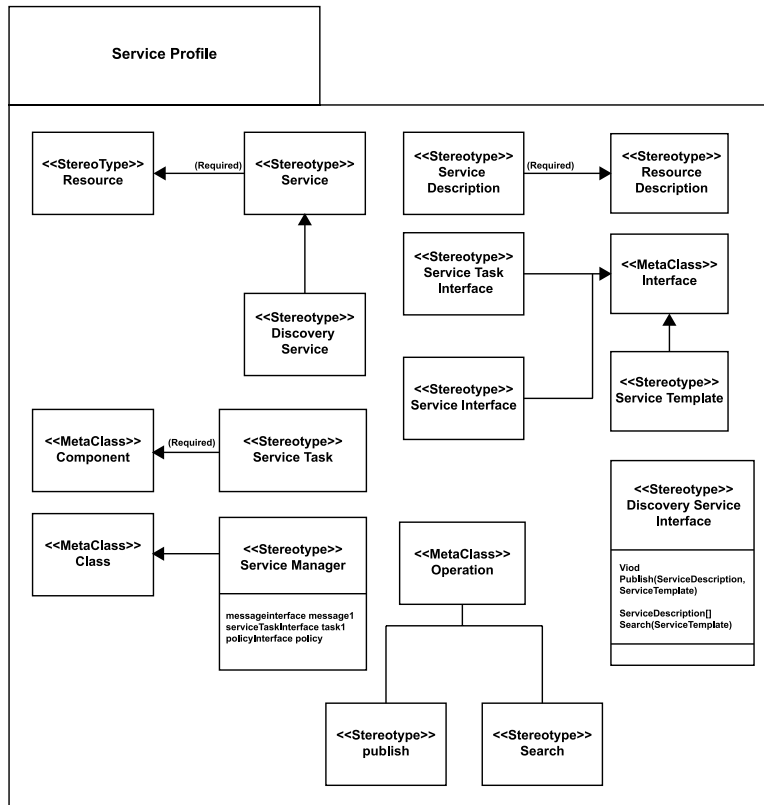


Figure 5 Service profile

Table 4 Notations

| Stereotype | Notation |
|-----------------------------|---|
| Service | <<service>> |
| Service Task | <<serviceTask>> |
| Service Manager | <<serviceManager>> |
| Service Intervace | <<serviceIntervace>> |
| Service Description |  |
| Service Task Interface | <<serviceTaskInterface>> |
| Discovery Service | <<discoveryService>> |
| Discovery Service Interface | <<discoveryServiceInterface>> |
| Service Template | <<serviceTemplate>> |
| Publish | <<publish>> |
| Search | <<search>> |

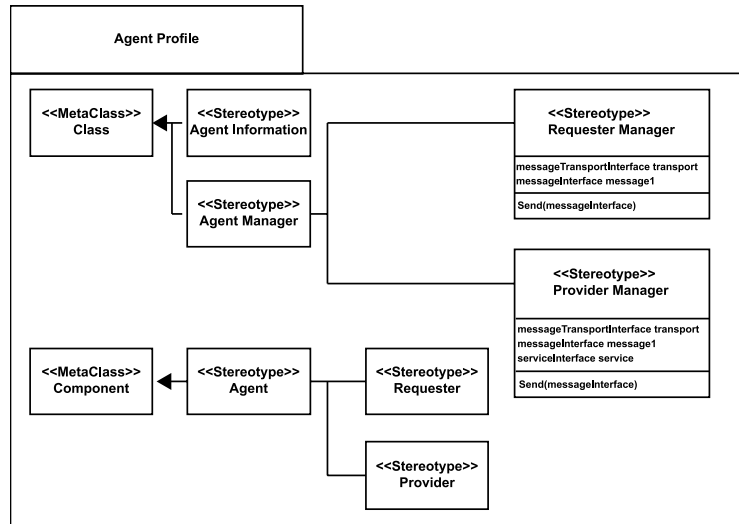


Figure 6 Agent profile

Table 5 Notations

| Stereotype | Notation |
|-------------------|----------------------|
| Agent | <<agent>> |
| Agent Information | <<agentInformation>> |
| Agent Manager | <<agentManager>> |
| Requester | <<requester>> |
| Provider | <<provider>> |
| Request Manager | <<requestManager>> |
| Provider Manager | <<providerManager>> |

component that can be either a Provider or a Requester. The Agent is characterized by the presence of a value object: Agent Information which carries all the information about this agent (address/phone/zip).

The Agent is controlled through the Agent Manager class that can be either a Requester Manager or a Provider Manager. The Requester Manager sends the messages to the service using the Message Transport Interface. The Provider Manager receives the messages using the Message Transport Interface, passes them and then sends them to the Service Interface of the service it is hosting. Fig. 6 illustrates The Agent Profile and Table 5 contain a summary of the used notations.

4. SOA Sample Model

Let us consider a case of a private marketplace that contains buyers and suppliers. The buyer’s needs are to inquire for items provided by suppliers. If the buyer’s inquiry returned true, the buyer will issue an order for the supplier with the given quantity of the item.

What is simply needed is to integrate the systems, such that we open the inventory system as a service that can be accessed by the trusted buyers only, and in

case an inventory system, does not exist we could store the items in a simple database and create a component that would access the database and convert the data to a service.

The buyers need to have a small system that would interact with their supplier functions. From the past requirement and the simple analysis performed we found that we need a Service Oriented Architecture that would link buyers with their suppliers.

We will mainly focus on the first function; (querying for the service for item availability).

Main Entities (Fig. 7):

According to our proposed profiles, the following entities will be needed:

1. Agents for the Buyer as a Requester and the Supplier as a Provider that will represent the actors of that system.
2. Supplier Service Components which represent the service of the Provider and Supplier Inventory Components that represent the Inventory component.
3. Messages for the Send and Response of the Service method.
4. Message Transport component for transporting the messages with an agreed protocol.

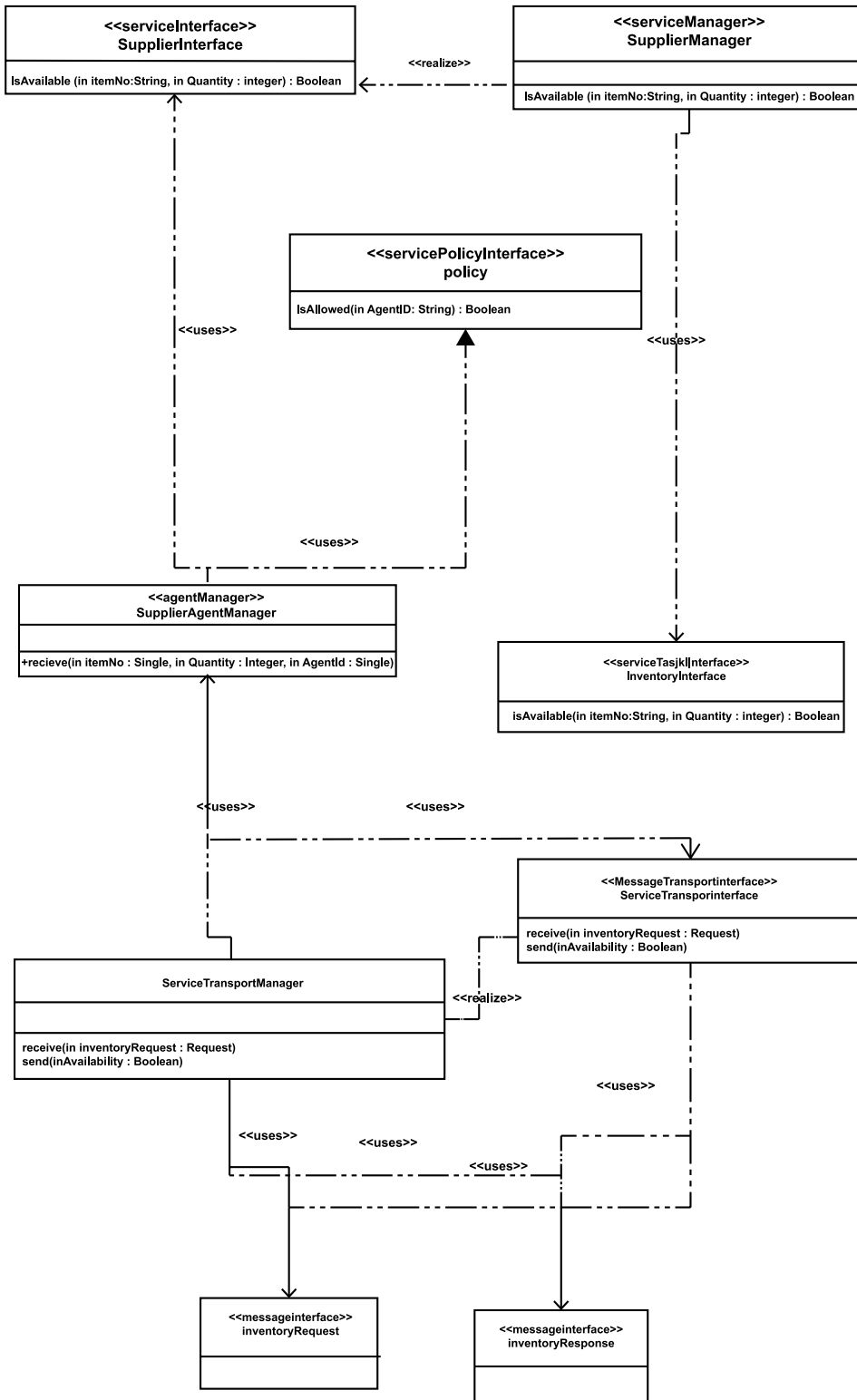


Figure 7 Sample Class Diagram

Fig. 8 illustrates a sample sequence diagram that describes the dynamic behavior of the proposed example. The first component (BuyerTransport Manager) sends a request message to the ServiceTransport Manager which is listening to any incoming message on a de-

defined identifier. The arrival of a message fires an event for a request message. This message is decoded using the parameters of the service function and sent to the Supplier Agent Manager. The Supplier Agent Manager asks the policy for the permission of sender agent to

call this operation. If the permission is granted the Supplier Agent Manager invokes the operation from the Supplier Interface (service interface) which in turn invokes the operation in the Inventory Interface (service task interface) and waits for the return till it reaches back to the Supplier Agent Manager.

The Supplier Agent Manager then calls its method to send the availability to the Service Transport Manager which then sends the response back to the buyer.

5. Conclusion

The technology of Web Services and SOA are migrating from research labs to software engineering centers. As the rate of this migration increases, it will become increasingly important to develop and make use of techniques for analyzing, specifying, designing, and verifying Web Services and SOA. Without such techniques, sac will not realize the potential it has. The UML Profiles presented in this paper are based on the newly presented web services architecture models. We have mapped these architectures into UML profiles. In this paper, we presented the notations and the stereotypes.

These profiles need further work especially in the area of the service choreography and web service

References

1. Object Management Group, UML 2.0 SuperStructure Final Adopted Specification. www.omg.org/cgi-bin/doc.ptc/2003-08-02, Accessed on 30 May , 2004.
2. Web Service Architecture. www.w3.org/TR/2004/NOTE-ws-arch-20040211/, Accessed on 30 May, 2004.
3. Amir Zeid Research Directions in Engineering Service Oriented Architectures, Proceedings of Second International Workshop on Engineering Web-services, in conjunction with OOPSLA 2004, Vancouver, Canada.

Amir Zeid, Rafik Amir

Faculty of Informatics and Computer Science (The British University in Egypt, The American University in Cairo).

azeid@bue.edu.eg,

rafikamir@hotmail.com

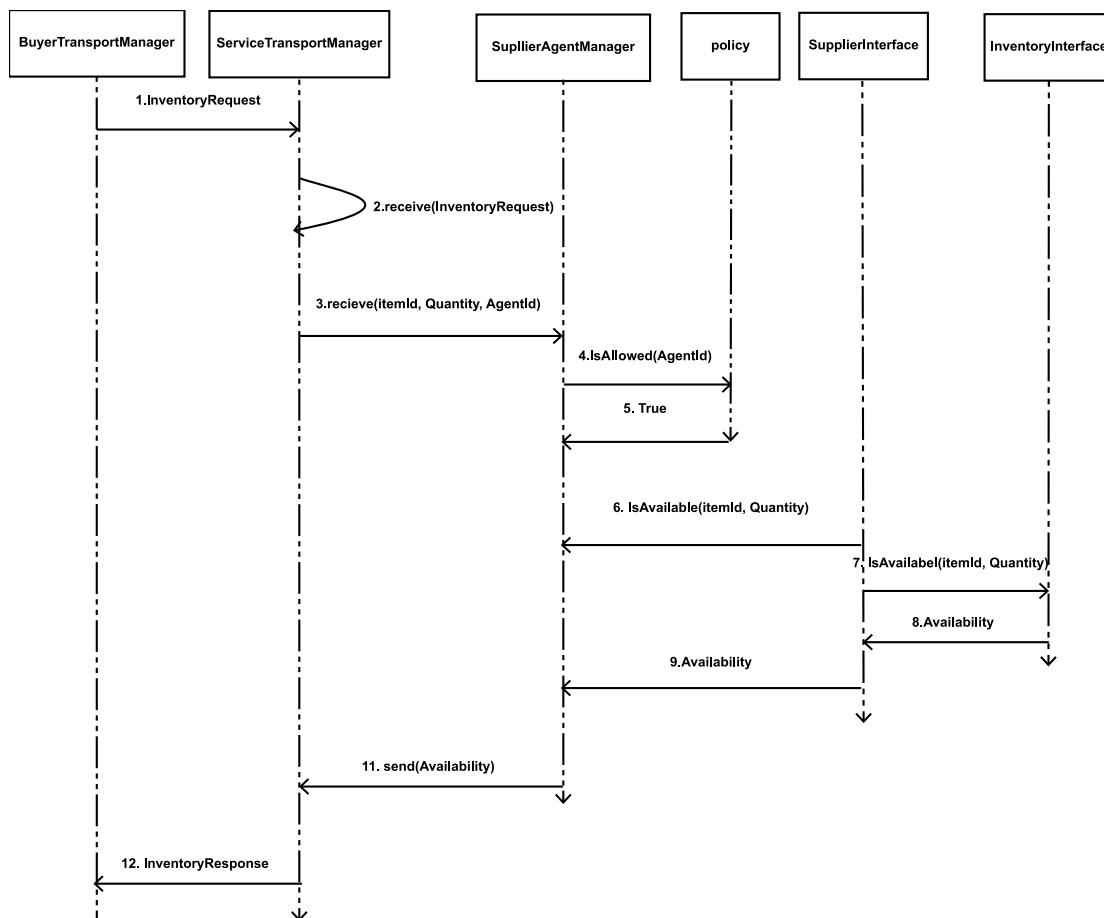


Figure 8 Sample sequence diagram

Using Change Propagation Probabilities to Assess Quality Attributes of Software Architectures 1

ABSTRACT

The study of software architectures is gaining importance due to its role in various aspects of software engineering, such as product line engineering, component based software engineering and other emerging paradigms. With the increasing emphasis on design patterns, the traditional practice of ad-hoc software construction is slowly shifting towards pattern-oriented development. Various architectural attributes like error propagation, change propagation and requirements propagation provide a wealth of information about software architectures. In this paper, we show that Change Propagation Probability (CP) is helpful and effective in assessing the design quality of software architectures. We study two different architectures (one that employs patterns versus one that does not) for the same application. We also analyze and compare the change propagation metric with respect to other coupling-based metrics.

Keywords: *Software Architecture, Architectural Attributes Design Quality, Design Patterns and Change Propagation Probability.*

1. Introduction

The study of software architectures is gaining importance due to its role in various aspects of software engineering, like product line engineering, component-based software engineering and other emerging paradigms. Various architectural attributes like error propagation, change propagation, requirements propagation were proposed to evaluate software architectures [12].

In this paper, we mainly plan to work with the specific architectural attribute Change Propagation (CP). CP reflects the probability of a change to be made in one or more of the components in architecture as a result of introducing a change in one of the components. This work is part of a larger effort to analyze and validate various architectural attributes like Error Propagation [2], Change Propagation [3], Requirements' Propagation [17], Diagonality [12], Product-Line Properties [18], etc. Our main objective is to show the role and use of CP in assessing the design quality (e.g., extensibility, maintainability, reusability etc.) of software architectures. We will illustrate how, in our view, the perspective and insights offered by CP complement the information provided by traditional object-oriented metrics.

The rest of this paper is organized as follows: In section 2, the definition and estimation of change propagation are given. Section 3 introduces the methodology used in the research. In section 4, a couple of sample applications and their results are discussed. In section 5, our change propagation metric is compared with other coupling-based metrics. In sections 6, related work is presented. In section 7, conclusion and future prospects are discussed.

2. Background

2.1 Design Patterns

A design pattern [8] is a solution to a design problem that recurs in a particular context. Since the idea was first communicated, design patterns have been considered an important aspect in the design of software architectures. The practice of ad-hoc software design is slowly shifting towards pattern-oriented development [16].

Designers can try to identify the various aspects of design problems associated with the application, and then they can choose some of the successful design patterns from a pattern repository to solve the problems. There are many advantages for using the various design patterns with respect to software architectures. Some of these advantages include: improving the reusability, extensibility, and maintainability of a software architecture.

2.2 Object-oriented metrics

Object-oriented metrics play a vital role in determining the design quality of software architectures. These reflect various design aspects like complexity, modularity, change proneness etc about the components or about an architecture in general.

In this paper we mainly deal with the Chidamber and Kemerer object oriented metrics [6] like Coupling Between Objects (CBO) [6], Response For a Class (RFC) [6] and Weighted Methods per Class (WMC) [6]. Apart from these, metrics like Message Passing Coupling (MPC) [5] and McCabe Cyclomatic Complexity (MCC) [10] have also been considered.

Coupling Between Objects (CBO) is defined as the number of the components coupled to a component in

an architecture. Response For a Class (RFC) is the sum of all the methods that can be invoked in response to a message to an object of a component or by a method of the component. Weighted Methods per Class (WMC) is the sum of the complexities of all the methods in a component. Message Passing Coupling (MPC) is the sum of the number of method calls made by all the methods in a component. McCabe Cyclomatic Complexity (MCC) is the sum of the number of flows in all the methods.

2.3 Change Propagation Probability

In this section, we introduce the definition of change propagation followed by a few equations to estimate change propagation. Let us consider a software architecture modeled by components and connectors. We are interested in the maintainability of the products instantiated from it. Change propagation probability $CP = [cp_{ij}]$ for an architecture is the conditional probability that a change originating in one component of the architecture requires changes to be made to other components. The estimation of the elements cp_{ij} of the change propagation matrix CP is based on the following definition [3]:

Definition. Given components C_i and C_j of a system S , the change propagation probability from C_i to C_j is denoted by cp_{ij} and defined as the following conditional probability:

$$cp_{ij} = \Pr([C_i] \neq [C_j'] | ([C_i'] \neq [C_j']) \wedge ([S] = [S']))$$

(1) where $[X]$ denotes the functionality of component/system X and S' is the system obtained from S by changing C_i into C_j' (and possibly C_j into C_j' as a consequence).

An architecture can be seen as a collection of components C_i , $i=1, \dots, N$. With every component C_i , we associate the set V_i of the interface elements of the provided functions of C_i . We determine the usage coefficient value π_v^{ij} for every interface element $v \in V_i$ and every other component C_j , $j \neq i$. They take binary values:

- $\pi_v^{ij} = 1$, if the interface element v provided by C_i is required by C_j . This means that any signature change in component C_i associated with interface element v will propagate to component C_j
- $\pi_v^{ij} = 0$, otherwise.

In [3], AbdelMoez *et al* proposed the following for estimating the change propagation probability cp_{ij} , for every pair of components C_i and C_j , $i \neq j$, based on the values of the usage coefficients π_v^{ij} by:

$$cp_{ij} = \frac{1}{|V_i|} \sum_{v \in V_i} \pi_v^{ij} \quad (2)$$

3. Methodology and Rationale

We have designed an experiment that compares architectures using object-oriented metric and change propagation matrices. The goal of the experiment is to assess to what extent the object-oriented metric on one hand and the CP matrices on the other hand are good predictors of architectural quality attributes. To this effect, we consider sample applications, and derive two candidate architectures for each: one that is based on design patterns (hence is presumably of higher quality) and one that is designed ad hoc, without predefined patterns. The following methodology has been applied:

1. Prepare a pair of architectures for the same application. One of the architectures is designed using design patterns while the other has no patterns.
2. Apply the CP metric on both architectures.
3. Apply other object-oriented metric on both architectures.
4. Analyse and compare the results. The architecture that employs software patterns should have better attributes that imply a higher quality in terms of extensibility and maintainability.

Since matrices are hard to compare, we introduce the Change Propagation Coefficient (CPC) that attempts to capture the information of a matrix in a single scalar, although not without some loss of information. CPC is a scalar that reflects the potential of an architecture to insulate its components from changes that can occur in other components. Obviously, the ideal CPC corresponds to a conditional change propagation matrix where only the diagonal cells are 1s and the rest of the cells in the matrix are 0s, i.e. an identity matrix. In such a case, components do not propagate changes to other components. At the other extreme, the worst possible CPC is one for which all cells of the conditional change propagation matrix are 1s. In this case, whenever a change arises in a component, it propagates to all other components. We wish to define the change propagation coefficient in such a way as to reflect, using a value between 0 and 1, how close we are to the ideal matrix and how far we are from the worst possible matrix. We estimate the change propagation coefficient by:

$$CPC = \frac{\sum_{i \neq j} cp_{ij}}{N^2 - N}, \quad (3)$$

where N is the number of components in the architecture. A low CPC value indicates an architecture where changes do not easily propagate between its components.

It is worth noting that we measure the CP and CPC for the architectures with the help of the Software Architecture Change Propagation Tool (SACPT) [1]. Cur-

rently our tool supports Java source code but we plan to extend it to support various other languages like C, C++, etc. Inputs to our tool are obtained with the help of the tool, Understand for Java [15]. SACPT generates the CP matrix of components in the architecture.

4. Sample Applications

We have performed the experiments on the source code of two sample applications using their architectural information. For each application, we experiment with two different architectures, one that employs patterns versus one that does not. Then, we compare the change propagation metric with other coupling-based, object oriented metric before and after applying the design pattern. Finally, we evaluate change propagation coefficient CPC for the entire architecture and compare the numerical indices of the two versions.

4.1. Job Application

Our first example is a simple application where an employer is seeking employment applications for the various jobs available, which are submitted through detailed electronic forms that must be validated. There are two versions; one is implemented as a simple switch case, while the other version is implemented using the Strategy pattern [8]. The Strategy design pattern comes into play when there are different implementations of an algorithm. The subclasses of the abstract class define the algorithm and define the implementations according to their needs. In this example, more flexibility is introduced when applying the pattern. Specifically, if there are new types of job positions to be supported by the software, rather than modifying the switch cases we just add another subclass to the abstract class that fulfils the new criteria.

We restrict the analysis to the components that exist before and after the application of the pattern. Fig. 1 and Fig. 2 show the reverse engineered class diagram and the change propagation probabilities of the example when using switch cases.

Fig. 3 and Fig. 4 show the reverse engineered class diagram and the change propagation probabilities of the example after applying the strategy design pattern. The Change Propagation Coefficient (CPC) for the architectures before and after using the design pattern are 0.18 and 0.11 respectively. Based on our assumption that a lower CPC value implies a better design, the architecture employing strategy design pattern, is better in design quality than the one that does not. Fig. 5 shows the Weighted Methods per Class (WMC) and McCabe Cyclomatic Complexity metric (MCC) for the components before and after applying the pattern.

The JobApplicantForm component has been improved in terms of these metric by employing strategy design pattern. However, much of the complexity has been displaced into the concrete validators and has not been shown in Fig. 5 as we compared components that existed before and after applying the pattern.

4.2. Colleague States

The second example is an application that tracks the states of colleague components. Each colleague will update its state according to its current state and the changes to the states of other colleagues. We have reverse engineered the architecture of the example using Rational Rose tool [13]. Fig. 6 shows the class diagram of the initial design with the colleague components directly coupled to each other. In Fig. 7, the mediator pattern [8] is used to let interactions of the colleagues be more independent with respect to each other and facilitate the addition of new colleagues to the architecture. Generally, the mediator pattern provides a way to encapsulate the various interactions of the other objects, increasing the cohesion of all components by con-



Figure 1 Class diagram of Job Application before applying strategy pattern.

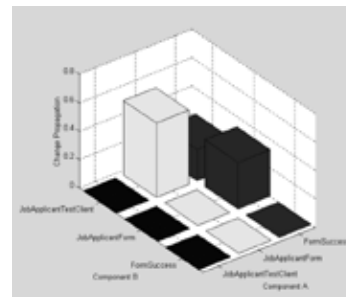


Figure 2 Change propagation of Job Application before applying strategy pattern.



Figure 3 Class diagram of Job Application after applying strategy pattern.

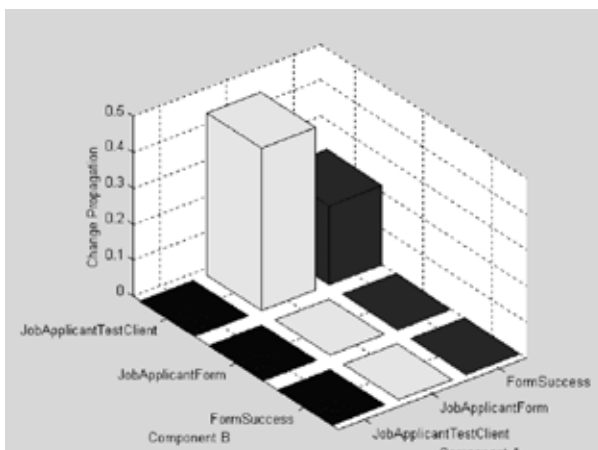


Figure 4 Change propagation of Job Application after applying strategy pattern.

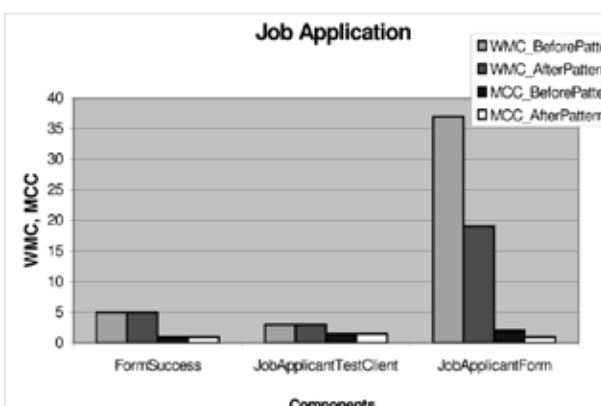


Figure 5 Weighted Methods per Class and McCabe Cyclomatic Complexity for Job Application

centrating the logic of the interactions in the mediator component as opposed to having it spread among the colleagues.

Fig. 8 and Fig. 9 show the change propagation probabilities of the architectures before and after applying the mediator pattern. In Fig. 8, we recognize that the three colleague components are tightly coupled to one another. In Figure 9, adding the mediator pattern decreased coupling between the colleague components. The three colleague components are completely decoupled with respect to one another, because they must interact via the mediator.

The Change Propagation Coefficient (CPC) for the architecture that does not employ any design pattern is 0.11, whereas the CPC value for the one with the mediator design pattern is 0.05. From the CPC values, the architecture employing a design pattern is better in design quality when compared to the same architecture that does not.

One important point here is that the change propagation coefficient (CPC) is calculated only to the components, which are present in both architectures. Actually these are the components which are most important because they are the ones that have the basic functionality of the application. The other components are just present due to the added design patterns and whose function is mainly to glue all the components present in the architecture.

Figure 10 shows the Weighted Methods per Class (WMC) and McCabe Cyclomatic Complexity (MCC) metrics for the architecture before and after using the mediator pattern. All the three colleague components

have been improved in terms of complexity when a mediator design pattern has been employed. Both the metrics WMC and MCC show this improvement as a decrease in value for the components in the architecture that employs a design pattern.

One of the effects of using the mediator design pattern is the centralization of the behavior of the components. Even though the distributed behavior of the components is localized to a few components in the architecture, the architecture that employs a mediator design pattern is more extensible and reusable than the one that does not. When adding new colleagues to the architecture, we need only to change the components

of mediator pattern. All the other colleagues will not be affected as they will not be directly coupled to the new colleague component.

5. Comparison of Change Propagation Metric with Other Metrics

In this section, the change propagation metric is compared with respect to three other coupling-based, object-oriented metrics: Coupling Between Objects (CBO), Response For a Class (RFC) and Message Passing Coupling (MPC) [5]. We restrict the analysis to the components that exist before and after the application

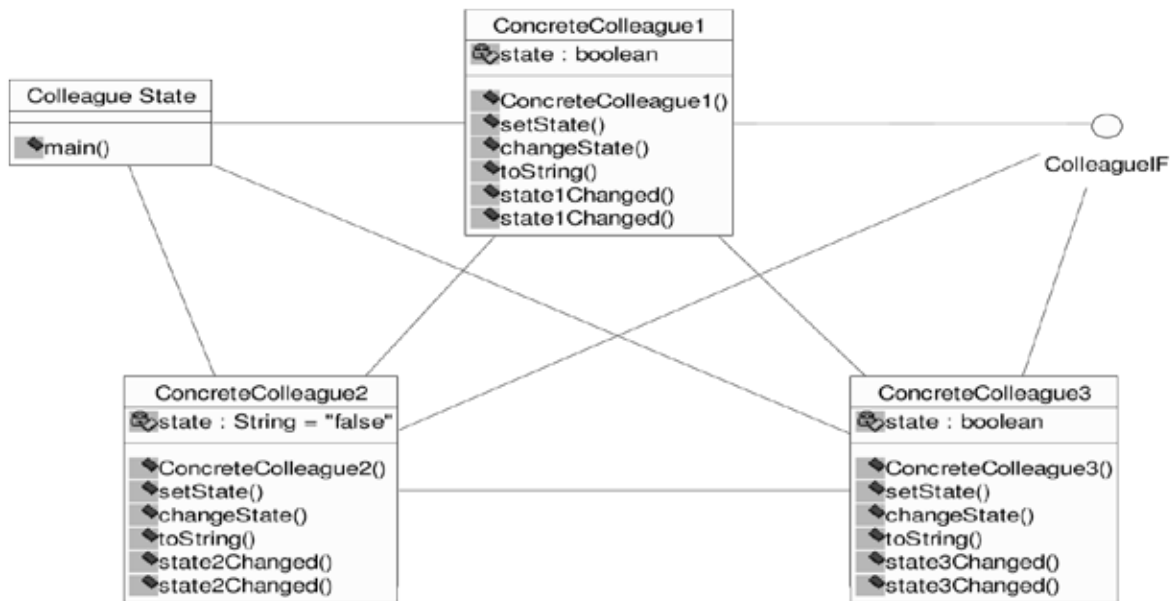


Figure 6 Class diagram of an initial design.

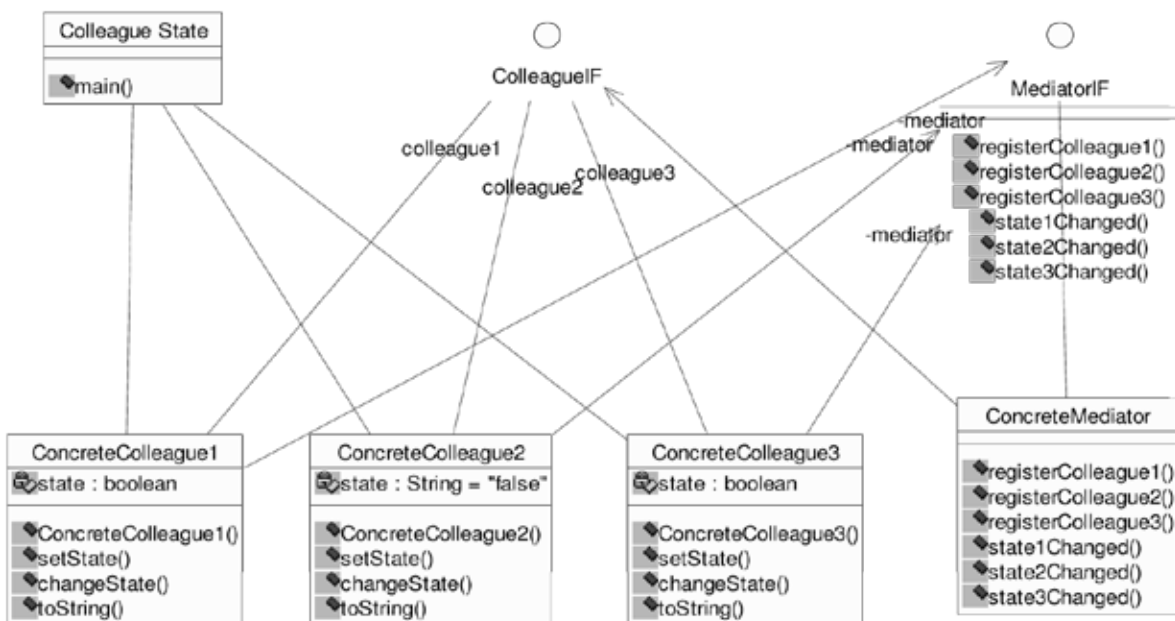


Figure 7 Class diagram of a design that uses mediator design pattern.

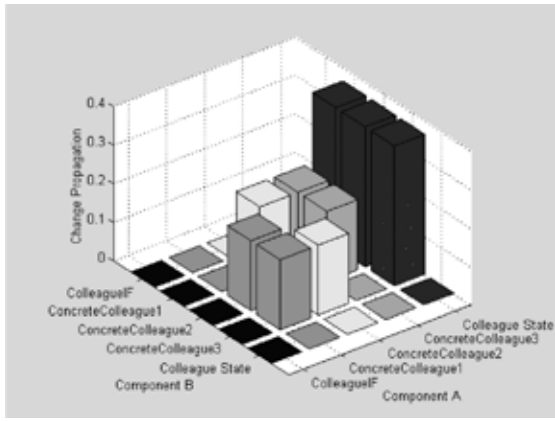


Figure 8 CP for the simple design for Colleague States.

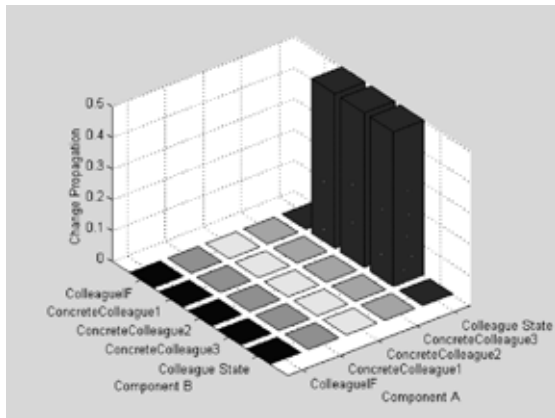


Figure 9: CP for the architecture employing mediator design pattern.

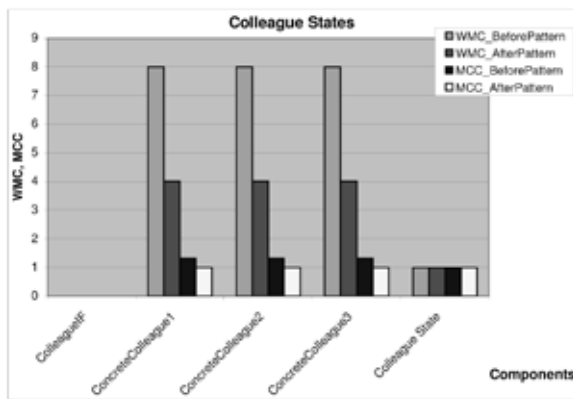


Figure 10: Weighted Methods per Class and McCabe Cyclomatic Complexity for the Colleague States example.

of the pattern. Figure 11 shows the Coupling Between Objects (CBO) for the two sample applications before and after the application of the design pattern. Observing Figure II, one can conclude that CBO metric is not sufficient to compare and state that an architecture is better in design quality when compared with another. Though there are improvements in the CBO values for the three colleague components in the Colleague States application, there is an increase in the CBO value for the JobApplication.Form component in the architec-

ture that implements the strategy pattern for Job Application example.

In Figure 12, the Response For a Class (RFC) metric could not show the difference between the two architectures in the Job Application example. In fact, it showed that the architecture that employs a simple design is better in design quality than the architecture that employs strategy design pattern. On the other hand, for the Colleague States example, the RFC metric confirmed a relative improvement of using design patterns. This shows that RFC metric may not be a good choice to compare between two candidate architectures.

Furthermore, the MPC metric showed no difference in design when applied to both the architectures on each of the two sample applications. Figure 13 shows the values for the MPC metric computed on the Job Application and the Colleague States examples. The MPC metric could not show the difference between the architectures in both cases.

On the other hand, the change propagation probability metric shows these variations and points out that one of the architectures is better than the other. Check the change propagation probability values for the three colleagues' components in the Colleague States example, Figures 8 and 9, and for the JobApplicationForm component in the Job Application example, Figures 2 and 4. The change propagation probability CP metric can show a different perspective and complements the usage of other object-oriented metrics: CBO, MPC and RFC in both examples.

6. Related Work

The work done by authors in [14], [11], [4] and [9] was more towards establishing the known benefits of design patterns like reusability, flexibility, extensibility etc. Since, there has been less insight and less work done in the area of design patterns so far, any amount of research done in this field is really helpful to a novice programmer. The various concepts related to design patterns are best understandable with the help of examples with source code as in [14], [4] and [9]. Although the examples considered in [14] were UML class diagrams, they were live examples.

Authors in [14] and [9] have done similar work when compared to ours. In [14], the authors have shown that the architecture employing a design pattern is more flexible than a simple design. However, our concern in this paper is to show the use of change propagation metric in the assessment of the design quality of software architectures.

In [9], the authors talk about the reduction of change proneness among the various components of the source code that employ design patterns but were not able to show that the architecture is less coupled. In

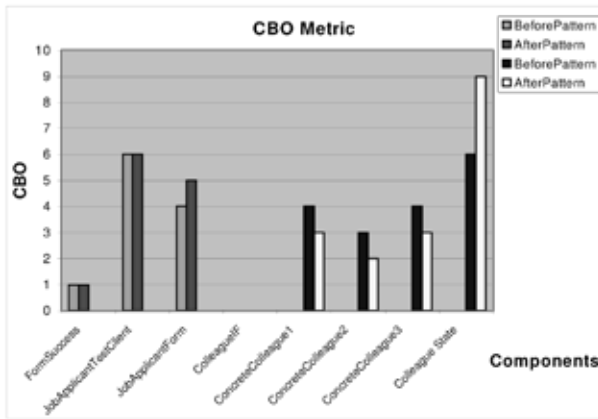


Figure 11 CBO for the sample applications of Job Application and Colleague States.

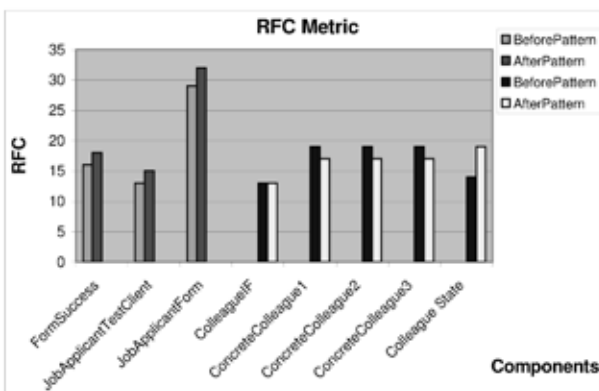


Figure 12 RFC for the Colleague States and Job Application examples.

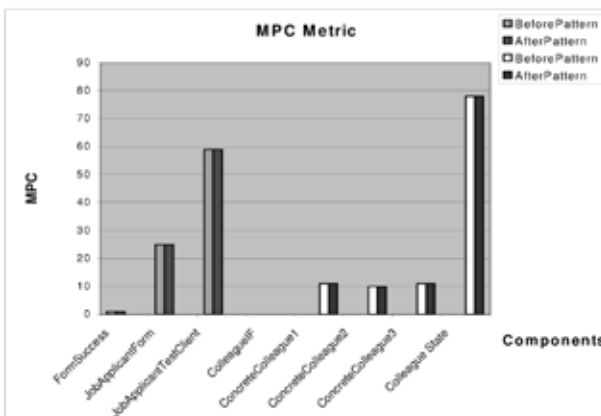


Figure 13 MPC for the Job Application and Colleague States examples.

general when the components of architecture are said to be less likely to change, then it is implied that they are less coupled which is what we have shown in this paper. We believe that only two object-oriented metrics -WMC (Weighted Methods per Class) and RFC (Response For a Class) –out of the six Chidamber and Kemerer set of object-oriented metrics support the fact that the source code that employs a design pattern is better in design quality. In addition, the MPC metric, when applied to our examples, did not show any mea-

sured improvement. All these results show that there is a need of a metric that can state the difference between two architectures in terms of criteria of a better design.

7. Conclusions and Prospects

In this paper, we have shown the applicability of the change propagation probability CP in assessing the design quality of software architectures. CP proved to give a different perspective than the one provided by the classical object-oriented metrics like the CBO, RFC and MPC. We have shown that these metrics (CBO, RFC and MPC) are not sufficient to state that an architecture is measurably better in design quality when compared to another architecture. We used the software architecture change propagation tool (SACPT) that analyzes Java source code to obtain the change propagation probability for an architecture.

This study is part of a larger project to analyze and validate various architectural attributes like Error Propagation (likelihood that an error in one of the components propagates to other components), and Requirements Propagation (likelihood that a change in the requirements in one of the components needs a change in the requirements in the other components), Diagonality etc. Significant work has been done on the architectural attribute Error Propagation while work is continuing on the Requirements Propagation.

Our future prospects include studying larger case studies in order to validate the applicability of change propagation probability to assess the design quality of the software architecture. Also, we need to automate the steps of the analysis methodology to facilitate applying it to more complex case studies.

References

- AbdelMoez W, Shereshevsky M, Gunnalan R, Yu Bo, Bogazzi S, Korkrnaz M, Mili A and Ammar H H, "Software Architectures Change Propagation Tool (SACPT)," Proc. Of the 20th international conference on Software Maintenance, Chicago, September 11-17, 2004.
- Abdelmoez W., D.M. Nassar, M. Shereshevsky, N. Gradetsky, R. Gunnalan, Mili. A and H.H. Ammar, "Error Propagation in Software Architecture," IEEE proceedings of the 10th International Symposium on Software Metrics, Chicago, September 14-16, 2004.
- AbdelMoez W., M. Shereshevsky, R. Gunnalan, H.H. Ammar, Bo Yu, S. Bogazzi, M. Korkrnaz, Mili A, "Quantifying Software Architectures: An Analysis of Change Propagation Probabilities", ACS/IEEE International Conference on Computer Systems and Applications (AICCSA 05), Cairo, Egypt, January 3-6, 2005.

7. Bieman J M, Straw G, Wang H, Munger P W and Alexander R T, "Design Patterns and Change Proneness: An Examination of Five Evolving Systems," Proc. of 9th International Symposium on Software Metrics, Sydney, Australia, September 3-5, 2003, pp 40-49.
8. Briand L.C, Wust J, Ikonomovski S. V and Lounis H, "Investigating Quality Factors in Object Oriented Designs: An Industrial Case Study," Proc. of the 1999 International Conference on Software Engineering, Los Angeles, May 16-22, 1999, pp 345-354.
9. Chidamber S.M and Kemerer C.F, "A Metrics Suite for Object Oriented Design," IEEE Transactions on Software Engineering, June 1994, pp 476-493.
10. Eric J Baude. Software Design: From Programming to Architecture. Wiley, 2003.
11. Gamma Erich, Richard Helm, John Vlissides and Ralph Johnson. Design Patterns: Elements of Object-Oriented Software. Addison Wesley Longman, 1994.
12. Masuda G, Sakamoto N and Ushijima K, "Redesigning of an Existing Software Using Design Patterns," Proc. International Symposium on Principles of Software Evolution, Kanazawa, Japan. November 1-2, 2000, pp 165-169.
13. McCabe, T. J., "A complexity measure", IEEE Transactions on Software Engineering SE-2, 1976, pp. 308-319.
14. Prechelt L, Unger B.; Tichy W F, Brossler P and Votta, L.G, "A Controlled Experiment in Maintenance: Comparing Design patterns to Simpler Solutions," IEEE transactions on Software Engineering, vol.27, no.12, pp.1134-1144, December, 2001.
15. Shereshevsky M., H. Ammari, N. Gradetsky, Mili A and H. H. Ammar, "Information Theoretic Metrics for Software Architectures," Computer Software and Applications Conference, Chicago, October 8-12, 2001.
16. The UML Tool, rational rose [Online]. Available: <http://www.ibm.com/software/rational>, last visited in May, 2005.
17. Tsantalis N, Alexander C, George S and Ignatios D, "Probabilistic Evaluation of Object-Oriented Systems." Proc. of the 10th International Symposium on Software Metrics, Chicago, September 14-16, 2004, pp 26-33.
18. [Online]. Available: Understand for Java, Scientific Toolworks Inc, <http://www.scitools.com>, last visited on May, 2005.
19. Yacoub S.M, Xue H and Ammar H H, "Automating the Development of Pattern-Oriented Designs for Application Specific Software Systems," Proc. of the 3M IEEE Application-Specific Systems and Software Technology Symposium, Texas, March 24-25, 2000, pp 163-170.
20. Yu Bo, Mili A, Abdelmoez W, Gunnalan R, Shereshevsky M and Ammar H H," Requirements Change Impact in Software Architecture," Proc. of 4th Int. Conf. On Information Science, Communications and Applications (ISA 2004), Miami, FL, April 2004.
21. Yu Bo, Mili A, Abdelmoez W, Gunnalan R, Shereshevsky M and Ammar H H," Assessing and Quantifying Attributes of Product Line Architectures," International Conference on Computing, Communications and Control Technologies, Austin, TX, August 14-17, 2004.
22. I Shaik², W. Abdelmoez, R. Gunnalan, M. Shereshevsky, A. Zeid³, H.H. Arnrnar Lane Department of Computer Science, West Virginia University Morgantown WV 26506 (isrars, mbie, gunnalan, smark, azeid, ammar} @ csee.wvu.edu
23. A. Mili College of Computer Science, New Jersey Institute of Technology Newark NJ 07102 mili@cis.njit.edu
24. C. Fuhrman Department of Software and IT Engineering Ecole de technologie superieure Montreal, Canada H3C 1K3 dlristopher.fuhrman@etsmtl.ca



Information Technology



Shymaa M. Arafat

Lecturer at the Computer Science Department, Faculty of Computer and Information Sciences, Ain Shams University. She was born on 25 July 1972 and graduated from Computer Science and Automatic Control Department, Faculty of Engineering, Alexandria University with degree of Honor.

In July 1997, she finished her master's degree with a thesis entitled "An Efficient Parallel Sample Sorting Algorithm". Four Years later in 2001, she completed her PhD in "Operating on Binary Code Trees". She continued her research and published more than 12 Publication in National and International Journals. In 2004, she won the BA/CSSP Research Grant, which was on *'Providing Secure Communications for Wireless and Wire Line Applications'*.

Providing Secure Communications for Wireless and Wireline Applications

Shymaa M. Arafat

Faculty of Computer and Information Sciences, Ain Shams University, Cairo, Egypt

1. Executive Summary

1.1 Introduction

There are many benefits associated with wireless networking. Roaming users can stay connected to the corporate network wherever they are. Consider the case of a patient in a hospital bed or in an ambulance, who needs to transfer his laboratory results, ECG, or the result of other monitoring device to the doctors at the moment while he is in place. This is also useful for industries like manufacturing, retail, healthcare, and services, where employees who are on the move can function much more effectively and eliminate errors by being connected at the point of service.

Wireless LANs (WLANs) eliminate the need to run wiring where it does not already exist, such as in schools, universities, hospitals, airports and remote offices; or in places where it may be impractical to run wiring, such as temporary offices or trade shows. Wireless technology can be combined with broadband networking to provide convenient Internet access for a variety of home devices and in public places such as hotels or conference venues.

This project is concerned with the security aspects of networks. The research mainly focused on authenticating messages and preventing un-authorized access in heterogeneous network environments, where wireless technology can be combined with broadband networking. The main outcome was a secure protocol for reliable communications in wireless and wired environments.

1.2 Motivations and Outcomes

This section presents the objectives we began with and the results achieved by the end of the project.

Rich Research Field

An important goal was to conduct and increase the research in the areas of wireless technology and mobile computing. Although security aspects was the main concern at the beginning, by digging into this area more research fields and aspects were investigated. A lot of postgraduate researches were conducted in wireless networks regarding security and other fields such as

sending multimedia data and power consumption. The aim was to provide the faculty with some simulation tools that facilitates such studies, many simulation tools were investigated free ones were downloaded and used like GlomoSim, nS2, OPNET.

2. Discussion

2.1 Introduction

In a wired network, transmissions travel through a guided medium such as copper wire or optical fiber, limiting the scope of user access. However, signal coverage in wireless networks effectively turns any space near the wireless transceiver into a point of access to the network, a one that an attacker can use to read or inject packets.

Another problem is that security programs usually involve extensive computations while most mobile nodes usually have limited power and computational resources. The bandwidth is also limited to occupy with security data.

Although I performed a research during the project in encryption algorithms, authentication rules and security in general, I consider the main research result of this project the design of efficient and reliable security protocols for authentication, exchanging session keys, and providing access control in mobile ad hoc networks. Thus, the first three sections will discuss wireless research only, then a separate section will consider a separate research in encryption algorithms.

2.2 First Phase of the project

At first it was necessary to establish a solid background before starting a research in wireless networks. Reading started from text books and survey papers to get a glance at the communication part and how wireless communications is actually done, documentations of known standards like IEEE 802.11 and Bluetooth, different network topologies, routing issues, and finally security issues.

Course Syllabus

I used such material to prepare a half semester elective course on wireless networks for 4th year Computer

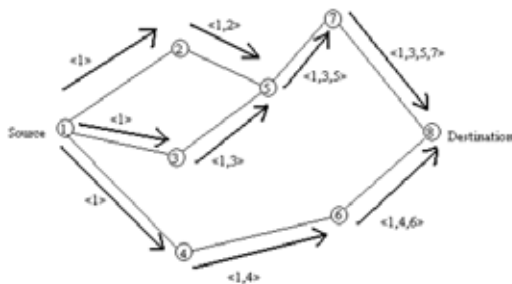
Science students. The syllabus of the course can be summarized as follows:-

Introduction to wireless communications (frequency ranges, difference from OSI-ISO 7 layers model, design issues and problems and different applications):

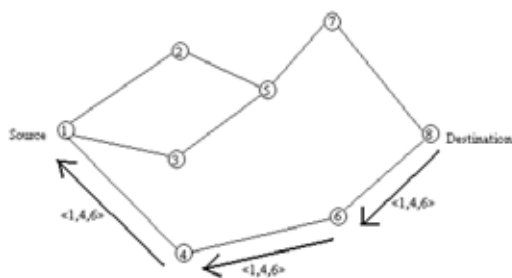
1. Wireless LANs (IEEE 802.11, architectures, operation modes, etc).
2. PANs, Bluetooth, ad hoc networks.
3. Routing protocols for mobile ad hoc networks (design issues, on demand *vs* table based, different protocols).
4. Securing wireless networks (problems, WEP, security of Bluetooth, securing wireless networks).

Ariadne Protocol

I also began my work with a Masters student on securing mobile ad hoc networks. By the end of this phase the survey was completed and we reached an existing secure MANET protocol (Ariadne) [17] that is based on TESLA multicast authentication protocol [11] and DSR routing protocol [6].



a. Propagation of a route request message



b. The route reply message

Figure 1 DSR route discovery example

Fig. 1 is an example of a route discovery process [4]

- Containing destination address, source address, and unique ID.
- Each node receiving a route request checks to see if it knows a route to the destination, otherwise it appends its own address to the packet and forwards it on out-going links.
- Once the message gets to the destination a Route Reply is sent through the reverse path to the source (although DSR supports anti symmetric links, we are concerned here with the case of symmetric links).

- Route maintenance is accomplished through route error packets generated at a node when the data link layer encounters a fatal transmission, and the route is canceled. Then, either another route is taken or a new route request is initiated.

DSR

Dynamic source routing is an on demand (reactive) routing protocol. On demand routing protocols, as opposed to table driven protocols, searches for a route only when it is needed [9]; an approach that was found more efficient for most ad hoc networks. DSR has two main phases; route discovery phase and route maintenance [1].

- Route discovery protocol uses a Route Request message.

TESLA

TESLA is a multicast authentication protocol to authenticate messages using message authentication codes (MACs) [5]. The idea is to make each node generate a key chain and then use it in reverse order.

- A random number K_n is generated then a key chain is constructed by making $K_i = H[K_{i+1}]$ where H is a one way hash function.
- A receiver accepts a message only if its key is not disclosed yet (otherwise it discards the packet). Then, when the key is disclosed it checks the MAC value of the message.
- Each sender pre-determines the disclosing schedule; picks K_i which will not be disclosed until $(T_i = T_0 + i \times \tau)$ it passes and adds MAC using K_i to the packet) Where T_0 is the time at which K_0 is published and τ is the key publication interval.

Two parameters are needed for the receiver to check the validity of the key; τ is the worst case end to end network delay, and Δ is the maximum time synchronization error. Following Fig. 2, the receiver accepts the message if the sending time $t_s \leq t_0 * i - \Delta$



Figure 2 Sending and receiving in TESLA

Ariadne

The Ariadne protocol embeds TESLA authentication information into the route request and route reply messages of DSR. Since we are presenting an enhancement on security operations of the protocol, while describing the protocol we will concentrate only on related features.

- When a sender wants to communicate with a certain destination he constructs a route request message. The message contains the source and destination addresses, a unique identifier of the message (called sequence number in DSR), and pessimistic expected arrival time at the destination. A MAC value (h_0) is appended using a secret key between the sender and the receiver. (Ariadne assumes such key is already established, section 3).
- The source floods the message to its neighboring nodes, and when a node receives it, the following operations are performed:
 - h_0 is chained into h_1 after adding the node address to it; h_1 is appended to M .
 - The node address (A) is appended to the message.
 - The node calculates the MAC of the resulting message using its current TESLA key and appends it to the message.
- The process is repeated till the request reaches the destination with the final hash chain value, addresses of intermediate nodes, and MACs of intermediate nodes.
- The target checks the hash chain value (it knows the secret key and the intermediate nodes), then if valid it constructs the route reply message with the source and destination addresses, the unique identifier, the routing nodes, and the MACs of the routing nodes (Note that D cannot check the validity of those MACs since their keys should not be disclosed yet, and thus leave it to the source). Finally the destination appends its MAC using the shared secret key between itself and the source.

Intermediate nodes append their key values to the reply message when they receive it, and forward it to the next node in the route. Ariadne can work in a similar manner with digital signatures or shared secret keys (and so is the proposed protocol). If digital signatures were used, they would replace the MAC values and the destination would be able to verify their values. If pairwise shared secret keys were used, intermediate nodes might add their MACs to the route request using the shared secret key with the destination, and then append MACs using the shared key with the source to the route reply. In both cases, although not mentioned explicitly

by the authors, it may not be necessary for intermediate nodes to complete the hash chain.

The strength of Ariadne comes from the fact that in order to change, add, or delete a node in the route, you need to rebuild the hash chain and recalculate the MAC values starting from that node. Consider the preceding Figure (with the route $S \rightarrow A \rightarrow B \rightarrow C \rightarrow D$).

If C desires to replace (or omit) A from the route, it needs to know the previous hash value (h_0) to build a new faked (h_1), and to recalculate the MAC value of B which is infeasible without knowing KB . Note however, that if a node is trying to change its immediate predecessor (B is trying to change A or C is trying to change B), it is enough to know the old hash value (h_0 for B or h_1 for C). Recalling that a passive attack is always possible, the hash chain cannot be considered a solution, this is why Ariadne assumes nodes in the route are trusted (to exclude C) and that a node can check the source address of the message it received so that no other node can deceive C to be in place of B .

Proposed Enhancement

We discovered an enhancement that saves time and network bandwidth and keeps the same security level (we thought so at the time).

Each node in the route appends its MAC to the route request packet, although the receiver (D) never checks these values; the MAC values are checked only by the sender in the route reply packet. Thus, it is not necessary for each node to append its MAC to the route request, it is more appropriate to keep only the last (chained) MAC value in the message.

Each node replaces the previous MAC with its MAC in a route request packet. With the final MAC value present, the sender will be able to verify the correctness of the MAC chain through the key values appended to the route reply. A malicious node trying to inject a wrong key value will be detected because it will lead to a wrong final MAC value.

The only drawback of this solution is that the sender will not be able to detect the source of a wrong MAC chain; that is exactly which of the MAC values was wrong, and also the sender will not have to perform the complete MAC chain to detect the error. Although this may help the sender to calculate statistics about suspicious nodes, a wrong MAC value may be caused by any active attacker, not necessarily the node in the route. This was a reasonable price to pay for saving packet length and network bandwidth.

Simulation

The plan for the next phase was to formulate the result with a detailed analysis on security and robustness against different attacks to prove the security of the modified protocol.

At the same time, search for a suitable simulation tool to measure the performance improvement. Although nS2 is the most popular, is an open source, and was used in the course labs, it needs a background on Unix, and takes from 3 to 6 months to practice it well enough to write a complete simulation. We looked for other alternatives, OPNET needed a licence so we studied the option of GlomSim.

Figs. 3 and 4 show the steps of the route request and route reply propagation.

Route to be found: $S \rightarrow A \rightarrow B \rightarrow C \rightarrow D$
 $M = [\text{Request}, S, D, id, ti]$
 $S: h0 = \text{MAC}_{KSD}(M)$
 $S^* : [M, h0, (), ()]$
 $A: h1 = H(A, h0)$
 $M_A = \text{MAC}_{KA ti} [M, h1, (A), ()]$
 $A^* : [M, h1, (A), (M_A)]$
 $B: h2 = H(B, h1)$
 $M_B = \text{MAC}_{KB ti} [M, h1, (A, B), (M_A)]$
 $B^* : [M, h2, (A, B), (M_A, M_B)]$
 $C: h3 = H(C, h2)$
 $M_C = \text{MAC}_{KC ti} [M, h3, (A, B, C), (M_A, M_B)]$
 $C^* : [M, h3, (A, B, C), (M_A, M_B, M_C)]$

Figure 3 Route request propagation

$M = [\text{Reply}, D, S, ti, (A, B, C), (M_A, M_B, M_C)]$
 $D: M_D = \text{MAC}_{KSD}(M)$
 $D^* : [M, M_D, ()]$
 $C^* : [M, M_D, (KC ti)]$
 $B^* : [M, M_D, (KC ti, KB ti)]$
 $A^* : [M, M_D, (KC ti, KB ti, KA ti)]$

Figure 4 Route reply steps

2.3 Second Phase of the Project

We started the simulation using GlomSim simulation tool and prepared a first version of the paper. However, after sending the paper to the first conference (MobiCom) one of the reviewers pointed out that the proposed protocol may prevent an attack he recently discovered against Ariadne. Thus, we read his paper [10], proved that our protocol prevents such attack then the paper was rewritten from a different point of view.

Attack Against Ariadne

The attack can be mounted by an active 1-2 adversary. This is a terminology of an attacker model introduced in [17]; it means an active attacker who owns two nodes in the network but has only a single corrupted key, say KA with identity A. Assume S is initiating a route discovery towards D, the two devices owned by A are in the way.

$S \rightarrow V \rightarrow A(1) \rightarrow Z \rightarrow \dots \rightarrow Z' \rightarrow A(2) \rightarrow W \rightarrow D$

The first node owned by A, A(1) will receive the following route request

$[M, h_V, (V), (M_V)]$

Now A(1) should replace h_V by h_A and append M_A to the message $[M, h_A, (V, A), (M_V, M_A)]$

Instead A(1) will send the following $[M, h_A, (V, A), (M_V, h_V)]$. None of the following intermediate nodes can detect the change, because they cannot check the value of M_A and even h_V has the same format (since MAC values are cryptographic hash functions that depend on a key). Thus, when the request reaches the second node owned by A, A(2), it will be as follows $[M, h_{Z'}, (V, A, Z, \dots, Z'), (M_V, h_V, M_Z, M_{Z'})]$

Now A(2) can remove all the nodes after A(1) from the route; i.e. the nodes $Z \dots Z'$, using the stored hash value; it will recalculate h_A , M_A and broadcast the following message to reach W $[M, h_A, (V, A), (M_V, M_A)]$. Neither W nor D will detect an error, and the route reply will reach A(2) as follows $[M_{rep}, M_D, (V, A, W), (K_W)]$, which it will recorrect to $[M_{rep}, M_D, (V, A, Z, \dots, Z', A, W), (K_W, K_A)]$.

The intermediate nodes will append their keys when the reply reaches them, till it reaches A(1) as follows $[M_{rep}, M_D, (V, A, Z, \dots, Z', A, W), (K_W, K_A, K_Z, \dots, K_{Z'})]$. A(1) will re omit the nodes $Z \dots Z'$, before it sends it to V. This way S will receive a "correct" route reply $[M_{rep}, M_D, (V, A, W), (K_W, K_A, K_V)]$ saying that the route to D is simply $S \rightarrow V \rightarrow A \rightarrow W \rightarrow D$ (wrong route!).

Preventing the Attack

Each node in the route appends its MAC to the route request packet, although the receiver (D) never checks these values; the MAC values are checked only by the sender in the route reply packet. Thus, it is not necessary for each node to append its MAC to the route request, it is more appropriate to keep only the last (chained) MAC value in the message.

If each node replaces the previous MAC with its MAC in a route request packet, the sender will still be able to verify the correctness of the MAC chain through the key values appended to the route reply.

With the final MAC value present, a malicious node trying to inject a wrong key value will be detected because it will lead to a wrong final MAC value. The previous attack will not be possible, since the second node A(2) will not be able to see or retrieve h_V because only $M_{Z'}$ will appear in the message $[M, h_{Z'}, (V, A, Z, \dots, Z'), (M_{Z'})]$. If a node tried to change its immediate predecessor, as mentioned in the last of section 2.2, (C is trying to change B for example) this would not be possible too, because the previous MAC value (MA) would not be available in the message.

The Proposed Protocol

After proving that the proposed approach prevents such attack and still prevents the attacks prevented by Ariadne, by removing the hash chain since the MAC chain now provide the same benefit, and embedding a session key exchange mechanism, the final proposal becomes as follows:

| |
|--|
| <p><u>Route Request</u></p> <p>Route to be found: $S \rightarrow A \rightarrow B \rightarrow C \rightarrow D$ $M = \langle \text{Request}, S, D, id, ti, E_{KSD}[R1], E_{KSD}[R2old] \rangle$ $S^* : \langle M, (), () \rangle$ $A : M_A = MAC_{KAti} \langle M, (A), () \rangle$</p> <hr/> <p>$A^* : \langle M, (A), (M_A) \rangle$ $B : M_B = MAC_{KBti} \langle M, (A, B), (M_A) \rangle$ $B^* : \langle M, (A, B), (M_B) \rangle$ $C : M_C = MAC_{KChi} \langle M, (A, B, C), (M_B) \rangle$ $C^* : \langle M, (A, B, C), (M_C) \rangle$</p> <p><u>Route Reply</u></p> <p>$M = \langle \text{Reply}, D, S, ti, (A, B, C), M_C, E_{KSD}[R2] \rangle$ $D : M_D = MAC_{KSD} (M)$ $D^* : \langle M, M_D, () \rangle$ $C : M_C = \langle M, M_D, (KChi) \rangle$ $B : M_B = \langle M, M_D, (KBti) \rangle$ $A : M_A = \langle M, M_D, (KAti) \rangle$</p> |
|--|

Figure 5 Route discovery of the proposed protocol

2.4 Third Phase of the Project

The simulation results were complete showing the improvement of different performance metrics (although it became second priority compared to the added security). The paper was published in the *International Journal of Global Engineering Science and Technology Society (GESTS): Transaction On Computer Science and Engineering*.

Simulation Details

We used GLObal MOBILE Information System Simulator (GloMoSim) [13], which is a scalable simulation library for wireless network systems.

2.4.1 Simulation Parameters

We used the following parameters in all simulation scenarios

- Simulation duration is 900 secs
- Number of Nodes 50
- Maximum Velocity (μ max) 20 m/s
- Dimensions of Space 1500 m * 300 m
- Nominal Radio Range 250 m
- Source-Destination Pairs 20
- Source Data Pattern (each) 4 packets/second
- Application Data Payload Size 512 bytes/packet

- Total Application Data Load 327 kbps
- Raw Physical Link Bandwidth 2 Mbps
- Node placement is uniform. Based on the number of nodes in the simulation, the physical terrain is divided into a number of cells. Within each cell, a node is randomly placed.
- MAC protocol 802.11 is used.
- IP is used as Network protocol

Performance Measures

Simple DSR (zero authentication overhead) is used as a basis of comparison for the two protocols, and the following performance measures were tested:

Average Network Throughput. The average network throughput is the average number of data bits transmitted throughout the network per unit time.

Average end to end delay [s]. The average time elapsed when a data packet is first sent to when it is first received at its destination.

Packet Delivery Ratio (PDR). The fraction of application level data packets sent that are actually received at the respective destination node.

2.5 Results

Figures 6, 7 and 8 show the results of the simulation.

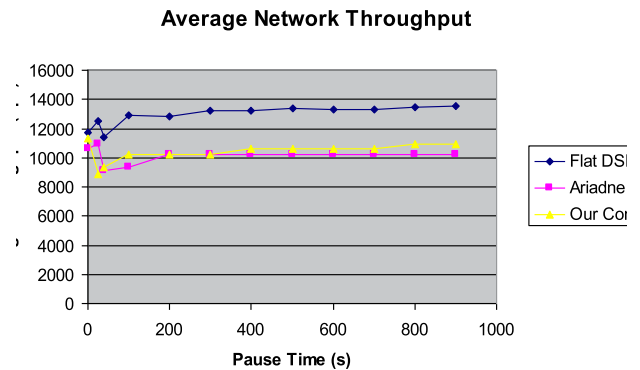


Figure 6 Network throughput of the three protocols

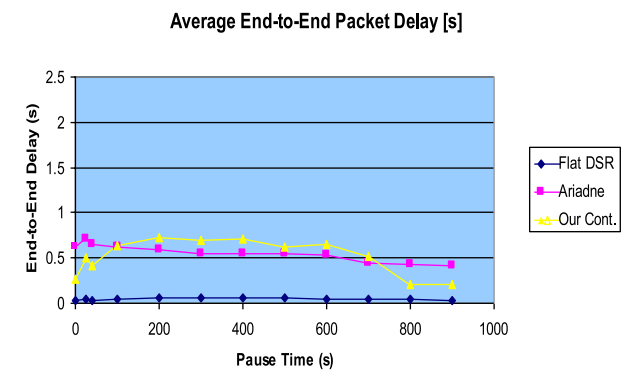


Figure 7 Average end-to-end packet delay of the three protocols

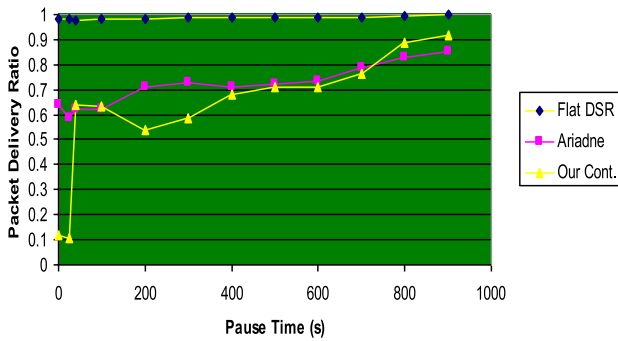


Figure 8 Packet delivery ratio of the protocols

As expected, the proposed protocol increases the network throughput; however, the enhancements in the delay and delivery ratio are only noticeable with larger pause times. The reason for this is that we have used different initial and maximum route request timeouts for different protocols according to the packet length and expected overhead for each. Typically, 0.5 and 10 seconds for DSR, 2 and 40 seconds for Ariadne, and 1.5 and 30 seconds for our proposal. Maybe these numbers need to be tuned, and the simulation needs to be repeated with the same values of timeouts so that the figures can reflect the improvement. This becomes more clear from the packet delivery ratio results; still, there is no reason to explain why the proposed protocol may have less packet delivery ratio in some points except that it has a shorter timeout interval.

However, we did not repeat the simulation for the time constrains, and since the simulation was just a tool to demonstrate the improvement as preventing more attacks is a sufficient advantage for the proposed algorithm.

2.6 Encryption

I had an ongoing research on an encryption algorithm. I started it in [11]. It was separate from the routing protocol, but since the project title included both wireless and wired communications I thought it could be included.

The Encryption Algorithm (ATC)

Alphabetic tree cipher was introduced as an idea in [11] to use a property of optimal alphabetic tree that can be used to encrypt data as nodes in the tree.

Theorem

If l_1, l_2, \dots, l_n are a valid set of levels for an OAT (the levels of some weight sequence) then the weight sequence $2^{l_1}, 2^{l_2}, \dots, 2^{l_n}$ has the same set of levels for its OAT

Corollary

If the weight list $w_1, w_2, \dots, w_i, \dots, w_n$ has the levels $l_1, l_2, \dots, l_i, \dots, l_n$ for its OAT then the weight list $(w_1 + k \cdot 2^{-l_1}), (w_2 + k \cdot 2^{-l_2}), \dots, (w_i + k \cdot 2^{-l_i}), \dots, (w_n + k \cdot 2^{-l_n})$, where k is a positive constant, has the same set of levels for its OAT

Alphabetic Tree Cipher

If the plain text is considered as nodes of an optimal alphabetic tree p_1, p_2, \dots, p_n , then the cipher text could be $(p_1 + k \cdot 2^{-l_1}), (p_2 + k \cdot 2^{-l_2}), \dots, (p_i + k \cdot 2^{-l_i}), \dots, (p_n + k \cdot 2^{-l_n})$ where k is derived from the secret key, Fig. 9.

Key Generation

To prevent known plaintext attacks, it was found that the key values should be an irreversible function of the secret key and the levels of the tree to get different key values for different trees. Two functions were tested; MD5 hash function and a simple squaring function for the sake of comparison $K_i = (k[\text{Index}] * l_i)^2 \text{ mod } 256$.

Experimental Results

After trying different values, the number of nodes was chosen as 8 nodes, where each node is a 64 bit block. Experiments were conducted to compare the two key functions and to compare the algorithm to known standards

Key Functions

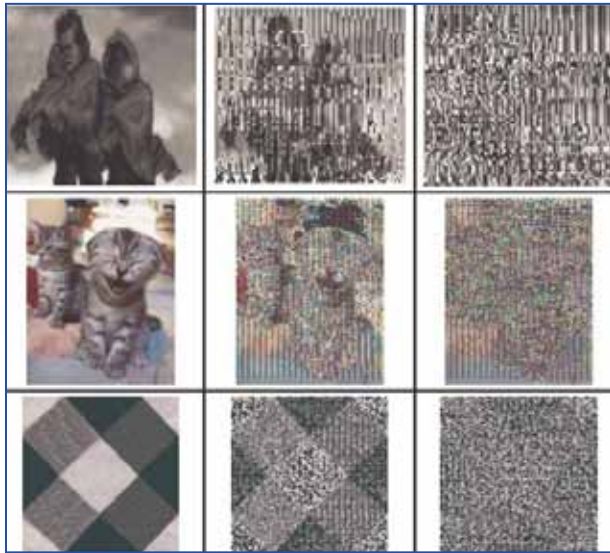
The results are shown for images to be more illustrative, Fig. 10, while the runtime comparisons are shown in Fig. 11.

```

ATC Encryption (INPUT: a set of  $n$  elements, Key)

//n: no. of nodes
//Phase 1: Level Calculation
Combination (In)
Level Assignment (T)
//Key Expansion
K = Md5 Function (Key, levels)
//Phase 2: Cipher Generation
for i = 1 to n
Ci = Pi + (K[Index] * 2li) //Index = 0 or 1 (key value part index)
    
```

Figure 9 ATC Encryption



a The original image b Squaring function c Using MD5

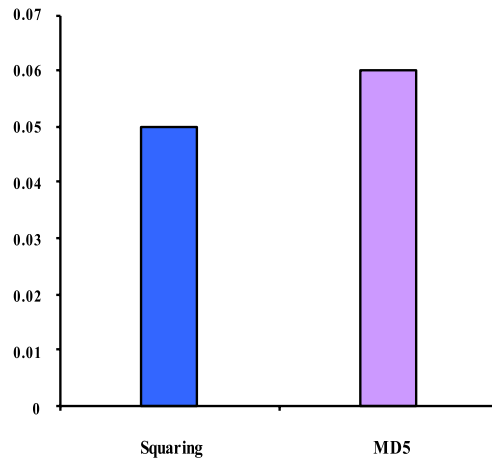


Figure 11 Runtime comparison for both functions

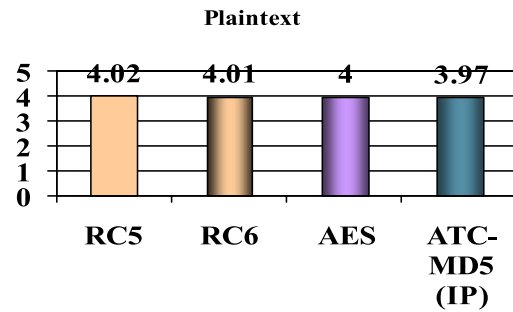
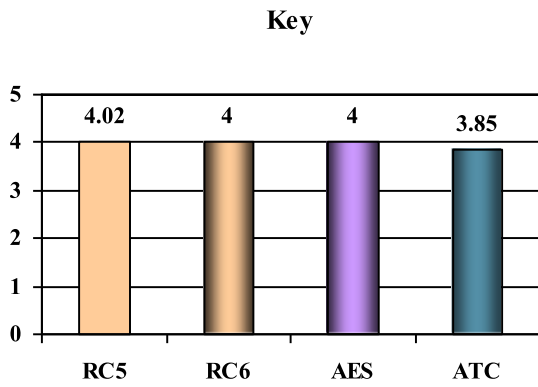


Figure 12 The avalanche effect for the four algorithms

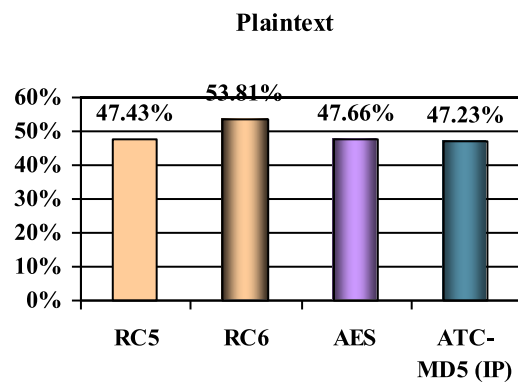
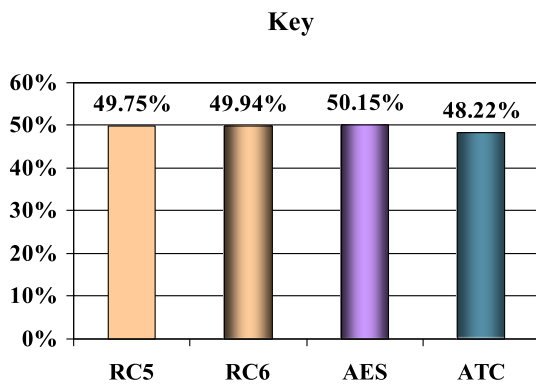


Figure 13 Bit randomness for the four algorithms

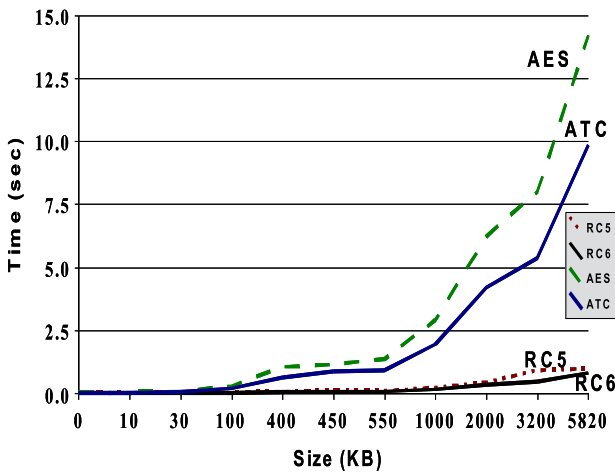


Figure 14 Average runtime of four algorithms

Comparing to Known Standards

The performance of the algorithm was compared to AES, RC5, RC6 encryption algorithms. The algorithms were compared according to their Avalanche Effect, Bit Randomness, and Runtime.

Avalanche Effect

The avalanche effect is defined as the hamming distance between two cipher text blocks when the hamming distance between their corresponding plaintext (or key values) is 1, Figure 12.

The ideal value for the avalanche effect is 50% of the bits which is scaled to 4 in the figure to normalize the different key and block sizes for the algorithms. It is worth mentioning that the first values for the plaintext case in ATC was very disappointing (0.18), analysis showed that this is due to the nature of optimal alphabetic trees. A change in 1 bit of a node in the tree is not likely to affect the resulting levels of the tree. Thus, we thought if we performed a random permutation of each block before encrypting, this would randomize the effect of each bit. The DES initial permutation was used as it is a tested random permutation. The results showed an incredible improvement in the results.

Bit Randomness

An ideal cipher text should be completely random, thus each cipher bit should have a probability $\frac{1}{2}$ of being 0 or 1. The bit randomness metric is defined as the average ratio of 1 (or 0) bits in the cipher text blocks for different plaintext (or key) values. An ideal value is 50%, Figure 13

Time Complexity

The runtime of the four algorithms is measured for different plain texts and the results are shown in Figure 14. All results show that the proposed algorithm is

comparable to these algorithms (although not superior of course).

Conclusions and Recommendations

With the advent of wireless technology enormous number of applications appeared ranging from military applications to multi player games. This variety of domains, where each domain has its specific needs and constraints, opened a lot of research areas in this field. These new hot topics are rich in both scientific and application levels, which make them tempting for investors as well as students and researchers. Recently a lot of graduation projects and master students chose this field.

To conduct a research in these areas two preliminary steps are needed; the first is to understand the technology and build a background on previous research. The second is to learn a simulation tool or study how to perform a simulation using a traditional programming language. This step involves studying movement patterns for nodes, arrival and service patterns for packets which are both dependant on the nature of the application. Thus, it would be much easier if the student learned these steps through his undergraduate courses where there is enough time to learn and practice the tool gradually through examples.

Published papers

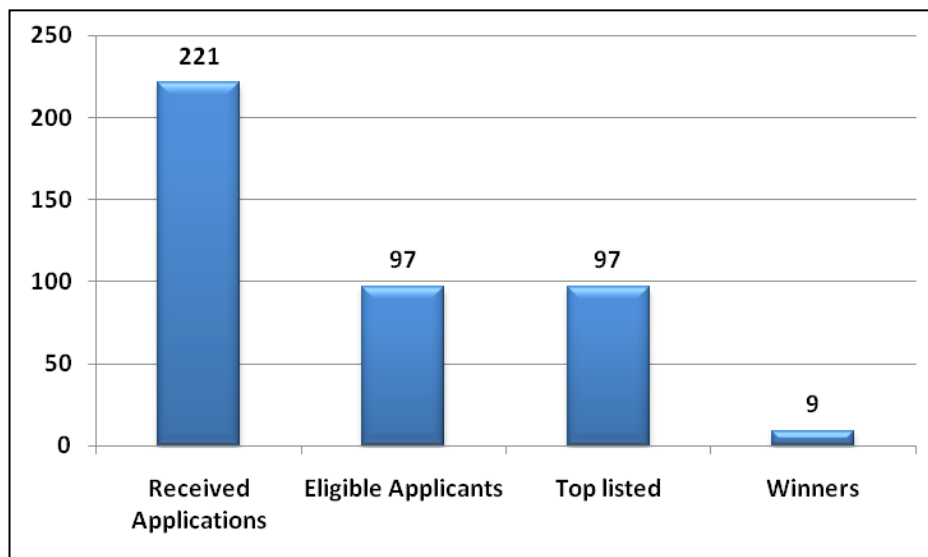
1. M. Tolba, S. Arafat, R. Kotb, "Analysis of Alphabetic Tree Cipher", the 4th International Multi conference in Computer Science and Information Technology, 5-7 April 2006, Amman, Jordan.
2. M. Tolba, S. Arafat, R. Kotb, "Comparing Alphabetic Tree Cipher (ATC) to RC5, RC6 and Rijndael", International journal on Intelligent Computing and Information Systems IJICIS, 2006.
3. S.Arafat, Y.Dakroury, A.Wahab, "An Efficient and Secure Ad hoc Routing Protocol", Global Engineering Science and Technology Society (GESTS) Transaction On Computer Science and Engineering, Vol. 32 and No.1, September 2006.

References

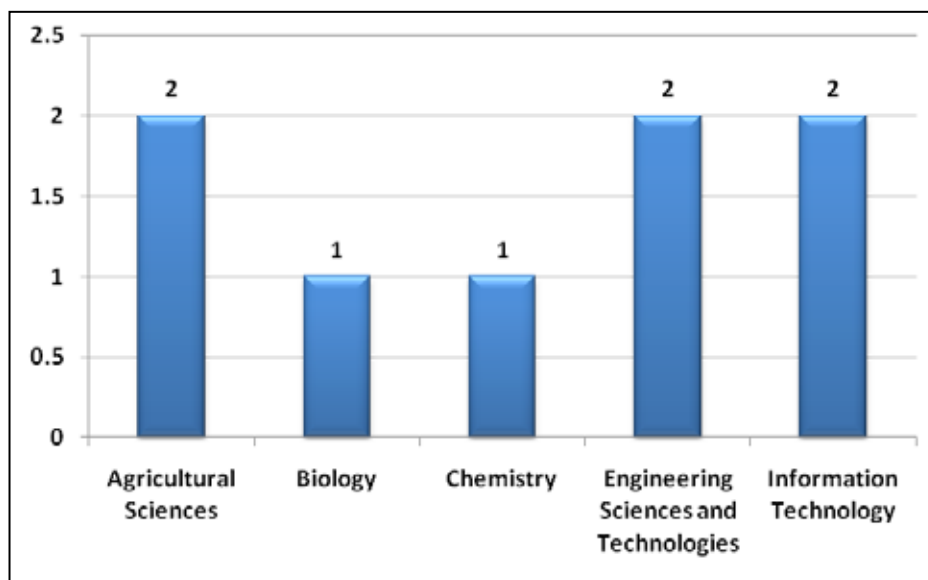
4. A. Aziz and W. Diffie. Privacy and Authentication in Wireless Local Area Networks. *IEEE Personal Communications*, First Quarter, 1994.
5. A. Perrig, R.Canetti, D.Song, and J.Taygar,"Efficient and Secure Source Authentication for Multicast". *In Network and Distributed System Security Symposium, NDSS'01*, February 2001.
6. B. RAMAN. Security in Wireless Networks, *Department of Computer Science Texas AandM University*, a Term paper, December 2001.

7. B. Xu, S. Hischke and B. Walke, "The Role of Ad Hoc Networking in Future Wireless Communications", Proceedings of ICCT 2003
8. Bharghavan, V. Secure Wireless LANs, In *ACM Conference on Computer and Communications Security*, November 1994, pp. 10-17.
9. David B. Johnson, Davis A. Maltz, "Dynamic Source Routing in Ad Hoc Networks", *Mobile Computing*, T. Imielinski and H. Korth, Eds., Kulwer, 1996, pp. 152-81.
10. E. Royer and C.Toh, "A review of Current Routing protocols for Ad Hoc Mobile wireless networks". *IEEE Personal Communications* April 1999, pp 46-55.
11. J. Hubaux, L. Buttyan, and S. Capkun, "The Quest for Security in Mobile Ad hoc Networks". In *Proceedings of the Second Symposium on Mobile Ad hoc Networking and Computing (MobiHoc 2001)*, Oct 2001.
12. K. Pahlavab, T. Probert, and M. Chase. Trends in Local Wireless Networks. *IEEE Communications Magazine*, March 1995.
13. L. Buttyan and I. Vajda, "Towards Provable Security for Ad Hoc Routing Protocols", Technical Report, July 2004.
14. S. Arafat, "Encryption Using Alphabetic Trees", the 3rd ACS/IEEE International Conference on Computer Systems and Applications, (AICCSA'05), January 2005, Cairo, Egypt.
15. S. Fluhrer, I. Mantin, and A. Shamir. *Weaknesses in Key Scheduling Algorithm of RC4*. August 2001.
16. UCLA Parallel Computing Laboratory and Wireless Adaptive Mobility Laboratory, GloMoSim: A Scalable Simulation Environment for Wireless and Wired Network Systems.
17. Uskela, Sami. Security in Wireless Local Area Networks, In *Proceedings of the Helsinki University of Technology, Seminars on Network Security*, Helsinki, Finland, 1997.
18. W. Stallng. *Wireless Communication and Networks*, 1st edition, Prentice Hall 2001.
19. *Wireless LAN Medium Access Control (MAC) and Physical Layer (PHY) Specifications*, IEEE 802.11 standards Draft, IEEE, 1999.
20. Y.Hu, A.Perrig, and D.Johnson, "Ariadne: A Secure On-Demand Routing Protocol for Ad Hoc Networks", *MobiCom'02*, USA

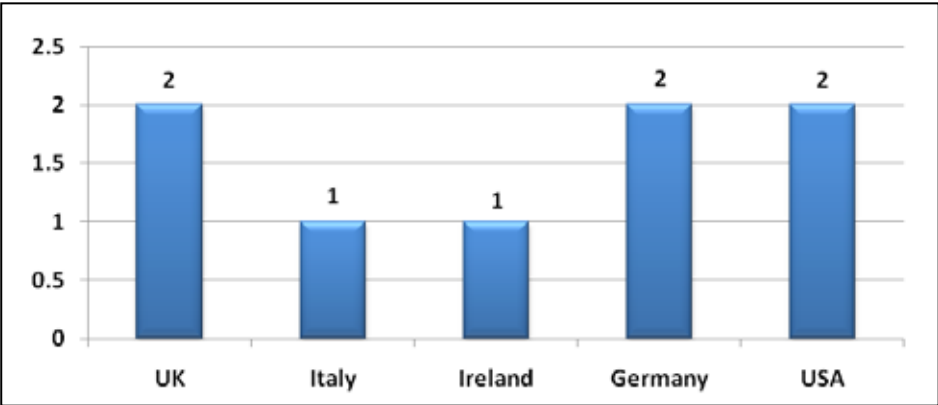
Research Grants 2004/2005 Statistics



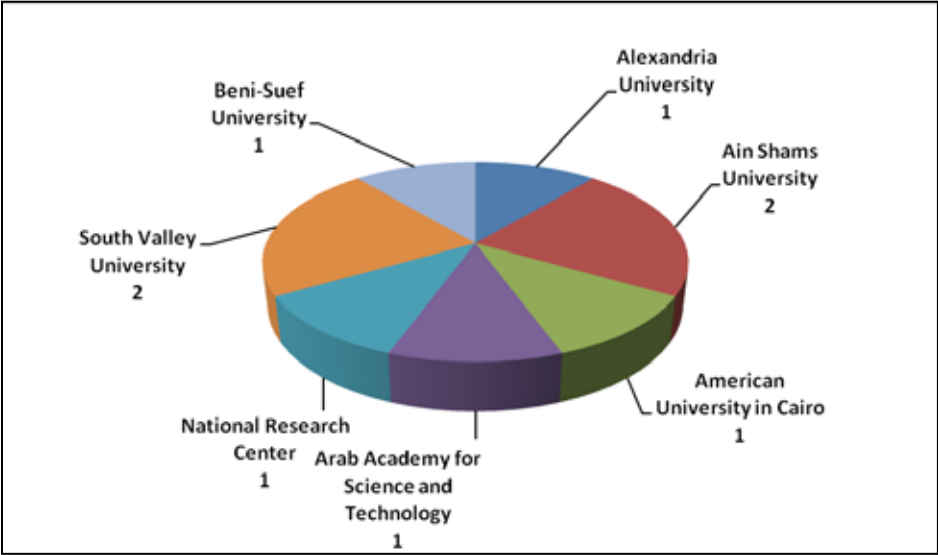
BA/CSSP Research Grants 2004/2005 Applications Results



BA/CSSP Research Grants 2004/2005 Winners by Field



BA/CSSP Research Grants 2004/2005 Research Counterparts by Country



BA/CSSP Research Grants 2004/2005 Winners by Institutes

